UC Berkeley
SEMM Reports Series

Title
Shake-table test response of bridge columns supported on rocking shallow foundations

Permalink
https://escholarship.org/uc/item/6bz1s4js

Authors
Antonellis, Grigorios
Gavras, G.
Panagiotou, Marios
et al.

Publication Date
2014-10-01

eScholarship.org Powered by the California Digital Library
University of California

Report No.
UCB/SEMM-2014/07

Structural Engineering
Mechanics and Materials

SHAKE-TABLE TEST RESPONSE OF BRIDGE COLUMNS SUPPORTED ON ROCKING SHALLOW FOUNDATIONS

By

G. Antonellis
G.A. Gavras
M. Panagiotou
B.L. Kutter
G. Guerrini
A. Sander
P.J. Fox
J.I. Restrepo
S.A. Mahin

October 2014

Department of Civil and Environmental Engineering
University of California, Berkeley

Shake Table Test Response of Bridge Columns Supported on Rocking Shallow Foundations

G. Antonellis[*], A.G. Gavras[†], M. Panagiotou[*], B. L. Kutter[†], G. Guerrini[‡], A. Sander[‡], P. J. Fox[‡], J. I. Restrepo[‡] and S. A. Mahin[*]

Structural Engineering Mechanics and Materials Report UCB/SEMM – 2014/07

Acknowledgements

This work was supported by the California Department of Transportation under Agreement 65A0487. Any contents, statements, or conclusions expressed in this report are those of authors, and are not necessarily endorsed by the sponsors. The authors would like to acknowledge the suggestions and assistance from Fadel Alameddine, Tom Shantz, Dan Radulescu, Paul Greco, Alex Sherman, Hector Vicencio, Raymond Hughey, Robert Beckley, Lawton Rodriguez and Darren McKay.

[*] University of California at Berkeley

[†] University of California at Davis

[‡] University of California at San Diego

Table of contents

List of figures

List of tables

1 Introduction

In this report the experimental setup and the results of a series of large-scale shake table tests of bridge columns supported on rocking shallow foundations are presented. The project was funded by the California Department of Transportation (Caltrans) and the tests were performed at the large outdoors facility of the Network for Earthquake Engineering Simulations (NEES) at the University of California at San Diego (UCSD). The purpose of this experimental and ongoing analytical study is to establish criteria for triggering of instability, to show that rocking foundations can be designed to remain stable and ultimately to develop a performance-based methodology for the design of bridges with rocking foundations.

This experimental work used the NEES large soil confining box (LSCB) which was already in place on top of the shake table platen for a previous test. Dry and well compacted sand was placed inside the soil box up to a height of 3.35 m. Two bridge column specimens were built, positioned on top of the sand and tested simultaneously. The footing of the first specimen was placed on an aligned configuration with respect to the direction of shaking (aligned specimen), whereas the footing of the second specimen was rotated 30^o counter-clock wise (skew specimen). Three different tests were conducted in May 2013; (a) one with no underground water (test 1), (b) a second with the water level 0.6 m below the footings (test 2) and (c) a third with the water level 1.2 m below the footings (test 3).

In section 2, following the introduction, the test configuration and specimens are presented. Section 3 discusses the preparation of the test, whereas the structural material and soil properties are presented in section 4. The instrumentation and measurements are discussed in section 5, followed by the ground motions and the test chronology in section 6. Finally, the main observed and measured responses are discussed in section 7.

Appendix A includes a complete set of construction drawings for the two specimens and the instrumentation drawings for the test can be found in appendix B. Appendix C presents additional critical plots from various response parameters, whereas raw plots for every sensor are included in appendix D.

2 Test configuration & test specimens

2.1 Specimens description & geometry

The basic geometric characteristics of the specimens are shown in Figure 1. Each specimen had a square footing with side dimension of 1.5 m and a circular column with a diameter of 0.46 m. The height of the footings was 0.51 m and the height of the column above the footing was 1.96 m. At the top 0.61 m of the column the circular cross section was changed into an enlarged square section with side dimension of 0.6 m. This part of the column, named here as load stub, was used for the connection of the prefabricated mass blocks to each test specimen. More specifically, four steel supporting beams were attached to the load stub, using post tensioned steel rods and the mass blocks were then attached to the steel beams. The total weight of the mass blocks per specimen was 235 kN resulting to an axial load at the base of each column equal to 5% of the column axial capacity, a typical value for bridge piers designed by Caltrans. In order to prevent excessive rotations of the footings and potential overturning of the specimens which could damage the soil box, a restraining system including additional steel and tapered wood beams was attached to each footing. Figure 2(a) shows one of the assembled specimens, where the restraining system is highlighted.

The reinforcing steel used for the construction of the specimens was A706, Grade 60, as typically used in bridge piers designed by Caltrans. The footings were reinforced with a grid of bundles of two #6 bars every 15cm, both at the top and the bottom side. Additionally, 96 vertical hooks (#4) were placed at every grid point, tying the bottom and top reinforcement layers, see Figure 2(b). Four high strength steel (HSS) pipes were placed vertically near the corners of the footings and they were used for mounting the restraining system. The longitudinal reinforcement of the columns consisted of 16 #6 bars placed on a single layer in bundles of two bars. The resulting reinforcing steel ratio of the column section was 2.8%, ensuring essentially elastic behavior of the columns during the rocking mechanism. The transverse reinforcement was a #3 spiral with a pitch of 5.1 cm and it was uniformly placed from the bottom of the footing and along the height of the column. The load stubs were reinforced with a grid of #4 square stirrups along all three directions. A complete set of the construction drawings can be found in Appendix A.

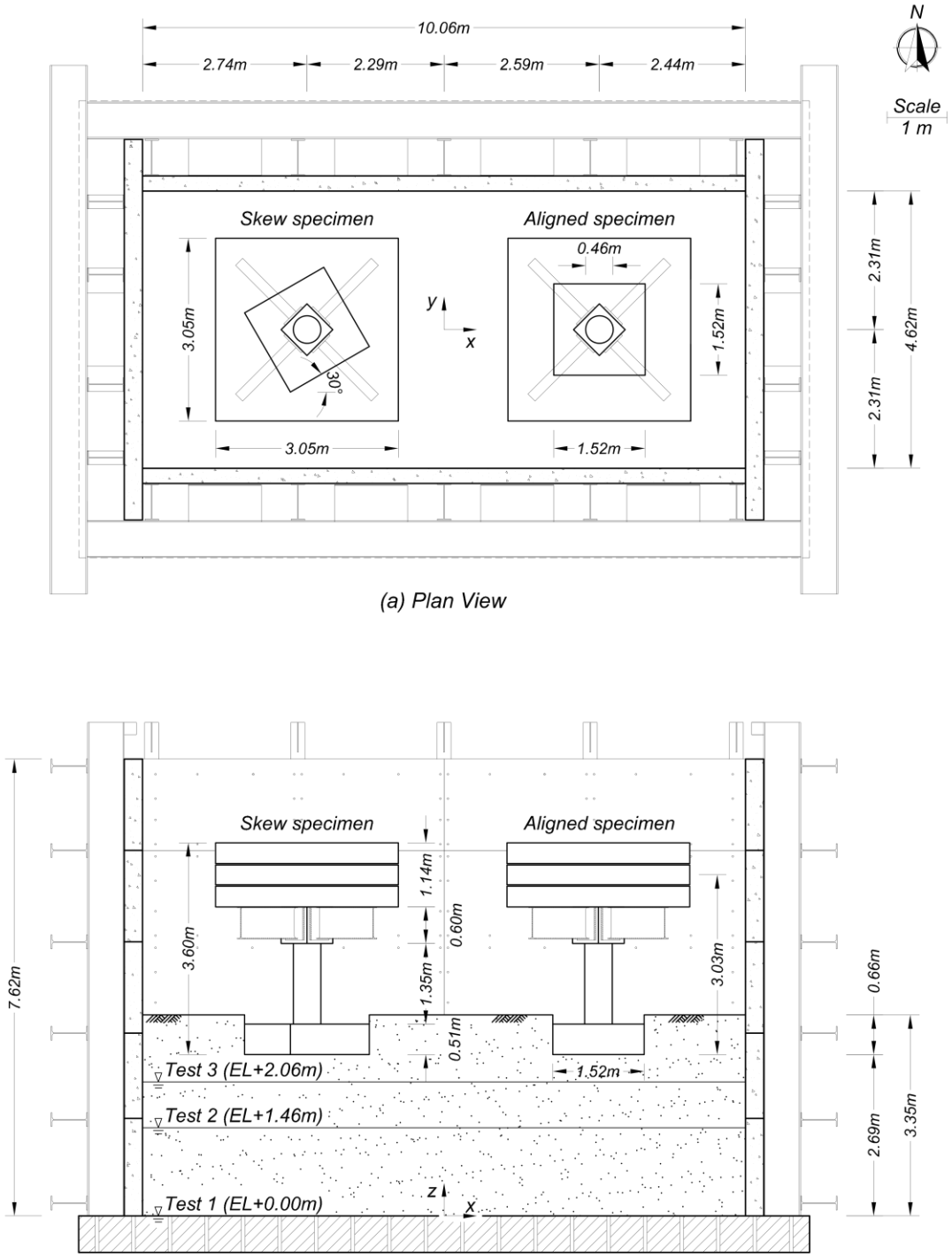

Figure 1. (a) Plan and (b) elevation view of the test setup and basic geometric characteristics of the soil confining box, the soil and the bridge column specimens. The direction of shaking is along the West-East direction.

Figure 2. (a) Picture of the assembled aligned specimen and (b) reinforcing steel cage for the footing and the column.

2.2 Test configuration

The test configuration is also shown in Figure 1, where for simplicity the restraining system of the specimens is not depicted. The soil box was filled up with dry and well compacted sand up to a height of 3.35 m. The elevation of the underground water was 0.0 (no water), 1.46 and 2.06 m, for test days 1, 2 and 3 respectively. The base of the footings was at an elevation of 2.69 m and they had an embedment height of 0.66 m. The aligned specimen was located near the east side of the soil box and the skew one near the west side. Both specimens were centered along the north south direction with respect to the shake table platen and the soil box. Figure 3 shows the embedded footing of the aligned specimen and a top view (from the west side looking east) of the test configuration.

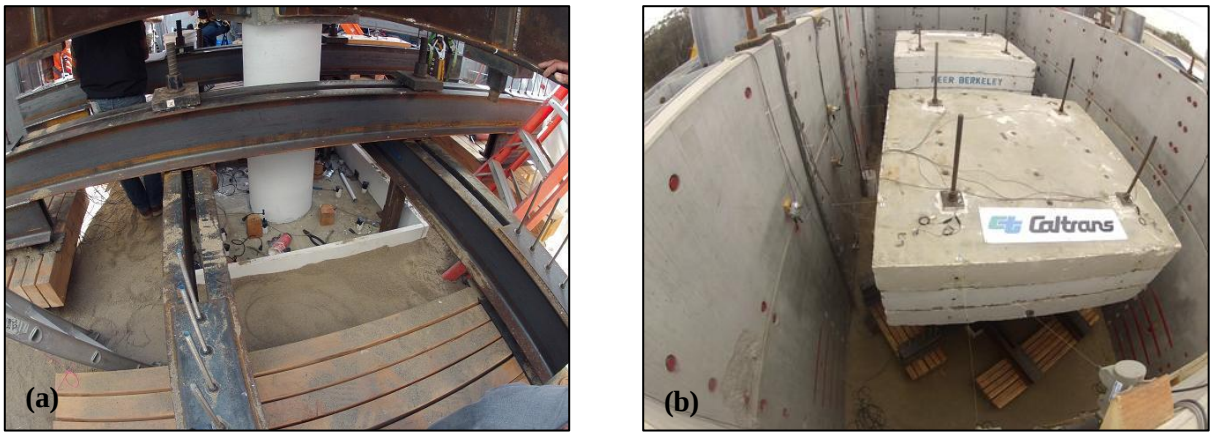

Figure 3. (a) Picture from inside the soil box after the placement of the specimens and (b) final configuration before test 1.

2.3 Coordinate system

The numeric position information contained in this report has been referenced to global and local coordinate systems. When the information is specific to a specimen it is referenced with respect to the specimen local coordinate system, while when it is not it referenced with respect to the global coordinate system. The global coordinate system has its origin at the top center of the shake table platen, with the positive x-axis extending towards the East, the positive y-axis extending towards the North, and the positive z-axis extending vertically upwards. The uniaxial direction of excitation is along the x-axis, i.e. East-West. The specimen local coordinate system is parallel to the global coordinate system but has its origin at the bottom center of the footing of the corresponding specimen. Specifically for the skew specimen, a secondary local to the footing coordinate system is defined having the same origin as the specimen local coordinate system but rotated positively about z-axis with $\theta_z = 30^o$.

In addition to the position information, accelerations and displacement data are defined positive in the same sense. However, when the vertical displacement is referred as settlement, then it is defined positive as the downwards movement.

Axial force is defined positive in compression. A positive bending moment and shear force are defined when the specimen bends and rotates such that the mass of the specimen displaces East relative to the footing base, or when the acceleration at the mass centroid in x-direction is negative.

3 Experiment preparation

3.1 Specimens construction & assembly

The specimens were constructed at the NEES outdoors facility in San Diego. The casting of concrete was done in two stages with the footings being casted first and the columns and load stubs two days later. Special care was taken for the curing of the concrete. Plastic sheets were used to cover the specimens and they were water-sprayed regularly for two weeks. Once the concrete was set, the specimens were transferred near the shake table area, where the restraining system, the supporting steel beams and the mass blocks were attached to the concrete specimens using the crane. Figure 4 shows pictures from the different construction stages of the specimens. For the restraining system, a steel rod was placed inside the HSS steel pipes which protruded vertically from each corner of the footings and they were then filled with grout. The horizontal steel beams for the restraining system were placed through the steel rods and were bolted in place. Finally the tapered wooden beams were positioned at the end of the horizontal steel beams using smaller steel rods. The vertical position of the wooden beams was therefore adjustable, controlling the foundation rotation after which the restraining system would be mobilized. Once the restraining system was assembled, the four steel supporting beams were placed on the sides of the load stub. For each pair of steel beams, four rods were used to tie them together with post-tensioning, which were passed through the load stub. The mass blocks were shipped from the Pacific Earthquake Engineering Research Center (PEER) facility in Berkeley and they were positioned one by one on top of the steel beams and the load stub. Hydro-stone was used between the steel beams and the mass blocks, as well as between the mass blocks, to allow for a smoother support surface and transfer of forces. Finally, four additional steel rods were post tensioned vertically tying the steel beams with the three mass blocks.

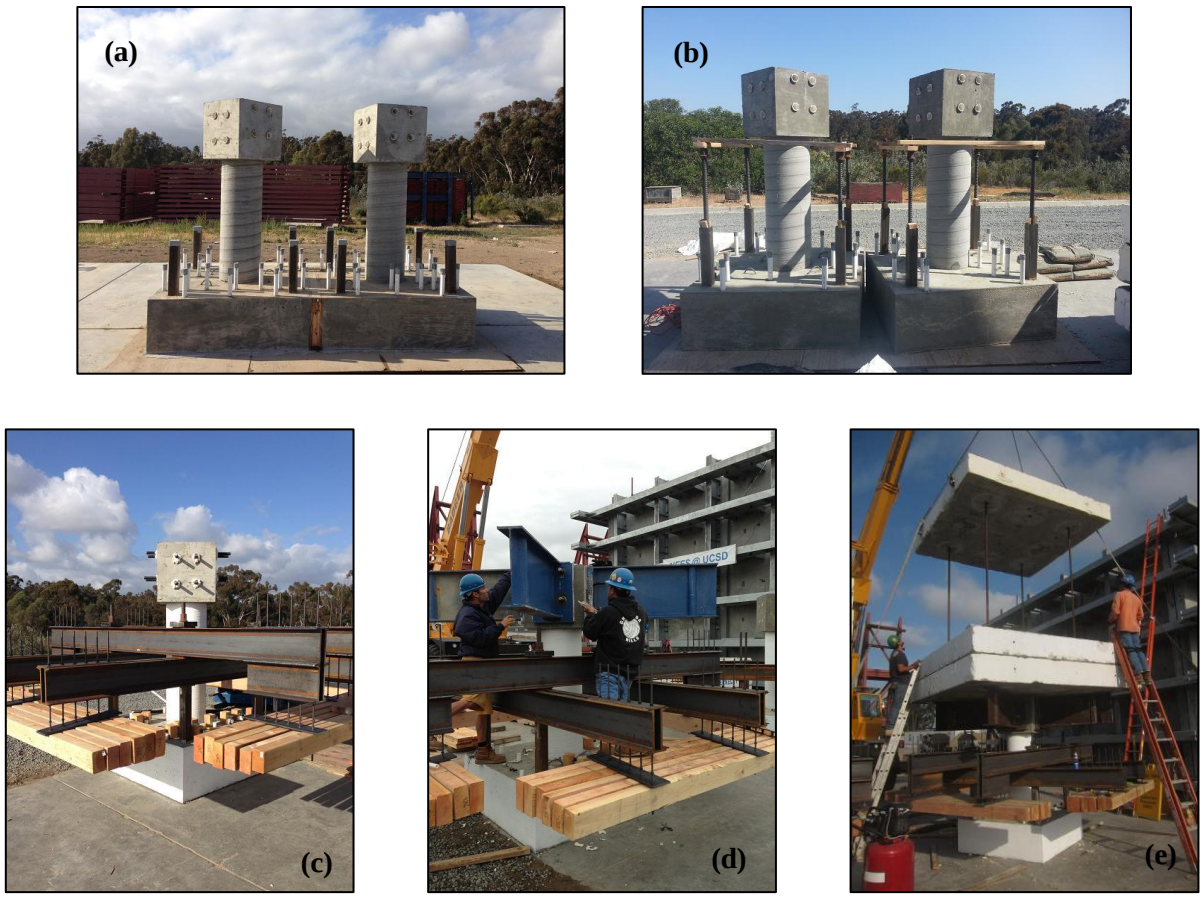

Figure 4. Photos from the assembly of the specimens; (a) concrete footings, columns and load stubs, (b) steel rods and grouting of the HSS pipes, (c) restraining system, (d) steel supporting beams and (e) placement of the mass blocks.

3.2 Soil box

The models described in this test were placed within the "rigid" NEES LSCB with internal dimensions of 10.06 m long × 4.62 m wide × 7.62 m high, see Figure 5 (a). The box was fixed to the shake table at the four corners and the mid-length sides of the box with PT rods that ran through the shake table platen. Iron angles were fixed to the shake table platen through PT rods to ensure good transfer of the accelerations from the shake table to the bottom of the soil profile (Figure 5 (b)).

Figure 5. (a) General view of the NEES Large Soil Confinement Box and (b) inside view of the LSCB showing the fixed iron angles at the shake table platen.

3.3 Liner system

To enable addition of water for tests 2 and 3, a system of liner protection was necessary to be installed. Chronically this project followed the "Earthquake Performance of Large-Scale MSE Retaining Walls" project that also utilized the LSCB and the same sand compacted at a relative density of D_R = 95%. Due to time limiting issues and in order to protect the liner system from the angle irons at the base of the box, the soil from the previous project was extracted up to an elevation of 0.60 m from the base, while a pile of well compacted soil had been kept covering the inner PT rods at the four corners of the box (Figure 6 (a)). The sand was wetted with a water hose and compacted by hand into a curvy surface aiming in better locking between the soil beneath and above the liner that would prevent soil-liner slipping and ensure good transfer of accelerations. Subsequently, a geotextile was attached at the sides of the box up to an elevation of 3.06 m to reduce the risk of the liner ripping from the concrete panels (Figure 6 (b,c)). The liner system consisted of two layers of plastic liner with an in between layer of geotextile. After flying the liner system with a crane within the box, it was unfolded and the top four sides of the liner were clamped at multiple locations to wood beams. Ropes were fixed to the C-clamps and the liner system was carefully lowered down. Figure 6(d) shows the liner system after installation with the ropes fixed at the top of the soil box holding vertical the sides of the liner. As the box was gradually filled with soil, the ropes holding the liner system were untied and the liner system was slightly lowered making sure that no gap is formed between the liner and the sides of the box. The liner was then tied back to the PT rods at the top of the box and the procedure was repeated until the soil reached the height of the liner, allowing for the ropes to be finally disengaged.

Figure 6. (a) Wetting and hand compaction the base soil into a curvy surface, (b) placing the geotextile at the sides of the box up to an elevation of 3.06 m, (c) general view of the installed geotextile and (d) general view of the lowered down liner system.

3.4 Saturation & drainage system

In addition to installing a liner protection system, a saturation and drainage system was also installed allowing a bottom-up saturation of the soil profile for tests 2 and 3 as well as desaturation of the soil before final excavation. The plastic liner was first covered with about 13 cm of soil compacted with a small diesel-operated vibratory compactor before installing the saturation and drainage system. The saturation system consisted of a 30.5 cm diameter vertical PVC pipe, long enough to extend from the final soil surface, open at the top and capped at the bottom, placed at the middle of the North side of the box (Figure 7 (a)). Holes were drilled near the bottom end of the vertical PVC pipe to accommodate 10.2 cm diameter perforated pipes (Figure 7 (c)) which were placed horizontally and spread radially from the vertical PVC pipe. The perforated pipes were split at various locations to equally cover the box plan view and were wrapped around with a geotextile. The saturation and drainage system was covered with another

13 cm layer of soil compacted with the small diesel-operated vibratory compactor before proceeding in compacting the sand as described in the next section.

Figure 7. (a) Vertical PVC pipe used to insert and pump out water during saturation and desaturation process, (b) horizontal perforated pipes extending radially from the vertical pipe used to spread the water across the box plan view and bottom-up saturate the soil and (c) close picture of the perforated pipes.

During saturation, the water hose was used to insert water into the vertical PVC pipe that was then transferred through the horizontal perforated pipes system across the bottom of the soil profile achieving bottom-up saturation, while during desaturation a submergible pump was lowered down at the bottom of the vertical PVC pipe to pump out the water.

To monitor and control the saturation process of the soil profile, four vertical observation PVC pipes of 5.7 cm diameter, sticking out from the final soil surface, were placed at the East side of the soil box near the perimeter. A geotextile was wrapped around the bottom of the observation pipes and secured with a zip-tie to prevent soil entering into the pipes. Figure 8 depicts the installed entry pipe and three of the four observation pipes in-situ. The water elevation in the observation pipes was measured using a laser meter from the top aiming against a small, thin wood disk floating in the water inside each pipe. Table 1 summarizes the measured elevation of water inside the entry pipe and the observation pipes for tests 2 and 3.

Figure 8. General view of the installed entry and observation pipes (photo taken from west side looking east).

Table 1. Measured water elevation inside the entry and observation pipes for tests 2 and 3.

Water elevation measurements, (m)	**Test 2**	**Test 3**
Target	1.47	2.08
Entry pipe, north center side	1.45	2.06
Observation pipe, north center side	1.47	2.07
Observation pipe, east side	1.46	2.06
Observation pipe, south east side	1.46	2.05
Observation pipe, south center side	1.45	2.05
Achieved	1.46	2.06

3.5 Placement of sand & compaction

The sand was transferred inside the soil box using a crane and a concrete hopper in lifts of 20 cm thick. It was spread around the soil box and compacted down to about 15 cm. The compaction was performed using a compact truck loader with a vibratory roller attachment making 6 passes per lift. For the area near the perimeter of the soil box, the small diesel-operated vibratory compactor has been used instead with 8 passes per lift. After the soil reached the elevation of footings base (i.e. 2.69 m), two square temporary wooden frames with dimensions 2.5 m × 2.5 m × 0.75m, slightly larger than the dimensions of the footings, were positioned at the two locations where the specimens were to be placed. The remaining lifts of sand up to the elevation of 3.35 m were placed and compacted outside the wooden frames with the diesel-operated vibratory compactor as shown in Figure 9. Hence, the purpose of adding the wooden frames was to allow placement and compaction of most of the soil above the foundation level prior to the placement of the specimens which would impose significant obstructions due to their restraining systems.

Figure 9. View of the temporary wooden frames used to allow placement and compaction of most of the soil above the foundation elevation prior to the placement of the specimens.

3.6 Placement & removal of specimens

Before placing the specimens inside the soil box for each test, the soil surface under the footings was leveled using a 1.83 m long level and it was also re-compacted by hand for tests 2 and 3. The elevation of the soil surface was measured and a set of strings forming an enlarged by 2.5 cm on each side of the footing footprint was established to aid in the placement of the specimens to the desired locations with sufficient accuracy. The assembled specimens were then transferred inside the soil box with a crane; see Figure 10(a). After the crane had the specimens partially rested on the soil, the position and rotation (i.e., twisting and tilting) of the temporarily placed specimens was measured again to ensure that they are acceptable. Adjustments were made where necessary before finalizing the placement of the specimens. Table 1 summarizes the position of the bottom center of the footing of the specimens for each test with respect to the global coordinate system described in section 2.3.

After each test the specimens were also removed with a crane. Before removing the specimens (except for test 3 for reasons described in the next section) the volume of the backfill soil extending approximately 0.30 m from the sides of the footing and a couple of centimeters below the foundation elevation was shoveled. Shoveling of the prescribed volume of backfill soil was done to prevent the backfill soil collapsing into the area of the footing footprint allowing taking post-test pictures of the soil surface under the footing; hence, capturing mechanisms such as rounding of the soil surface due to rocking and sand sliding from the backfill under the gapping side of the footing. Shoveling of the backfill soil resulting to an enlarged hole was conducted for practical reasons too, such as easier compaction and leveling of the "damaged" soil surface and accommodation of the upcoming placement of the specimens for the next test. Figure 10(b) depicts the enlarged hole (front hole) after test 1 prepared to accommodate the

placement of aligned specimen; the set of strings used to guide the specimen placement are barely visible.

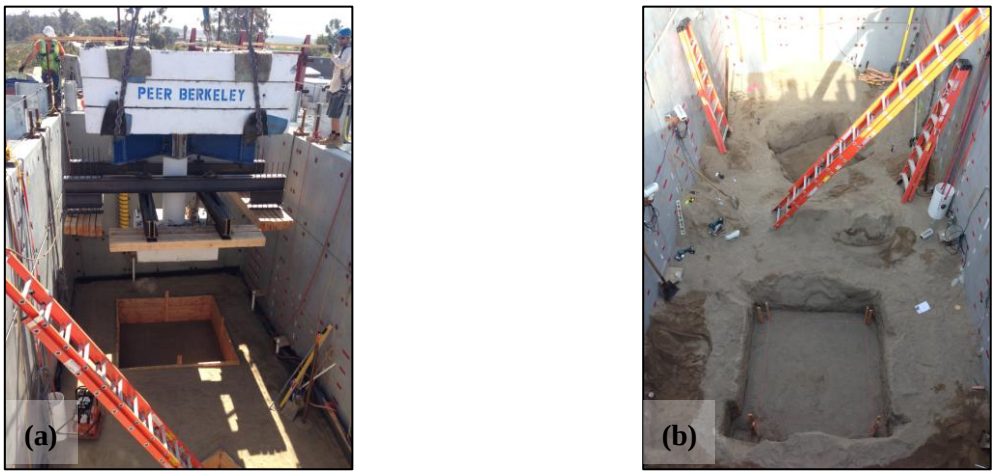

Figure 10. (a) Placement of aligned specimen for test 1 and (b) enlarged hole after test 1 prepared to accommodate placement of aligned specimen; sets of string used for guidance are barely visible.

Table 2. Measured position of the bottom center of the footings of the specimens for each test with respect to the global coordinate system.

Test	Specimen	x (m)	y (m)	z (m)
1	Aligned	2.62	0.00	2.67
	Skew	-2.28	0.00	2.65
2	Aligned	2.59*	0.00*	2.64
	Skew	-2.29*	0.00*	2.63
3	Aligned	2.59	-0.01	2.65
	Skew	-2.26	0.00	2.63

* (x,y) measurements were not taken for test 2; instead, theoretical values are listed.

3.7 Backfilling around the footings

Backfilling around the footings followed the placement of specimens inside the soil box. For test 1 only, the two temporary square wooden frames used during placement and compaction of the soil layers above foundation elevation had to be removed before backfilling the footings. The gaps between the footings and the surrounding soil for tests 1 and 2 were filled with sand which was compacted using a hand compactor due to space limitations; see Figure 11(a).

The procedure for backfilling around the footings described above turned out to be critical and affected significantly the overall behavior of the rocking shallow foundations. For test 1, the sand used to backfill the footings was taken from the soil pit near the shake table. A

light rain during the days preceding test 1 caused the sand to be slightly moist allowing for a better compaction and an apparent cohesive behavior. On the other hand, the sand used to backfill the footings for test 2 was the same backfill soil used in test 1 that was shoveled and spread around the enlarged holes before the removal of the specimens after test 1; the described backfill soil can be identified in Figure 11(a) from its darker color due to the contained moisture. This fact, along with lack of rain, caused the backfill sand for test 2 to be much less moist than for test 1. The reduced moisture also reduced the effectiveness of the hand compaction of the backfill. As a result, during test 2 the backfill sand near the foundations slid under the gapping side of the footings at large rotations, causing significant residual rotations as described in section 8.

This procedure was changed for test 3 aiming to prevent the falling sand mechanism observed in test 2. Weak concrete was casted in place of the sand at the perimeter of the foundations before test 3; see Figure 11(b and c). This concrete extended up to 0.30 m away from the sides of the footings and was as deep as the foundation level. The sides of the footings were covered with plastic sheet before casting to prevent bonding of the concrete to the footing sides, minimizing related foundation moment overstrength. Vertical thin wooden boards wrapped around with plastic were placed between the footing sides and the soil to create joints such that the casted concrete can easily break into smaller pieces, allowing footing rocking kinematics and preventing overstrength. The estimated compressive strength of the weak concrete at the day of test equals 3.5 MPa.

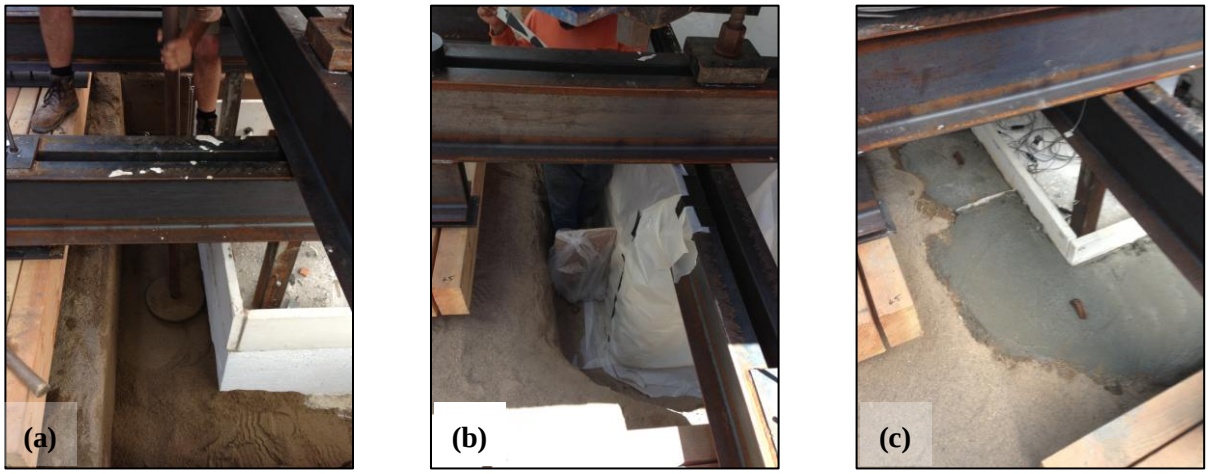

Figure 11. (a) Compaction by hand of the backfill sand for tests 1 and 2, and construction detail around the footings for test 3 (b) before and (c) after weak concrete casting.

4 Material properties

4.1 Structural materials

As mentioned above, the concrete placement for the specimens was done in two separate phases. The concrete had a specified strength of 41.3 MPa (6 ksi) and a maximum aggregate size of 9.5 mm. The footings were casted first, followed by the columns and load stubs two days later. For each concrete batch, slump tests were performed prior to casting and cylinder samples were taken to be tested at a later time. For construction purposes and due to the high congestion of the steel reinforcement throughout the height of the columns, concrete with higher slump was used for the columns and the load stubs. This was achieved by increasing the water content of the concrete mixture in-situ and it resulted into a lower than the specified compressive strength. The slump for the concrete of the footings and the columns were 14 and 22 cm respectively. Three cylinder samples were tested from each batch after approximately 1, 2 and 4 weeks as well as on the day of tests 1 and 2. At the day of test 1, the concrete of the footings had a compressive strength of 42.1 MPa (6.1 ksi) whereas the concrete used in the columns had a compressive strength equal to 30.3 MPa (4.4 ksi).

Reinforcing steel samples were tested in tension. For the longitudinal reinforcement of the column, the experimentally calculated yield stress was equal to 495 MPa (71.8 ksi), the yield strain was 0.27% and the ultimate stress was 660 MPa (95.7 ksi). Using the calculated values for the yield stress of steel and the column concrete compressive strength, the moment curvature of the as built column section was performed and compared against the design moment curvature. An axial load of 260 kN, equal to the gravity load at the base of the column was used for these analyses. The as built yielding moment, calculated for peak steel strain $\varepsilon_s = 0.5\%$, was equal to 365 kN-m. This value was 8% larger than the design value, despite the decreased concrete strength of the as built section due to the higher yield stress of the reinforcing steel.

4.2 Soil properties

The model bridges were built upon moist, poorly-graded (uniformly graded and gap-graded), Carroll Canyon type II ASTM C33 washed concrete sand (supplied by Hanson Aggregates, West Region, San Diego, CA). Selected soil properties for the coarse sand used in the test are documented in Table 3.

Table 3. Selected soil parameters for sand mixture used in the test.

Classification		Poorly-graded, coarse sand; SP
Specific gravity, G_S		2.63 *
Grain size, D_{50} (D_{10})	[μm]	737 (186) *
Coeff. of uniformity, C_u		5.3
Coeff. of curvature, C_c		0.9
Dry unit weight, $\gamma_{d,min}$ ($\gamma_{d,max}$)	[kN/m^3]	14.41 (17.72) †
Void ratio, e_{max} (e_{min})		0.790 (0.456)
Friction angle, φ_{pk} (φ_{cv})	[deg.]	43 (39) ‡
Relative density in-situ, D_r	[%]	≈ 90 ‖

* Manufacturers' supplied datasheet

† From personal communication with Sander

‡ Direct shear tests by Group Delta Consultants, Inc., San Diego, CA

‖ In-situ sand cone tests

The strength parameters summarized in Table 3 were obtained from consolidated, drained direct shear tests conducted by Group Delta Consultants, Inc., San Diego, CA. In total, three direct shear tests were conducted at normal effective stresses of 47.9, 95.8 and 191.5 kPa with the samples prepared at a relative density of D_r = 79.8% (γ_d = 16.9 kN/m^3) with a water content of w = 18.7%.

To estimate the relative density of the built soil profile, a total of 16 sand cone tests were performed at different stages of the construction; see Figure 12. The calculated relative density and water content values are summarized in Table 4. From those sand cone tests that result to reliable measurements, it is considered that an estimate of D_r = 90% for the as-built soil is reasonable. In addition, due to the significant residual rotation of the specimens in test 2 resulted from the sand sliding under the gapping side of the footing during rocking, water content samples were taken from the backfill of the footings about 30 minutes after test 2 was completed. The water content values are also tabulated in Table 4.

Using the soil properties described above, the corresponding factor of safety against vertical loads of the aligned footing, FS_v, was 24. The critical contact area ratio A/A_c was equal to 11 and the base shear coefficient for rocking C_r was 0.26.

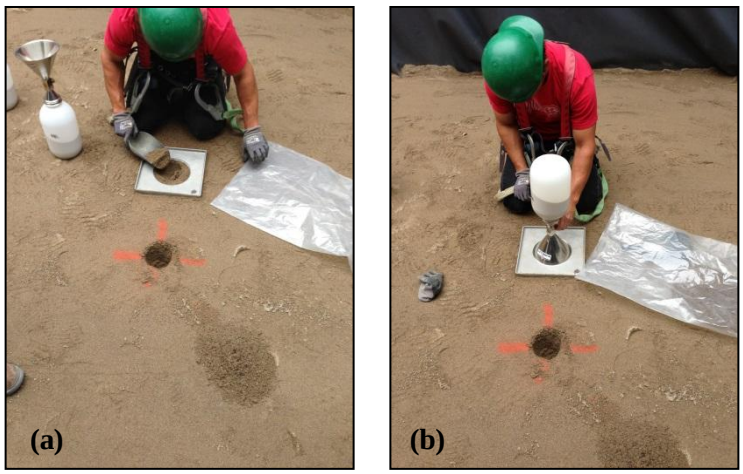

Figure 12. Sand cone test.

Table 4. Summary of sand cone tests and water content samples.

Test type	Description	Location			Relative density, D_r (%)	Water content, w (%)
		x (m)	y (m)	z (m)		
Sand cone	Under skew footing center	-2.29	0.30	0.97	86.9	5.1
Sand cone	Under aligned footing center	2.59	0.30	0.97	72.8	4.4
Sand cone	Under skew footing center	-2.29	0.30	1.83	105.7	5.2
Sand cone	Under aligned footing center	2.59	0.30	1.83	95.3	5.7
Sand cone	Under skew footing center	-2.29	0.30	2.49	91.3	3.8
Sand cone	Under aligned footing center	2.59	0.30	2.49	78.4	4.5
Sand cone	Under skew footing center	-2.29	0.00	2.69	68.1	4.9
Sand cone	Under aligned footing center	2.59	0.00	2.69	83.0	4.9
Sand cone	Skew footing backfill before test 1, SE corner	-0.92	-0.36	3.35	352.8	4.1
Sand cone	Skew footing backfill before test 1, SE side middle	-1.79	-0.86	3.35	88.6	4.4
Sand cone	Aligned footing backfill before test 1, SE corner	3.58	-0.99	3.35	69.5	3.4
Sand cone	Aligned footing backfill before test 1, S side middle	2.59	-0.99	3.35	95.7	3.2
Water content	Skew footing backfill after test 2, NE side middle	-1.43	0.86	3.35	-	2.1
Water content	Skew footing backfill after test 2, NE side middle	-1.43	0.86	3.02	-	2.6
Water content	Aligned footing backfill after test 2, E side middle	3.58	0.00	3.35	-	1.9
Water content	Aligned footing backfill after test 2, E side middle	3.58	0.00	3.02	-	2.2
Sand cone	Center of aligned footing after test 2	2.59	0.00	2.69	74.3	3.8
Sand cone	SE corner of aligned footing after test 2 (fallen sand)	3.12	-0.53	2.69	34.5	2.3
Sand cone	Skew footing center before test 3	-2.29	0.00	2.69	64.5	5.5
Sand cone	Aligned footing center before test 3	2.59	0.00	2.69	86.9	5.8

5 Instrumentation

5.1 Sensors

The test was heavily instrumented using a total of 140 sensors. Table 5 summarizes the type and number of sensors used in the test.

Table 5. Type and number of sensors used.

Sensor type	Location	Description	Test 1	Test 2	Test 3
MEMS accelerometers	Shake table	3 acceleration DoF at top center of shake table platen	3	3	3
	Soil box	Soil box acceleration response*, correction of string potentiometers' mounting points†	4*, 8†	4*, 8†	4*, 8†
	Soil, free-field	Free-field acceleration response	10	10	10
	Soil, under footings	Acceleration in soil beneath the footings	10‡, 11§	10‡, 11§	10‡, 11§
	Footing	6 acceleration DoF of footings	7‡, 8§	7‡, 8§	7‡, 8§
	Mass blocks	6 acceleration DoF of mass blocks	8‡, 8§	8‡, 8§	8‡, 8§
	Restraining system	Correction of soil-footing string potentiometers' mounting points	1‡, 2§	1‡, 2§	1‡, 2§
			80	*80*	*80*
String potentiometers	Footing	6 displacement DoF of footings	6‡, 6§	6‡, 6§	6‡, 6§
	Mass blocks	6 acceleration DoF of footings	6‡, 6§	6‡, 6§	6‡, 6§
	Soil-footing	Soil settlement at foundation elevation in the footings' vicinity	4‡, 4§	4‡, 4§	0‡, 0§
	Soil, free-field	Free-field soil settlement	0	0	1
			32	*32*	*25*
Linear potentiometers	Footing	Mapping of soil-footing contact area	10‡, 10§	10‡, 10§	10‡, 10§
			20	*20*	*20*
Pore pressure transducers	Soil	Excess pore pressure at free-field and under footings	8	8	8
Total no. of sensors			140	140	133

‡ Aligned specimen related sensor.

§ Skew specimen related sensor.

MEMS accelerometers were placed at the shake table platen, the soil box, the soil, the footings, the restraining system and the mass blocks. The soil accelerometers were first mounted within a switch and outlet electrical box that could accommodate up to three sensors before being placed in the soil. The selected method aimed to prevent damage to the sensors due to vibrations induced by the vibratory roller attachment of the compact truck loader. A 15 cm long rod sticking out from the base of the electrical box penetrating into the soil below in combination with well burying the electrical box before spreading and compacting the new soil lift eliminated possible displacement and rotation of the sensors. To attach the accelerometers at the concrete surfaces of the soil box, the footings and the mass blocks, a 2.5 cm-deep hole was drilled into the concrete and a factory-made 2.5 cm × 2.5 cm × 2.5 cm aluminum block was fixed through a threaded rod anchored in the concrete hole. The aluminum block had pairs of threaded holes at its five free sides allowing screwing the accelerometers on them. Figure 13(a) depicts the installation of the soil accelerometers under the aligned footing, while Figure 13(b) shows one of the installed accelerometers at the top of the mass blocks of the skew specimen.

String potentiometers were primarily used to measure the relative to the soil box displacements of the footings and the mass blocks, as well as the relative vertical displacements between the soil at the foundation elevation in the vicinity of the footings and the restraining system. Mounting of the string potentiometers at the concrete panels of the soil box was done similarly to the mounting of accelerometers at the concrete surfaces of the footings and mass blocks. A wooden wedge or slab was tied to an anchor inserted into a 2.5 cm-deep hole drilled in the concrete and the string potentiometer sensor was directly screwed in the wooden wedge or slab. For the other end of the string, an open-eye eyebolt was anchored to the concrete of the masses and footings (all string potentiometers on mass blocks and inclined string potentiometer for aligned footing; see Figure 13(b)) or welded to the legs of the restraining system (all string potentiometers for skew footing and horizontal string potentiometers for aligned footing). Figure 13(c) shows the connected string potentiometers to the mass of the skew specimen in the direction of shaking.

Figure 13. (a) Installation of soil accelerometers under the aligned footing, (b) installed accelerometers at the top of skew mass and (c) installed string potentiometers measuring the relative to the soil box displacement of the skew mass.

String potentiometers were also used to measure the vertical displacement of the soil at the foundation elevation in the vicinity of the footings relative to the footings. To achieve the measurement a special assembly was made consisting of a 10.1 cm × 10.1 cm × 1.3 cm steel plate and a 0.6 cm diameter threaded rod long enough to stick out from the final soil surface, attached at its bottom to a coupling nut welded to the steel plate and with an open-eye eyebolt at its top to accommodate the wire from the string potentiometers (Figure 14(a)). The hand-made assemblies were placed near the sides of the footings at foundation elevation and subsequently were covered with soil during the backfilling around the footings (Figure 14(b)). Figure 14(c) shows the covered assemblies connected to the soil-footing string potentiometers before testing. The string potentiometer sensors were screwed to a wood board placed at the top of the triggering beams of the restraining system extending to one side. Fixity of the string potentiometers mounting wood board was achieved by tying it against a series of wood boards placed at the bottom of the triggering beams using rods passing through the gap between the back of the channel beams.

Figure 14. (a) Prepared hand-made assemblies used to measure the soil vertical displacement at foundation elevation near the footings' vicinity, (b) placing the assemblies near the footing sides and (c) covered assemblies, connected to the soil-footing string potentiometers before testing.

Pore pressure transducers were placed in the soil at the free-field and under the footings to measure excess pore pressure and potential triggering of liquefaction during tests 2 and 3. In place of a porous stone, a stainless steel corrosion-resistant breather vent, able to trap particles down to 100 microns, was attached through an adapter at the end of the pressure sensor to isolate pore pressure measurement from total stress. De-aired silicon oil with kinematic viscosity of 200 cSt was used to saturate the cavity of the sensors and the breather vents while Teflon tape was applied to the pipe threads to prevent leakage of the saturation fluid in the cavity after installation. The breather vents had been saturated by submerging them within the de-aired silicon oil for a full day before sensor installation so that trapped air bubbles could dissolve in the silicon oil. Just before installation, the pressure transducer-adapter was submerged within the silicon oil to saturate the cavity and the breather vent was tied down to the adapter ensuring that all the parts remained submerged during assembly (Figure 15(a)). The assembled pore pressure transducer was deployed vertically with the breather vent facing up in a 12 cm-deep hole and it was then backfilled with soil until only the top of the adapter and breather vent were sticking out of the soil (Figure 15(b)). Honey was poured on top of the sensor and the sensor was then fully backfilled with soil. Honey was used to form a viscous seal that would dissolve after the water was added for tests 2 and 3, preventing de-saturation of the sensors during the 2.5 weeks period they remained in unsaturated soil conditions.

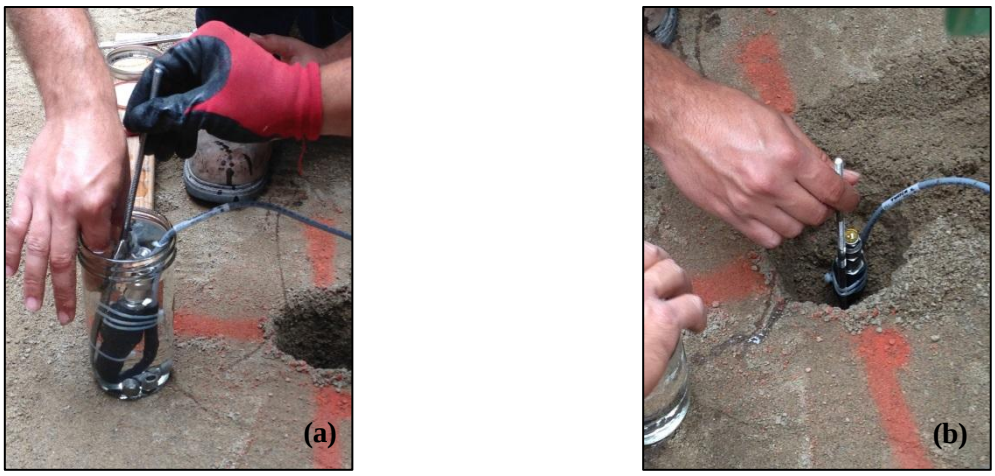

Figure 15. (a) Saturating the sensor cavity and assembling pressure transducer-adapter with breather vent under the silicon oil and (b) deploying the assembled sensor in situ.

Special gap-no gap instruments using linear potentiometers were installed through the footings mapping the soil surface under the footings and the uplifting mechanism. Figure 16 illustrates the construction details of the gap-no gap instruments. The gap-no gap instruments had an inner and an outer mechanism. The outer mechanism consisted of a 4.2 cm outer diameter PVC pipe with a PVC hex bushing attached at its bottom and a 0.3 cm thick super soft neoprene rubber wrapped around the bushing and secured with a hose clamp (Figure 17(a)). The assembled outer mechanism was placed within the footings and it was secured against the cage and the formwork such that no concrete would flow under the neoprene rubber during casting or displace the pipes (Figure 17(b)). Two 2.7 cm outer diameter PVC pipes with a compressed spring in between were inserted inside the outer mechanism. The top inner PVC pipe was secured with 4 screws against the outer PVC pipe such that the spring reacting against the top inner PVC pipe would constantly push the bottom inner PVC pipe downwards. Therefore, when a gap was formed under the instrument due to uplifting of the footing the unsupported by soil neoprene rubber would deflect downwards. PVC disks were glued to the top and bottom of the inner bottom and top PVC pipes, respectively, to provide the needed area against which the force of the spring was applied. The disks had a center hole and a PVC rod was glued to the disk of the bottom inner PVC pipe while passing through the center hole of the disk of the top inner PVC pipe. The PVC rod was used to prevent buckling of the spring but also to allow measuring the vertical movement of the bottom inner PVS pipe, and hence the neoprene rubber membrane deflection, using a linear potentiometer. The linear potentiometer landed on a PVC disk placed on top of the previously described PVC rod and was attached to a wood block glued with epoxy to the concrete surface of the footings. Another PVC disk was glued at the bottom of the bottom inner PVC pipe such that it prevented plunging in the soil beneath but also allowing adequate downwards deflection of the membrane under the spring force. Figure 17(c) depicts the constructed internal mechanisms while Figure 17(d) shows the installed gap-no gap instruments

of the aligned footing. Finally, Figure 17(e) shows the pattern and deflection of the gap-no gap instruments of the skew footing while flying the specimen into the box.

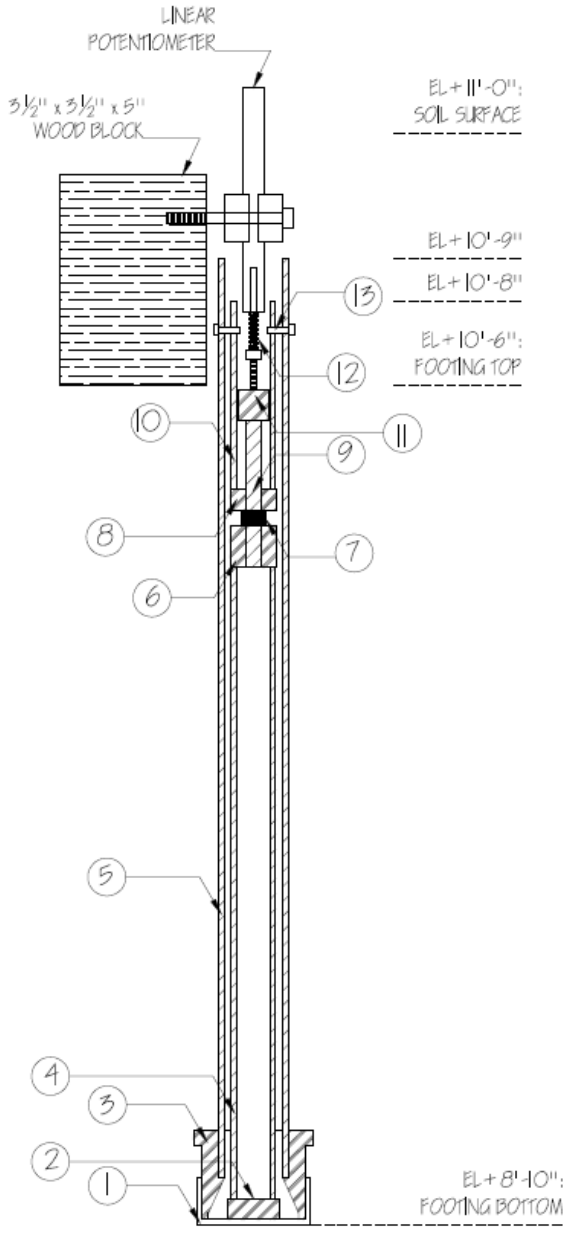

No.	Description	Notes
1	Super-soft Neoprene Rubber, 1/8" thickn., Durometer Hardness 10A	Wrapped around part 3 and tied with hose clamp.
2	PVC rod 1¼" Dia., ½" Thickn.	To be glued with PVC cement & primer to part 4.
3	PVC Hex Bushing 2½" Pipe End Male x 1¼" Socket Female	-
4	¾" ND PVC pipe, Sch. 40, 1'-3" Lg., 1.05" OD, 0.824" ID	To be glued with PVC cement & primer to parts 2 & 6.
5	1¼" N.D. PVC pipe, Sch. 40, 1'-11" Lg., 1.66" OD, 1.38" ID	To be cut 3" higher than the concrete surface of the footing.
6	PVC rod 1⅛" Dia., 1" Thickn.	1) Drill 25/64" center through hole. 2) To be glued with PVC cement & primer to parts 4 & 9.
7	Compression Spring, 2.188" Overall Lg., 0.59" OD, 0.51" ID, 0.38" Compressed Lg., 6.80 lbs Max Load, 3.80 lbs/ in Rate, Closed Ends	To be fully compressed in its initial position.
8	PVC rod 1⅛" Dia., ½" thickn.	1) Drill 7/16" center through hole. 2) To be glued with PVC cement & primer to part 10.
9	PVC rod ⅜" Dia., 3½" Lg.	To be glued with PVC cement & primer to part 6.
10	¾" ND PVC pipe, Sch. 40, 4½" Lg., 1.05" OD, 0.824" ID	To be glued with PVC cement & primer to part 8.
11	PVC rod ¾" Dia., ¾" thickn.	-
12	Compression Spring, 3.0" Overall Lg., 0.240" OD, 0.182" ID, 0.93" Compressed Lg., 5.0 lbs Max Load, 3.60 lbs/ in Rate, Closed Ground Ends	To be fully compressed in its initial position.
13	No. 6 x ½" Pan Head Serrated-Thread Screw for Plywood	Use 4 of them per sensor to provide reaction for the top inner PVC pipe against the outer PVC pipe.

NOTES:

1. 30 x 50mm STROKE LPs + 9 x 100mm STROKE LPs (since 30 50mm stroke LPs are currently available).

Figure 16. Construction details of the gap-no gap instruments.

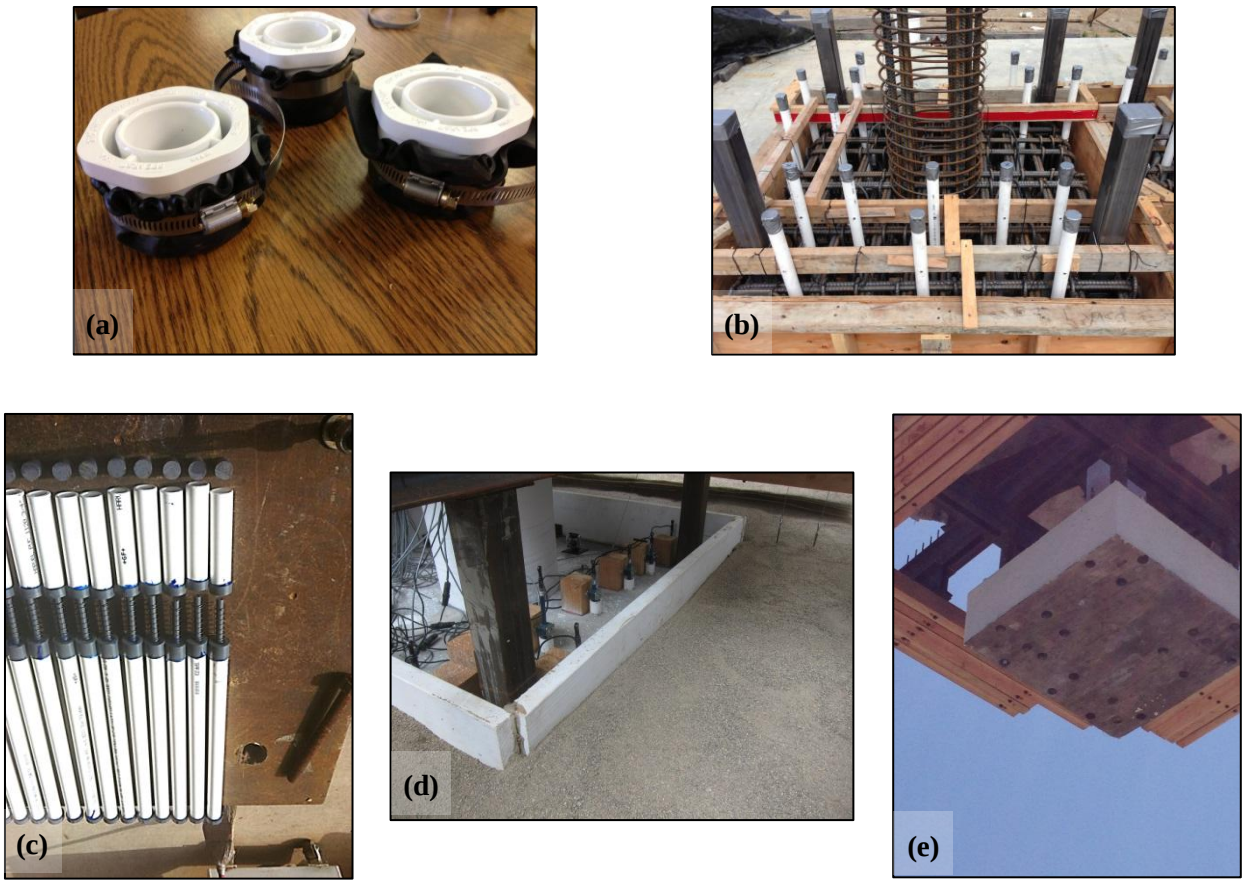

Figure 17. (a) Hex bushing attached at the bottom of outer PVC pipe with neoprene rubber wrapped around, (b) placed and secured against cage and formwork outer mechanisms for aligned footing before casting, (c) constructed internal mechanisms, (d) view of the installed gap-no gap instruments for aligned footing and (e) bottom view of skew footing while flying specimen in the box showing pattern and deflection of gap-no gap instruments.

Having described the instruments used in the test series, it is worth pointing out the used instruments naming convection. Each sensor was assigned with a unique alphanumeric ID up to seven characters to reflect adequate information about the sensor type, position and orientation. Naming a sensor in a unique way was important for recording and post-processing the data. The naming convention is categorized in Table 6. For instance, sensor AMTSWE is a MEMS accelerometer at the south-west corner of the skew specimen mass oriented towards East.

Table 6. Alphanumeric naming convention of sensors.

A: *Accelerometer*					
T: Table platen	**F**: Free-field	**S**: South	**E**: East	**S**: South	**0**: EL+0m
B: Soil box	**Z**: Aligned	**M**: Middle	**M**: Middle	**N**: North	**1**: EL+1.17m
S: Soil	specimen	**N**: North	**W**: West	**E**: East	**2**: EL+1.83m
F: Footing	**T**: Skew	position in	position in	**W**: West	**3**: EL+2.49m
M: Mass	specimen	S-N plane	E-W plane	**U**: Upwards	**4**: EL+2.69m
				orientation	
S/LP: *String/linear potentiometer*					
F: Footing	**Z**: Aligned	**S**: South	**E**: East	**S**: South	**H**: Horizontal
M: Mass	specimen	**M**: Middle	**M**: Middle	**N**: North	(within ±15o)
S: Soil	**T**: Skew	**N**: North	**W**: West	**E**: East	**V**: Vertical
G: Gap-no gap	specimen	position in	position in	**W**: West	(within ±15o)
	F: Free-	S-N plane	E-W plane	**D**: Diagonal	**I**: Inclined
	field	**1,2,..**: No.		**V**: Vertical	(otherwise)
				orientation of	**1,2,..**: No.
				(x,y) projection	
PP: *Pore pressure transducer*					
F: Free-field	**S**: South	**E**: East	**1**: EL+0.91m		
Z: Aligned	**M**: Middle	**M**: Middle	**2**: EL+1.83m		
specimen	**N**: North	**W**: West			
T: Skew	position in	position in			
specimen	S-N plane	E-W plane			
AC: *Correction accelerometer*					
P: Protection	**Z**: Aligned	**S**: South	**1,2,..**: No.		
system	specimen	**N**: North			
B: Soil box	**T**: Skew	**E**: East			
	specimen	**W**: West			
	S: South	**U**: Upwards			
	N: North	**D**: Downwards			
	E: East	**1,2,..**: No.			
	W: West				
	box wall				

Tables Table 7 and Table 8 tabulate the coordinates of the string potentiometers and the rest of the instruments, respectively, the node and channel through which were connected to the Data Acquisition system (DAQ), the directional unit vector where appropriate, and the engineering units output.

The instrument ID is distinguished between "as-built" and "corrected" where necessary so as the corrected ID complies with the naming convention of Table 6. Such cases include using already installed or connected to DAQ instruments from the previous retaining wall shake table test (e.g. shake table platen accelerometers and most of soil box accelerometers), changing location or orientation of the instrument in situ upon reevaluation of conditions (e.g. PPFSE2 and some of the soil accelerometers directly under the footings) and introducing a new sensor just before testing (e.g. SSFSMV) where technical staff has assigned a non-conflicting sensor ID.

To vectorize the (x,y,z) coordinates of the instruments different coordinate systems are used as they are described in section 2.3. Sensors, or parts of sensors that are not mounted on specimens are defined with respect to the global coordinate system. Sensors, or parts of sensors mounted on the specimens are defined with respect to the specimen local coordinate system. In addition, specifically for instruments mounted on the skew footing, the secondary local to the footing coordinate system is used where it is thought to be more practical.

A directional unit vector is introduced such that the measurements of the instrument comply with the sign convention described in section 2.3. For accelerometers, this information is also included in the ("corrected") instrument ID. For instance, an accelerometer with East orientation has a unit vector of 1, while an accelerometer with West orientation will have a unit vector of -1. Same approach applies to accelerometers with different orientations. Correction accelerometers mounted on the restraining system and which do not include orientation information in their respective ID's have all an upward orientation; hence a unit vector of 1. String and linear potentiometers are always positive in extension. All linear potentiometers used in these test series, the soil-footing and free-field soil settlement string potentiometers, are vertical with the extension of the stroke being towards the negative z-axis. The rest of the string potentiometers have variable orientations with the (x,y,z) coordinates of the fixed and moving point of each string potentiometer revealing its respective orientation.

The instrumentation drawings due to their extent are attached separately at Appendix B.

Table 7. Instrumentation list for string potentiometers.

Group	Sub-group	Instrument ID		Fixed point			Moving point			Node	Channel	Engr.
		as-built	corrected	x (m)	y (m)	z (m)	x (m)	y (m)	z (m)			units
Aligned specimen	Mass*	SMZNEWH	-	4.893	0.914	6.344	1.473	0.914	3.651	12	45	in
		SMZNEWI	-	4.878	0.914	7.505	1.473	0.914	3.651	12	47	in
		SMZNESH	-	3.505	2.175	6.344	0.914	1.473	3.651	12	39	in
		SMZNWSI	-	1.676	2.161	7.505	-0.914	1.473	3.651	12	37	in
		SMZNWSH	-	1.676	2.175	6.344	-0.914	1.473	3.651	12	40	in
		SMZSEWI	-	4.878	-0.914	7.505	1.473	-0.914	3.651	12	41	in
	Footing*	SFZSEWI	-	4.893	-0.203	5.567	0.533	-0.203	0.559	12	43	in
		SFZNEWI	-	4.893	0.305	5.567	0.533	0.305	0.559	12	50	in
		SFZNEDH	-	4.678	2.175	3.778	0.622	0.699	0.813	12	38	in
		SFZNESI	-	2.896	2.175	5.567	0.305	0.533	0.559	12	44	in
		SFZNWSI	-	2.286	2.175	5.567	-0.305	0.533	0.559	12	49	in
		SFZNWDH	-	0.503	2.175	3.740	-0.622	0.699	0.813	12	42	in
	Soil-footing†§	SSZSEV1	-	0.762	-0.914	1.440	0.762	-0.914	0.787	12	32	in
		SSZSEV2	-	0.914	-0.422	1.173	0.914	-0.422	0.787	12	30	in
		SSZSEV3	-	1.067	-0.422	1.173	1.067	-0.422	0.787	12	31	in
		SSZSWV1	SSZSEV4	0.762	-1.067	1.440	0.762	-1.067	0.787	12	28	in
Skew Specimen	Mass*	SMTNESI	-	-1.372	2.161	7.505	0.914	1.473	3.651	12	51	in
		SMTNESH	-	-1.372	2.175	6.344	0.914	1.473	3.651	12	48	in
		SMTNWSH	-	-3.200	2.175	6.344	-0.914	1.473	3.651	12	46	in
		SMTNWEI	-	-4.878	0.914	7.505	-1.473	0.914	3.651	12	58	in
		SMTNWEH	-	-4.893	0.914	6.344	-1.473	0.914	3.651	12	57	in
		SMTSWEI	-	-4.878	-0.914	7.505	-1.473	-0.914	3.651	12	56	in
	Footing*	SFTNEDI	-	-1.703	2.175	5.572	0.189	0.916	0.813	12	53	in
		SFTNEDH	-	-1.703	2.173	3.723	0.189	0.916	0.813	12	55	in
		SFTNWDI	-	-4.893	0.685	5.572	-0.887	0.294	0.813	12	59	in
		SFTNWDH	-	-4.888	0.684	3.723	-0.887	0.294	0.813	12	54	in
		SFTSWDI	-	-2.869	-2.175	5.572	-0.189	-0.916	0.813	12	60	in

Table 7. (continued).

Group	Sub-group	Instrument ID		Fixed point			Moving point			Node	Channel	Engr.
		as-built	corrected	x (m)	y (m)	z (m)	x (m)	y (m)	z (m)			units
Skew	Footing*	SFTSWDH	-	-2.869	-2.170	3.723	-0.189	-0.916	0.813	12	52	in
Specimen	Soil-footing‡§	SSTSEV1	-	1.067	-0.422	1.173	1.067	-0.422	0.787	12	36	in
		SSTSEV2	-	0.914	-0.422	1.173	0.914	-0.422	0.787	12	33	in
		SSTSEV3	-	0.727	-0.914	1.440	0.727	-0.914	0.787	12	35	in
		SSTSEV4	-	0.727	-1.067	1.440	0.727	-1.067	0.787	12	34	in
Soil	Free-field*‖	SPSWADD	SSFSMV	0.894	0.000	4.572	0.894	0.000	3.353	12	63	in

* Fixed point (x,y,z) coordinates with respect to global coordinate system, moving point (x,y,z) coordinates with respect to specimen local coordinate system.

† Fixed and moving point (x,y,z) coordinates with respect to specimen local coordinate system.

‡ Fixed and moving point (x,y,z) coordinates with respect to footing local coordinate system.

§ Instrument used in tests 1 and 2.

‖ Instrument used in tests 2 and 3.

Table 8. Instrumentation list for accelerometers, pore pressure transducers and linear potentiometers.

Instrument type	Group	Sub-group	Instrument ID		x (m)	y (m)	z (m)	Node	Channel	Unit vector	Engr. units
			as-built	corrected							
MEMS accelerometer	Shake table platen*		ABC0C1	ATMME0	0.000	0.000	0.000	11	14	1	g
			ABC0C2	ATMMN0	0.000	0.000	0.000	11	8	1	g
			ABC0C3	ATMMU0	0.000	0.000	0.000	11	13	1	g
	Box*		ABC3E1	ABMEE4	5.334	0.000	2.692	11	4	1	g
			ABC4E1	ACBEE1	5.334	0.305	5.715	11	11	1	g
			ABC5E1	ACBEE2	5.334	1.183	6.401	11	3	1	g
			ABC3W1	ABMWE4	-5.334	0.000	2.692	11	6	1	g
			ABC4W1	ACBWE1	-5.334	0.749	5.715	11	15	1	g
			ABS5W1	ACBWE2	-5.334	-0.722	7.315	11	7	1	g
			ABS3C2	ABSMN4	1.219	-2.565	2.692	11	2	1	g
			ABN3C2	ABNMN4	1.219	2.565	2.692	11	9	1	g
			ACBNN4	-	2.896	2.565	5.715	11	1	1	g
			ACBNN1	-	-1.676	2.565	3.747	11	12	1	g
			ABN5C2	ACBNN3	-1.676	2.565	5.715	11	5	1	g
			ABN4C2	ACBNN2	-1.372	2.565	7.214	11	10	1	g
	Soil	Free-field*	ASFMME1	-	0.000	0.000	1.213	11	17	1	g
			ASFMMU1	-	0.000	0.000	1.213	11	18	1	g
			ASFMME2	-	-0.051	-0.152	1.878	11	19	1	g
			ASFMMU2	-	-0.051	-0.152	1.878	11	20	1	g
			ASFMME4	-	0.000	0.000	2.737	11	27	1	g
			ASFMMN4	-	0.000	0.000	2.737	11	25	1	g
			ASFMMU4	-	0.000	0.000	2.737	11	26	1	g
			ASFMWE4	-	-4.267	0.000	2.737	11	32	1	g
			ASFMWN4	-	-4.267	0.000	2.737	11	28	1	g
			ASFMWU4	-	-4.267	0.000	2.737	11	31	1	g

Table 8. (continued).

Instrument type	Group	Sub-group	Instrument ID as-built	Instrument ID corrected	x (m)	y (m)	z (m)	Node	Channel	Unit vector	Engr. units
MEMS accelerometer	Soil	Under aligned specimen*	ASZNEU3	-	3.251	0.660	2.534	11	50	1	g
			ASZNEE3	ASZNEW3	3.251	0.660	2.534	11	51	-1	g
			ASZNEN3	ASZNES3	3.251	0.660	2.534	11	49	-1	g
			ASZMEU3	-	3.251	0.000	2.534	11	54	1	g
			ASZMEE3	ASZMEW3	3.251	0.000	2.534	11	53	-1	g
			ASZMMU3	-	2.591	0.000	2.534	11	52	1	g
			ASZMWU3	-	1.930	0.000	2.534	11	44	1	g
			ASZNWU3	-	1.930	0.660	2.534	11	43	1	g
			ASZNWE3	-	1.930	0.660	2.534	11	35	1	g
			ASZNWN3	-	1.930	0.660	2.534	11	47	1	g
		Under skew specimen*	ASTSEU3	-	-1.384	-0.241	2.534	11	46	1	g
			ASTSEE3	ASTSEW3	-1.384	-0.241	2.534	11	33	-1	g
			ASTSEN3	ASTSES3	-1.384	-0.241	2.534	11	45	-1	g
			ASTMEU3	-	-1.715	0.330	2.534	11	41	1	g
			ASTMEE3	ASTMEW3	-1.715	0.330	2.534	11	34	-1	g
			ASTMEN3	ASTMES3	-1.715	0.330	2.534	11	42	-1	g
			ASTMMU3	-	-2.286	0.000	2.534	11	38	1	g
			ASTMWU3	-	-2.858	-0.330	2.534	11	48	1	g
			ASTNWE3	-	-3.188	0.241	2.534	11	36	1	g
			ASTNWN3	-	-3.188	0.241	2.534	11	37	1	g
			ASTNWU3	-	-3.188	0.241	2.534	11	39	1	g
Pore pressure transducer	Soil	Free-field*	PPFMM1	-	0.000	0.305	1.120	11	22	-	psi
			PPFMM2	-	-0.051	0.152	1.866	11	40	-	psi
			PPFSE2	PPFNE2	2.438	1.549	1.808	11	21	-	psi
		Under aligned specimen*	PPZMM1	-	2.591	0.000	1.136	11	16	-	psi
			PPZMM2	-	2.489	-0.025	1.821	11	29	-	psi
			PPZME2	-	3.213	-0.051	1.820	11	30	-	psi

Table 8. (continued).

Instrument type	Group	Sub-group	Instrument ID as-built	Instrument ID corrected	x (m)	y (m)	z (m)	Node	Channel	Unit vector	Engr. units
Pore pressure transducer	Soil	Under skew specimen*	PPTMM1	-	-2.286	0.000	1.225	11	23	-	psi
			PPTMM2	-	-2.235	-0.076	1.777	11	24	-	psi
MEMS accelerometer	Aligned specimen	Mass†	AMZNEN	-	1.219	1.219	3.600	12	22	1	g
			AMZNEU	-	1.219	1.219	3.600	12	24	1	g
			AMZMEE	-	1.219	0.000	3.600	12	18	1	g
			AMZSEU	-	1.219	-1.219	3.600	12	21	1	g
			AMZSWE	-	-1.219	-1.219	3.600	12	23	1	g
			AMZSWU	-	-1.219	-1.219	3.600	12	19	1	g
			AMZNWN	-	-1.219	1.219	3.600	12	20	1	g
			AMZNWU	-	-1.219	1.219	3.600	12	25	1	g
		Footing†	AFZNEU	-	0.660	0.660	0.508	8	16	1	g
			AFZNEE	-	0.660	0.660	0.508	8	15	1	g
			AFZSEU	-	0.660	-0.660	0.508	8	2	1	g
			AFZSWE	-	-0.660	-0.660	0.508	8	7	1	g
			AFZSWU	-	-0.660	-0.660	0.508	8	9	1	g
			AFZNWU	-	-0.660	0.660	0.508	8	3	1	g
			AFZNMN	-	0.000	0.660	0.508	8	19	1	g
		Protection sys.†	ACPZ1	-	1.067	-0.422	1.359	12	27	1	g
	Skew specimen	Mass†	AMTNEN	-	1.219	1.219	3.600	12	15	1	g
			AMTNEU	-	1.219	1.219	3.600	12	9	1	g
			AMTMEE	-	1.219	0.000	3.600	12	12	1	g
			AMTSEU	-	1.219	-1.219	3.600	12	16	1	g
			AMTSWE	-	-1.219	-1.219	3.600	12	10	1	g
			AMTSWU	-	-1.219	-1.219	3.600	12	11	1	g
			AMTNWN	-	-1.219	1.219	3.600	12	14	1	g
			AMTNWU	-	-1.219	1.219	3.600	12	13	1	g

Table 8. (continued).

Instrument type	Group	Sub-group	Instrument ID		x (m)	y (m)	z (m)	Node	Channel	Unit vector	Engr. units
			as-built	corrected							
MEMS accelerometer	Skew specimen	Footing†	AFTSEU	-	0.902	-0.242	0.508	11	62	1	g
			AFTSEN	-	0.902	-0.242	0.508	11	60	1	g
			AFTSWE	-	-0.242	-0.902	0.508	11	59	1	g
			AFTSWU	-	-0.242	-0.902	0.508	11	63	1	g
			AFTNWU	-	-0.902	0.242	0.508	11	57	1	g
			AFTNWN	-	-0.902	0.242	0.508	11	64	1	g
			AFTNEU	-	0.242	0.902	0.508	12	5	1	g
			AFTNEE	-	0.242	0.902	0.508	11	61	1	g
		Protection system‡	ACPT1	-	1.067	-0.422	1.359	12	29	1	g
			ACPT2	-	0.727	-1.067	1.626	12	26	1	g
Linear potentiometer	Aligned specimen	Footing†	LPGZ1	-	-0.445	-0.699	0.000	8	1	-1	in
			LPGZ2	-	-0.692	-0.456	0.000	8	17	-1	in
			LPGZ3	-	-0.470	-0.446	0.000	8	12	-1	in
			LPGZ4	-	-0.278	-0.451	0.000	8	14	-1	in
			LPGZ5	-	0.011	-0.446	0.000	8	13	-1	in
			LPGZ6	-	0.265	-0.446	0.000	8	10	-1	in
			LPGZ7	-	0.464	-0.443	0.000	8	4	-1	in
			LPGZ8	-	0.697	-0.443	0.000	8	18	-1	in
			LPGZ9	-	-0.700	0.148	0.000	8	5	-1	in
			LPGZ10	-	-0.470	0.138	0.000	8	11	-1	in
	Skew specimen	Footing‡	LPGT1	-	0.437§ -0.017‖	-0.691§ -0.456‖	0.000	12	4	-1	in
			LPGT2	-	0.300	-0.456	0.000	12	8	-1	in
			LPGT3	-	0.433	-0.457	0.000	12	6	-1	in
			LPGT4	-	0.692	-0.446	0.000	12	1	-1	in
			LPGT5	-	0.448	-0.164	0.000	12	2	-1	in

Table 8. (continued).

Instrument type	Group	Sub-group	Instrument ID		x (m)	y (m)	z (m)	Node	Channel	Unit vector	Engr. units
			as-built	corrected							
Linear potentiometer	Skew specimen	Footing‡	LPGT6	-	0.560	-0.119	0.000	12	3	-1	in
			LPGT7	-	-0.276	0.184	0.000	11	55	-1	in
			LPGT8	-	-0.695	0.448	0.000	11	56	-1	in
			LPGT9	-	0.425	0.462	0.000	11	58	-1	in
			LPGT10	-	0.684	0.438	0.000	12	7	-1	in

* Instrument (x,y,z) coordinates with respect to global coordinate system.

† Instrument (x,y,z) coordinates with respect to specimen local coordinate system.

‡ Instrument (x,y,z) coordinates with respect to footing local coordinate system.

§ For test 1.

‖ For tests 2 and 3.

5.2 Video cameras

In addition to the instruments placed at and around the specimens a total of 21 cameras were placed around the periphery of the specimens and the soil box to record video streams of the dynamic behavior of the specimens during shaking events. Three different types of cameras were used; namely, coaxial cameras (8), GoPro2 cameras (11) and Sony video cameras (2). Coaxial cameras recorded live video streams at 768 × 494 pixels and 30 frames per second (fps) that could be played back during testing. They were used to capture the overall response of each specimen as well as the gap evolution between the soil and the bottom of the restraining system, in order to track whether the restraining system had been mobilized during large shaking events. Wireless, battery-supported GoPro2 cameras that record video streams at 1920 × 1080 pixels and 30 fps were used to capture the overall response as well as details of the rocking specimens. Videos recorded by the GoPro2 cameras could only be played back after the end of test when the memory cards were collected. Lastly, battery-supported, man-operated Sony video cameras recorded video streams at 1920 × 1080 pixels and 30 fps and as GoPro2 cameras could only be played back after the test. Both Sony video cameras were located outside the soil box as nobody could be within the soil box during testing. One Sony video camera was used to capture the overall response of the two specimens from a man lift raising high above the top of soil box, while a second one was used for tests 2 and 3 to capture the general soil box movement from the South-West corner. Figure 18 illustrates the position of each camera relative to the specimens and the soil box in plan view, while Table 9 describes the position and target of each camera. Table 10 summarizes the available video streams for dynamic events per test since in some cases the battery of the camera was drained before the end of testing or the wireless camera failed to be activated.

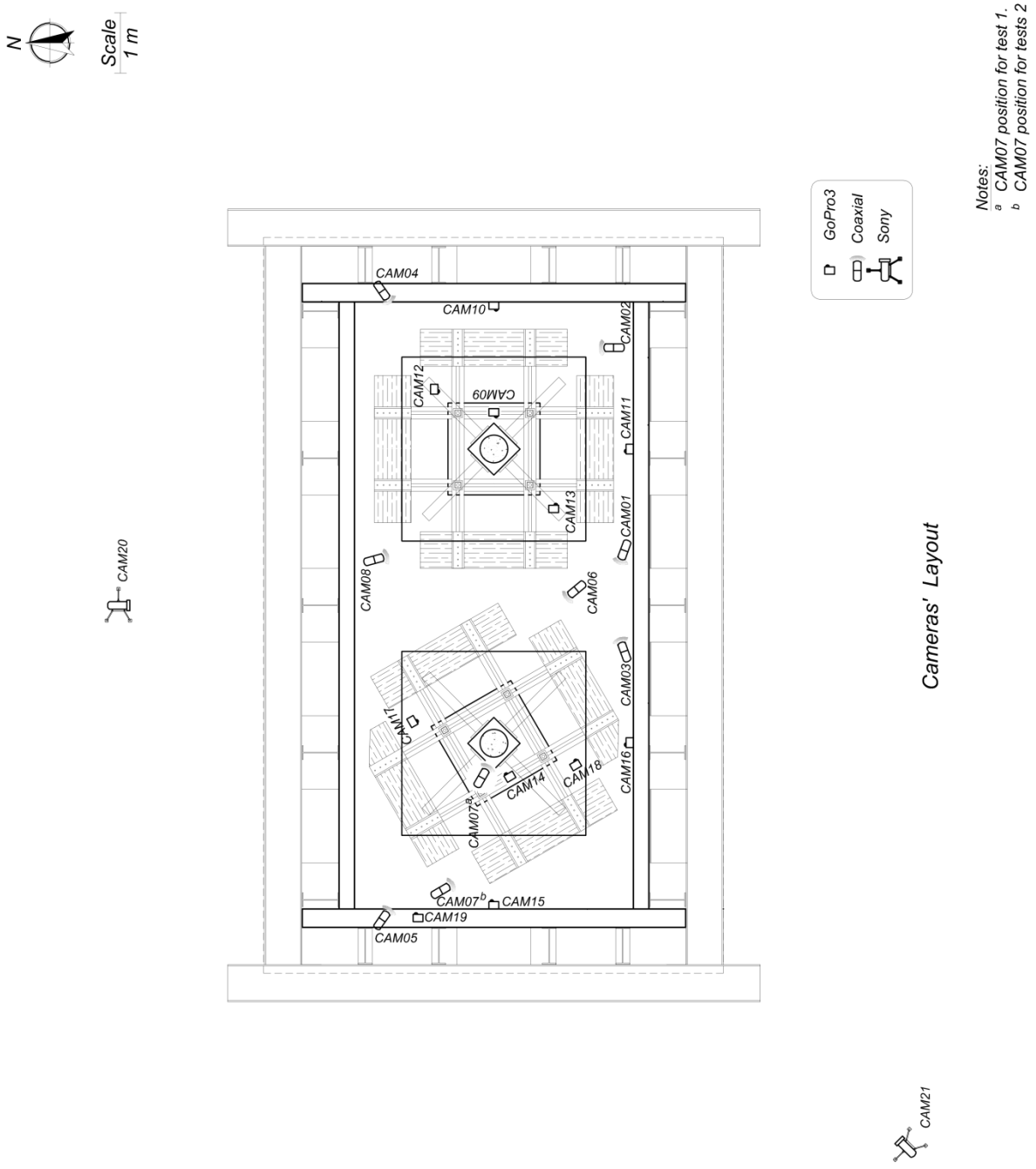

Figure 18. Position of cameras around the specimens.

Table 9. Location and type of cameras used.

Camera type	Camera ID	Mounting location	Target
Coaxial	CAM01	Middle of south wall at load stub height	SE elevation view of skew specimen
	CAM02	South east wood stoppers of aligned specimen, at soil surface	Soil-wood stoppers gap evolution
	CAM03	Middle of south wall at load stub level	SW elevation view of aligned specimen
	CAM04	NE top of soil box	NE top view of aligned specimen
	CAM05	NW top of soil box	NW top view of skew specimen
	CAM06	SE of skew specimen's NE and SE wood stoppers at soil surface	Soil-wood stoppers gap evolution
	CAM07	West of skew specimen's column at footing top *	Column base of skew specimen
	CAM07	NW of skew specimen's NW and SW wood stoppers at soil surface †	Soil-wood stoppers gap evolution
	CAM08	North of aligned specimen's west wood stoppers at soil surface	Soil-wood stoppers gap evolution
GoPro3	CAM09	East of aligned specimen's column at footing top	Column base of aligned specimen
	CAM10	Middle of east wall at load stub level	East elevation view of aligned specimen
	CAM11	South wall across aligned specimen at load stub height	South elevation view of aligned specimen
	CAM12	NE corner of aligned footing	Aligned footing edge from NE to SE corner
	CAM13	SW corner of aligned footing	Aligned footing edge from SW to SE corner
	CAM14	West of skew specimen's column at footing top	Column base of skew specimen
	CAM15	Middle of west wall at load stub height	West elevation view of skew specimen
	CAM16	South wall across skew specimen at load stub height	South elevation view of skew specimen
	CAM17	NE corner of skew footing	Skew footing edge from NE to SE corner
	CAM18	SW corner of skew footing	Skew footing edge from SW to SE corner
	CAM19	NW top of soil box	NW top view of skew specimen
Sony	CAM20	North of soil box at man lift higher than soil box top	Top view of soil box and specimens
	CAM21	SW of soil box at reference elevation	SW elevation view of soil box

* CAM07 location for test 1.

† CAM07 location for tests 2 and 3.

Table 10. Available videos by camera view for each test day (ground motion numbering according to Table 11).

Camera type	Camera ID	Test 1	Test 2	Test 3
Coaxial	CAM01	✓	✓	✓
	CAM02	✓	✓	✓
	CAM03	✓	✓	✓
	CAM04	✓	✓	✓
	CAM05	✓	✓	✓
	CAM06	✓	✓	✓
	CAM07	✓	✓	✓
	CAM08	✓	✓	✓
GoPro3	CAM09	×	1-4	6
	CAM10	1-4, 6	✓	×
	CAM11	1, 4	×	×
	CAM12	2-4, 6	✓	6, 7
	CAM13	2-4	1-4, 6	1-6
	CAM14	2-4, 6	×	2-4
	CAM15	1-4, 6	✓	×
	CAM16	1-4	✓	1-6
	CAM17	2-4, 6	✓	1-8
	CAM18	2-4, 6	✓	1-6
	CAM19	2-4, 6	×	2-9
Sony	CAM20	1	✓	1-7
	CAM21	×	✓	✓

✓ All videos are available.

× None video is available.

6 Ground motions and test chronology

The test protocol involved real ground motion recordings to achieve increasing targeted drift ratios. Numerical models similar to the ones presented in part I where used for the selection of the ground motion amplitude scale factors. Since the specimens were assumed to be built at a 1/3 scale, the time of the ground motions was scaled by $\sqrt{1/3}$ = 0.577. Table 6 lists the test protocol used for tests 1, 2 and 3. As shown, the majority of the motions used were records from historic earthquakes in California. Note that the Pacoima dam record was filtered with a 5 Hz low pass filter to remove high frequency spikes which could damage the soil box. White noise was also applied before every motion, as well as in the end of every test, for system identification purposes. Motions 7, 8 and 9 were used only in test 3. Xxx plots the acceleration and displacement spectra of the recorded free field soil acceleration at the elevation of the base of the footings. In this plot, the recordings are from test 3 and a damping ratio of 3% was used.

Table 11. Test protocol for test days 1, 2 and 3.

No.	Station	Earthquake location, year	Amplitude scale factor	Target drift ratio, (%)
1	Gilroy #1	Loma Prieta, CA, 1989	1.0	< 0.5
2	Corralitos	Loma Prieta, CA, 1989	0.8	1.0
3	El Centro #6	Imperial Valley, CA, 1979	1.1	2.0
4	Pacoima dam*	Northridge, CA, 1994	0.8	4.0
5	Takatori	Kobe, Japan, 1995	0.5	6.0
6	Takatori	Kobe, Japan, 1995	1.0	> 8.0
7†	Parachute test site	Superstition Hills(B), CA, 1987	1.0	> 8.0
8†	Parachute test site	Superstition Hills(B), CA, 1987	-1.0	> 8.0
9†	Parachute test site	Superstition Hills(B), CA, 1987	1.1	> 8.0

* Filtered at 5Hz.

† Only for test 3.

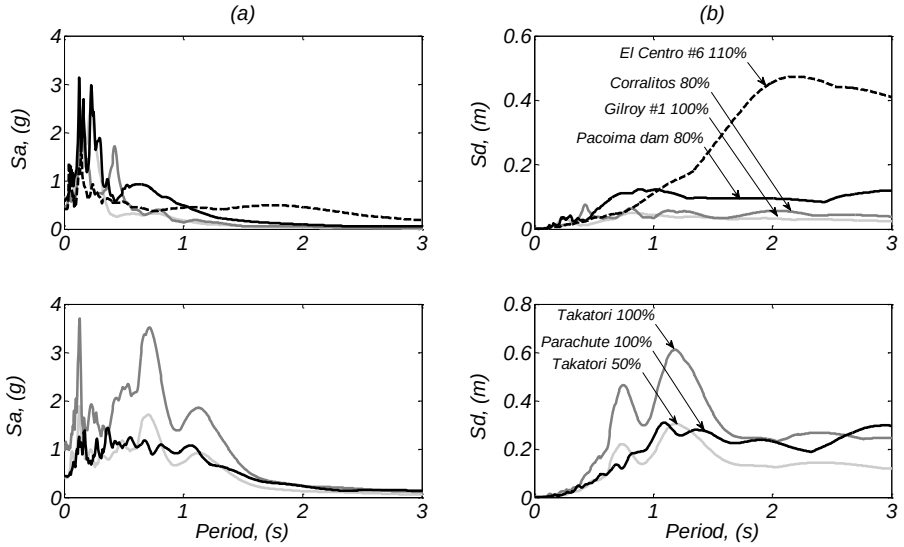

Figure 19. (a) Linear acceleration and (b) displacement spectra for the recorded free field soil acceleration at the elevation of the base of the footings (ζ = 3%).

7 Observed and measured test response

Table 12 presents the peak column drift ratios, defined as the displacement at the centroid of the mass block in any direction divided by the height to the base of the footing. The residual values of the column drift ratio are also shown in parentheses. The residual rotations were negligible (<0.1%) and small (< 0.5%) for peak drift ratios equal to 2.2% and 3.9% respectively. For motion 5 (Takatori 50%), the peak drift ratios of the aligned specimen were 6.8% and 6.9%, for test day 1 and 2 respectively. The corresponding residual rotations were 0.9% and 1.4%, indicating the effect of the sand falling under the gapping side of the footings. This effect became more profound during motion 6 (Takatori 100%) where for peak rotations of 11.6% and 13.7%, for test day 1 and 2 respectively, the residual rotations were 3.4% and 7.8%. The construction detail around the footings in test day 3 resulted into slightly smaller peak rotations (10.1%) due to larger moment capacity of the foundation, but with significantly smaller residual ones (2.1%). This can be also seen in Figure 20 which plots the drift ratio time history for motions 4, 5, and 6. Test day 3 involved three additional strong motions resulting to peak drift ratio during the last shake equal to 13.8% for the aligned specimen, with a corresponding residual rotation of 3.5%. The skew specimen resulted to smaller peak drift ratios and residual rotations in the East- West direction. Larger drifts were observed in the out-of-shaking North-South direction compared to the aligned specimen (not shown here).

Using the data from the white noise runs before each shake, the fundamental period of each specimen was estimated as the period for which the amplification ratio of the acceleration response spectrum (ARS) of the horizontal acceleration at the centroid of the mass to the ARS of the soil free field acceleration was maximized. The resulting periods are shown in Figure 21. It is noted that for test days 1 and 3 the fundamental period tends to increase (up to motion 6) after each shake due to the rounding of the soil surface under the footing during the rocking mechanism [3] that eventually reduces the effective contact area at the end of shaking. For test day 3, the period elongation after motion 6 is larger than that observed for test 1 because the concrete blocks casted around the footings are pushed away from the sides of the footing and do not contribute to the stiffness of the system during the white noise. On the other hand, the period remains almost constant for test day 2. This is because sand fell under the footings mainly during test day 2, since it was looser and drier as explained above, and helped retain the soil-footing contact area near the edges that mainly contribute to the rocking stiffness of the footing. The resulting soil surfaces under the aligned specimen after test days 1 and 2 are shown in Figure 22. This indicates that the falling sand during test day 2 resulted in a gap between the footing and the soil near the center of the footing.

Figure 23 shows the recorded foundation moment-rotation relation for motions 4, 5, and 6. The equivalent foundation rotation-settlement diagrams are shown in Figure 24. Even for very

large rotations (13%), the cumulative residual settlement of the footing was about 0.02 m which corresponds to only 1.3% of the foundation width. The sand falling under the footing reduces the settlements during test day 2 but increases the residual rotations. The re-centering behavior is enhanced by preventing this during test day 3 resulting to larger settlements.

No signs of triggering of liquefaction were either observed or recorded using the pore pressure transducers in the soil during test days 2 and 3 (with underground water).

Table 12. Peak and residual (in parentheses) column drift ratios for the aligned and skew specimens.

	Aligned specimen			**Skew specimen**		
Motion No.	**Test day 1**	**Test day 2**	**Test day 3**	**Test day 1**	**Test day 2**	**Test day 3**
1	0.7 (0.0)	0.9 (0.0)	0.8 (0.0)	0.7 (0.0)	0.7 (0.1)	0.9 (0.0)
2	1.0 (0.1)	1.5 (0.1)	1.1 (0.0)	0.9 (0.0)	1.0 (0.1)	1.0 (0.1)
3	1.5 (0.1)	2.2 (0.1)	1.4 (0.0)	1.3 (0.1)	1.4 (0.1)	1.5 (0.1)
4	3.7 (0.4)	3.9 (0.5)	3.3 (0.2)	3.5 (0.2)	3.4 (0.3)	3.3 (0.3)
5	6.9 (0.9)	6.9 (1.4)	5.9 (0.5)	5.2 (0.8)	4.5 (1.8)	5.7 (0.9)
6	11.6 (3.4)	13.7 (7.8)	10.1 (2.1)	11.7 (2.0)	9.9 (2.2)	10.9 (0.7)
7	-	-	12.9 (2.5)	-	-	9.7 (0.8)
8	-	-	8.8 (2.7)	-	-	8.3 (1.1)
9	-	-	13.8 (3.5)	-	-	10.1 (1.1)

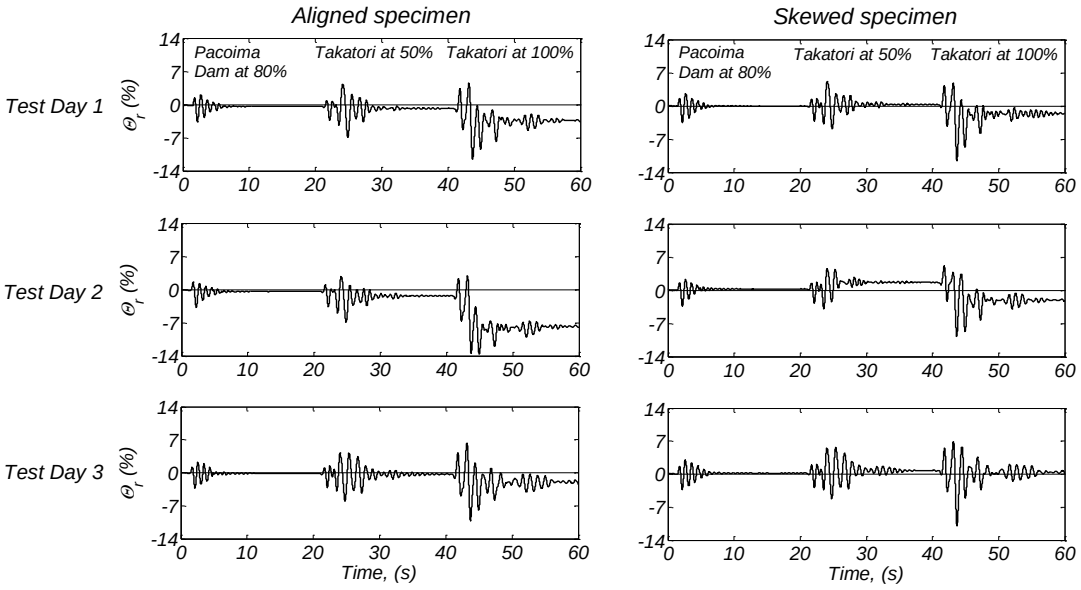

Figure 20. Recorded column drift ratio time histories (WE direction) for motions 4, 5 and 6.

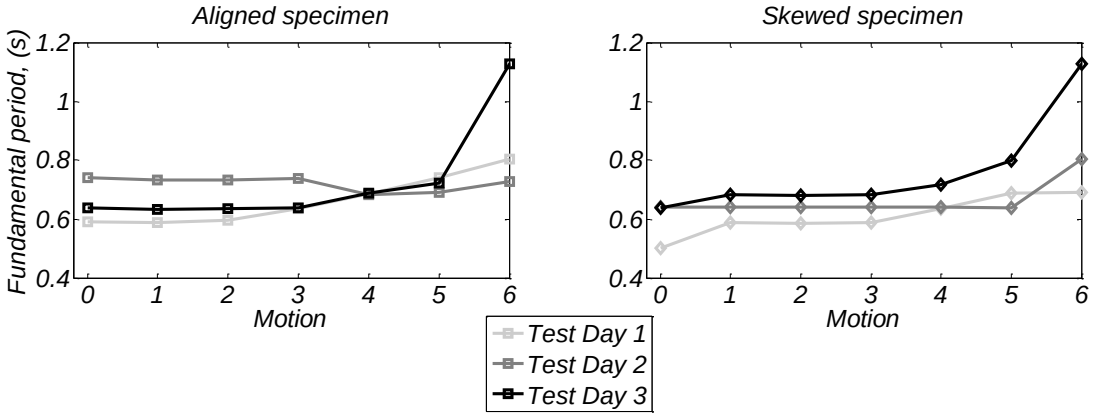

Figure 21. Fundamental periods of the specimens measured using white noise excitations after each motion (motion 0 corresponds to initial period).

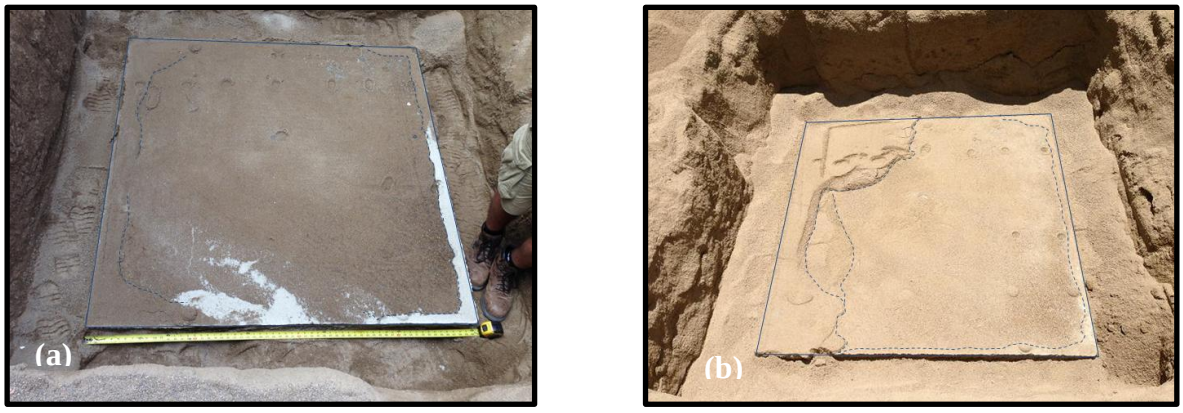

Figure 22. Falling sand area under the aligned footing after (a) test day 1 and (b) test day 2.

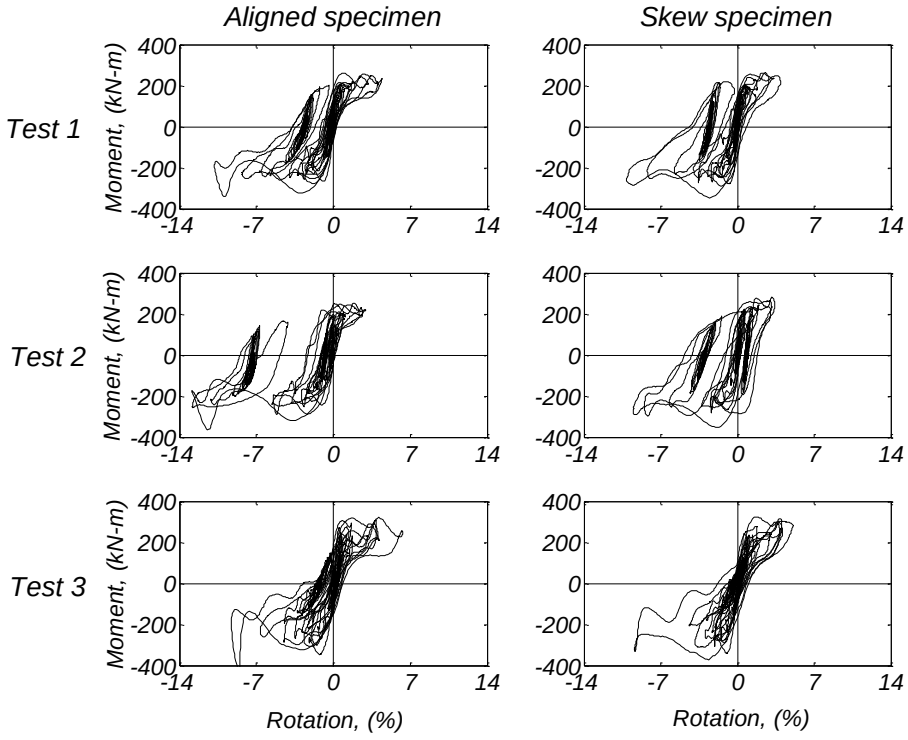

Figure 23. Recorded foundation moment-rotation diagram for motions 4, 5, and 6.

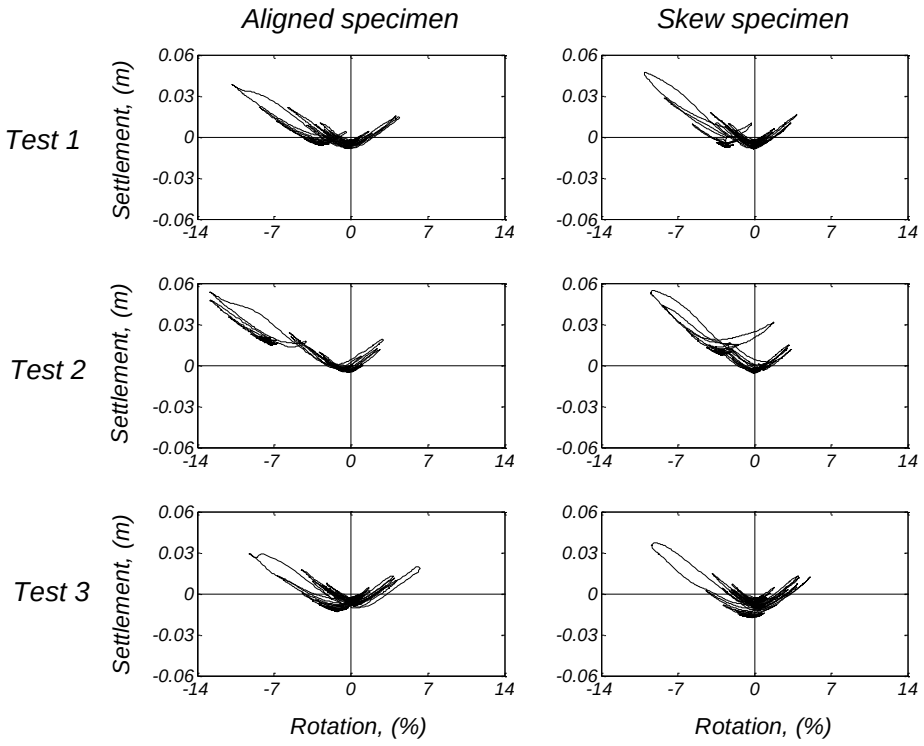

Figure 24. Recorded foundation rotation-settlement diagrams for motions 4, 5, and 6.

8 Conclusions

This experimental study involved two one-third scale specimens of bridge piers placed inside a soil confining box on top of 2.7 meters of well compacted clean sand (D_r > 90%), in an aligned and skew configuration with respect to the direction of shaking. Dry conditions, as well as with the underground water 1.2 m and 0.6 m below the footings were tested where no triggering of liquefaction was observed. These tests lead to the following observations;

Shallow rocking foundations were observed to reliably accommodate earthquake induced deformations corresponding to drift ratios of 3.3% and 5.9% with minimal residual drift ratios (0.2% and 0.5%). These peak drift ratios are similar to expected drift demands for design and maximum considered earthquakes respectively [2].

Loose and dry cohesionless backfill can fall under the footing during the uplifting of the rocking foundation potentially resulting in significant residual drifts. Residual drifts increased significantly for peak drift ratios larger than 6.9%. The casting of weak concrete around the footings for test day 3 was successful in limiting material falling under the gapping side of the footing, leading to minimal residual drifts for peak drift ratios up to 5.9%. The resulting foundation moment overstrength due to the concrete around the footing was 15%.

The sand falling under the footing during the uplifting mechanism reduces the settlements but also reduces the re-centering tendency. On the other hand sand falling under the footing keeps the edges of the footing in contact with the soil, helping to maintain the rocking stiffness of embedded footings. Without sand falling under the edges of the footing, degradation of stiffness was apparent. The degradation of stiffness may be explained by the formation of a rounded soil-footing interface during rocking.

Appendix A: Construction drawings

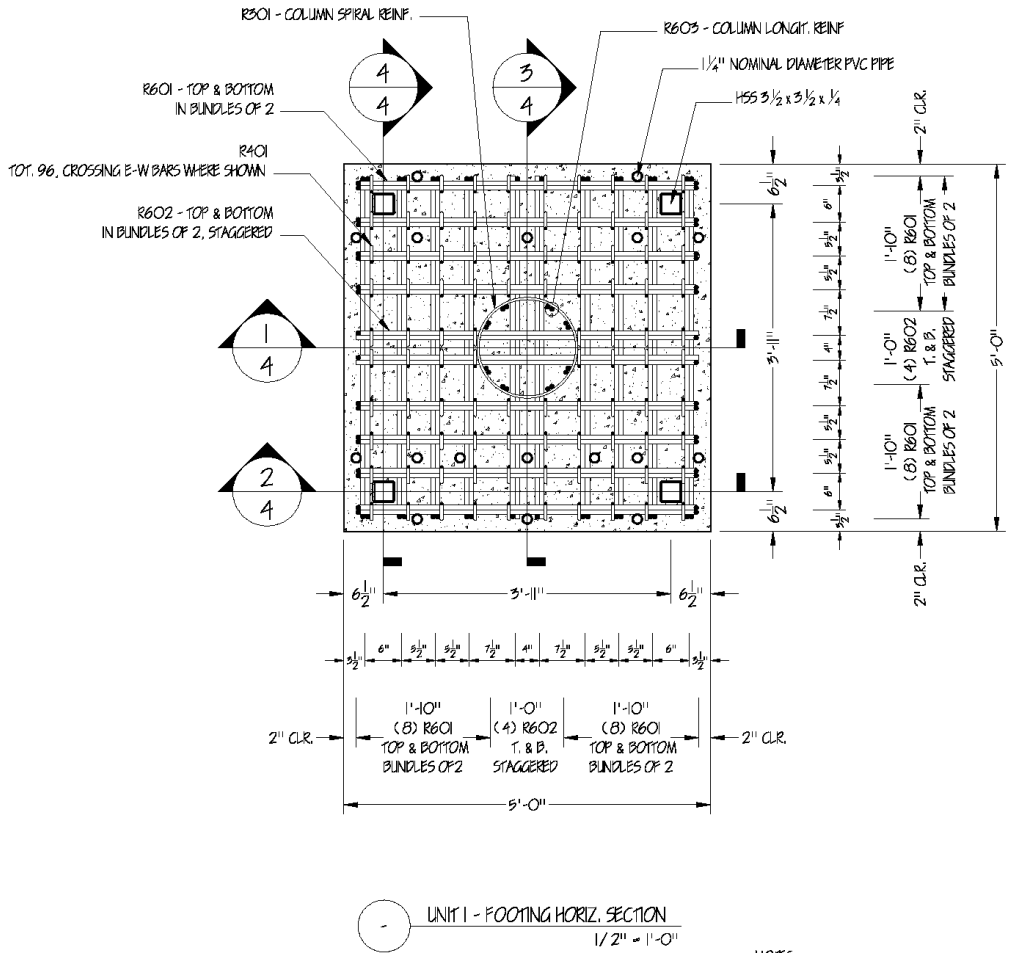

Figure A1. Reinforcement of aligned footing.

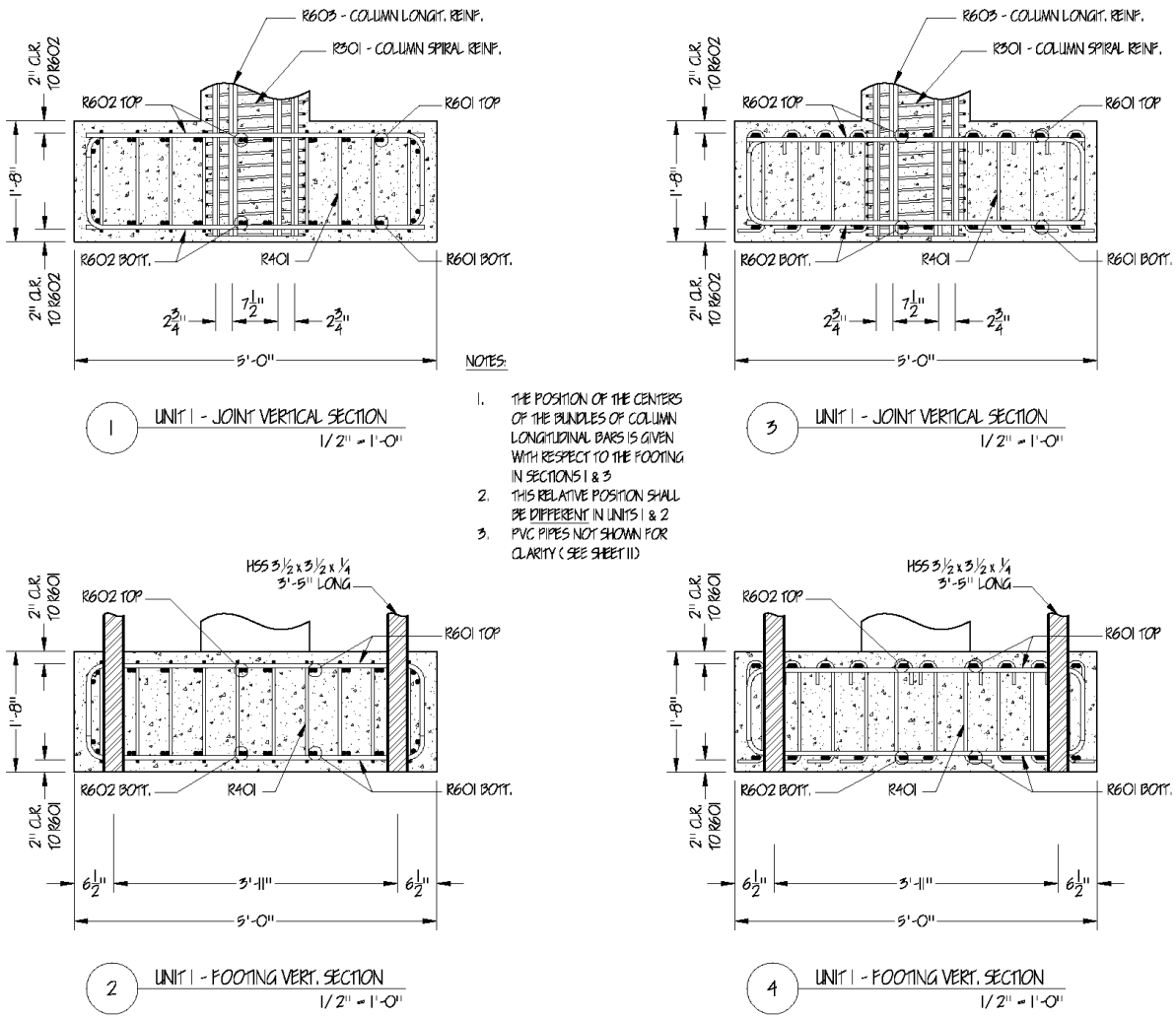

Figure A2. Footing – column joint details for aligned footing.

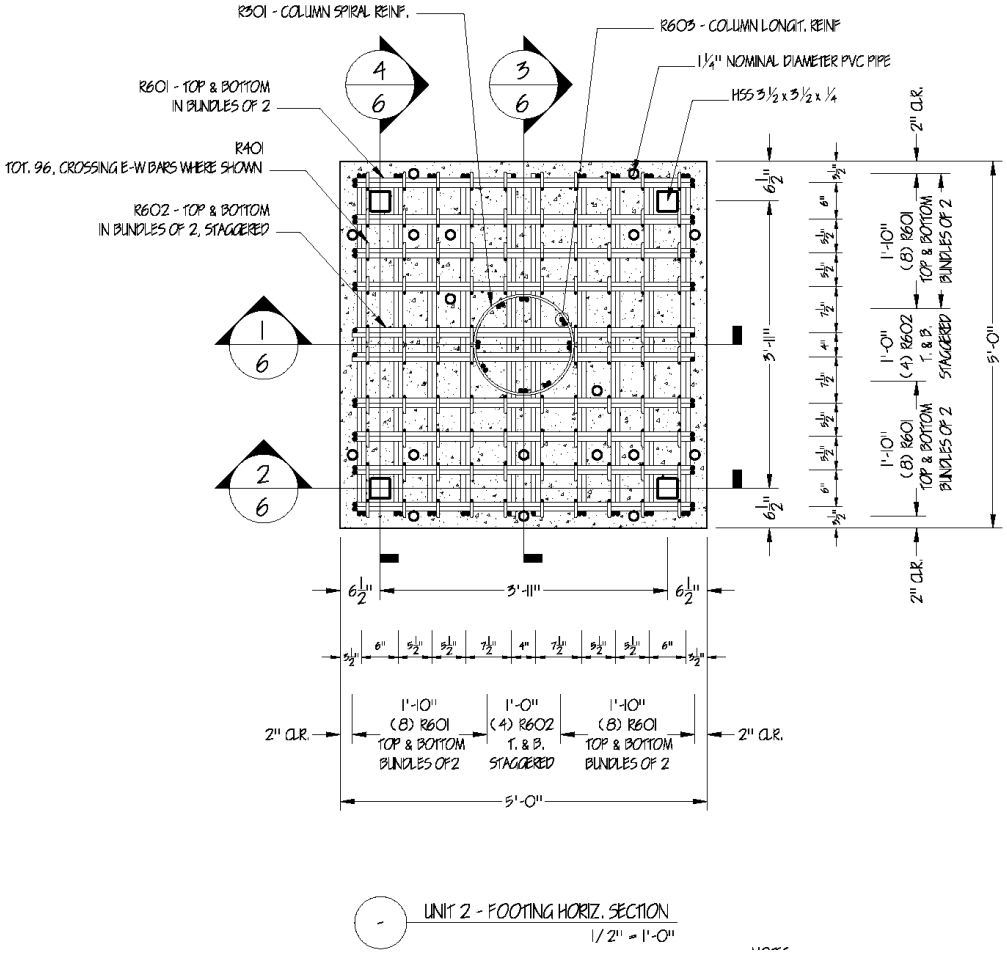

Figure A3. Reinforcement of skew footing.

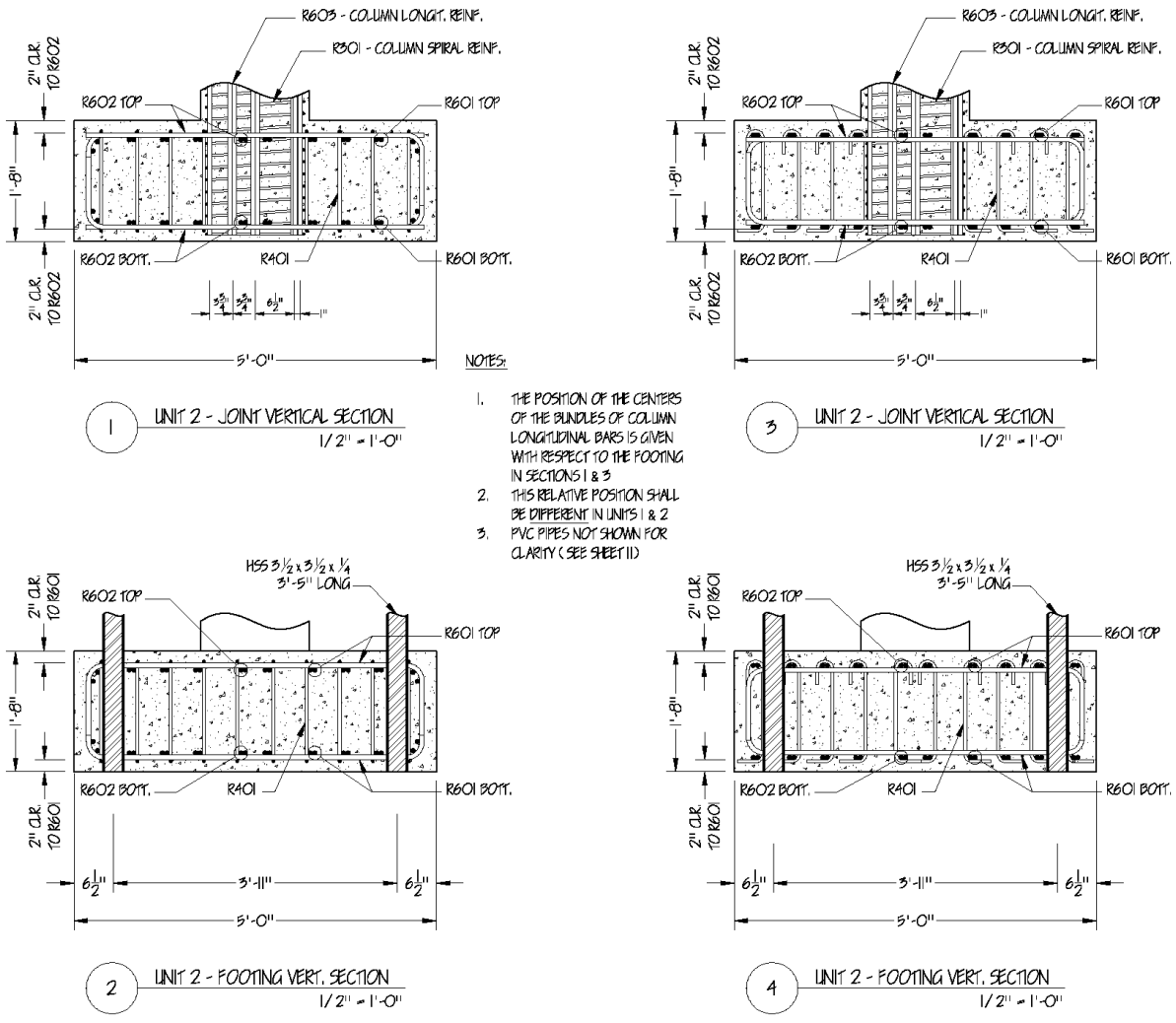

Figure A4. Footing – column joint details for skew footing.

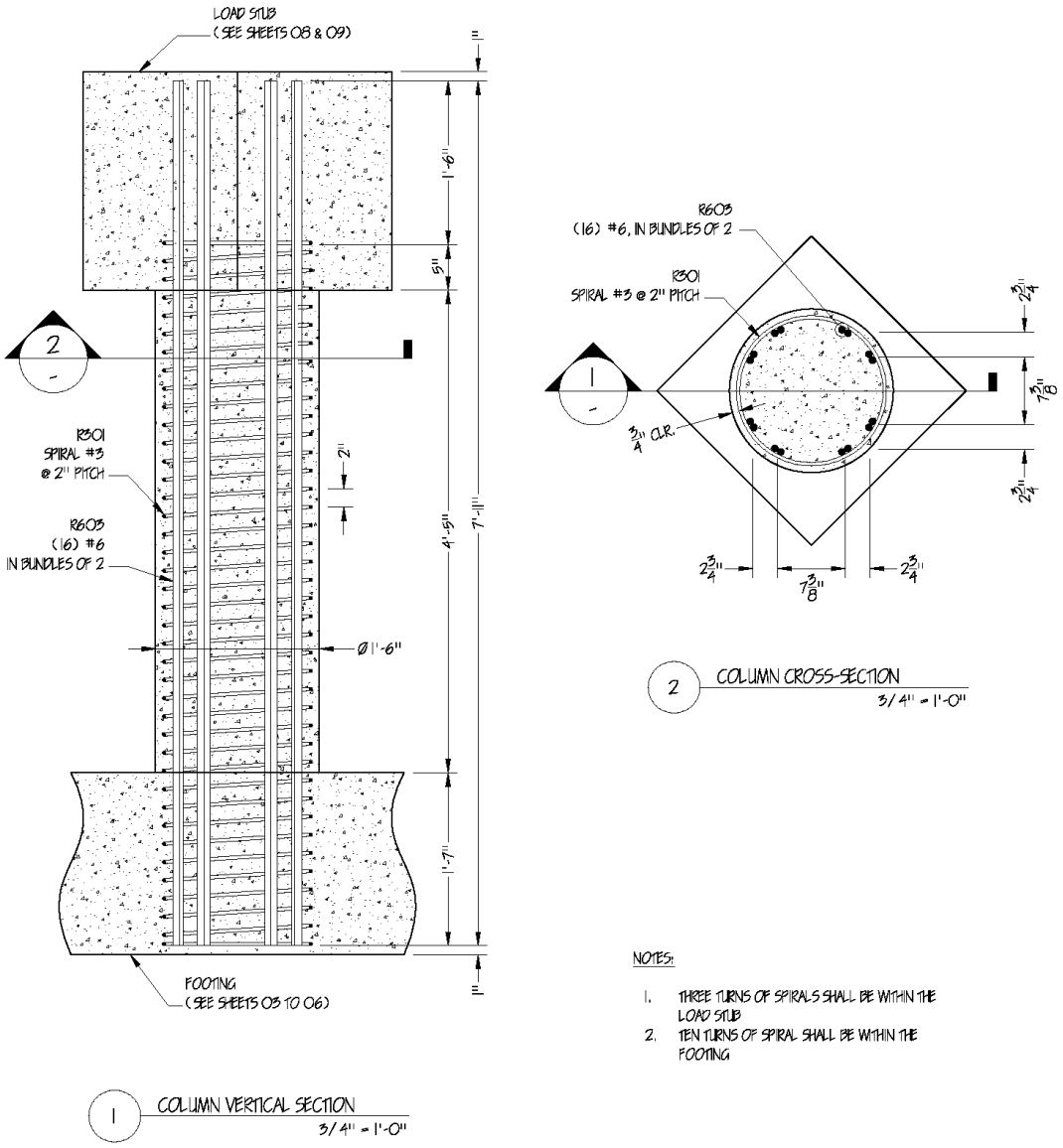

Figure A5. Column reinforcement for both specimens.

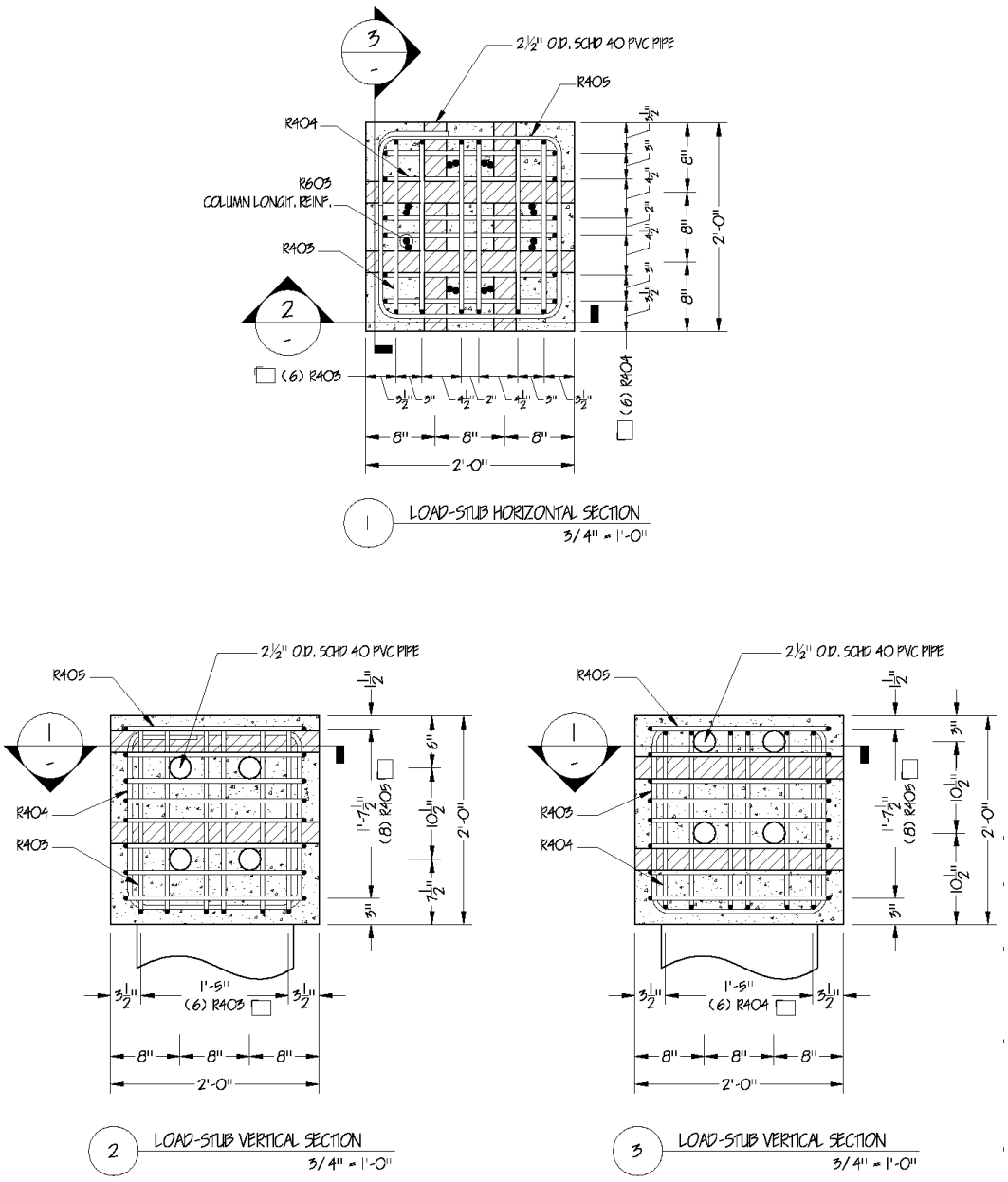

Figure A6. Load stub reinforcement for both specimens.

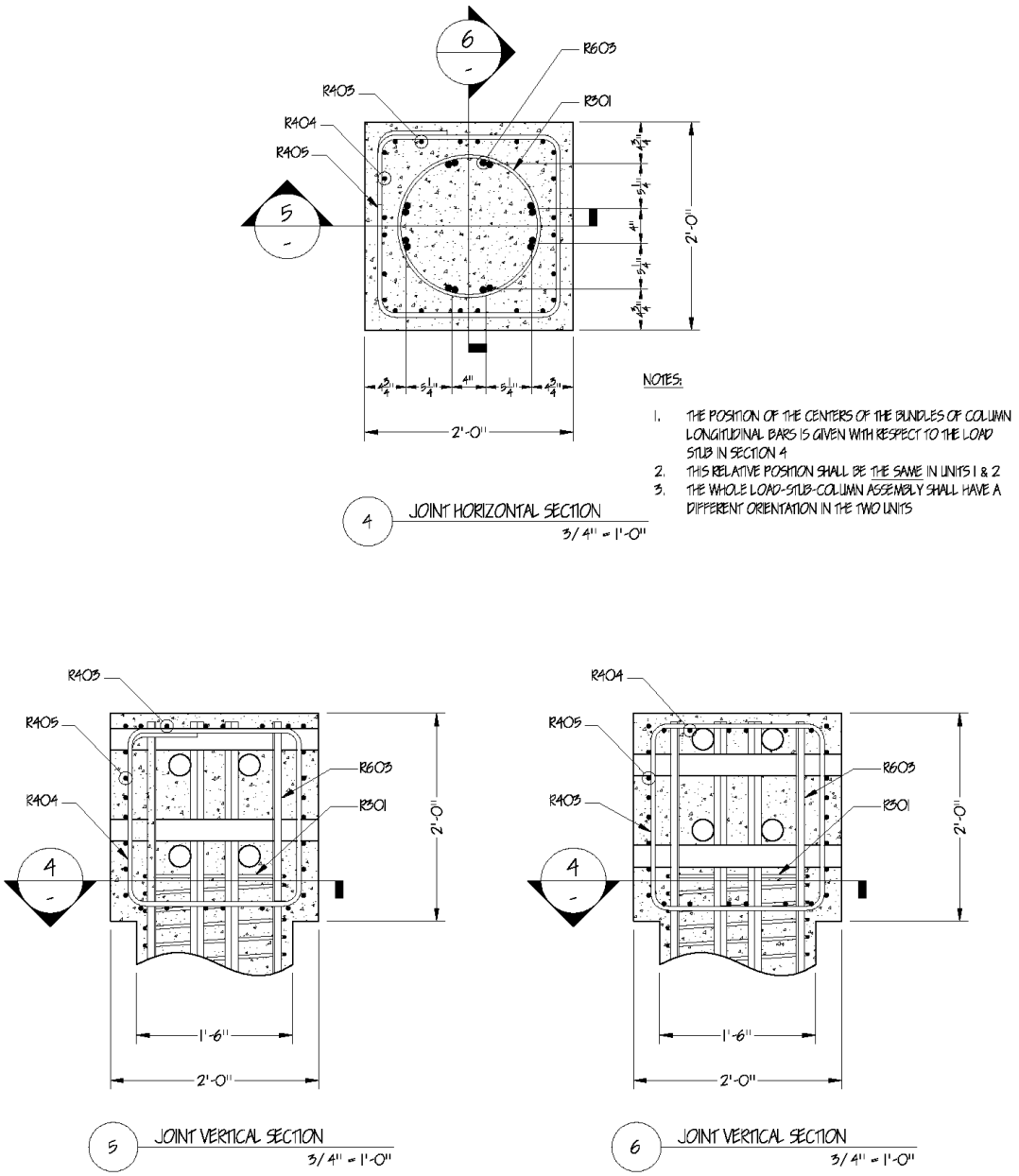

Figure A7. Load stub – column connection details for both specimens.

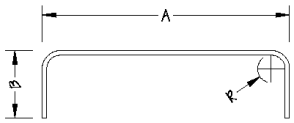

DESIGN.	ASTM	GRADE	BAR SIZE	A	B	R	QTY
R601	A706	60	#6	4'-8"	1'	2¼"	128

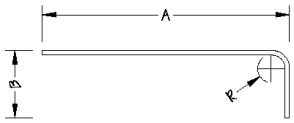

DESIGN.	ASTM	GRADE	BAR SIZE	A	B	R	QTY
R602	A706	60	#6	4'-8"	1'	2¼"	32

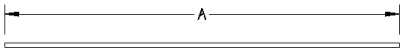

DESIGN.	ASTM	GRADE	BAR SIZE	A	QTY
R603	A706	60	#6	7'-11"	32

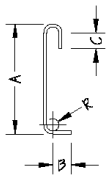

DESIGN.	ASTM	GRADE	BAR SIZE	A	B	C	R	QTY
R401	A706	60	#4	1'-5"	3"	2½"	1"	192

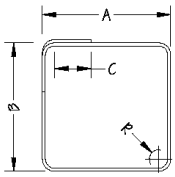

DESIGN.	ASTM	GRADE	BAR SIZE	A	B	C	R	QTY
R403	A706	60	#4	1'-8"	1'-9½"	6"	1½"	12
R404	A706	60	#4	1'-8"	1'-8½"	6"	1½"	12
R405	A706	60	#4	1'-9"	1'-9"	6"	1½"	16

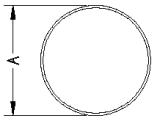

*** SPRIAL REINFORCEMENT ***

DESIGN.	ASTM	GRADE	BAR SIZE	A	TURNS	PITCH	QTY
R301	A706	60	#3	1'-4½"	40	2"	2

Figure A8. Reinforcement details.

Appendix B: Instrumentation drawings

Figure B1. Elevation view of accelerometers mounted on (a) East and (b) West soil box wall.

Figure B2. Elevation view of accelerometers mounted on South soil box wall.

Figure B3. Elevation view of accelerometers mounted on North soil box wall.

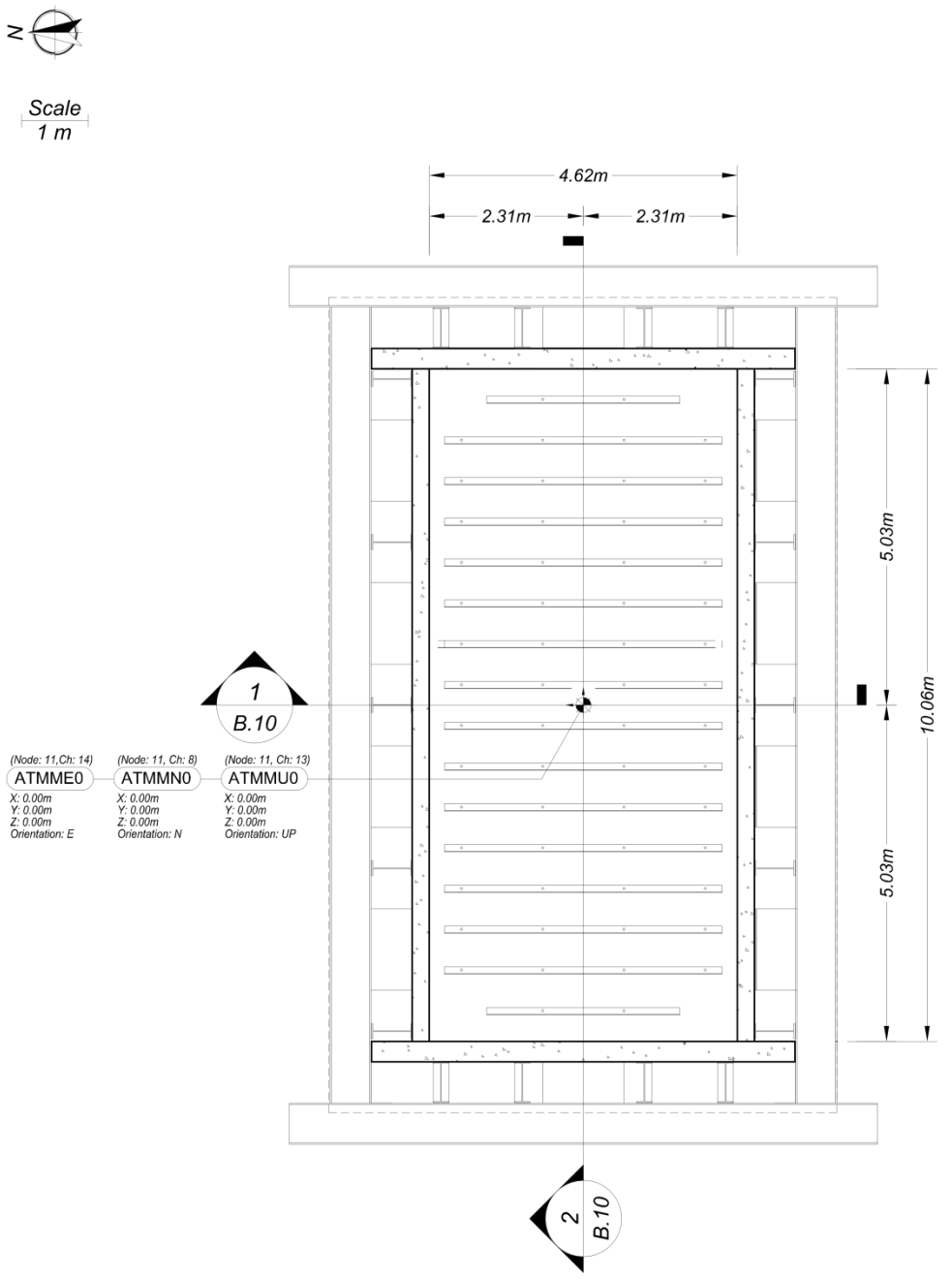

Plan View of Empty Soil Box

Notes:
1. *(x,y,z) coordinates are with respect to global coordinate system.*

Figure B4. Plan view of accelerometers mounted on top center of shake table platen at EL +0.00m.

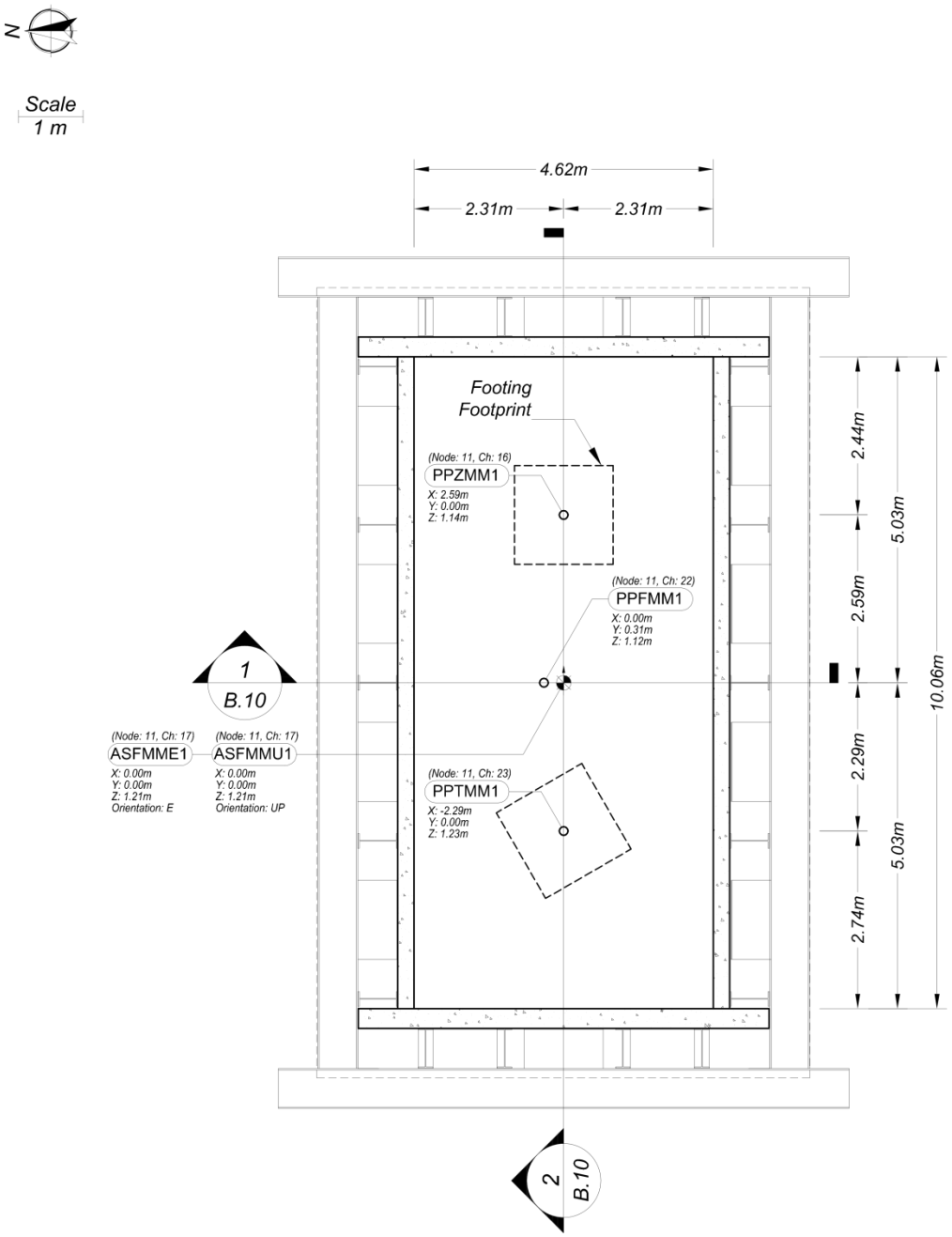

Plan View at EL+1.17m

Notes:
1. *(x,y,z) coordinates are with respect to global coordinate system.*

Figure B5. Plan view of accelerometers and pore pressure transducers placed in the soil at EL+1.17m.

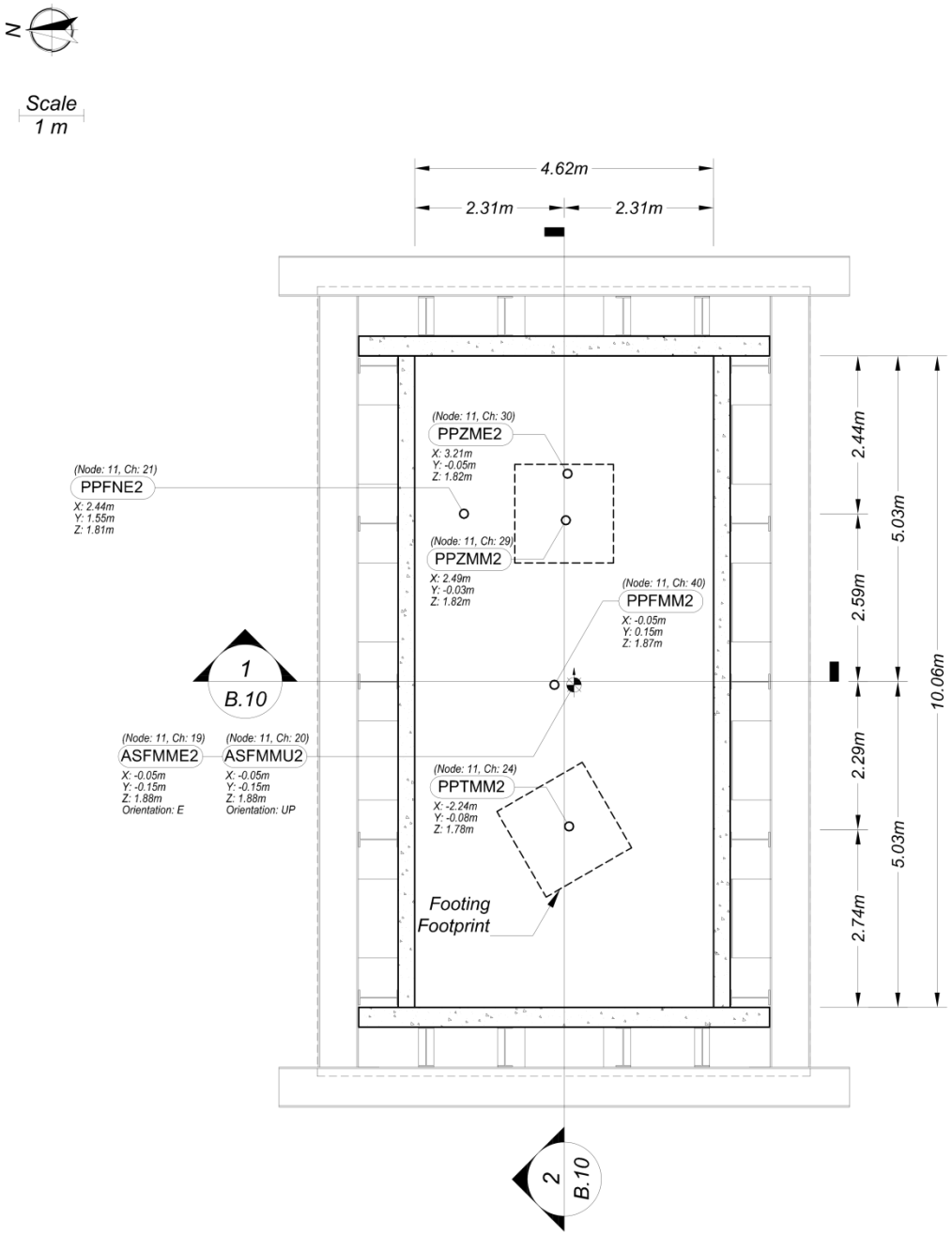

Plan View at EL+1.83m

Notes:
1. *(x,y,z) coordinates are with respect to global coordinate system.*

Figure B6. Plan view of accelerometers and pore pressure transducers placed in the soil at EL+1.83m.

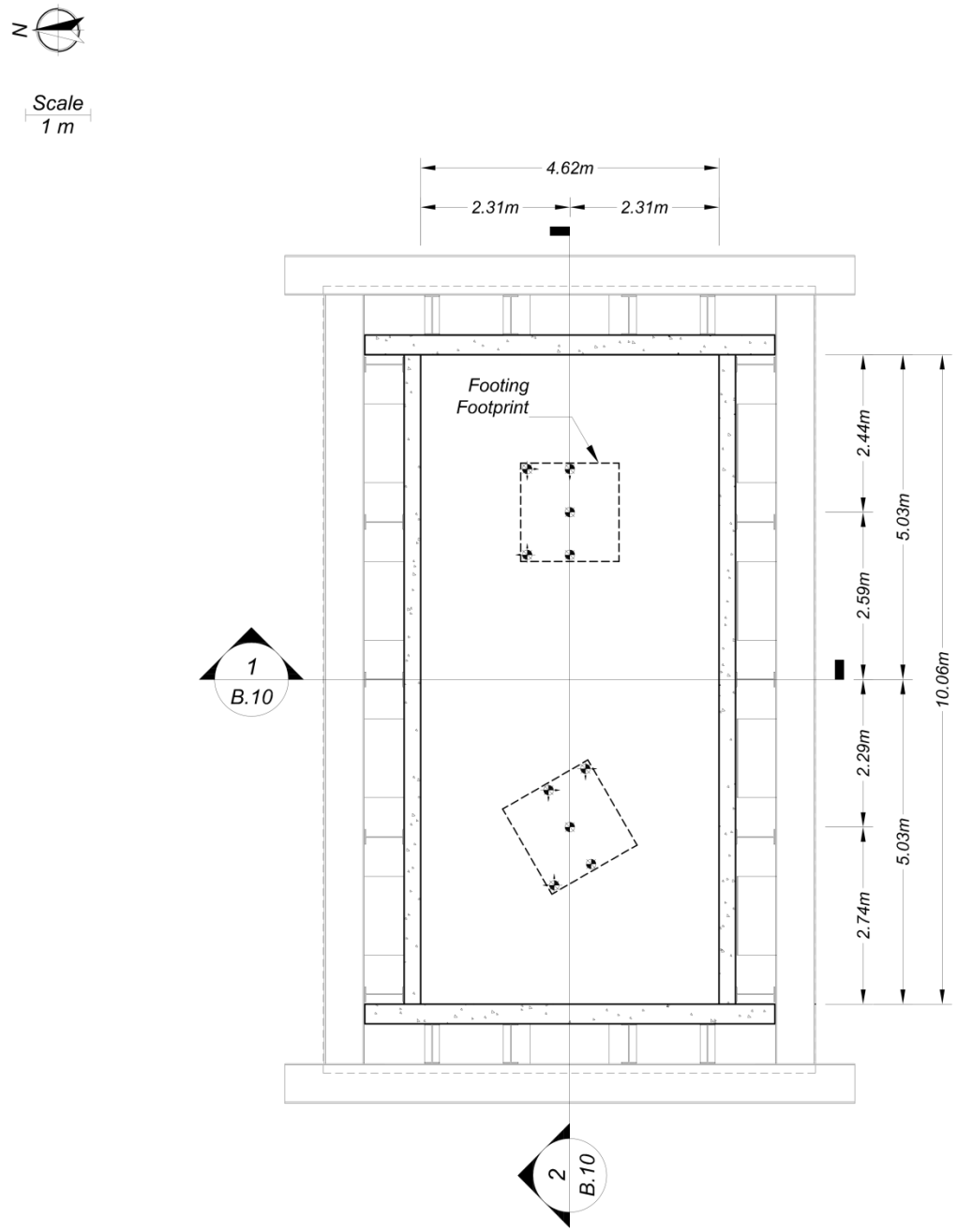

Figure B7. General plan view of accelerometers placed in the soil under the footings at EL+2.49m.

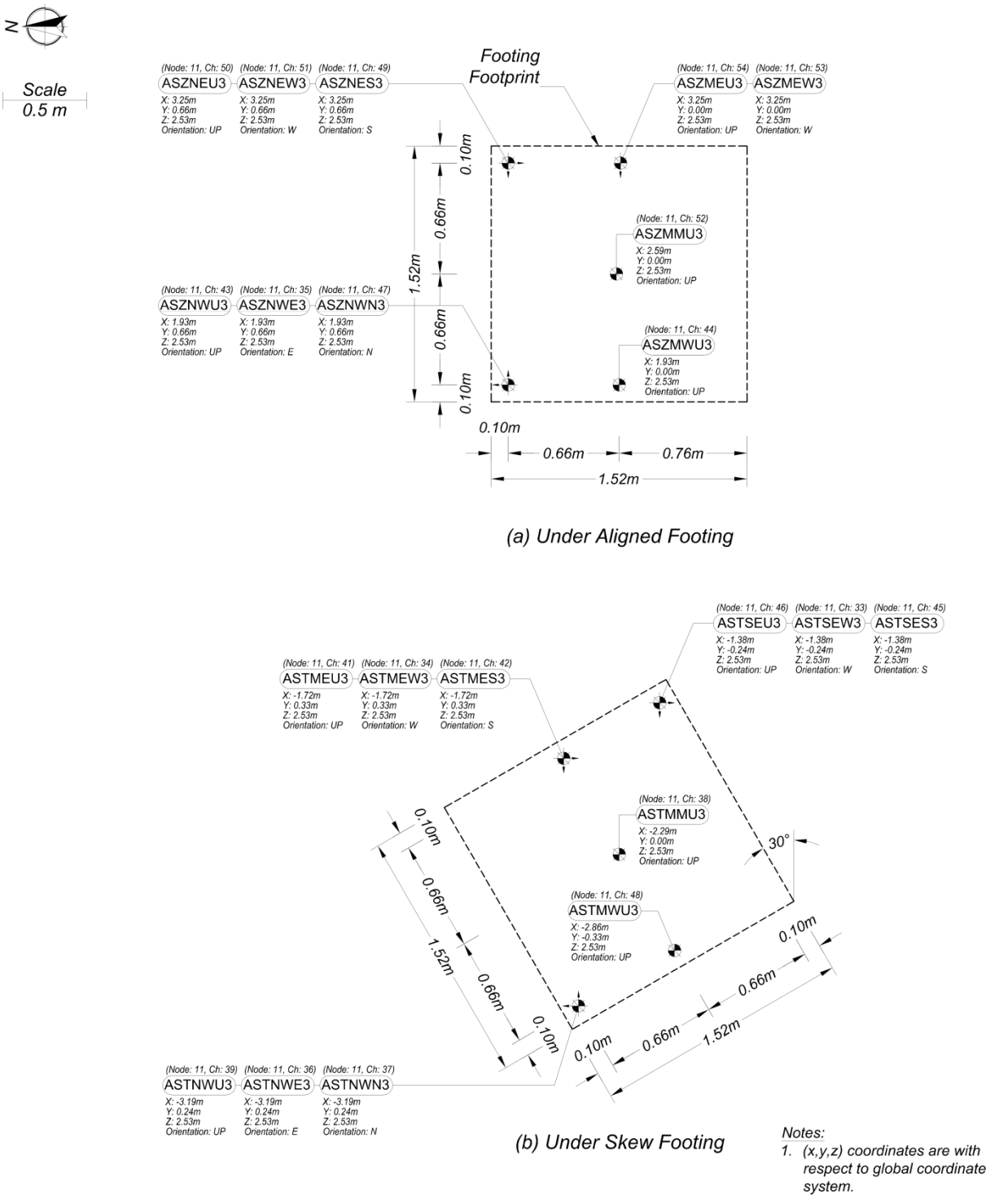

Figure B8. Detailed plan view of accelerometers placed in the soil under the (a) aligned and (b) skew footing at EL+2.49m.

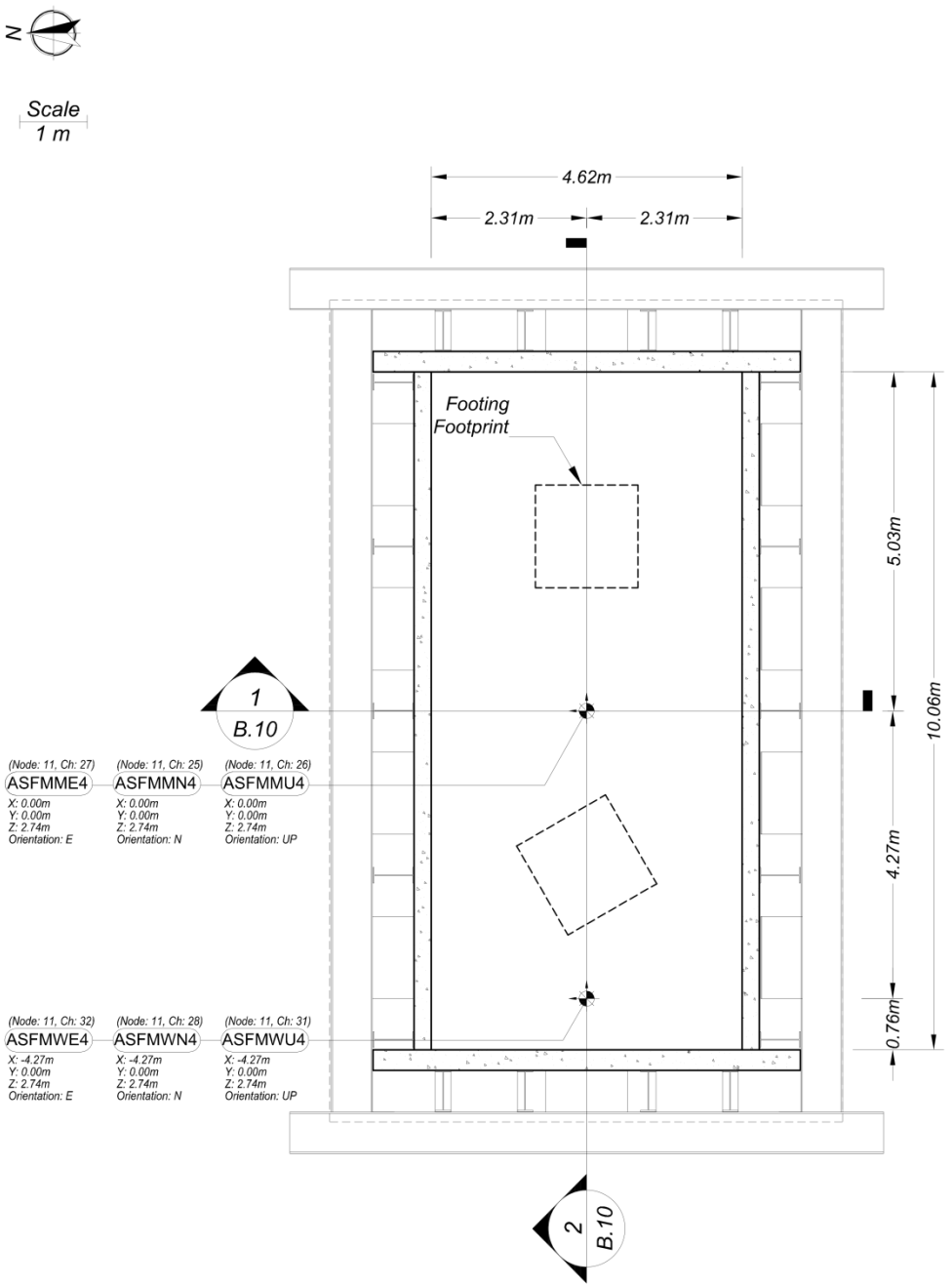

Plan View at EL+2.69m

Notes:
1. *(x,y,z) coordinates are with respect to global coordinate system.*

Figure B9. Plan view of accelerometers placed in the soil at EL+2.69m.

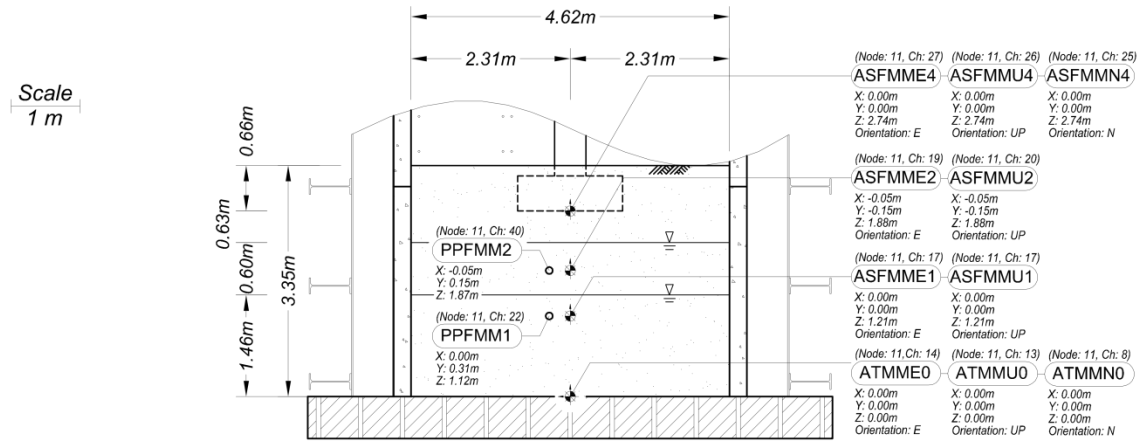

(a) West Elevation View 1

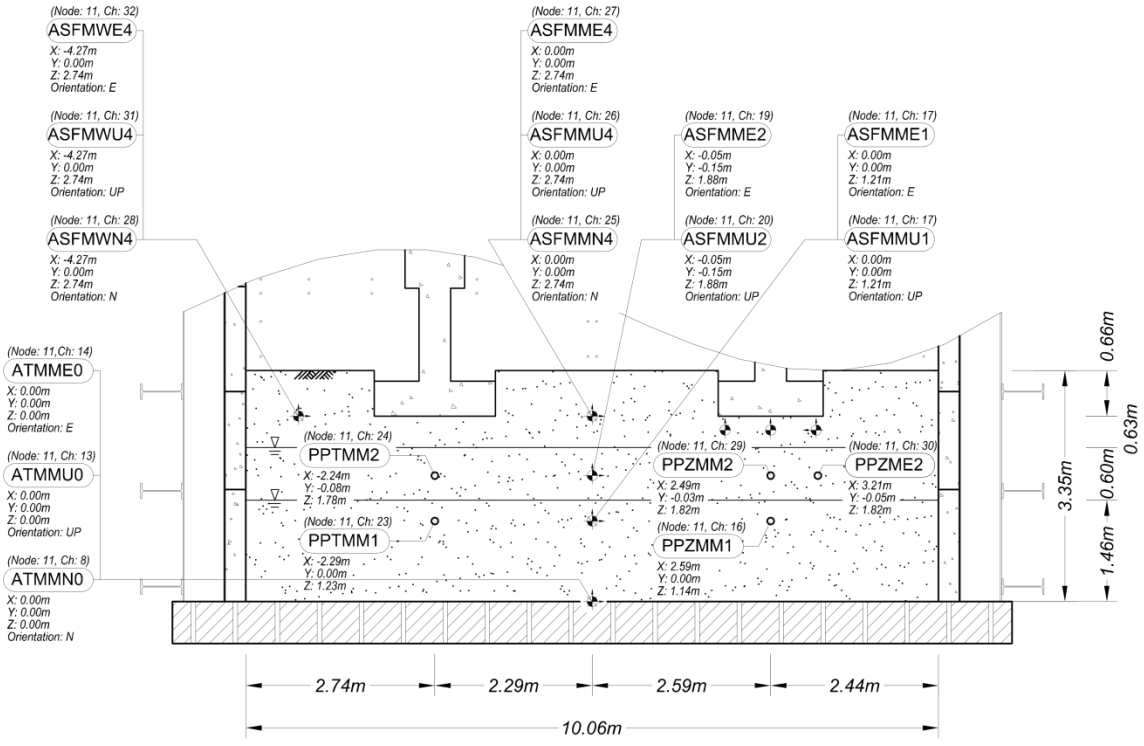

(b) South Elevation View 2

Figure B10. Elevation view of accelerometers and pore pressure transducers placed in the soil for section along (a) y-axis and (b) x-axis.

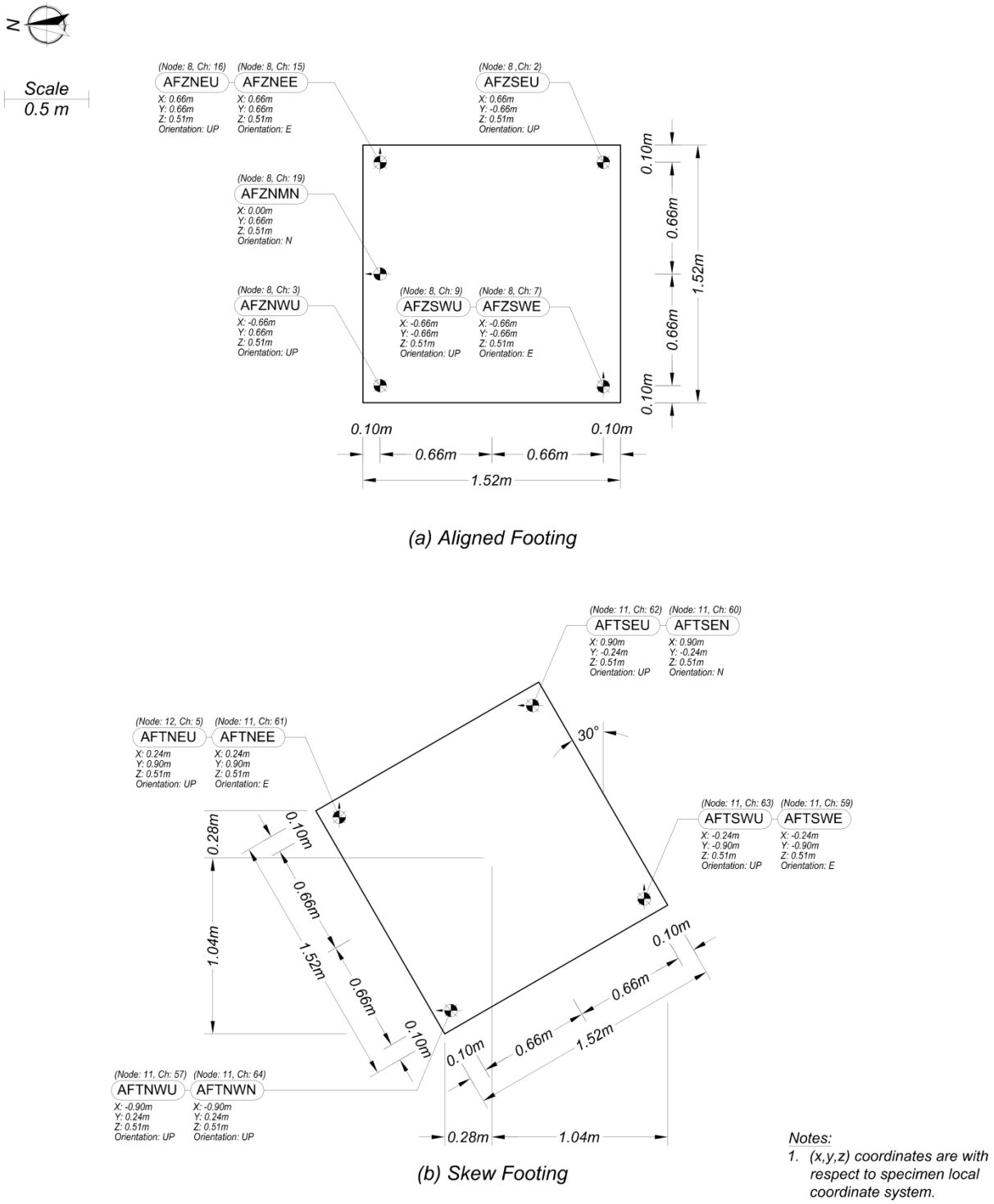

Figure B11. Plan view of accelerometers mounted on top of the (a) aligned and (b) skew footing.

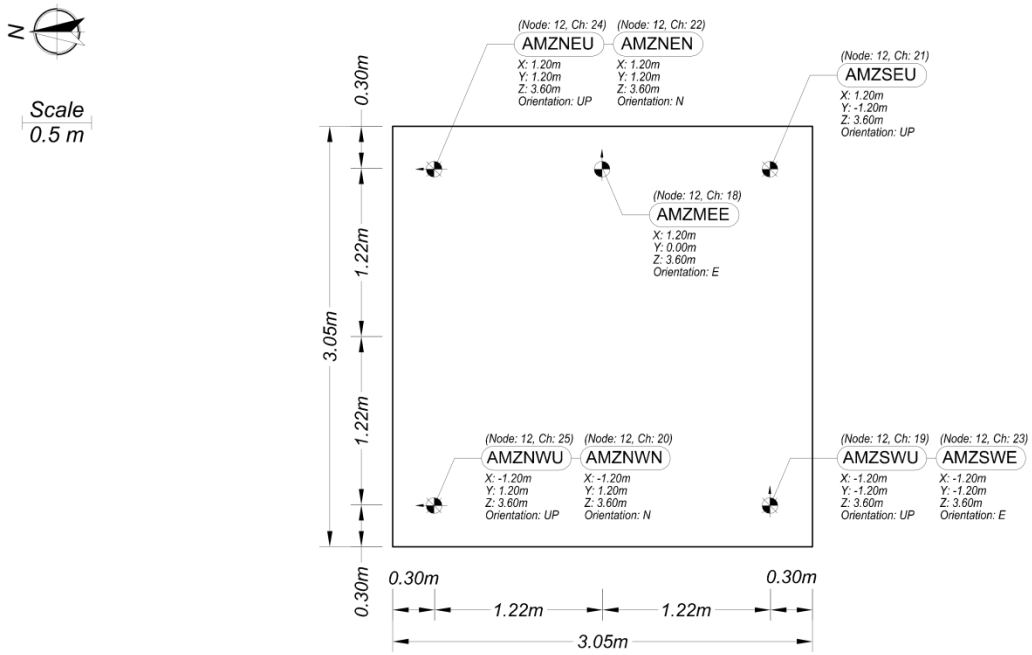

(a) Aligned Mass

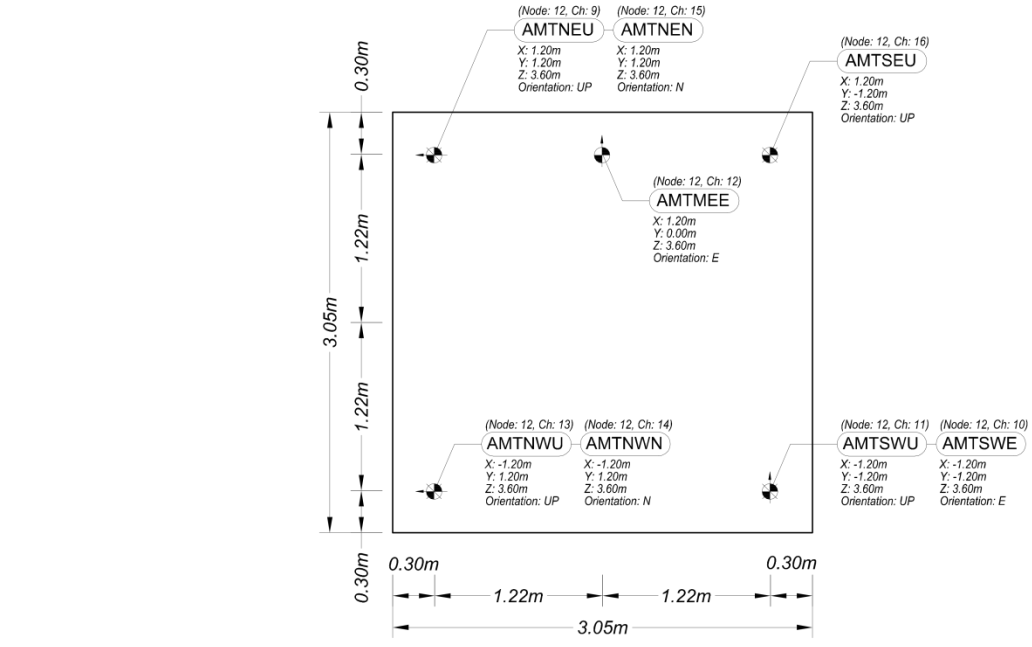

(b) Skew Mass

Figure B12. Plan view of accelerometers mounted on top of the R/C mass blocks of (a) aligned and (b) skew specimen.

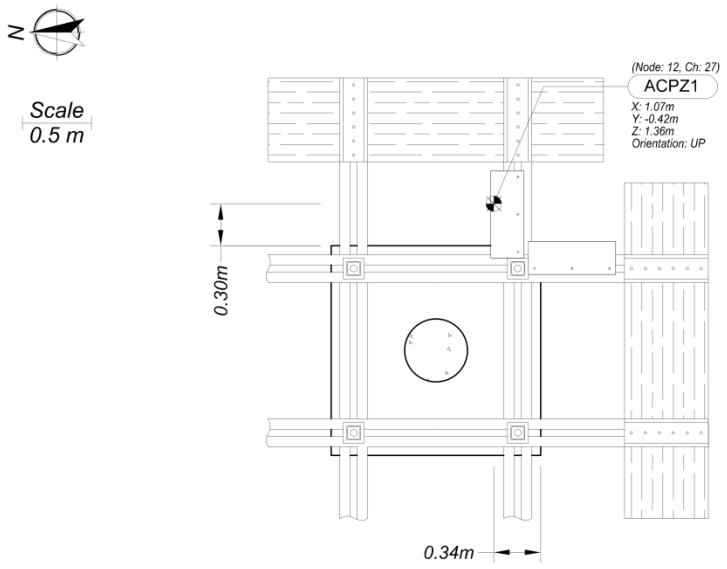

(a) Aligned Footing, Plan View at EL+4.55m

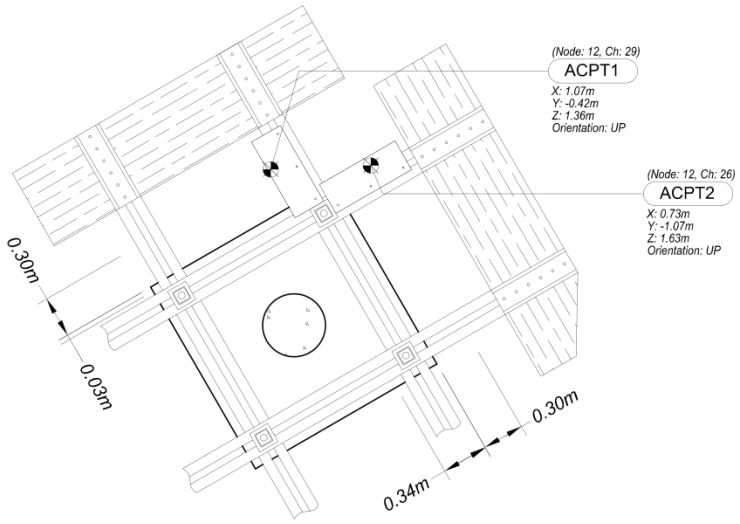

(b) Skew Footing, Plan View at EL+4.55m

Notes:

1. *(x,y,z) coordinates are with respect to specimen and footing local coordinate system for aligned and skew footing, respectively.*

Figure B13. Plan view of accelerometers mounted on the restraining system of (a) aligned and (b) skew specimen.

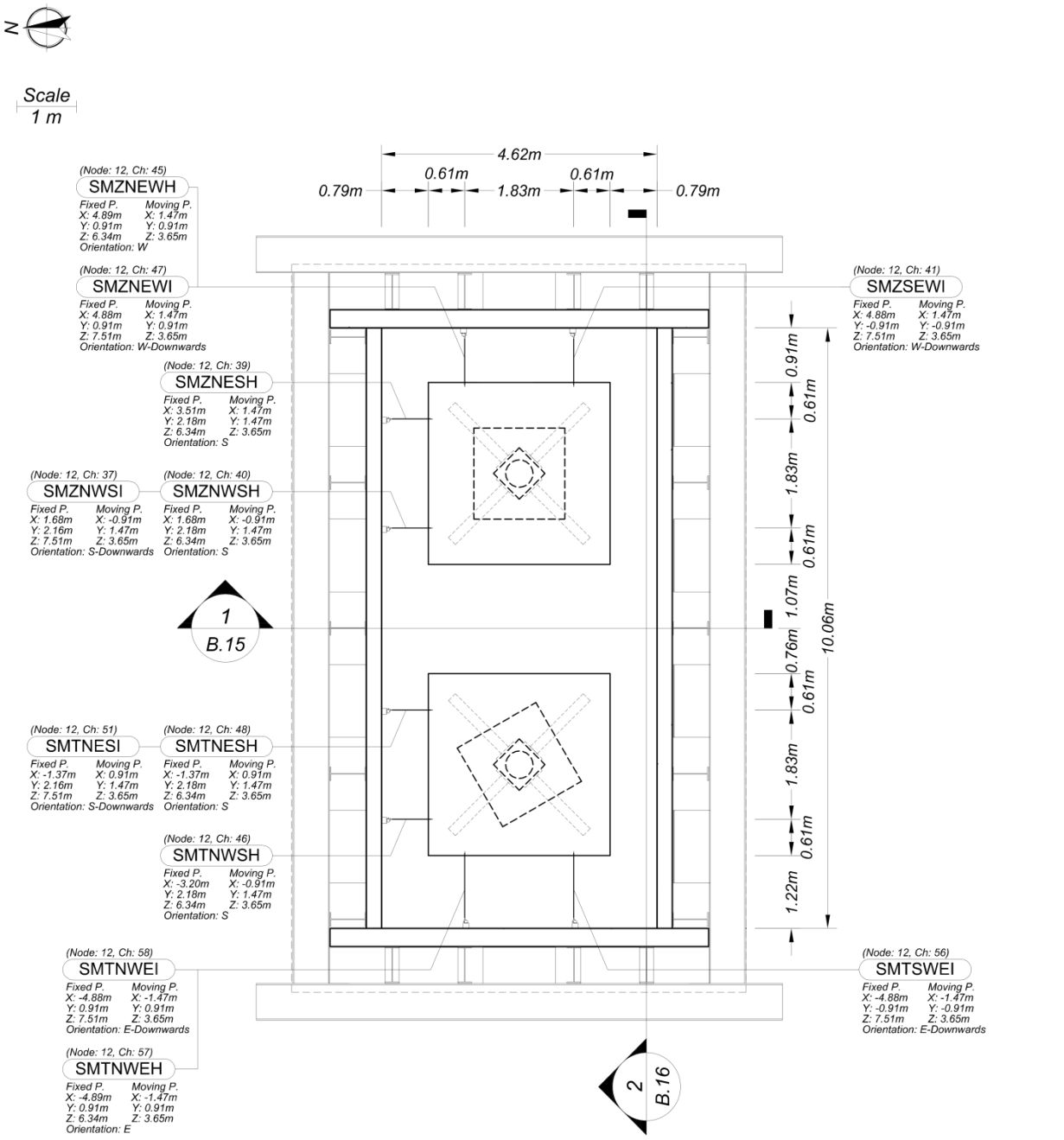

Figure B14. Plan view of string potentiometers mounted on top of the R/C mass blocks.

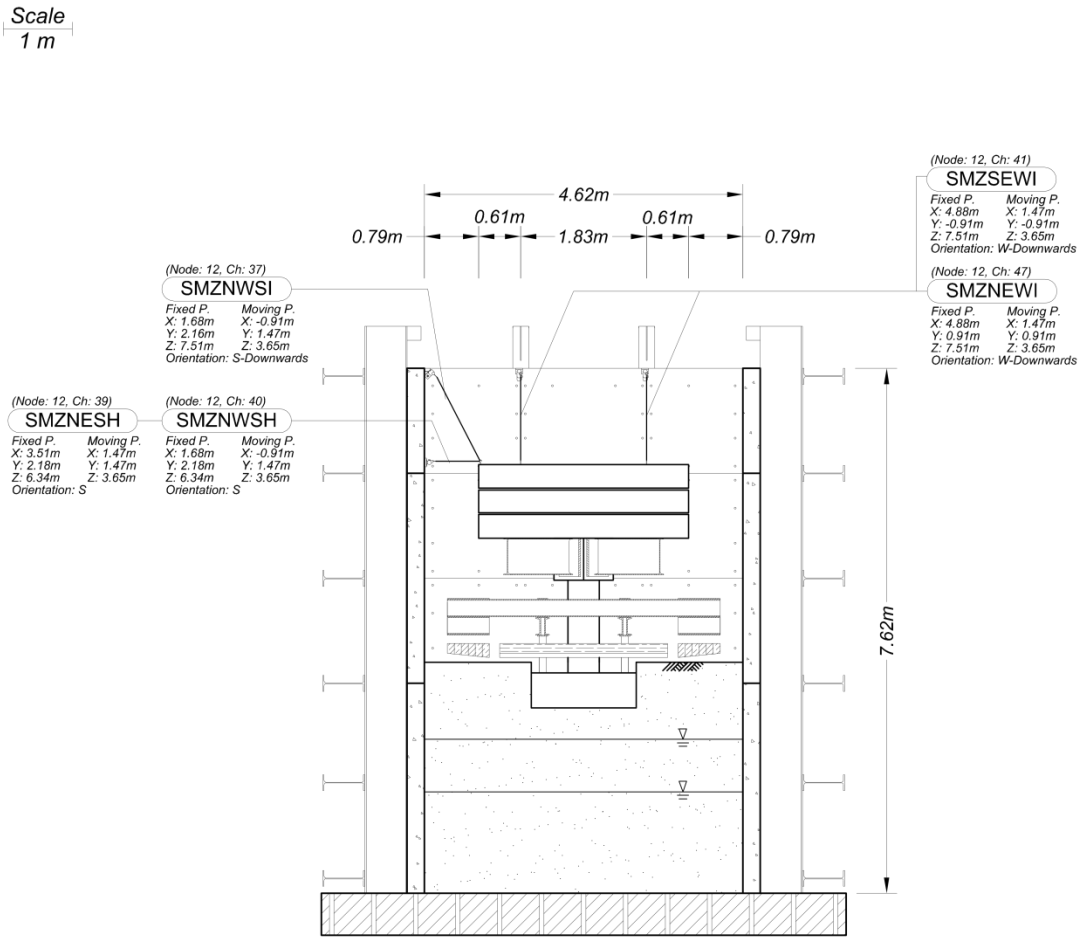

Aligned Specimen, West Elevation View 1

Notes:
1. *(x,y,z) coordinates for fixed points are with respect to global coordinate system.*
2. *(x,y,z) coordinates for moving points are with respect to specimen local coordinate system*

Figure B15. West elevation view of string potentiometers mounted on top of the R/C mass blocks of the aligned specimen.

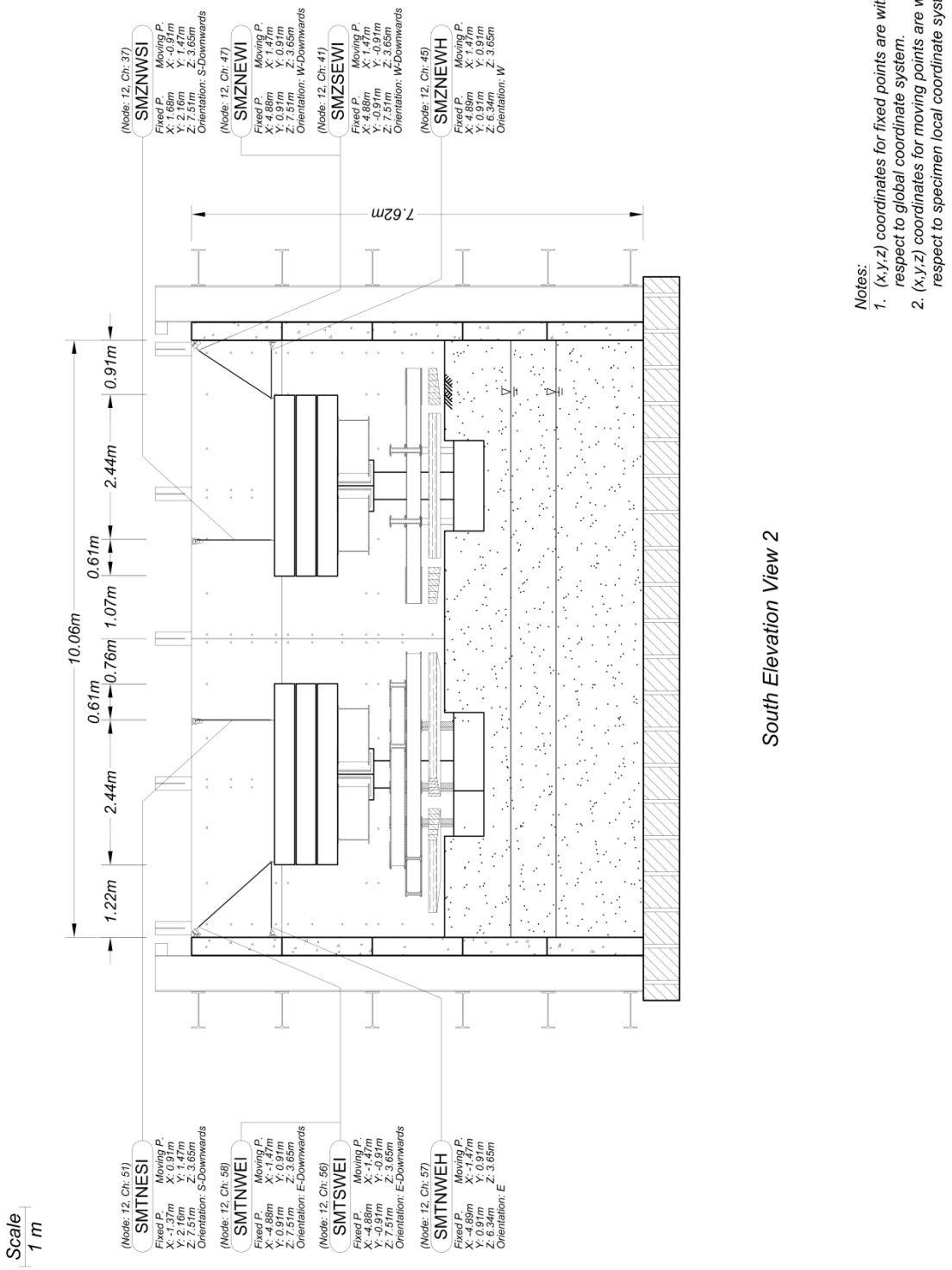

Figure B16. South elevation view of string potentiometers mounted on top of the R/C mass blocks.

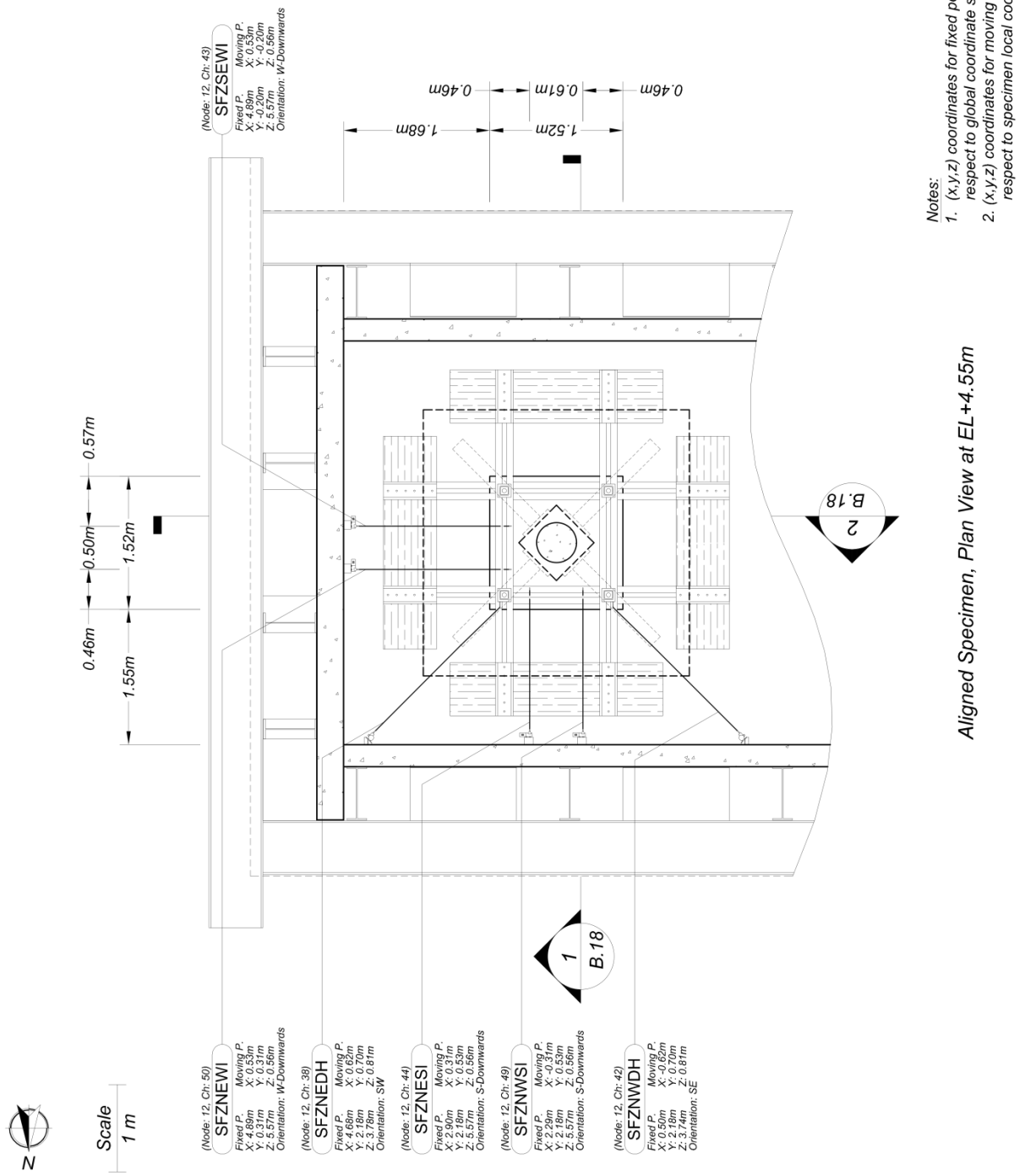

Figure B17. Plan view of string potentiometers mounted on the aligned footing.

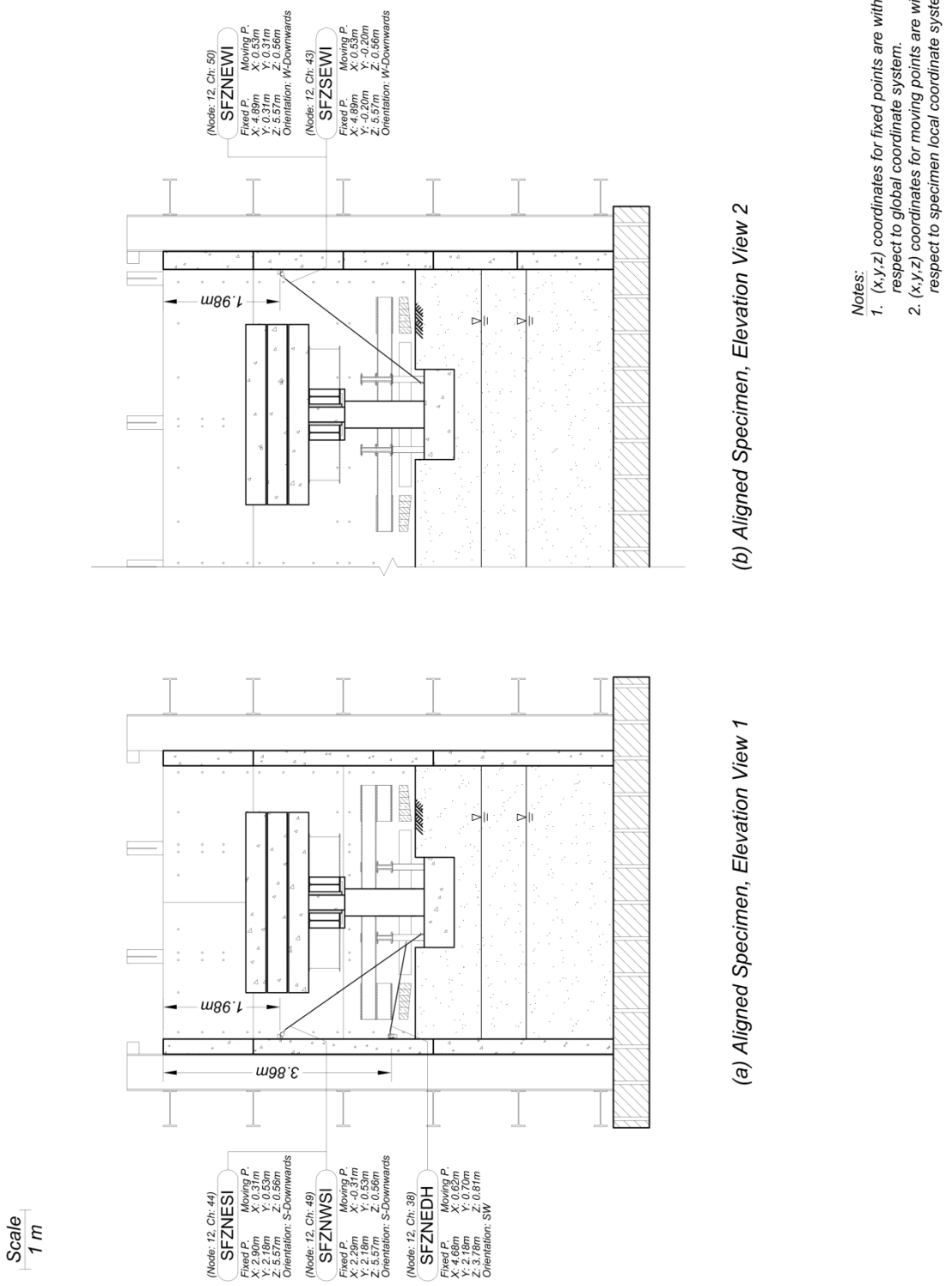

Figure B18. Elevation views (a) 1 and (b) 2 of string potentiometers mounted on the aligned footing.

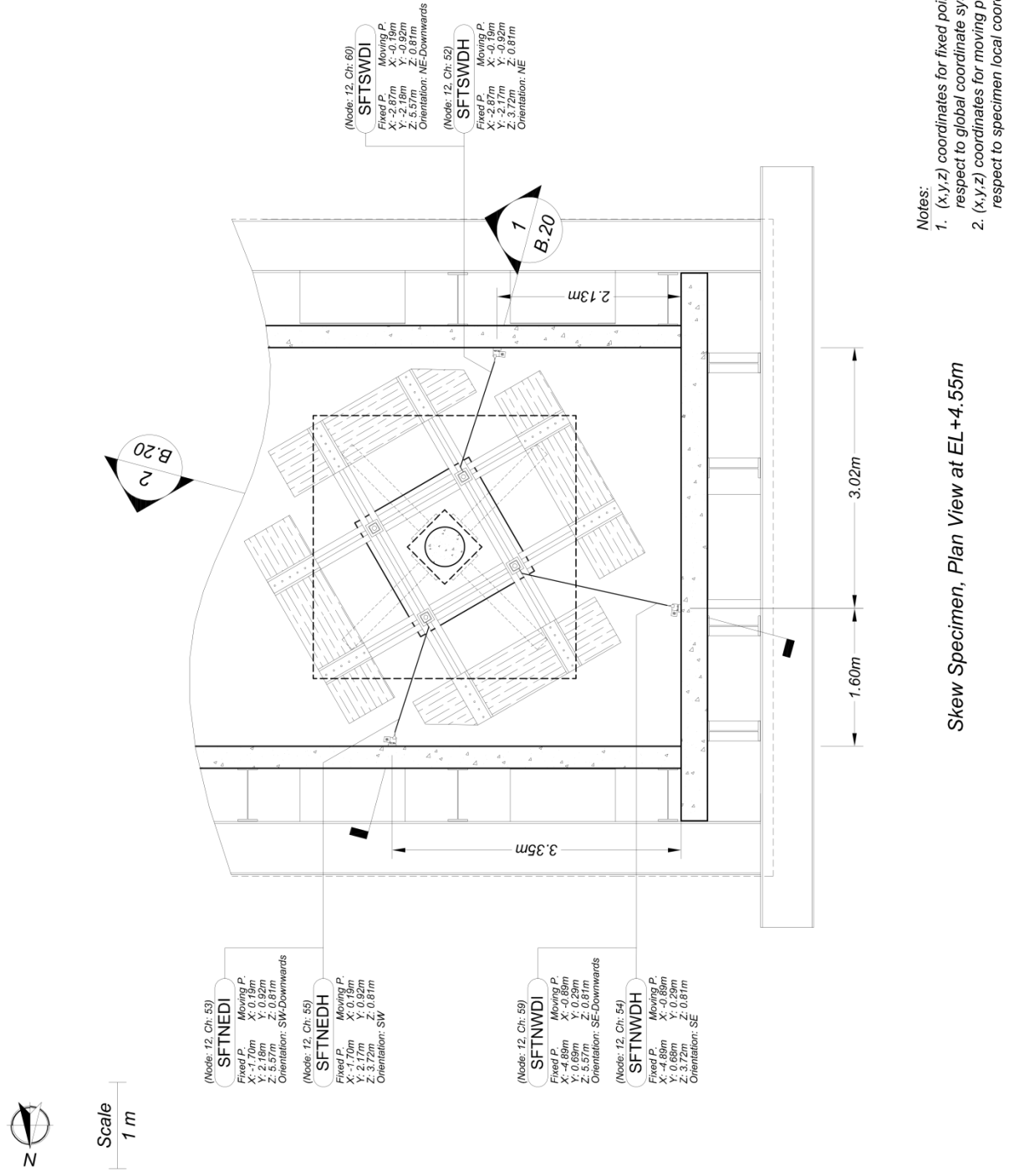

Figure B19. Plan view of string potentiometers mounted on the skew footing.

Figure B20. Elevation views (a) 1 and (b) 2 of string potentiometers mounted on the skew footing.

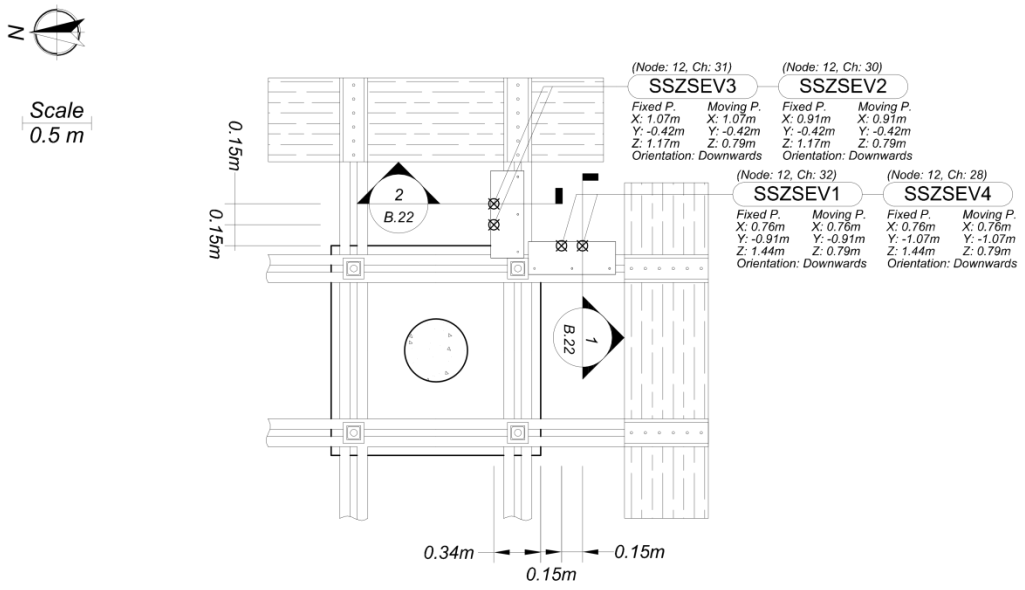

(a) Aligned Footing, Plan View at EL+4.55m

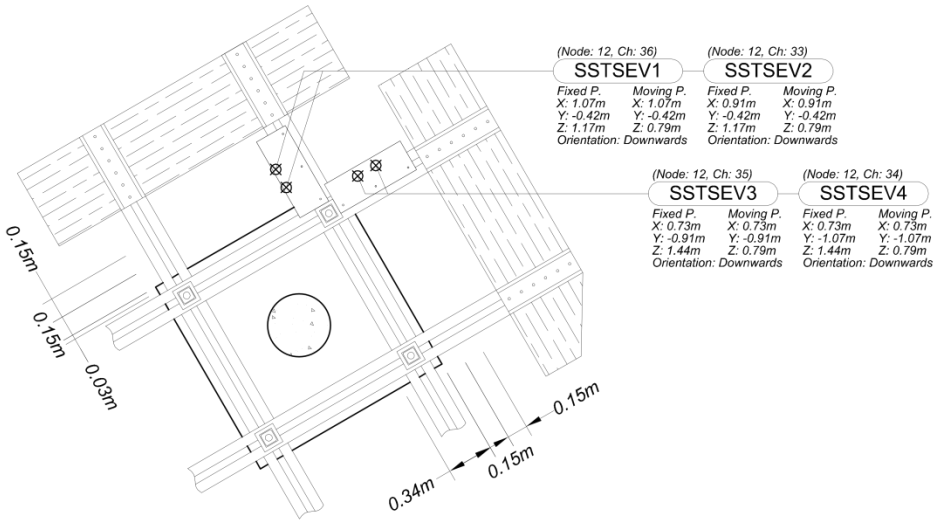

(b) Skew Footing, Plan View at EL+4.55m

Notes:

1. *(x,y,z) coordinates are with respect to specimen and footing local coordinate system for aligned and skew footing, respectively.*

Figure B21. Plan view of soil-footing string potentiometers of (a) aligned and (b) skew footing.

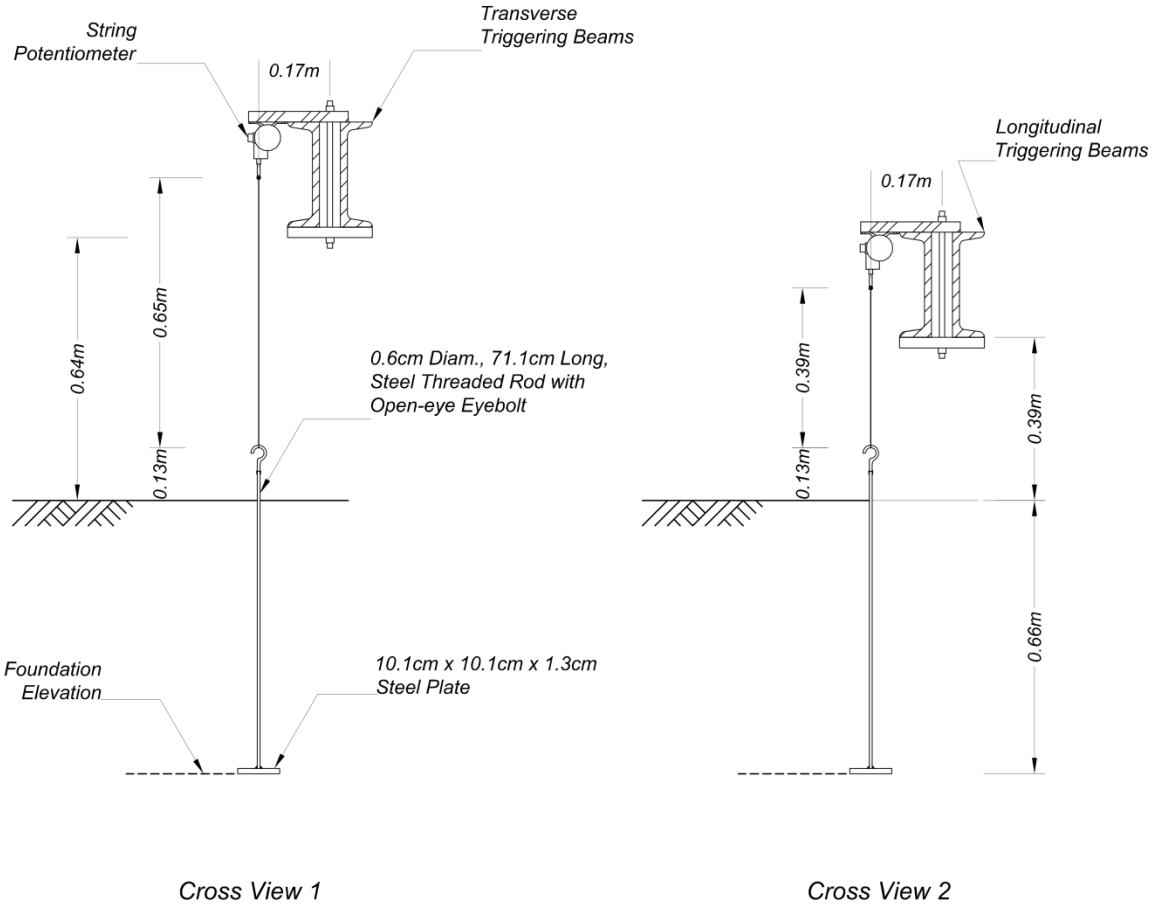

Notes:

1. *The string potentiometer sensor is mounted on the top wooden board that is secured against the bottom wooden board through a 1.3cm diam. threaded rod passing between the gap of the triggering C-beam backs.*

Figure B22. Elevation view construction details of the soil-footing string potentiometers.

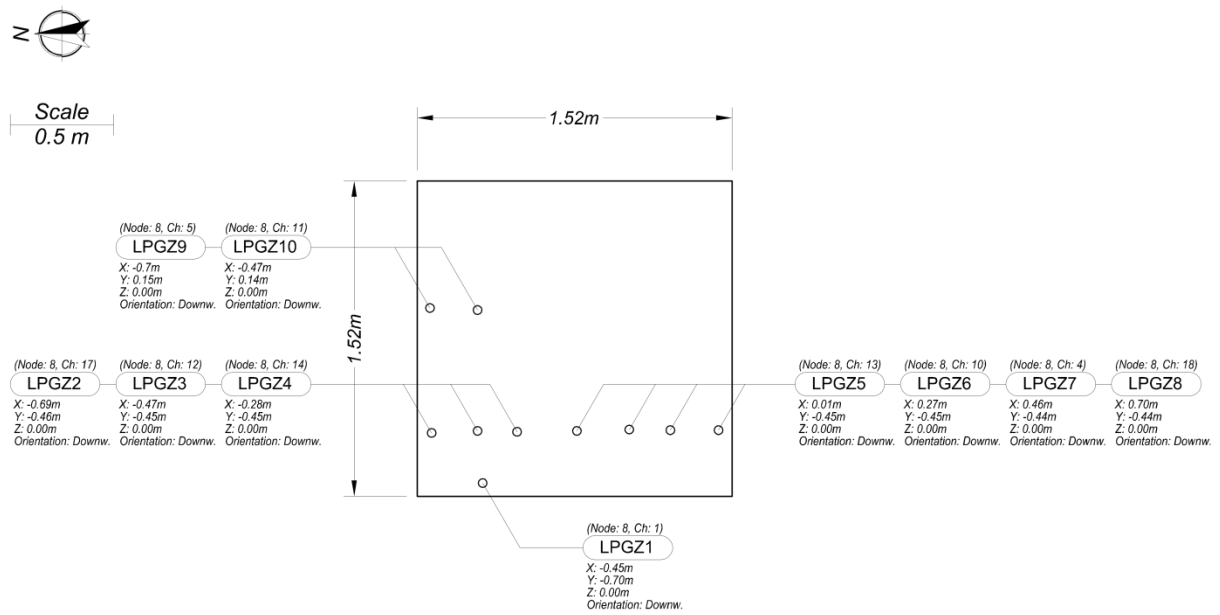

(a) Aligned Footing

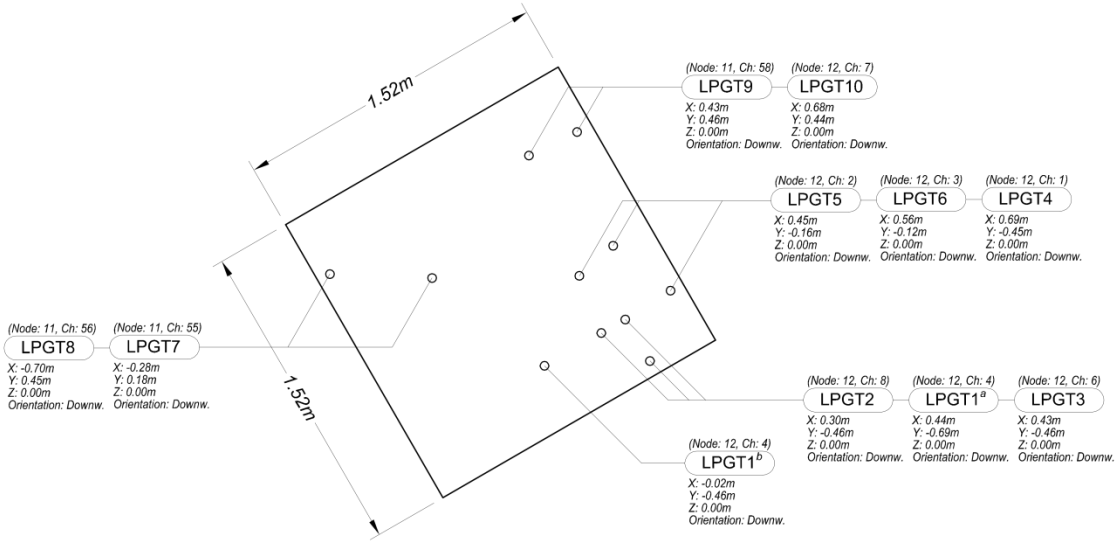

(b) Skew Footing

Notes:

1. *(x,y,z) coordinates are with respect to specimen and footing local coordinate system for aligned and skew footing, respectively.*

[a] *Sensor used in test 1.*

[b] *Sensor used in tests 2 and 3.*

Figure B23. Plan view of gap-no gap instruments of (a) aligned and (b) skew footing.

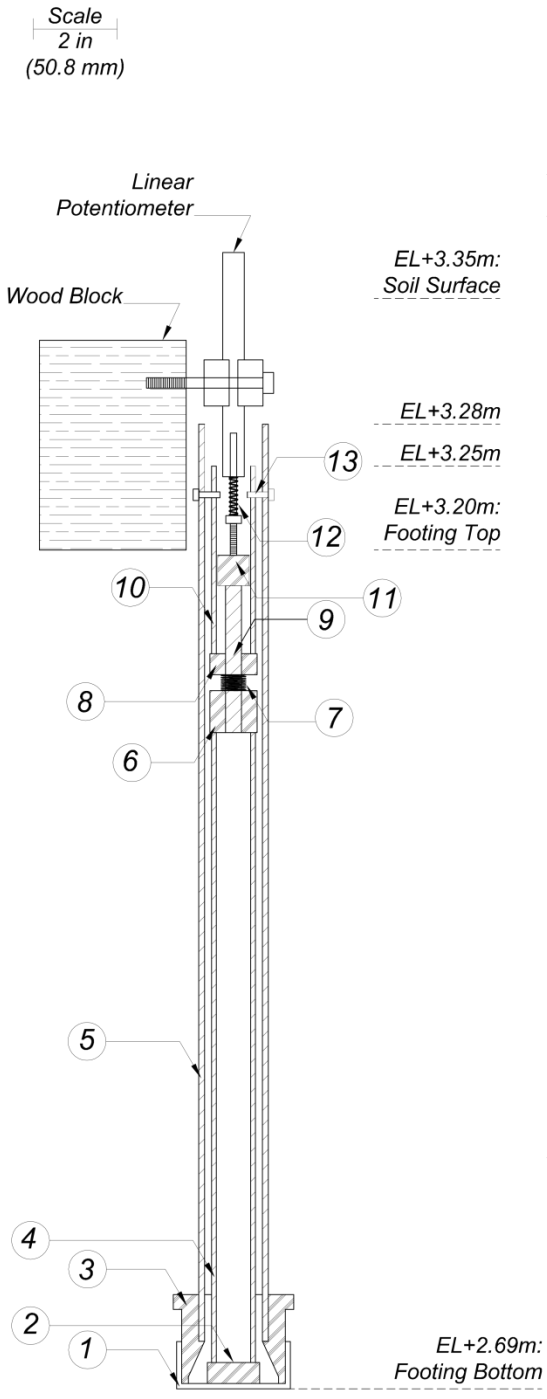

No.	Description	Notes
1	Super-soft neoprene rubber, 1/8" thickn., Durometer hardness 10A	Wrapped around part 3 and tied with hose clamp.
2	PVC rod 1 1/4" Dia., 1/2" Thickn.	Glued with PVC cement & primer to part 4.
3	PVC Hex Bushing 2 1/2" Pipe End Male x 1 1/4" Socket Female	
4	3/4 " N.D. PVC pipe, Sch. 40, 1'-3" Lg., 1.05" O.D., 0.824" I.D.	Glued with PVC cement & primer to parts 2 & 6.
5	1 1/4" N.D. PVC pipe, Sch. 40, 1'-11" Lg., 1.66" O.D., 1.38" I.D.	Exceeds by 3" the top of the footing.
6	PVC rod 1 1/8 " Dia., 1" Thickn.	Drilled 25/64" center through hole, glued with PVC cement & primer to parts 4 & 9.
7	Compression Spring, 2.188" Overall Lg., 0.59" O.D., 0.51" I.D., 0.38" Compressed Lg., 6.80 lbs Max Load, 3.80 lbs/in Rate, Closed Ends	Fully compressed in its initial position.
8	PVC rod 1 1/8 " Dia., 1/2 " thickn.	Drilled 7/16" center through hole, glued with PVC cement & primer to part 10.
9	PVC rod 3/8" Dia., 3 1/2 " Lg.	Glued with PVC cement & primer to part 6.
10	3/4 " N.D. PVC pipe, Sch. 40, 4 1/2" Lg., 1.05" O.D., 0.824" I.D.	Glued with PVC cement & primer to part 8.
11	PVC rod 3/4" Dia., 3/4 " thickn.	
12	Compression Spring, 3.0" Overall Lg., 0.240" O.D., 0.182" I.D., 0.93" Compressed Lg., 5.0 lbs Max Load, 3.60 lbs/in Rate, Closed Ground Ends	Fully compressed in its initial position.
13	No. 6 x 1/2" Pan Head Serrated-Thread Screw for Plywood	Use 4 of them per sensor to provide reaction for the top inner PVC pipe against the outer PVC pipe.

Figure B24. Elevation view construction details of the gap-no gap instruments.

Appendix C: Critical plots

Day 1, Gilroy #1 1.0 Motion

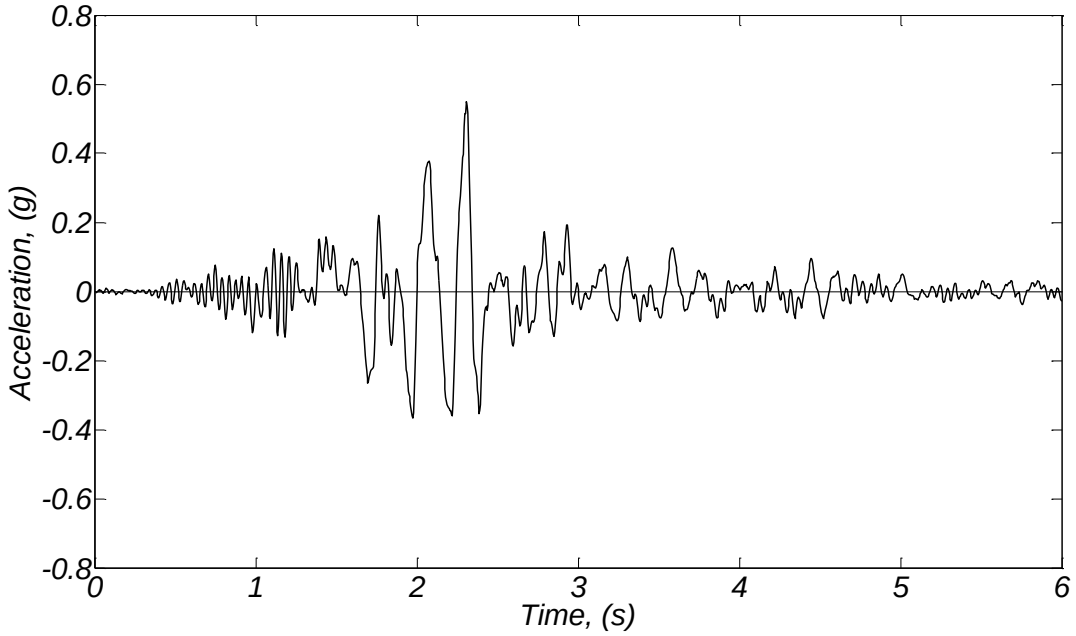

Figure C1. Soil free field acceleration time history (direction of shaking).

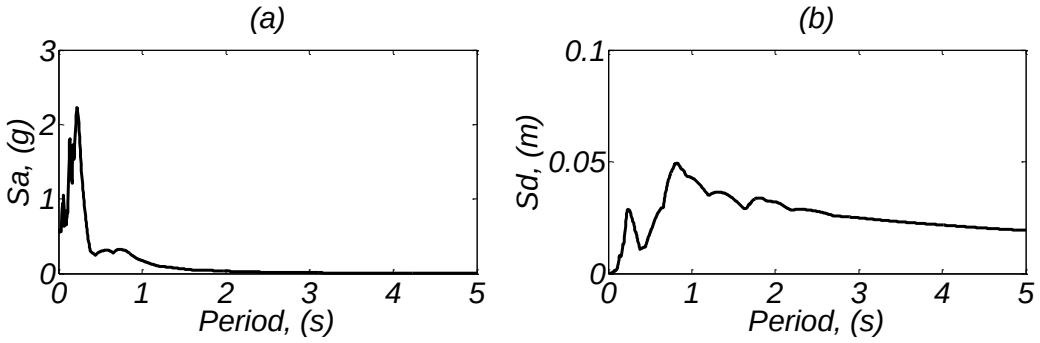

Figure C2. (a) Acceleration and (b) displacement response spectra for the recorded soil free field acceleration (direction of shaking) for damping ζ = 3%.

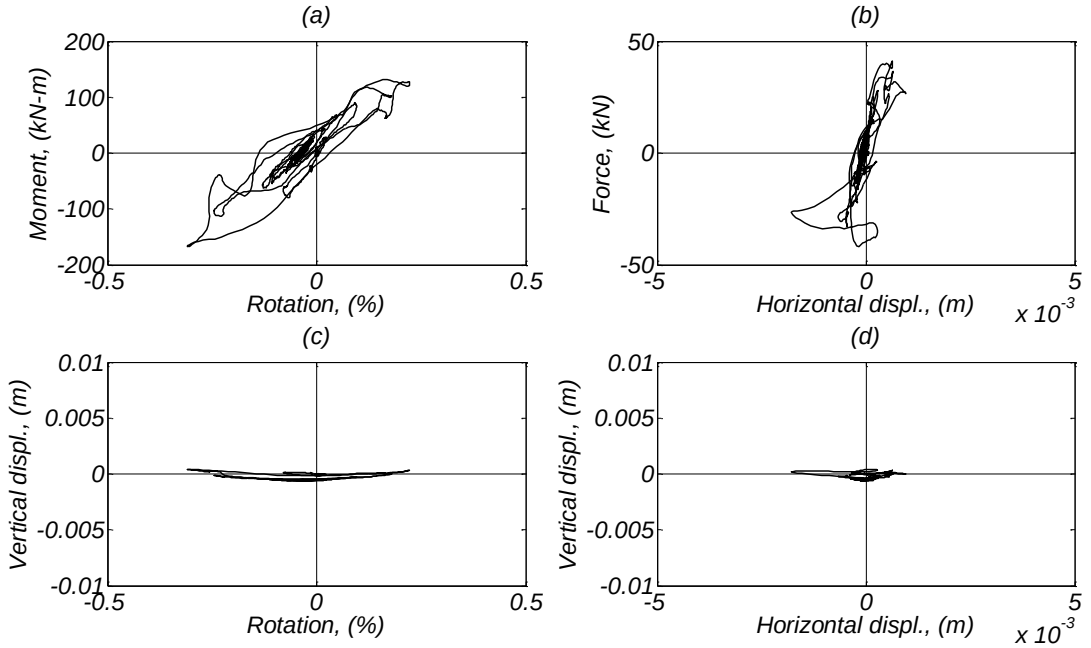

Figure C3. Aligned footing response; (a) moment vs rotation diagram (around NS direction), (b) base shear vs horizontal displacement (EW direction), (c) vertical displacement vs foundation rotation, and (d) vertical displacement vs horizontal displacement in the EW direction.

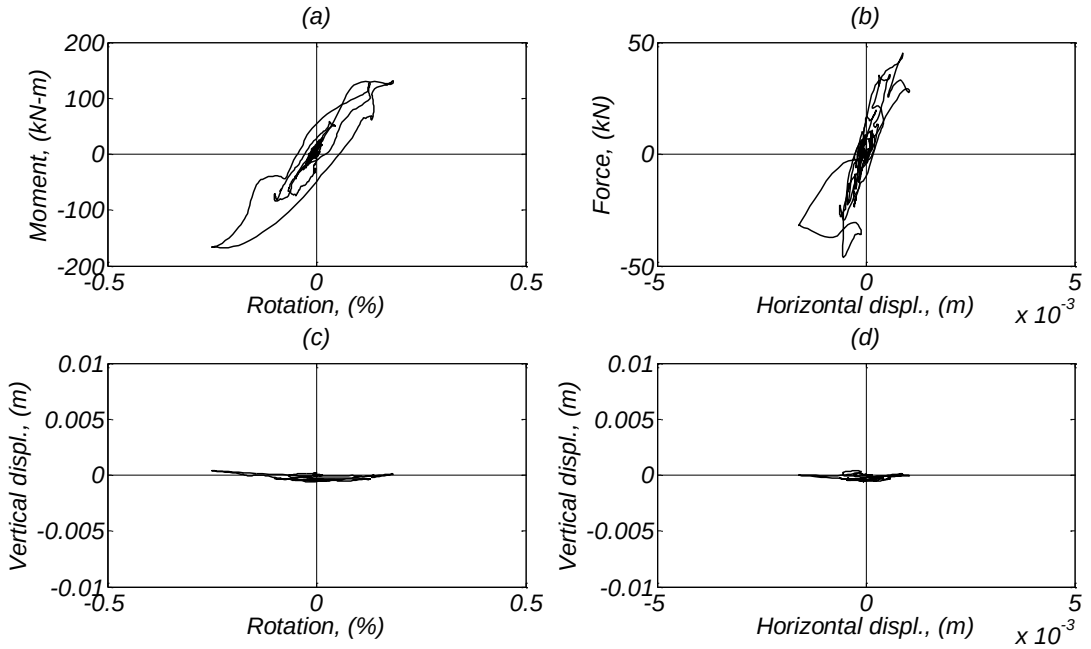

Figure C4. Skew footing response; (a) moment vs rotation diagram (around NS direction), (b) base shear vs horizontal displacement (EW direction), (c) vertical displacement vs foundation rotation, and (d) vertical displacement vs horizontal displacement in the EW direction.

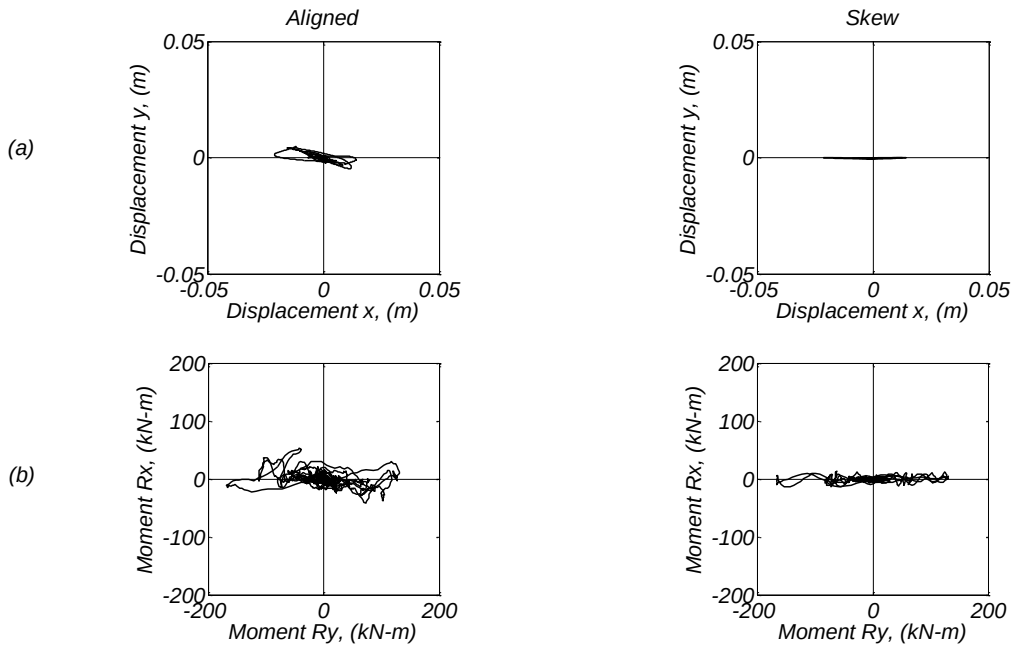

Figure C5. Bilateral response for the aligned and skew specimens; (a) mass displacement for the EW(x) and NS(y) direction, and (b) foundation moment for the corresponding directions.

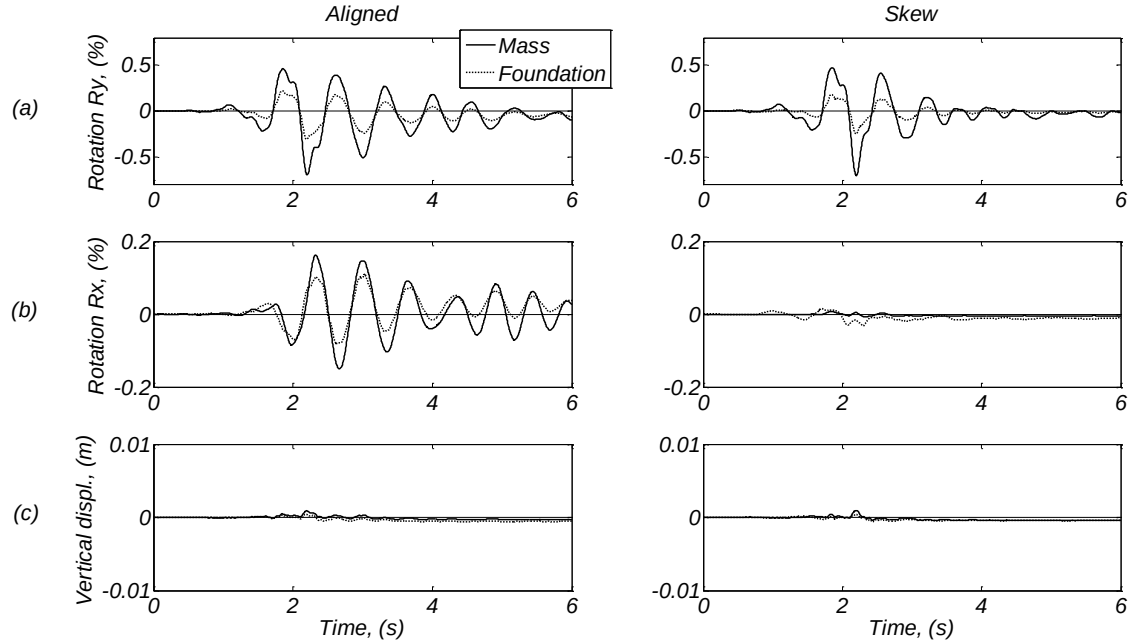

Figure C6. Time histories for the aligned and skew specimens; (a) mass drift ratio for the EW direction and equivalent foundation rotation, (b) mass drift ratio for the NS direction and equivalent foundation rotation, and (c) mass and footing vertical displacements.

Day 1, Corralitos 0.8 Motion

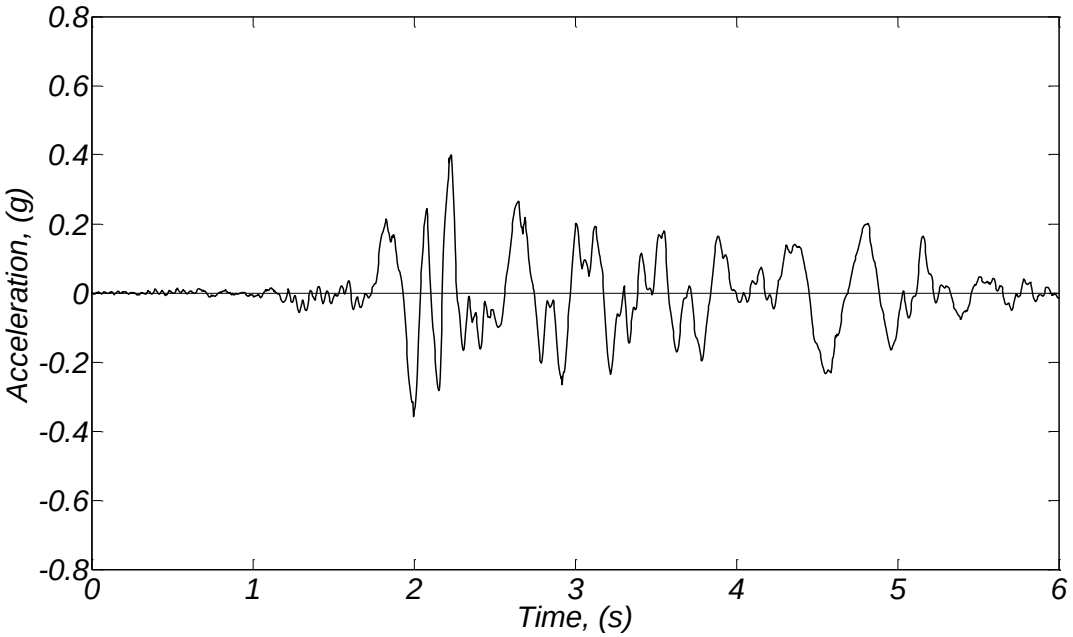

Figure C7. Soil free field acceleration time history (direction of shaking).

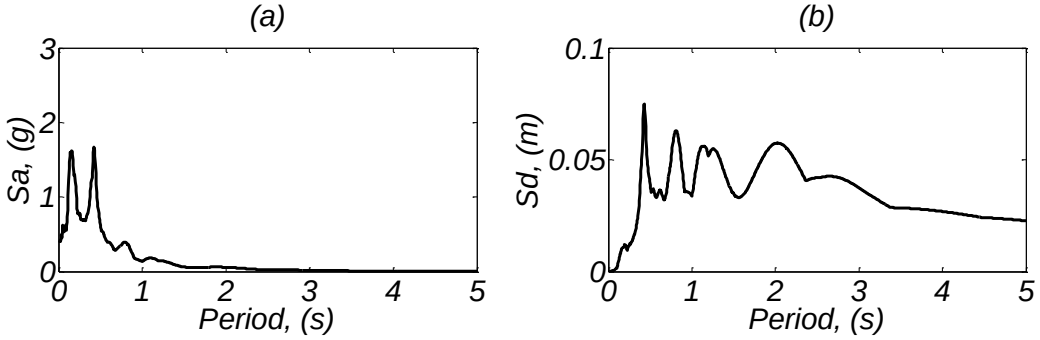

Figure C8. (a) Acceleration and (b) displacement response spectra for the recorded soil free field acceleration (direction of shaking) for damping ζ = 3%.

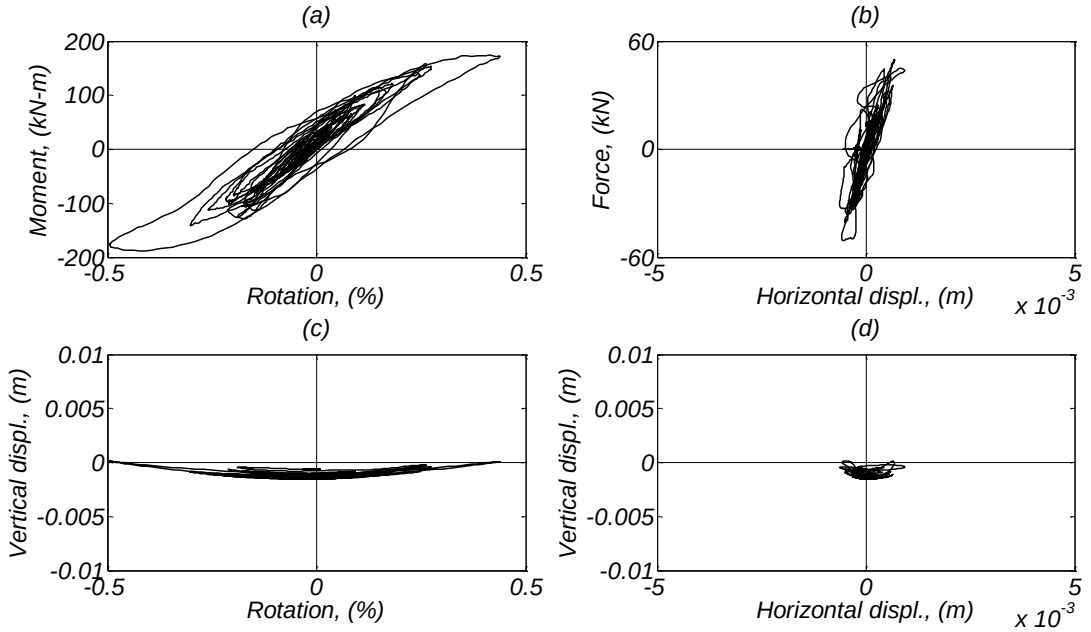

Figure C9. Aligned footing response; (a) moment vs rotation diagram (around NS direction), (b) base shear vs horizontal displacement (EW direction), (c) vertical displacement vs foundation rotation, and (d) vertical displacement vs horizontal displacement in the EW direction.

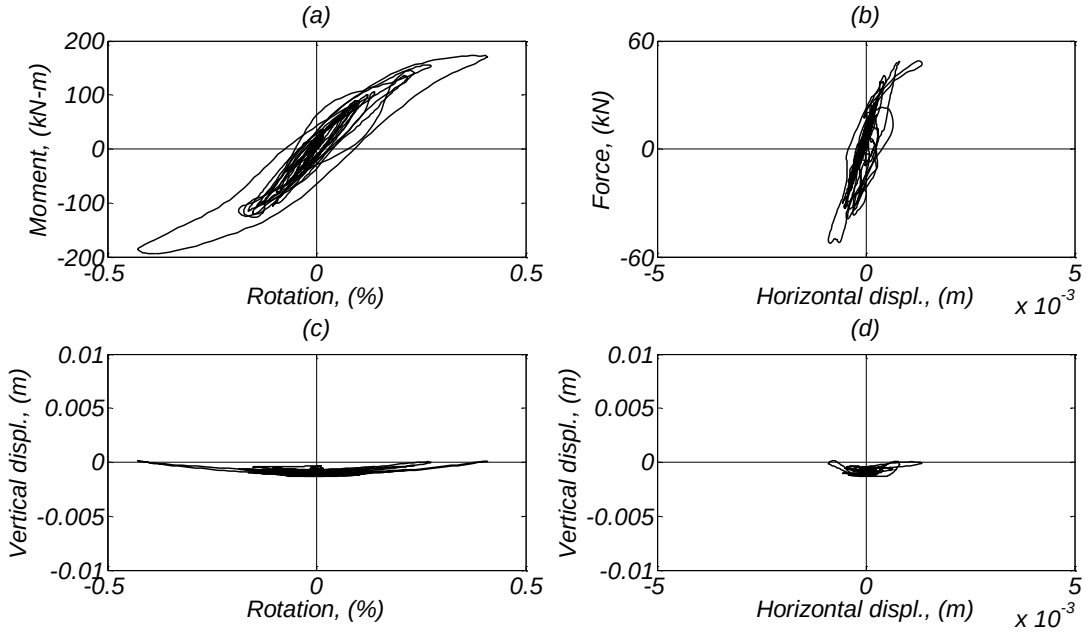

Figure C10. Skew footing response; (a) moment vs rotation diagram (around NS direction), (b) base shear vs horizontal displacement (EW direction), (c) vertical displacement vs foundation rotation, and (d) vertical displacement vs horizontal displacement in the EW direction.

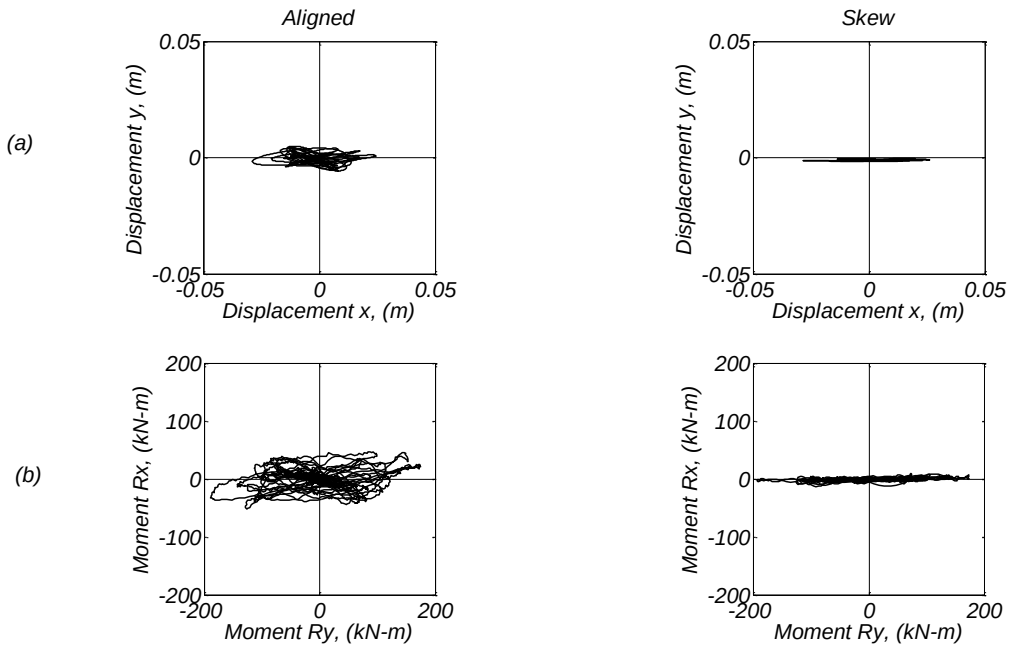

Figure C11. Bilateral response for the aligned and skew specimens; (a) mass displacement for the EW(x) and NS(y) direction, and (b) foundation moment for the corresponding directions.

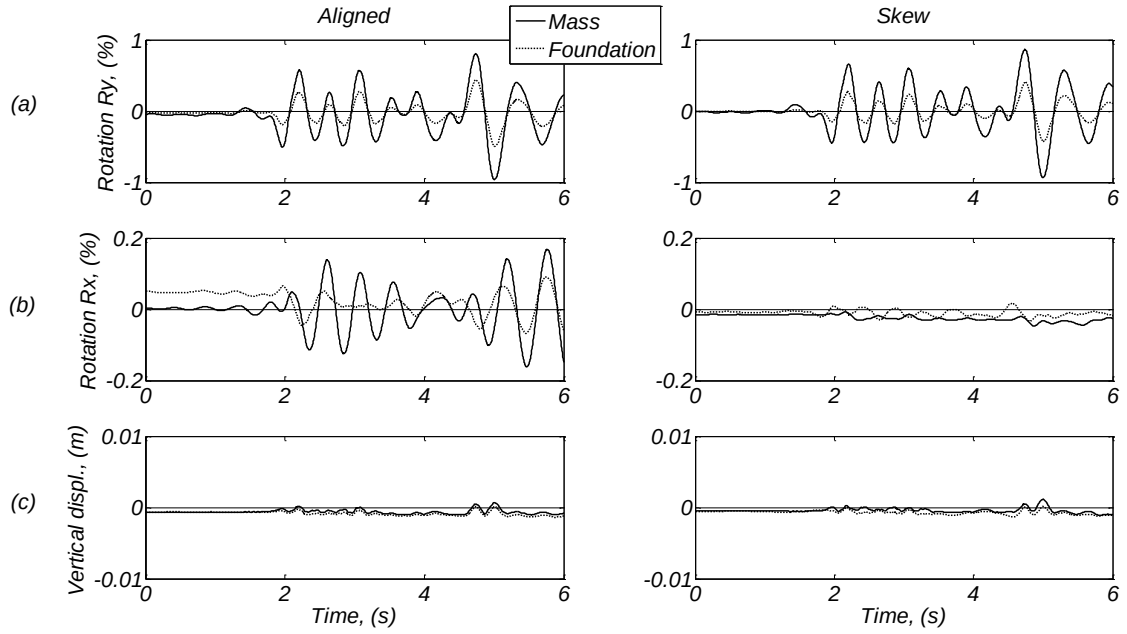

Figure C12. Time histories for the aligned and skew specimens; (a) mass drift ratio for the EW direction and equivalent foundation rotation, (b) mass drift ratio for the NS direction and equivalent foundation rotation, and (c) mass and footing vertical displacements.

Day 1, El Centro #6 1.1 Motion

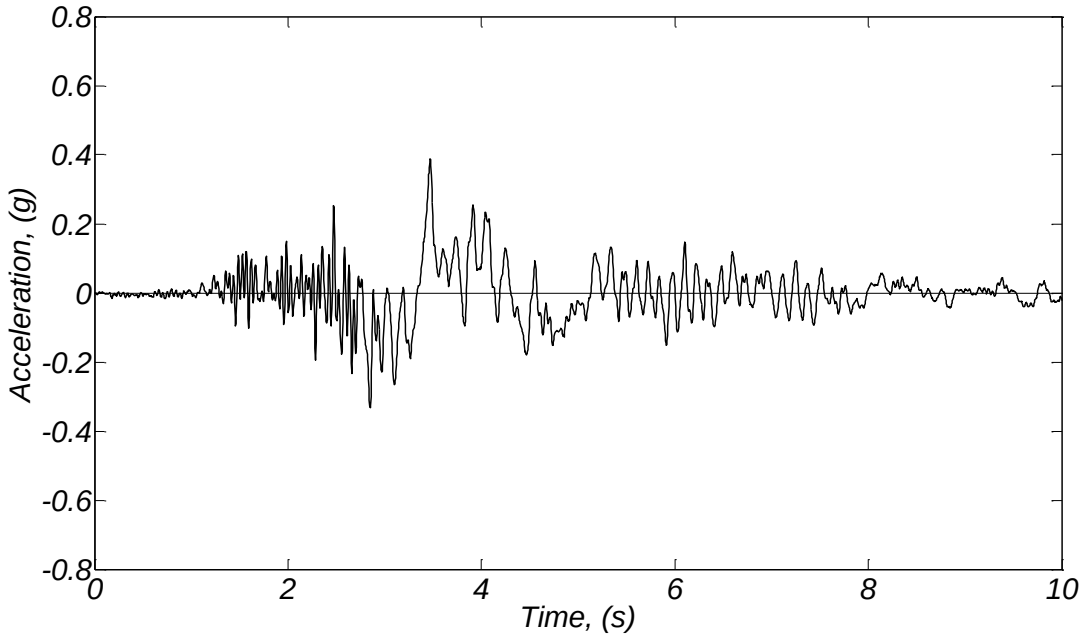

Figure C13. Soil free field acceleration time history (direction of shaking).

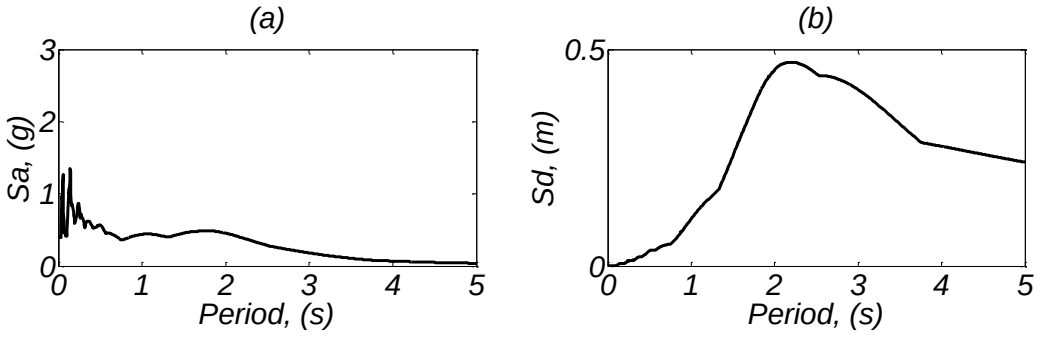

Figure C14. (a) Acceleration and (b) displacement response spectra for the recorded soil free field acceleration (direction of shaking) for damping $\zeta = 3\%$.

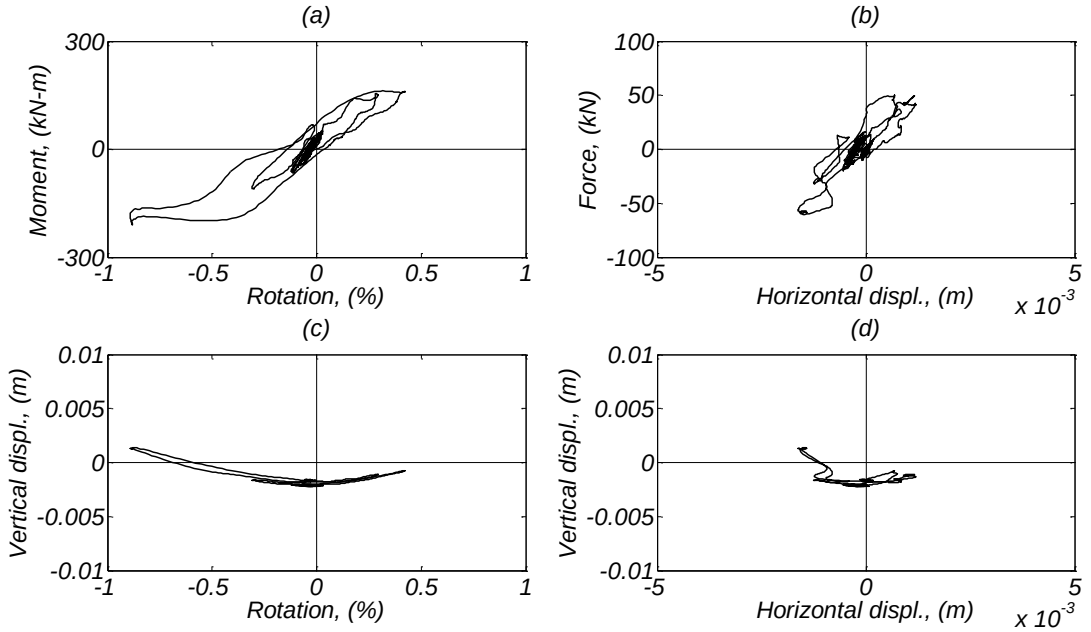

Figure C15. Aligned footing response; (a) moment vs rotation diagram (around NS direction), (b) base shear vs horizontal displacement (EW direction), (c) vertical displacement vs foundation rotation, and (d) vertical displacement vs horizontal displacement in the EW direction.

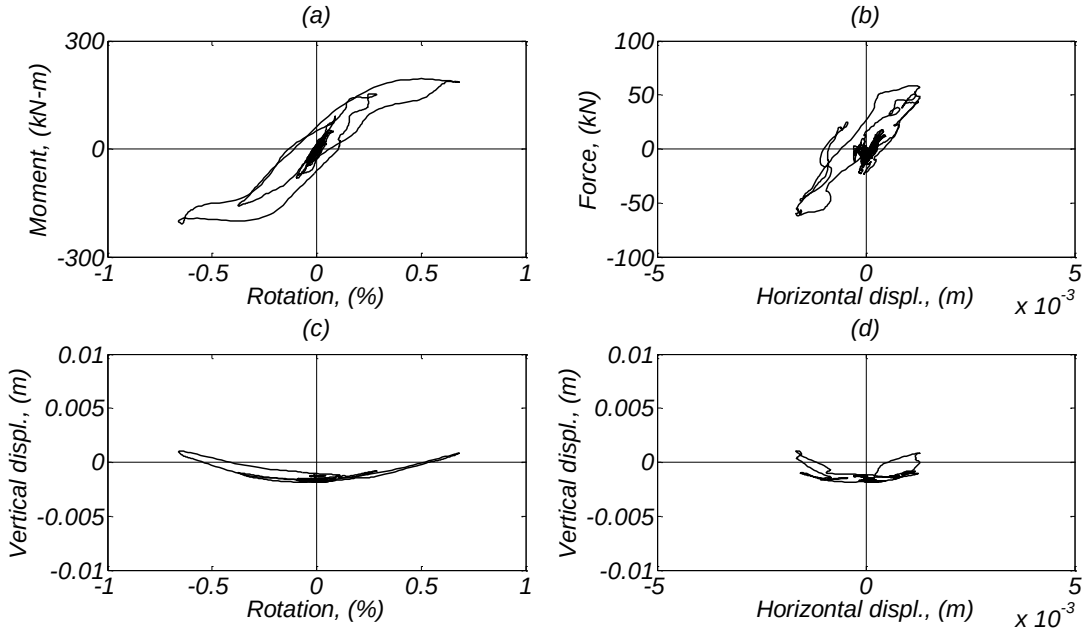

Figure C16. Skew footing response; (a) moment vs rotation diagram (around NS direction), (b) base shear vs horizontal displacement (EW direction), (c) vertical displacement vs foundation rotation, and (d) vertical displacement vs horizontal displacement in the EW direction.

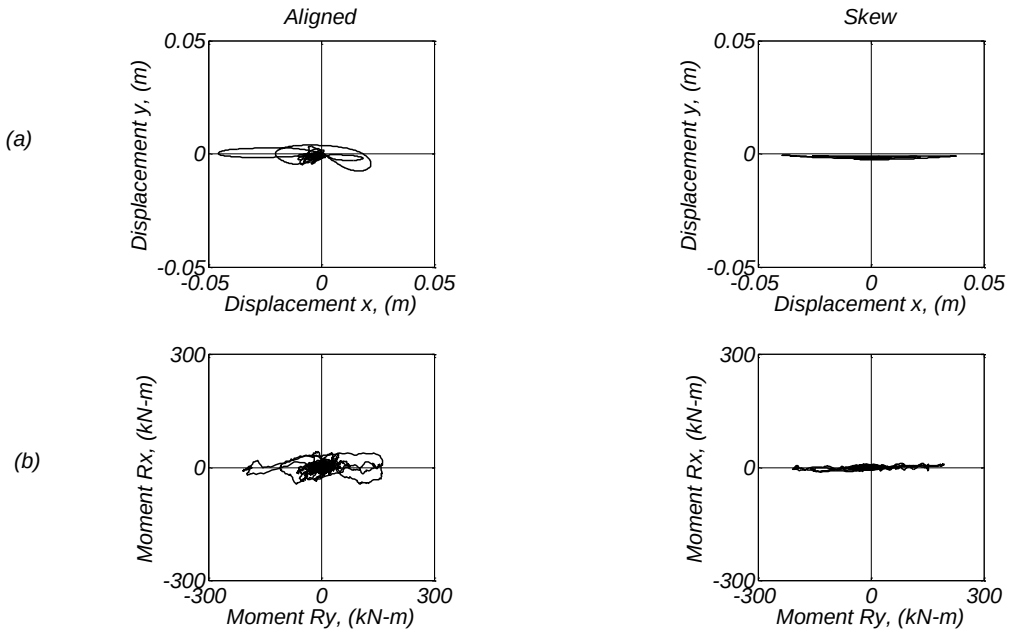

Figure C17. Bilateral response for the aligned and skew specimens; (a) mass displacement for the EW(x) and NS(y) direction, and (b) foundation moment for the corresponding directions.

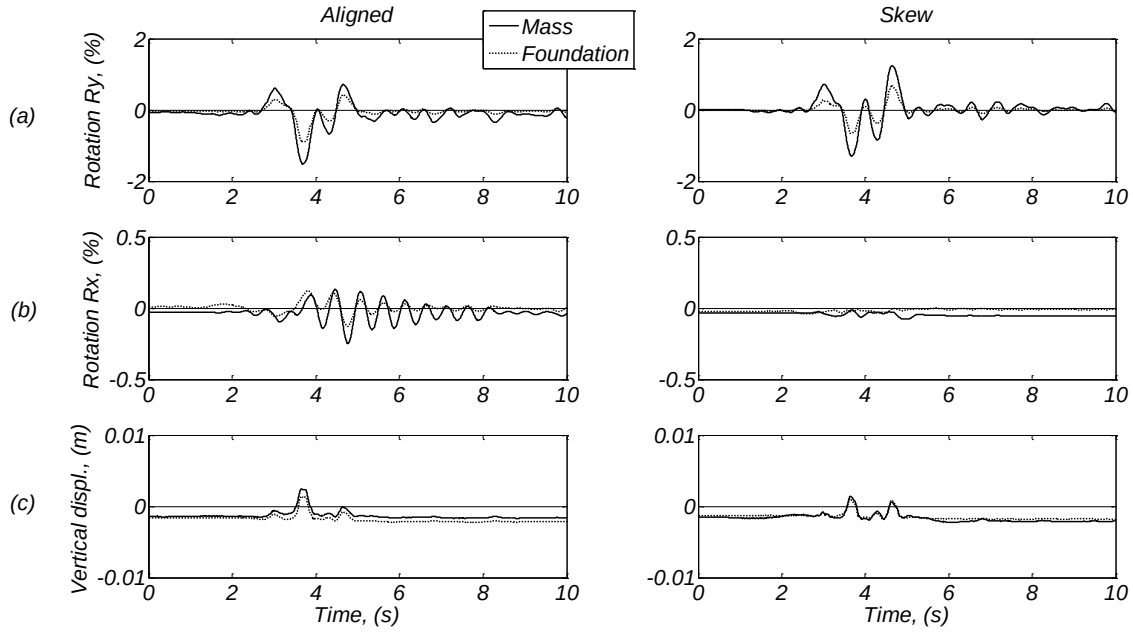

Figure C18. Time histories for the aligned and skew specimens; (a) mass drift ratio for the EW direction and equivalent foundation rotation, (b) mass drift ratio for the NS direction and equivalent foundation rotation, and (c) mass and footing vertical displacements.

Day 1, Pacoima Dam 0.8 Motion

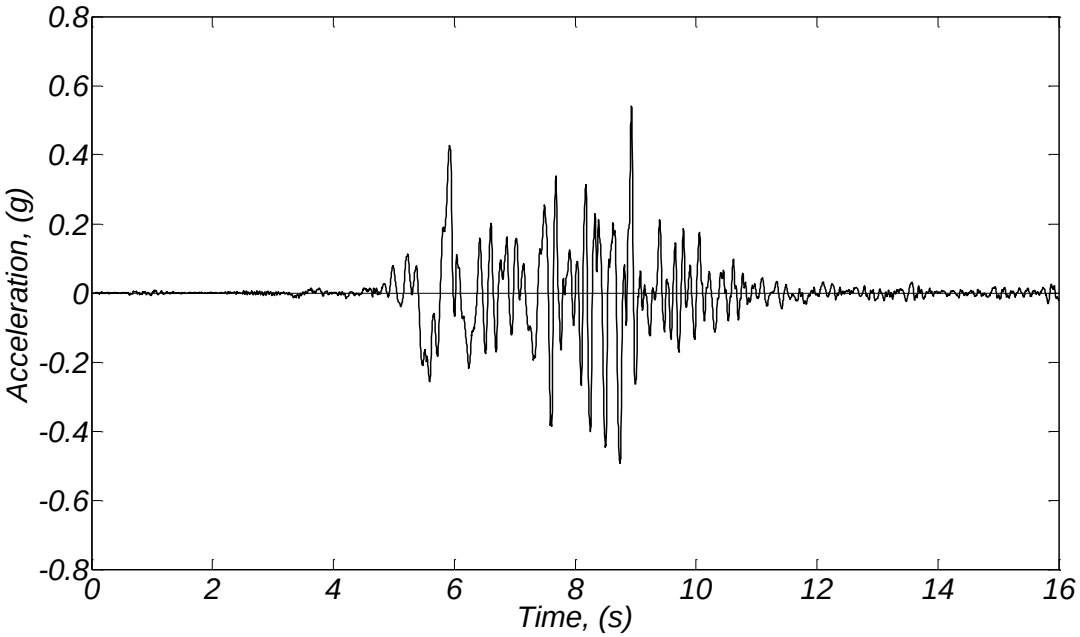

Figure C19. Soil free field acceleration time history (direction of shaking).

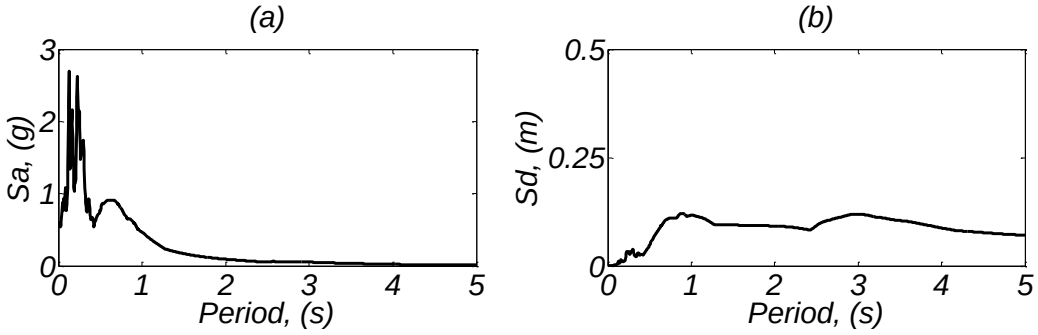

Figure C20. (a) Acceleration and (b) displacement response spectra for the recorded soil free field acceleration (direction of shaking) for damping $\zeta = 3\%$.

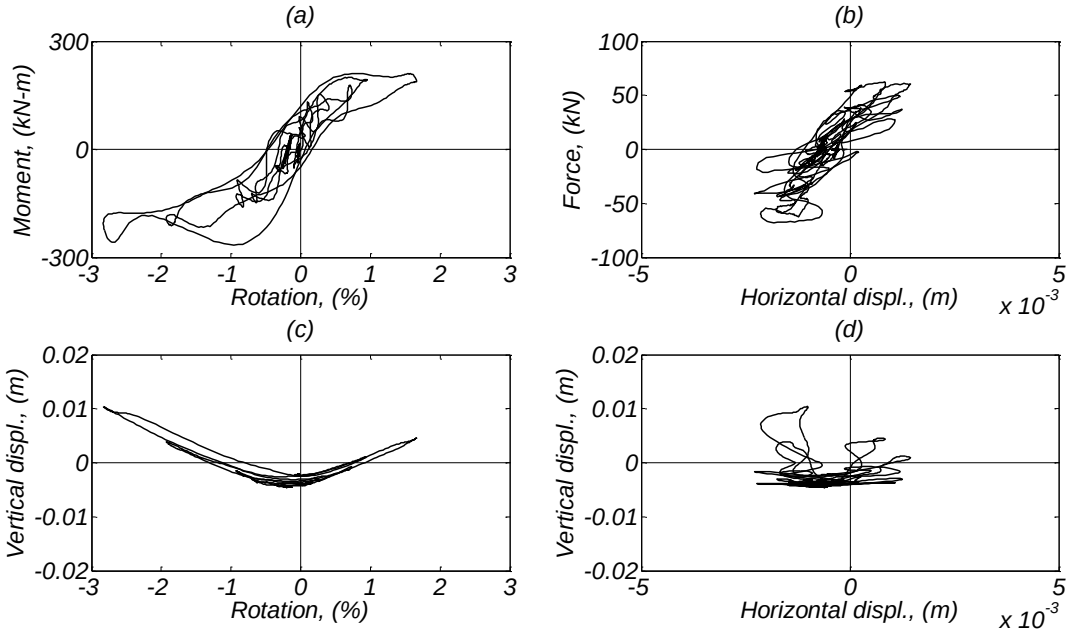

Figure C21. Aligned footing response; (a) moment vs rotation diagram (around NS direction), (b) base shear vs horizontal displacement (EW direction), (c) vertical displacement vs foundation rotation, and (d) vertical displacement vs horizontal displacement in the EW direction.

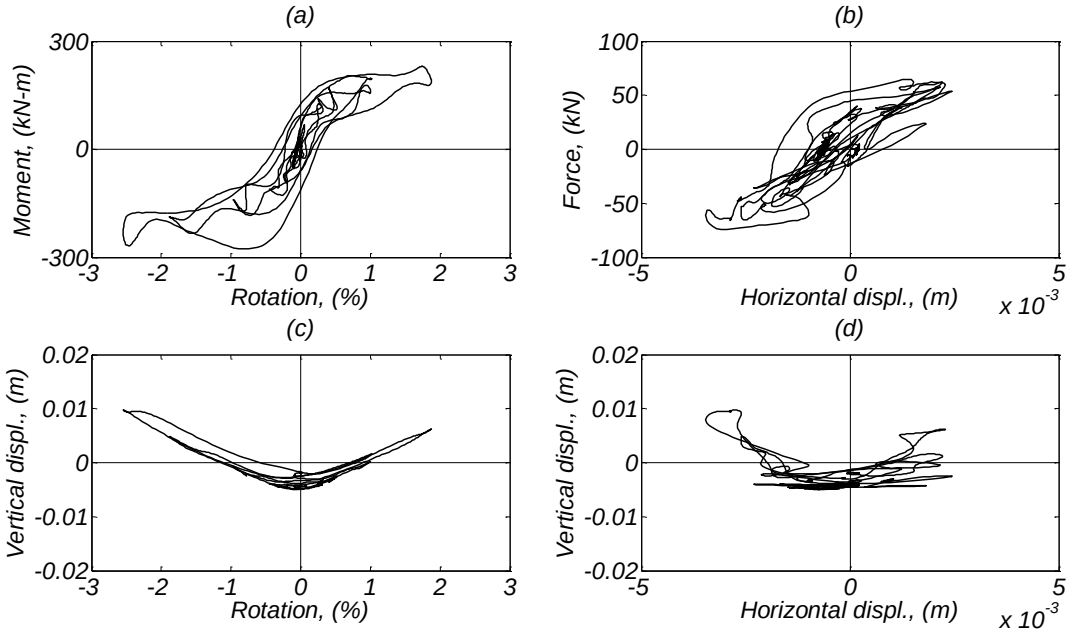

Figure C22. Skew footing response; (a) moment vs rotation diagram (around NS direction), (b) base shear vs horizontal displacement (EW direction), (c) vertical displacement vs foundation rotation, and (d) vertical displacement vs horizontal displacement in the EW direction.

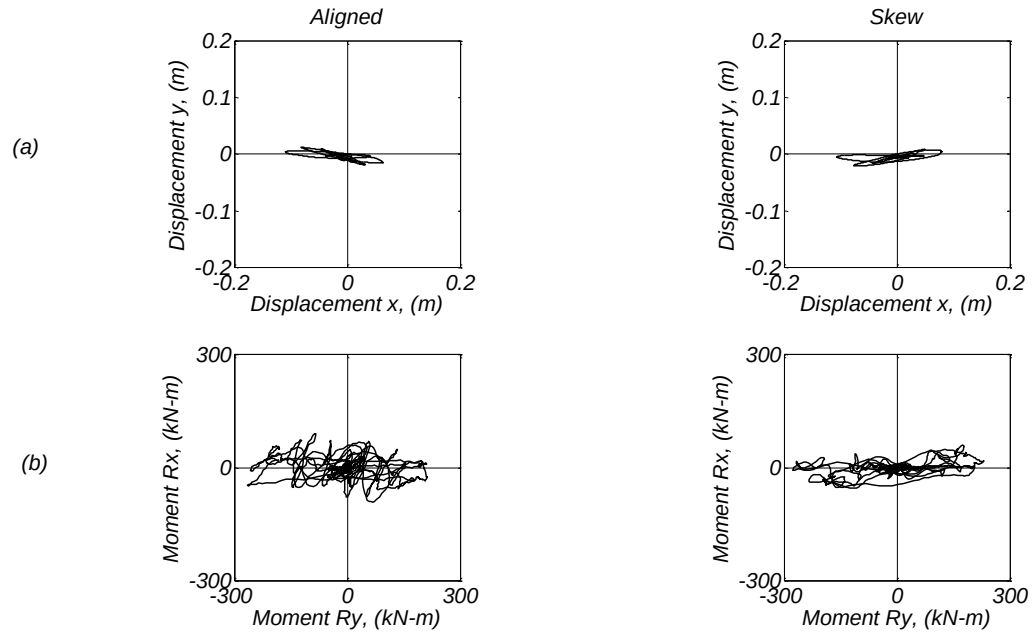

Figure C23. Bilateral response for the aligned and skew specimens; (a) mass displacement for the EW(x) and NS(y) direction, and (b) foundation moment for the corresponding directions.

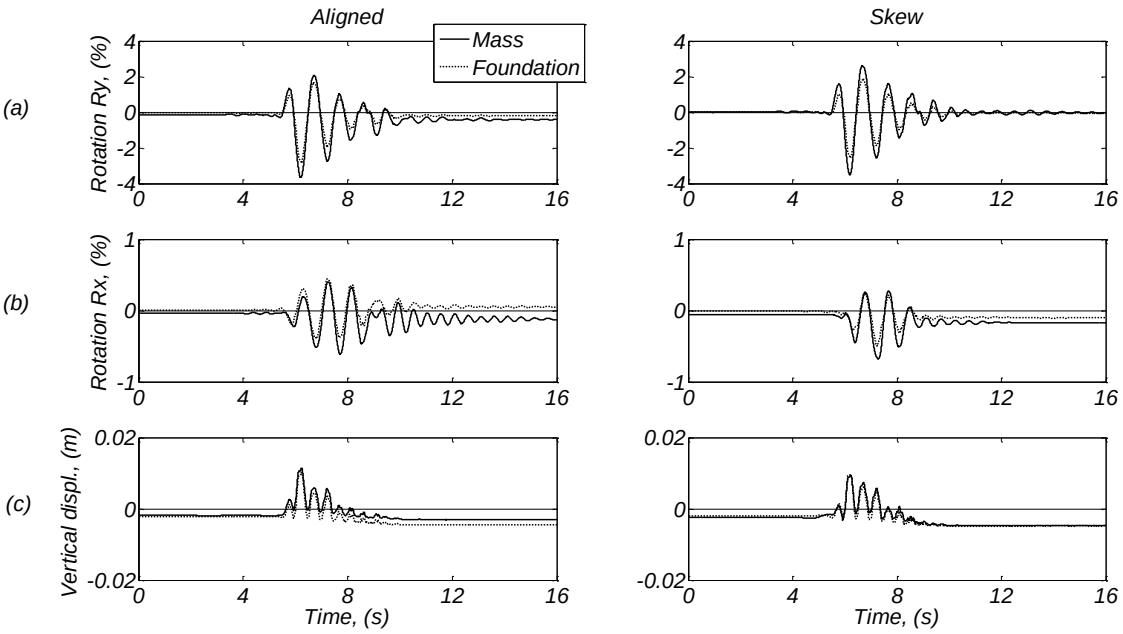

Figure C24. Time histories for the aligned and skew specimens; (a) mass drift ratio for the EW direction and equivalent foundation rotation, (b) mass drift ratio for the NS direction and equivalent foundation rotation, and (c) mass and footing vertical displacements.

Day 1, Takatori 0.5 Motion

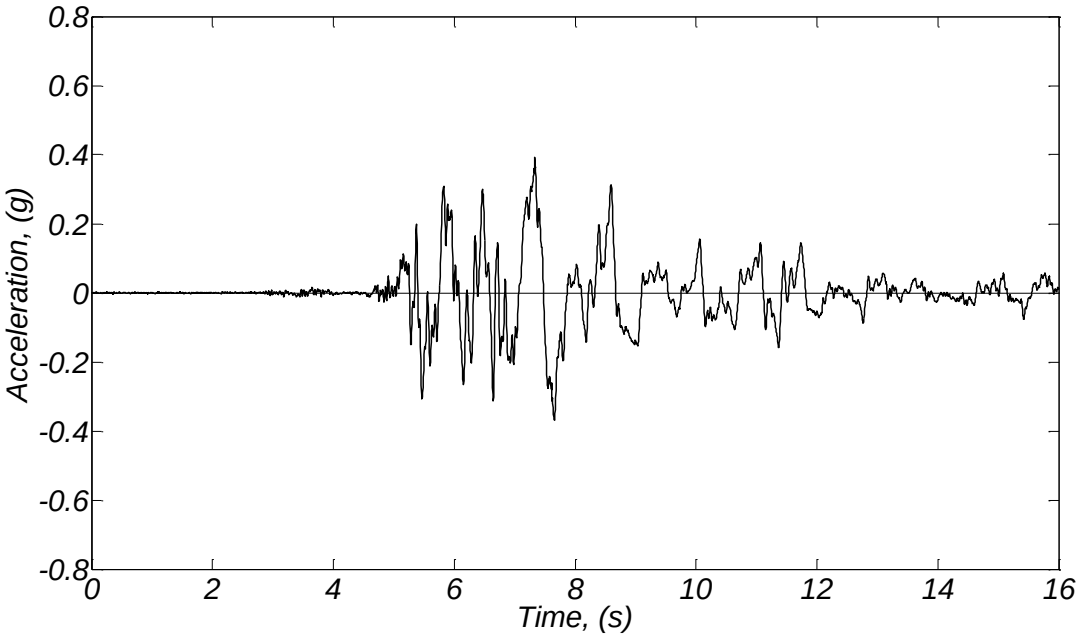

Figure C25. Soil free field acceleration time history (direction of shaking).

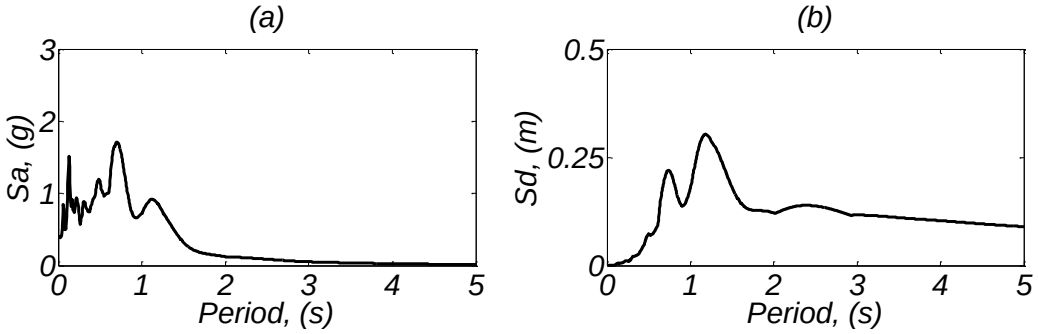

Figure C26. (a) Acceleration and (b) displacement response spectra for the recorded soil free field acceleration (direction of shaking) for damping ζ = 3%.

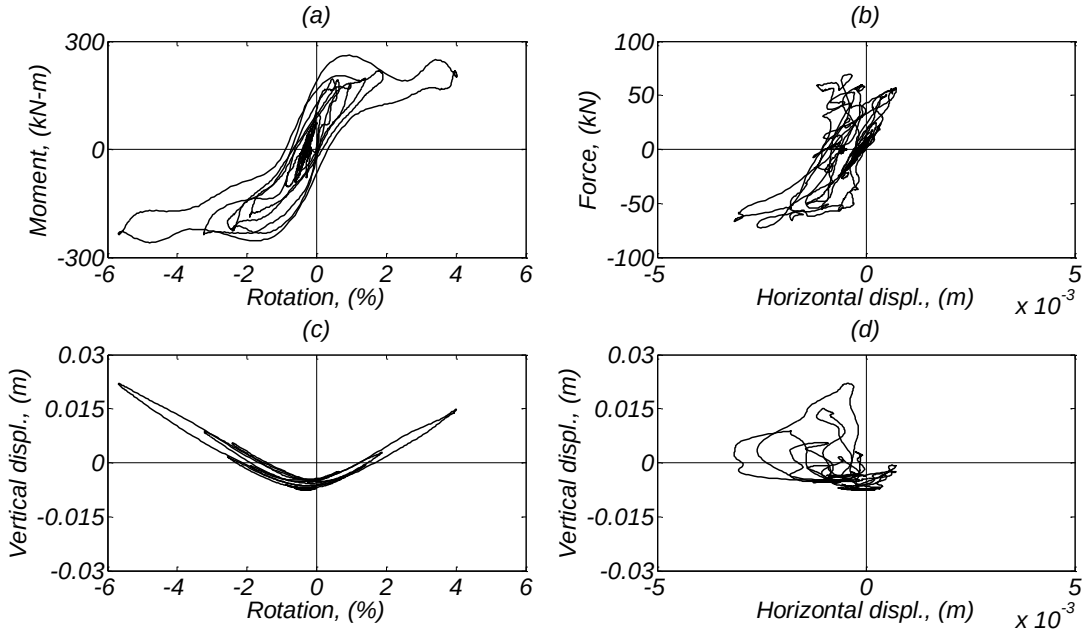

Figure C27. Aligned footing response; (a) moment vs rotation diagram (around NS direction), (b) base shear vs horizontal displacement (EW direction), (c) vertical displacement vs foundation rotation, and (d) vertical displacement vs horizontal displacement in the EW direction.

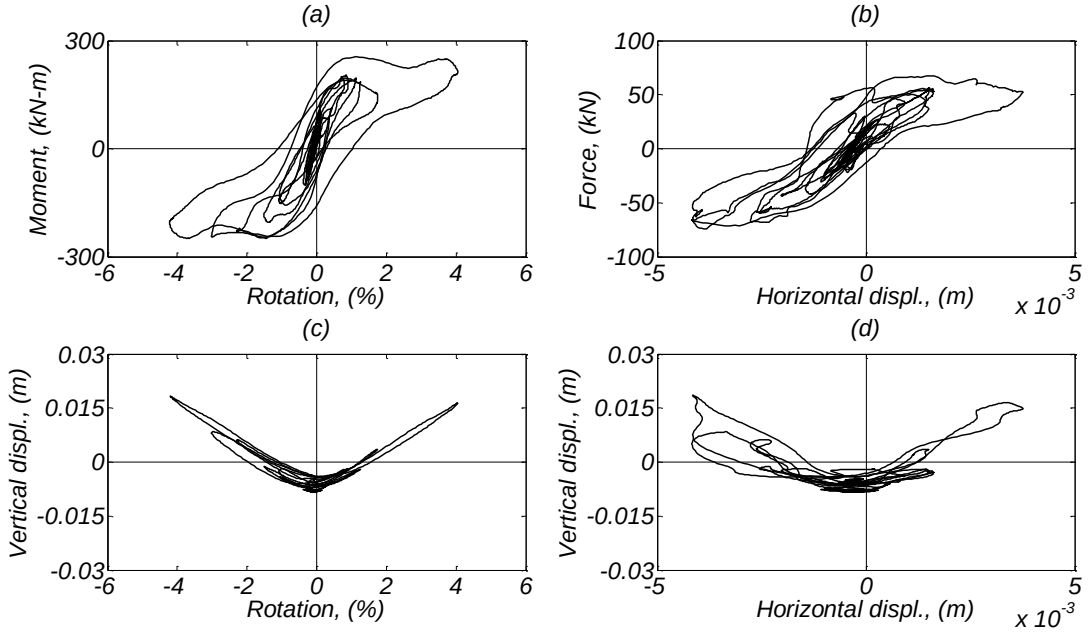

Figure C28. Skew footing response; (a) moment vs rotation diagram (around NS direction), (b) base shear vs horizontal displacement (EW direction), (c) vertical displacement vs foundation rotation, and (d) vertical displacement vs horizontal displacement in the EW direction.

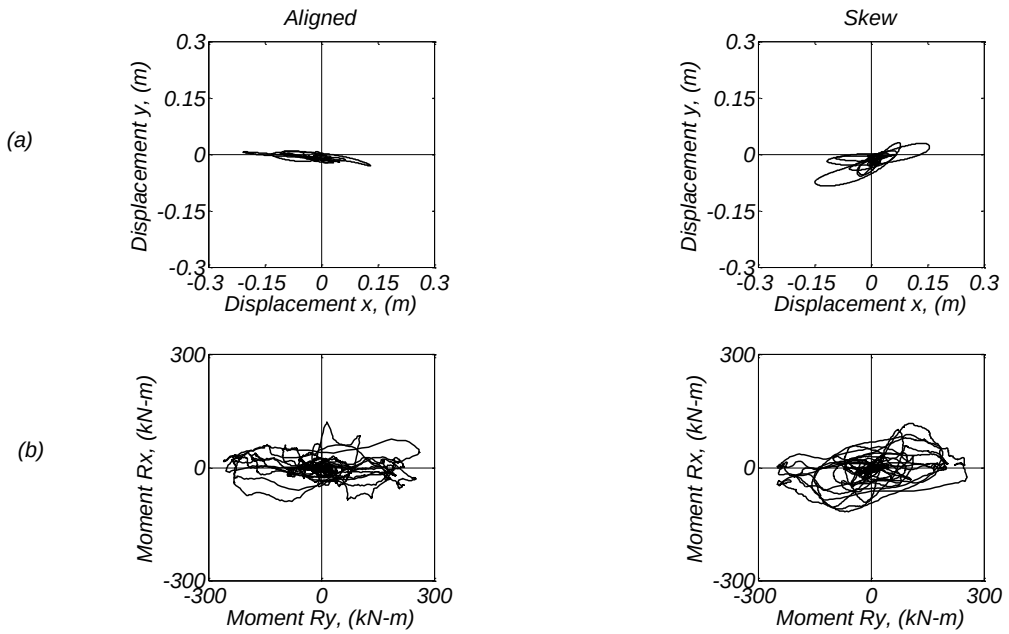

Figure C29. Bilateral response for the aligned and skew specimens; (a) mass displacement for the EW(x) and NS(y) direction, and (b) foundation moment for the corresponding directions.

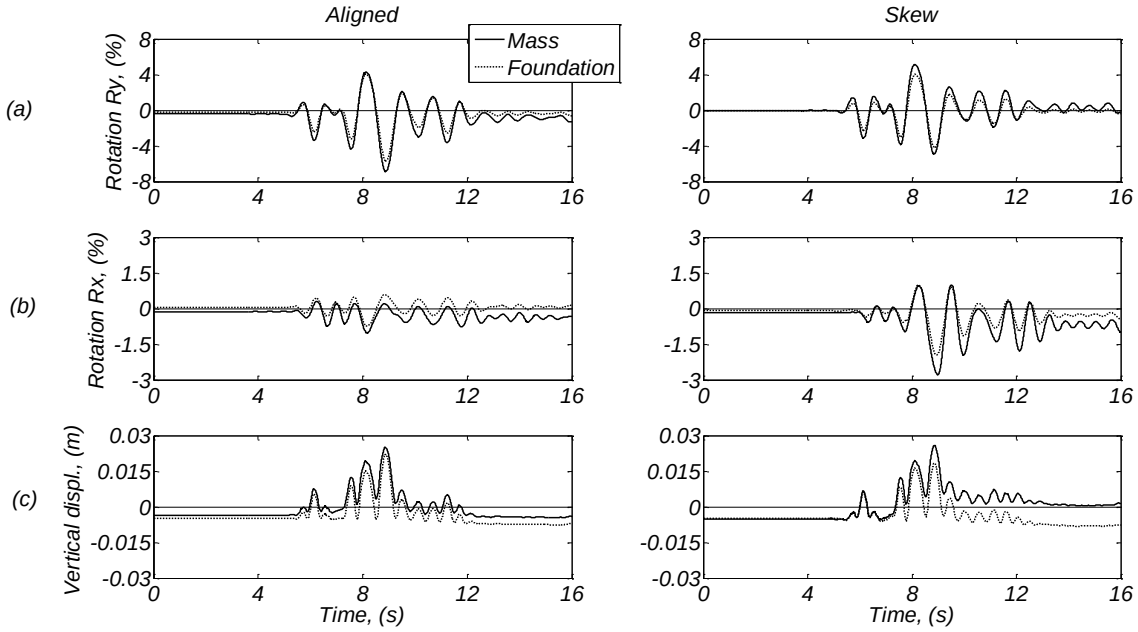

Figure C30. Time histories for the aligned and skew specimens; (a) mass drift ratio for the EW direction and equivalent foundation rotation, (b) mass drift ratio for the NS direction and equivalent foundation rotation, and (c) mass and footing vertical displacements.

Day 1, Takatori 1.0 Motion

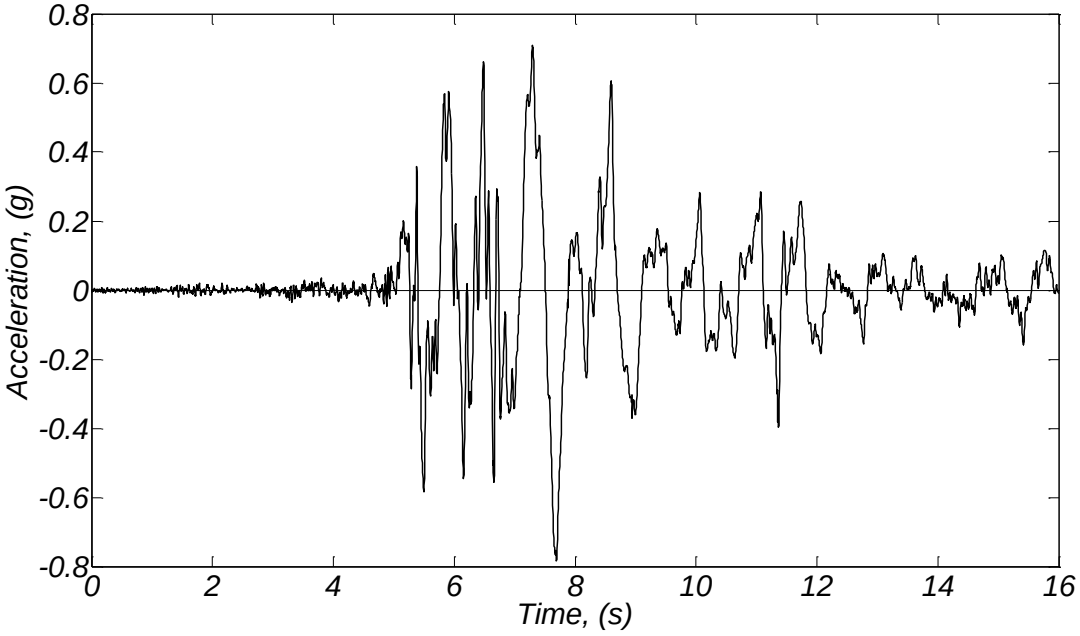

Figure C31. Soil free field acceleration time history (direction of shaking).

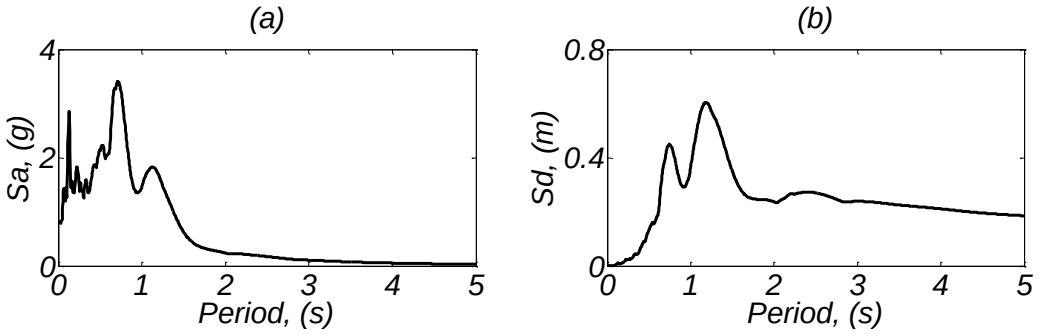

Figure C32. (a) Acceleration and (b) displacement response spectra for the recorded soil free field acceleration (direction of shaking) for damping ζ = 3%.

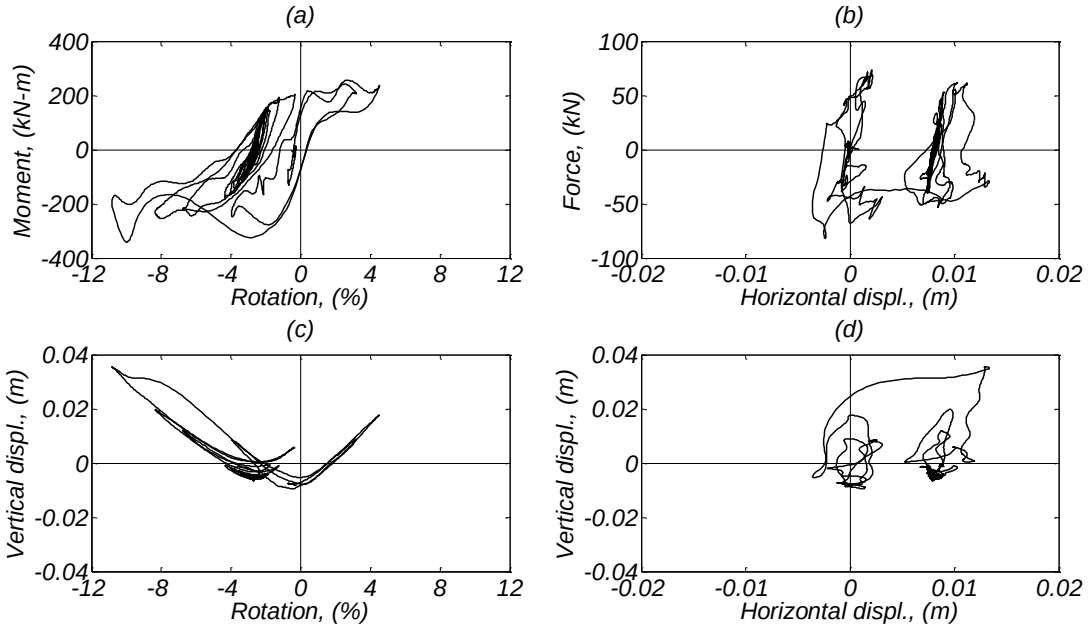

Figure C33. Aligned footing response; (a) moment vs rotation diagram (around NS direction), (b) base shear vs horizontal displacement (EW direction), (c) vertical displacement vs foundation rotation, and (d) vertical displacement vs horizontal displacement in the EW direction.

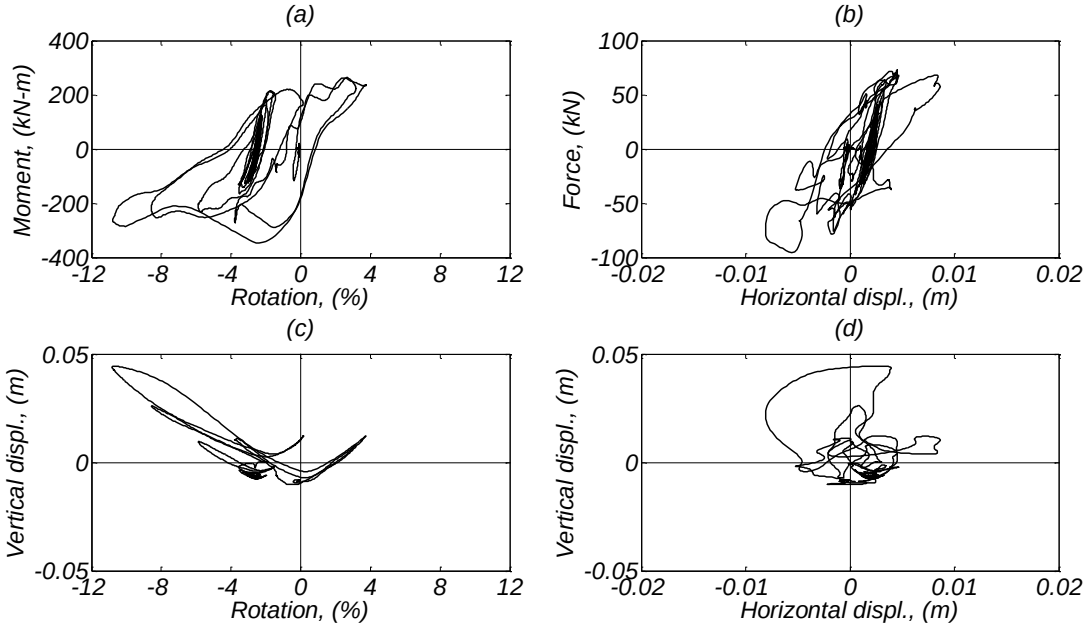

Figure C34. Skew footing response; (a) moment vs rotation diagram (around NS direction), (b) base shear vs horizontal displacement (EW direction), (c) vertical displacement vs foundation rotation, and (d) vertical displacement vs horizontal displacement in the EW direction.

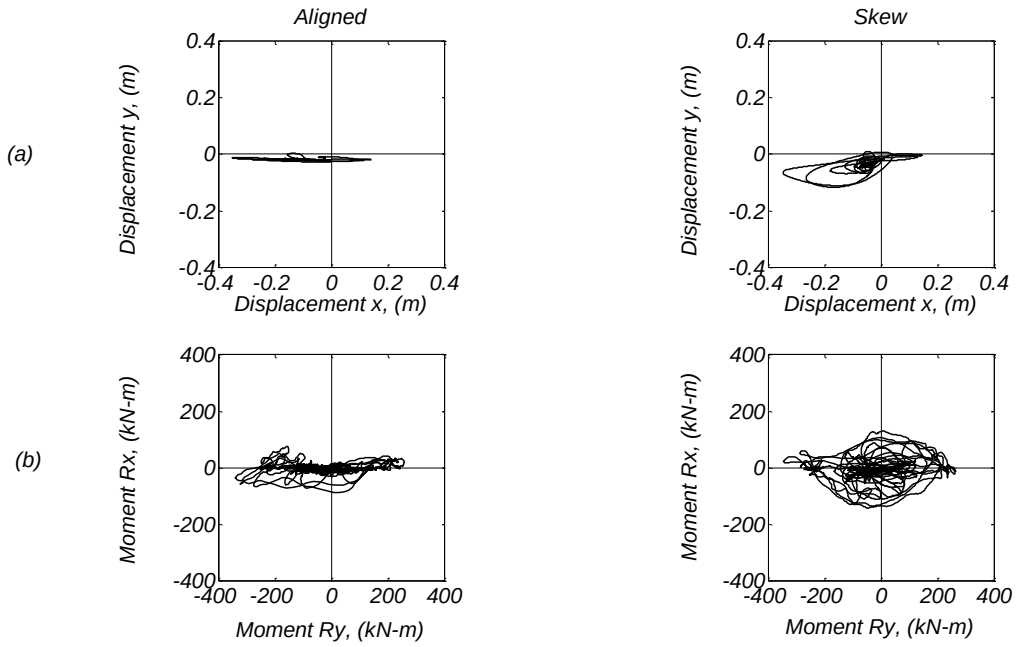

Figure C35. Bilateral response for the aligned and skew specimens; (a) mass displacement for the EW(x) and NS(y) direction, and (b) foundation moment for the corresponding directions.

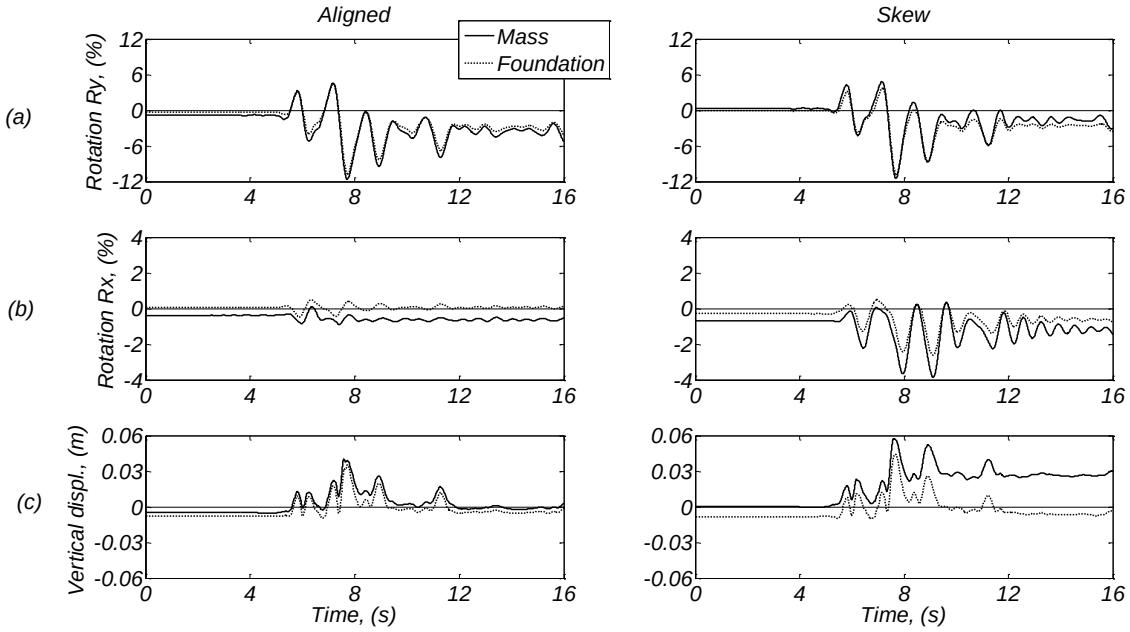

Figure C36. Time histories for the aligned and skew specimens; (a) mass drift ratio for the EW direction and equivalent foundation rotation, (b) mass drift ratio for the NS direction and equivalent foundation rotation, and (c) mass and footing vertical displacements.

Day 2, Gilroy #1 1.0 Motion

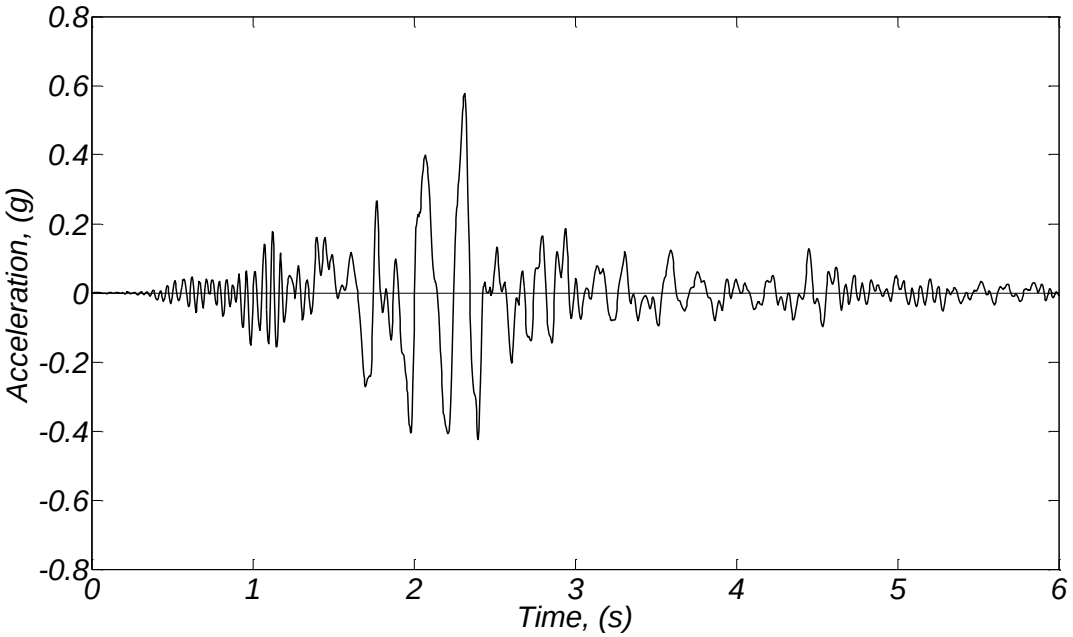

Figure C37. Soil free field acceleration time history (direction of shaking).

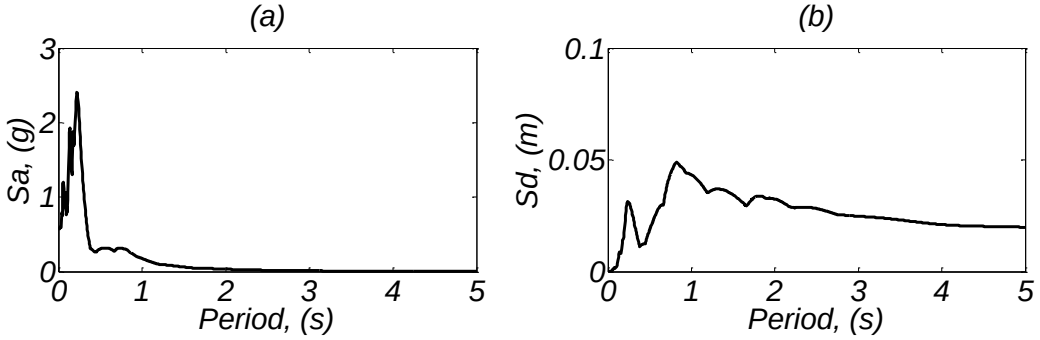

Figure C38. (a) Acceleration and (b) displacement response spectra for the recorded soil free field acceleration (direction of shaking) for damping ζ = 3%.

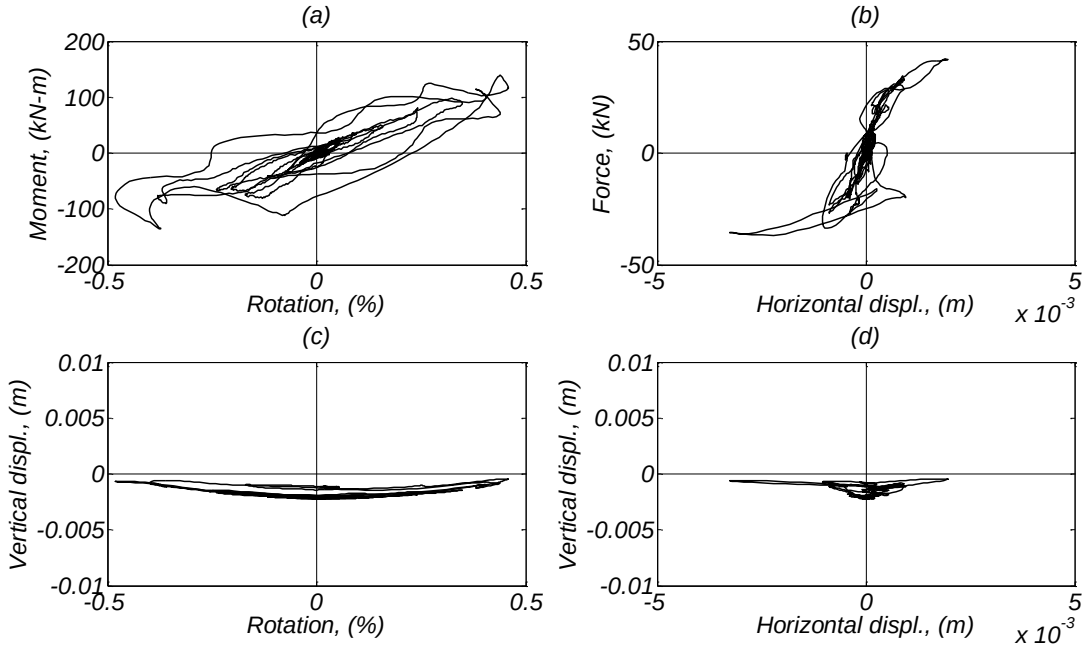

Figure C39. Aligned footing response; (a) moment vs rotation diagram (around NS direction), (b) base shear vs horizontal displacement (EW direction), (c) vertical displacement vs foundation rotation, and (d) vertical displacement vs horizontal displacement in the EW direction.

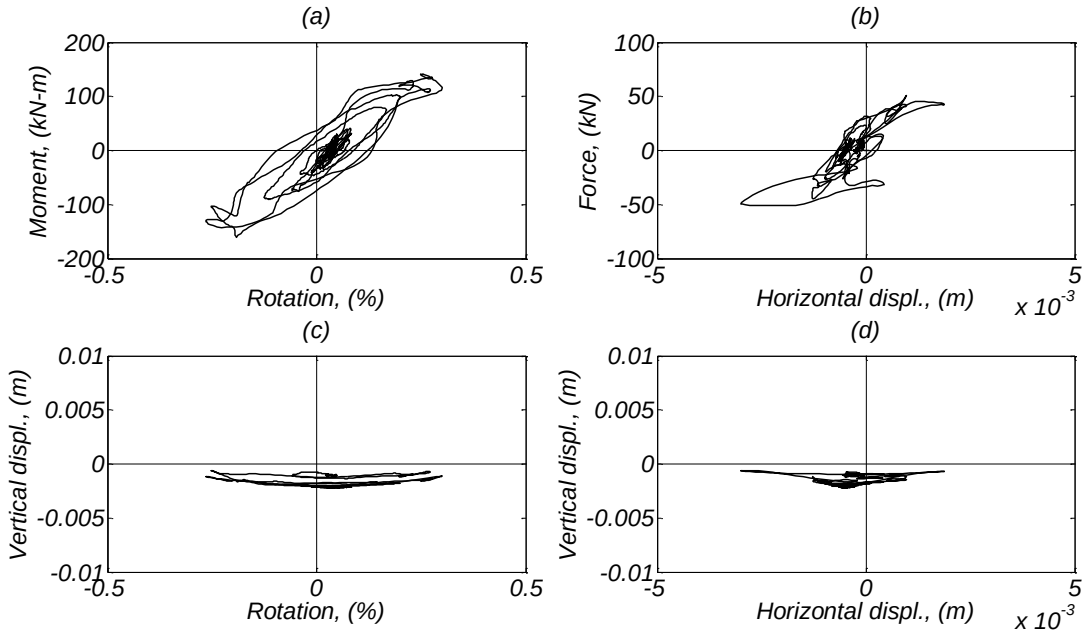

Figure C40. Skew footing response; (a) moment vs rotation diagram (around NS direction), (b) base shear vs horizontal displacement (EW direction), (c) vertical displacement vs foundation rotation, and (d) vertical displacement vs horizontal displacement in the EW direction.

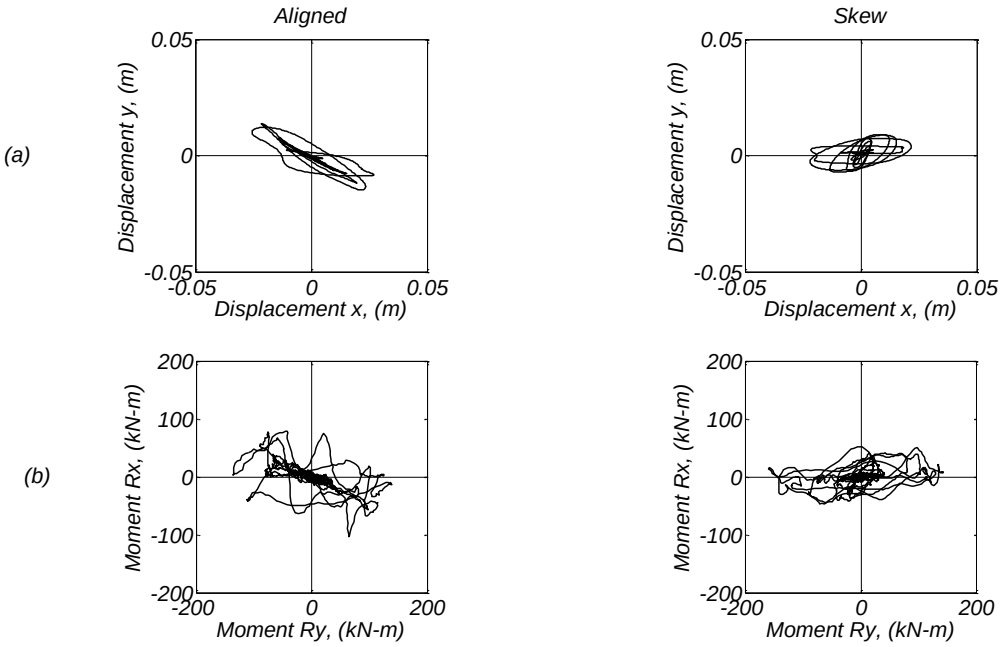

Figure C41. Bilateral response for the aligned and skew specimens; (a) mass displacement for the EW(x) and NS(y) direction, and (b) foundation moment for the corresponding directions.

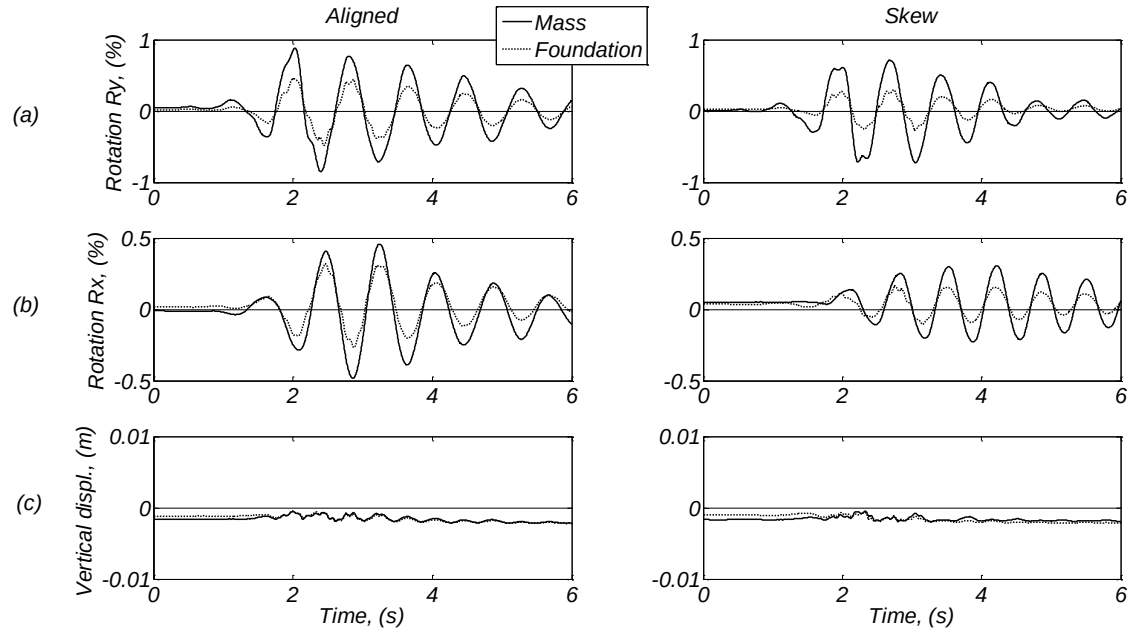

Figure C42. Time histories for the aligned and skew specimens; (a) mass drift ratio for the EW direction and equivalent foundation rotation, (b) mass drift ratio for the NS direction and equivalent foundation rotation, and (c) mass and footing vertical displacements.

Day 2, Corralitos 0.8 Motion

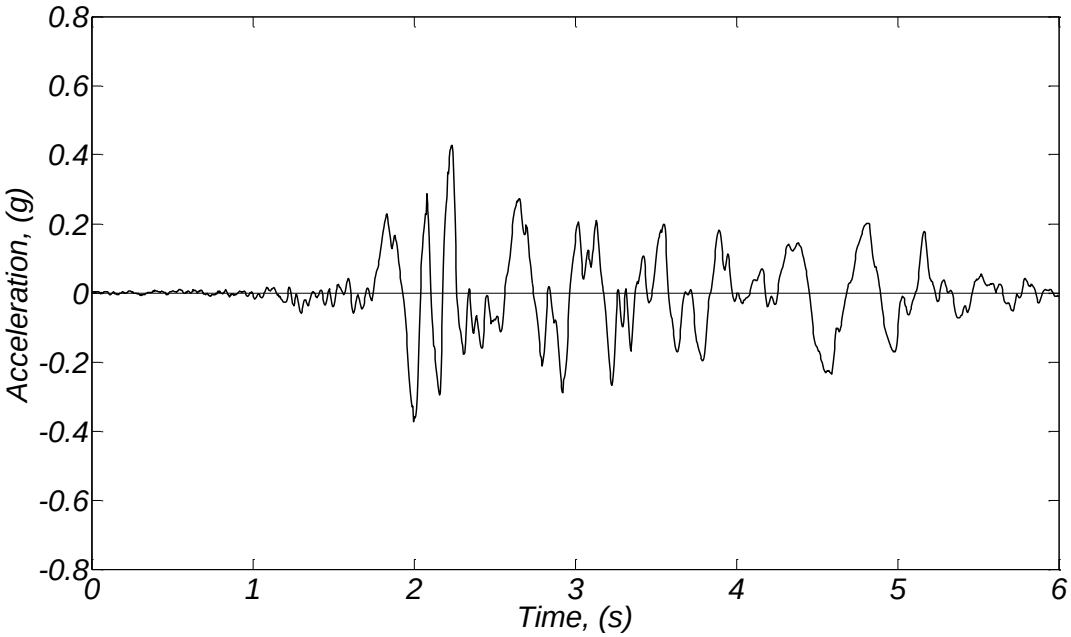

Figure C43. Soil free field acceleration time history (direction of shaking).

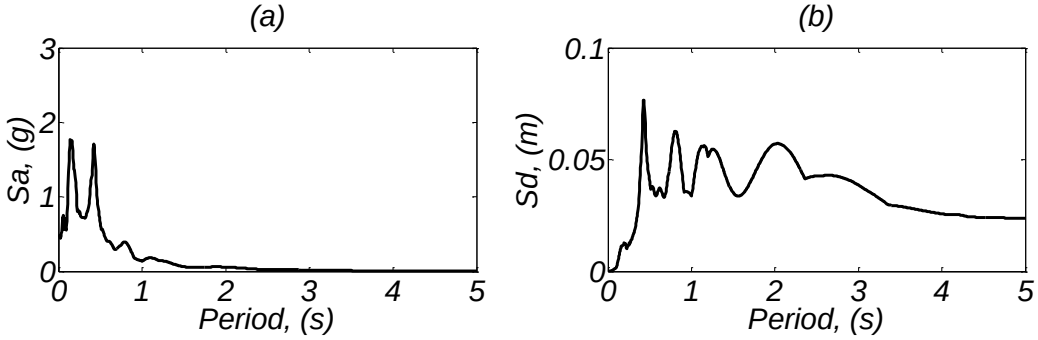

Figure C44. (a) Acceleration and (b) displacement response spectra for the recorded soil free field acceleration (direction of shaking) for damping $\zeta = 3\%$.

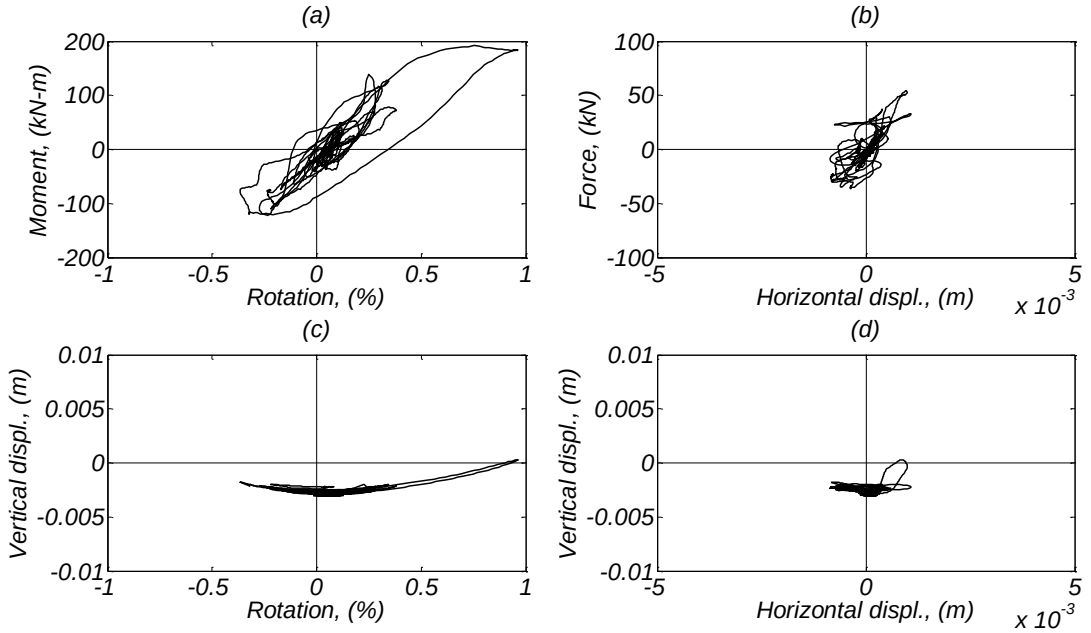

Figure C45. Aligned footing response; (a) moment vs rotation diagram (around NS direction), (b) base shear vs horizontal displacement (EW direction), (c) vertical displacement vs foundation rotation, and (d) vertical displacement vs horizontal displacement in the EW direction.

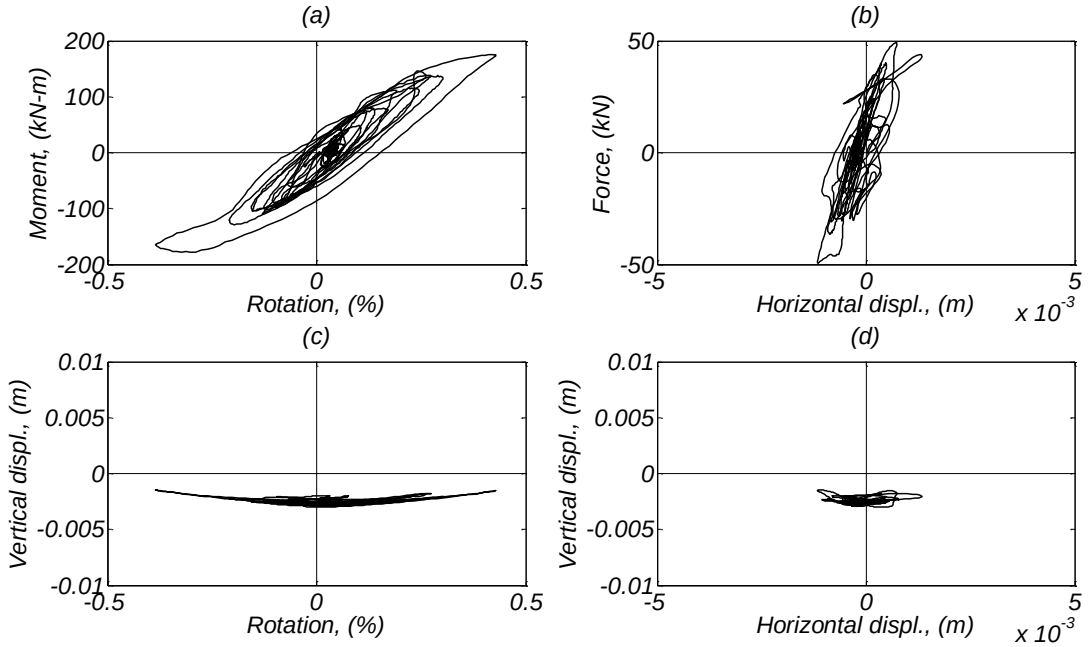

Figure C46. Skew footing response; (a) moment vs rotation diagram (around NS direction), (b) base shear vs horizontal displacement (EW direction), (c) vertical displacement vs foundation rotation, and (d) vertical displacement vs horizontal displacement in the EW direction.

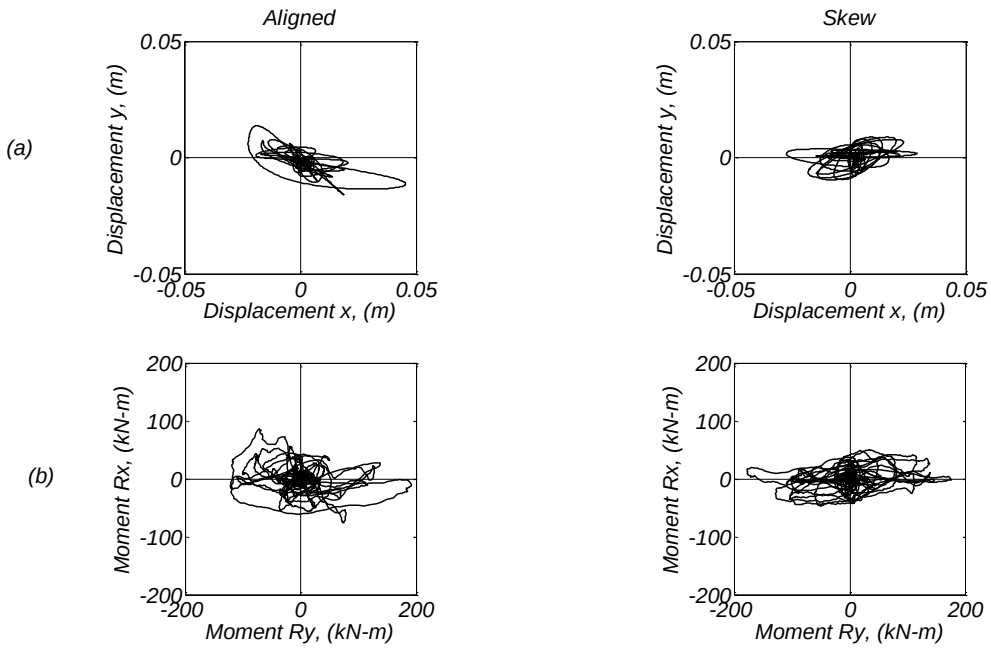

Figure C47. Bilateral response for the aligned and skew specimens; (a) mass displacement for the EW(x) and NS(y) direction, and (b) foundation moment for the corresponding directions.

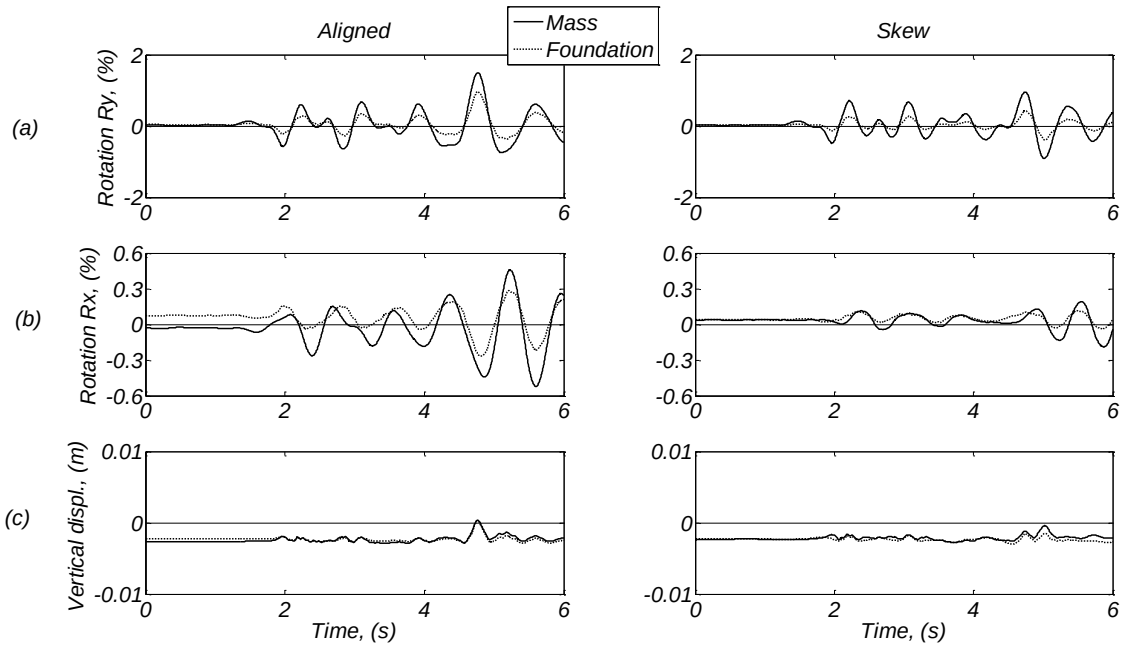

Figure C48. Time histories for the aligned and skew specimens; (a) mass drift ratio for the EW direction and equivalent foundation rotation, (b) mass drift ratio for the NS direction and equivalent foundation rotation, and (c) mass and footing vertical displacements.

Day 2, El Centro #6 1.1 Motion

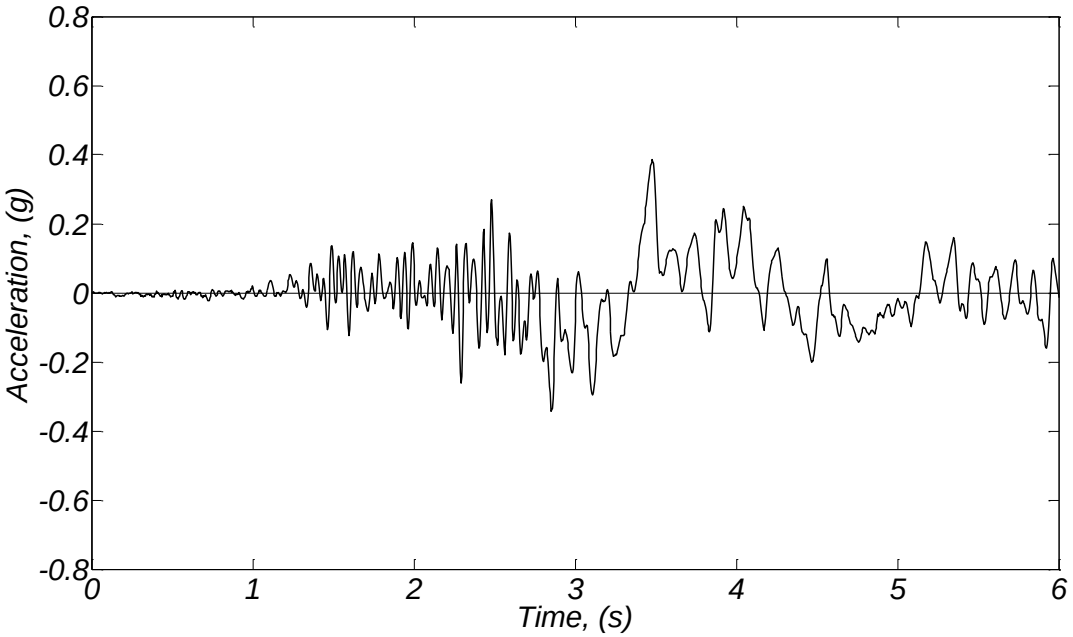

Figure C49. Soil free field acceleration time history (direction of shaking).

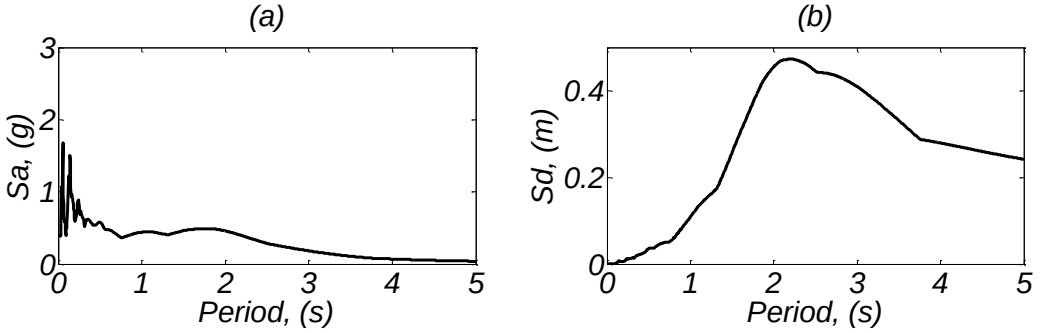

Figure C50. (a) Acceleration and (b) displacement response spectra for the recorded soil free field acceleration (direction of shaking) for damping ζ = 3%.

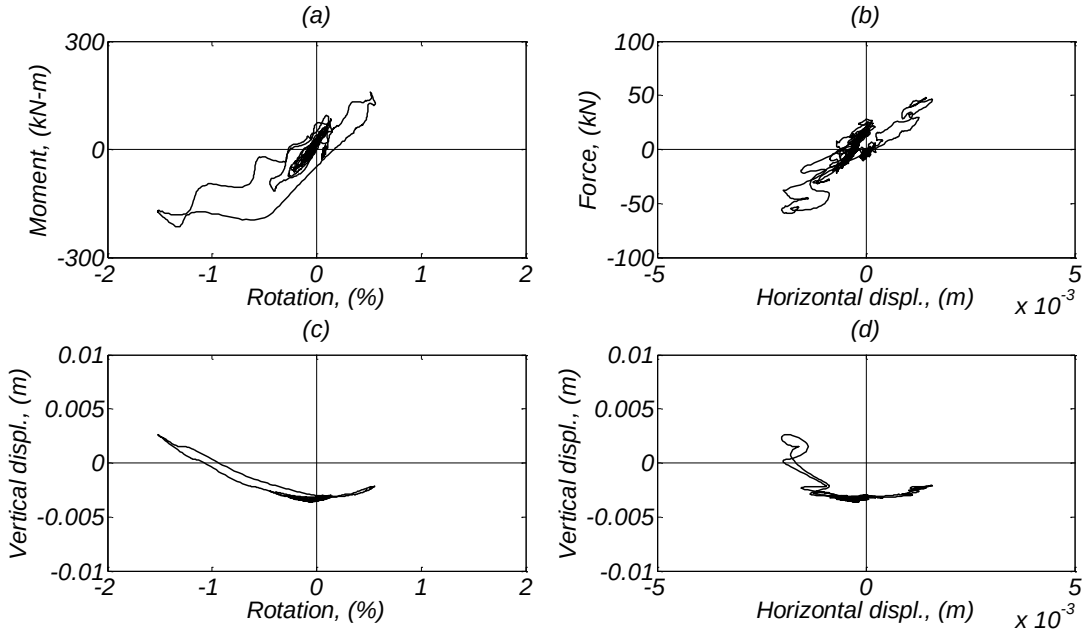

Figure C51. Aligned footing response; (a) moment vs rotation diagram (around NS direction), (b) base shear vs horizontal displacement (EW direction), (c) vertical displacement vs foundation rotation, and (d) vertical displacement vs horizontal displacement in the EW direction.

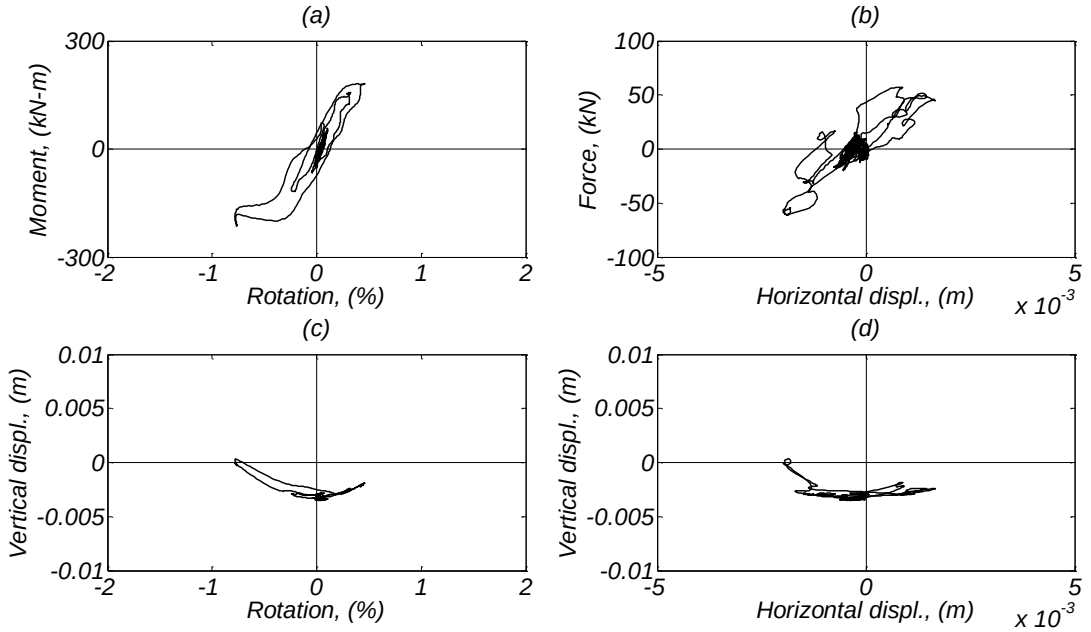

Figure C52. Skew footing response; (a) moment vs rotation diagram (around NS direction), (b) base shear vs horizontal displacement (EW direction), (c) vertical displacement vs foundation rotation, and (d) vertical displacement vs horizontal displacement in the EW direction.

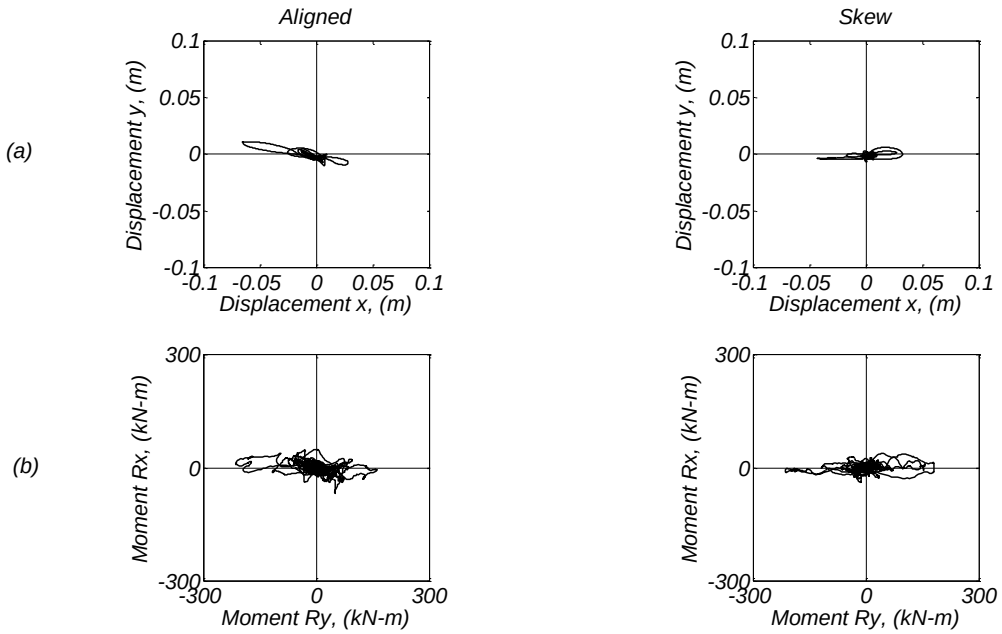

Figure C53. Bilateral response for the aligned and skew specimens; (a) mass displacement for the EW(x) and NS(y) direction, and (b) foundation moment for the corresponding directions.

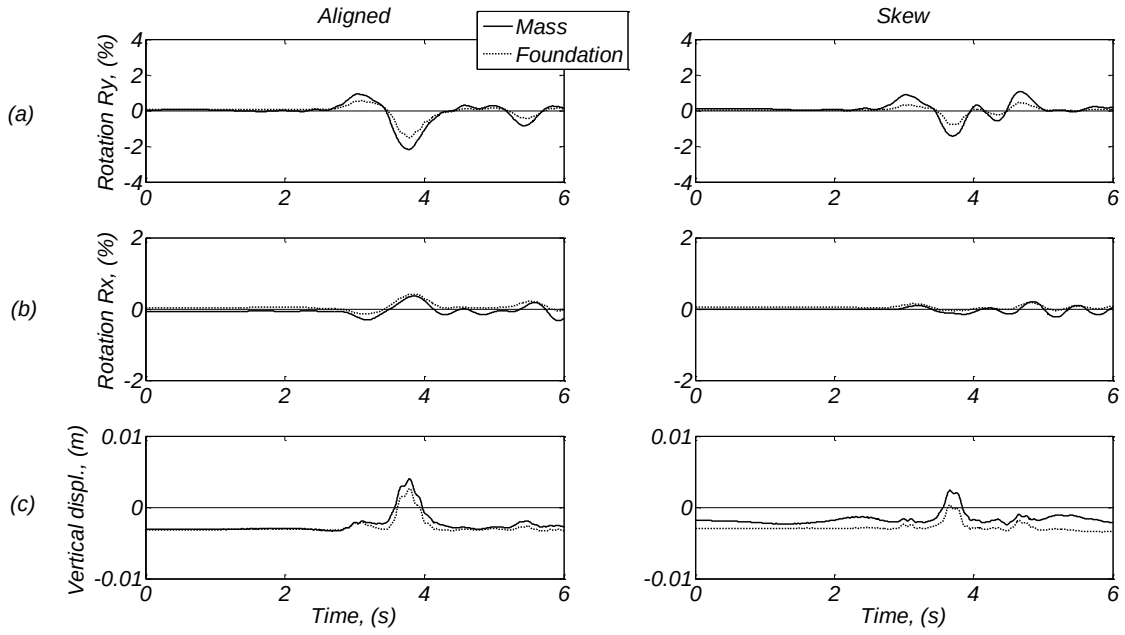

Figure C54. Time histories for the aligned and skew specimens; (a) mass drift ratio for the EW direction and equivalent foundation rotation, (b) mass drift ratio for the NS direction and equivalent foundation rotation, and (c) mass and footing vertical displacements.

Day 2, Pacoima dam 0.8 Motion

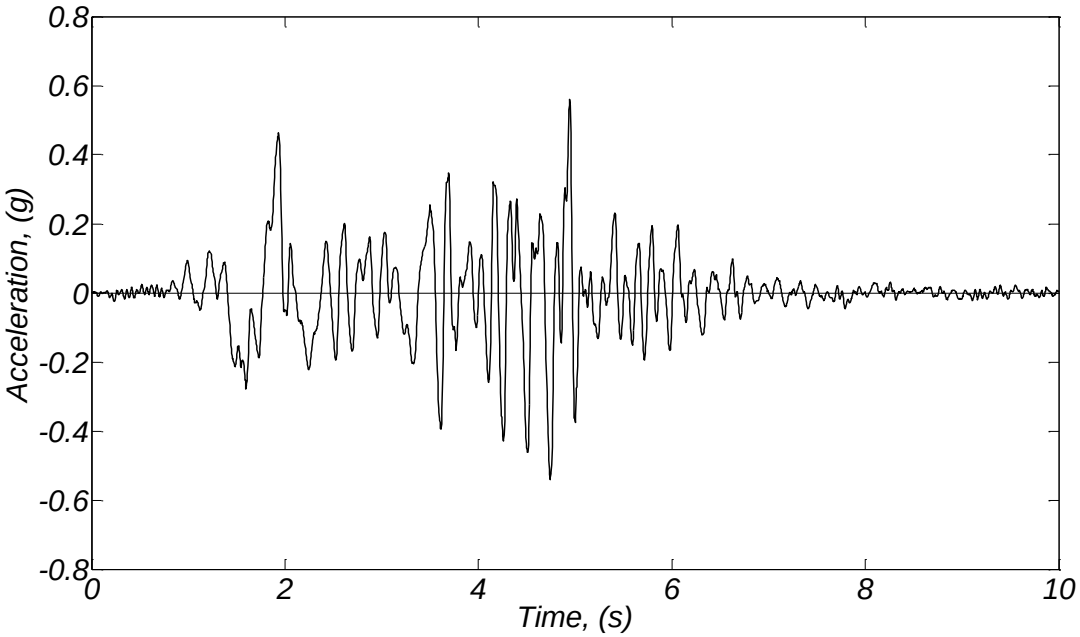

Figure C55. Soil free field acceleration time history (direction of shaking).

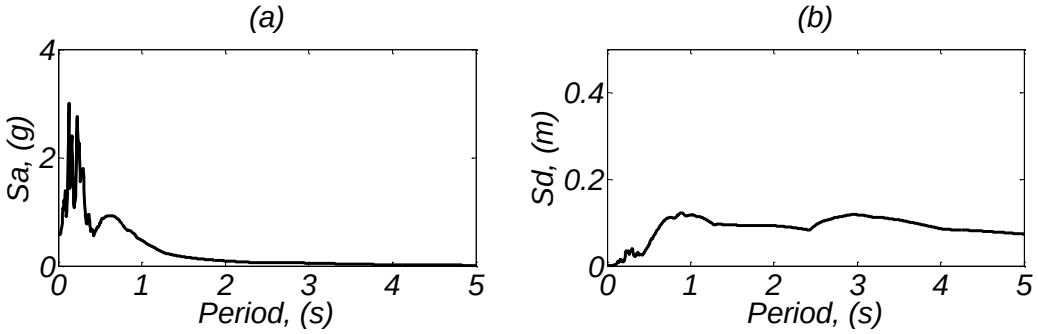

Figure C56. (a) Acceleration and (b) displacement response spectra for the recorded soil free field acceleration (direction of shaking) for damping ζ = 3%.

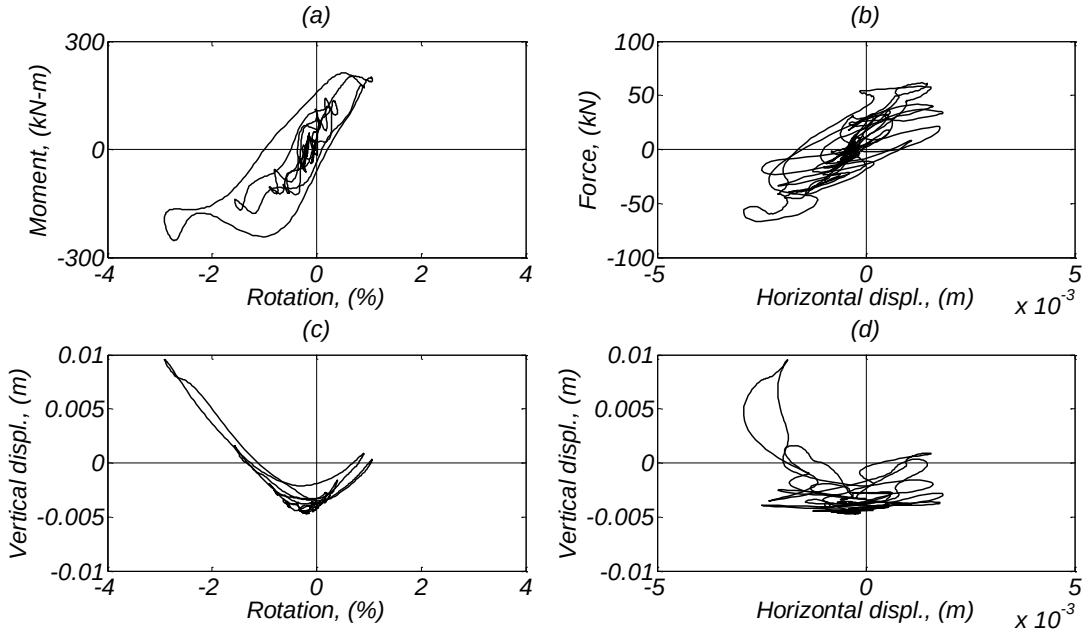

Figure C57. Aligned footing response; (a) moment vs rotation diagram (around NS direction), (b) base shear vs horizontal displacement (EW direction), (c) vertical displacement vs foundation rotation, and (d) vertical displacement vs horizontal displacement in the EW direction.

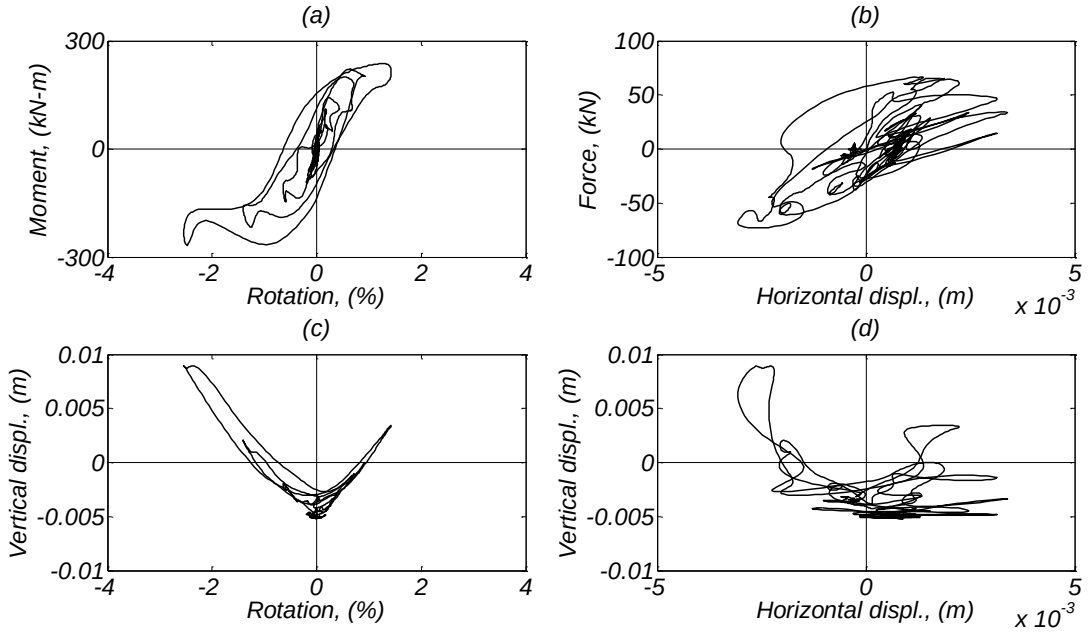

Figure C58. Skew footing response; (a) moment vs rotation diagram (around NS direction), (b) base shear vs horizontal displacement (EW direction), (c) vertical displacement vs foundation rotation, and (d) vertical displacement vs horizontal displacement in the EW direction.

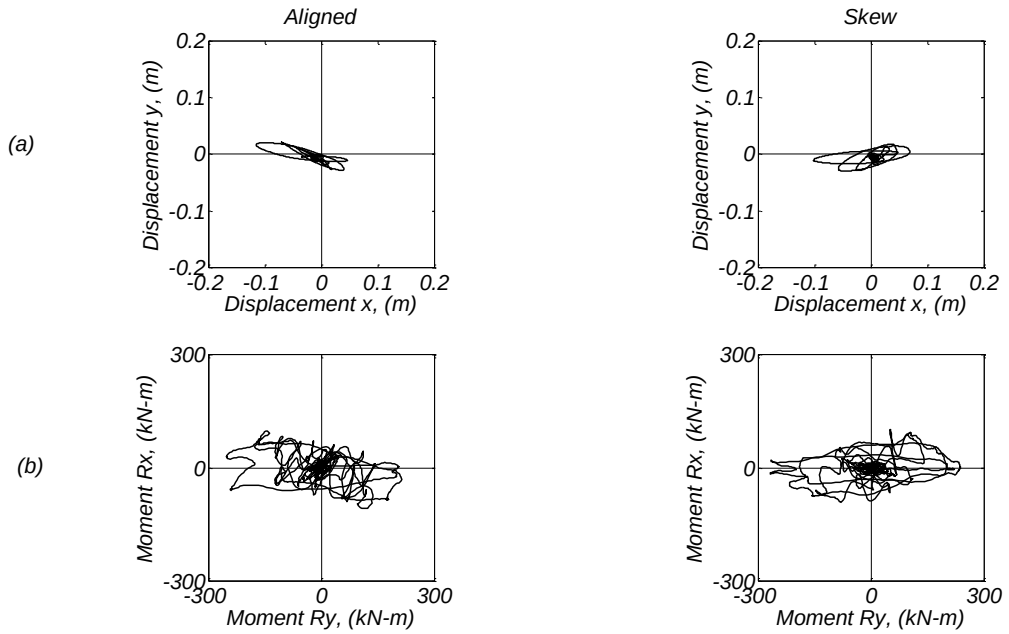

Figure C59. Bilateral response for the aligned and skew specimens; (a) mass displacement for the EW(x) and NS(y) direction, and (b) foundation moment for the corresponding directions.

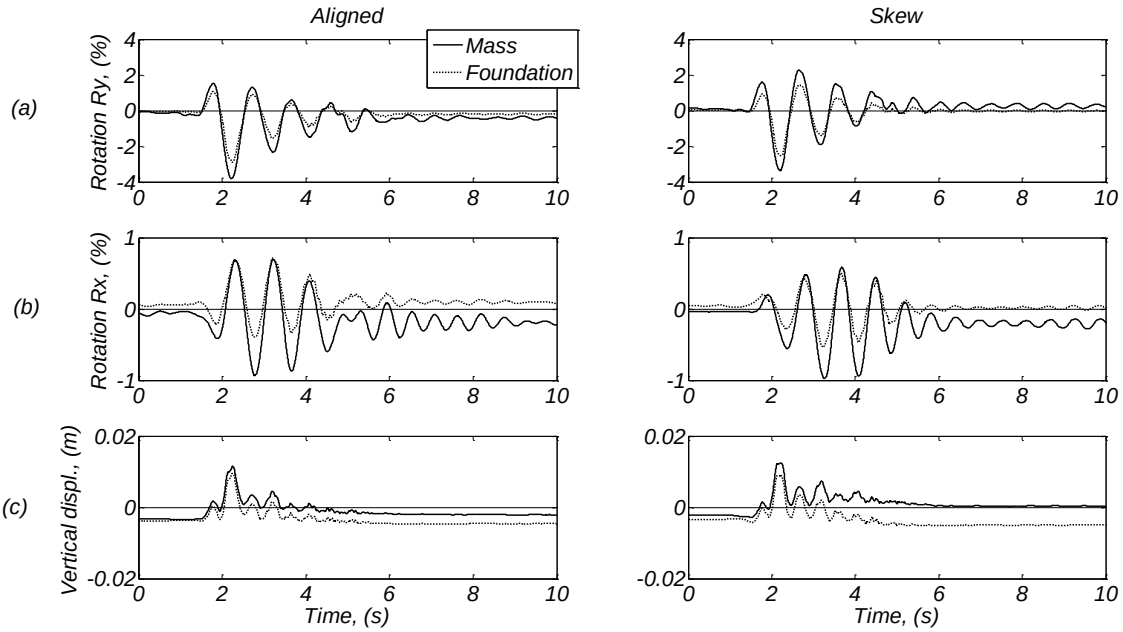

Figure C60. Time histories for the aligned and skew specimens; (a) mass drift ratio for the EW direction and equivalent foundation rotation, (b) mass drift ratio for the NS direction and equivalent foundation rotation, and (c) mass and footing vertical displacements.

Day 2, Takatori 0.5 Motion

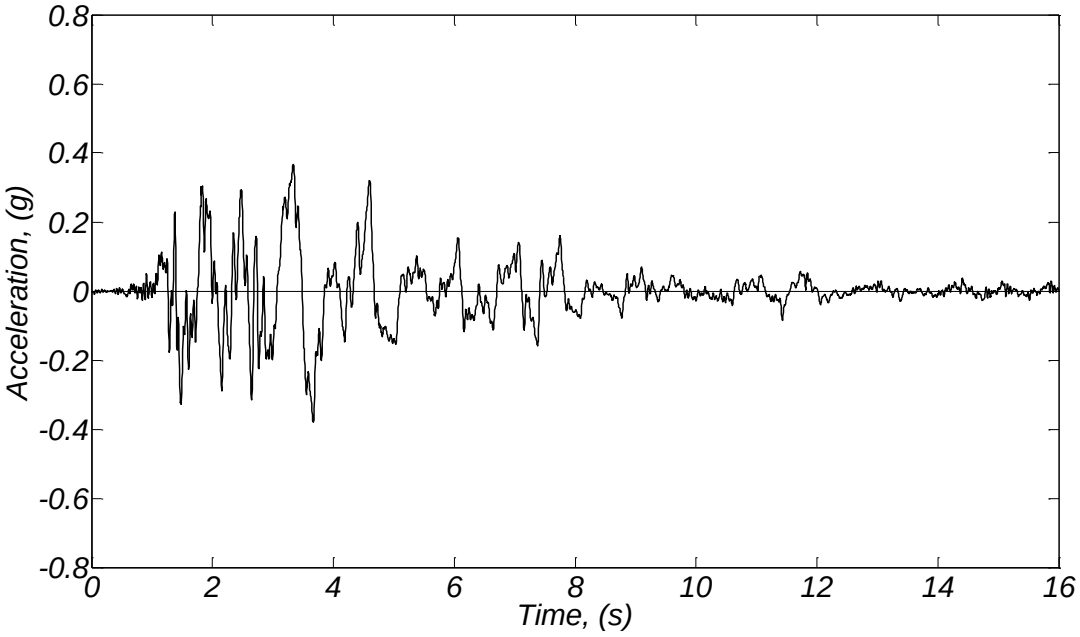

Figure C61. Soil free field acceleration time history (direction of shaking).

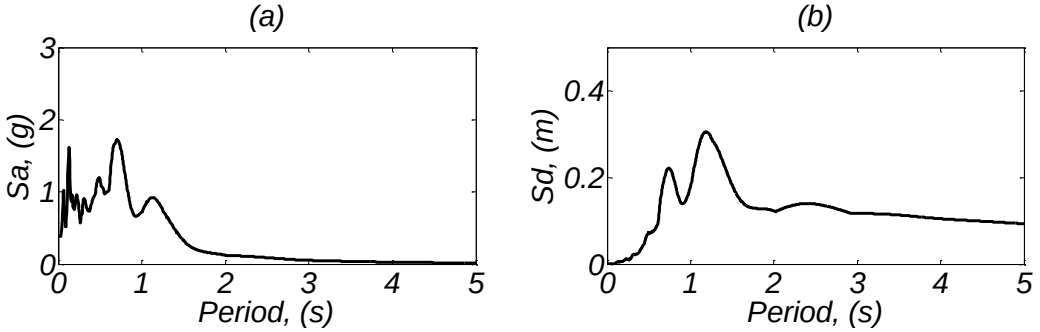

Figure C62. (a) Acceleration and (b) displacement response spectra for the recorded soil free field acceleration (direction of shaking) for damping $\zeta = 3\%$.

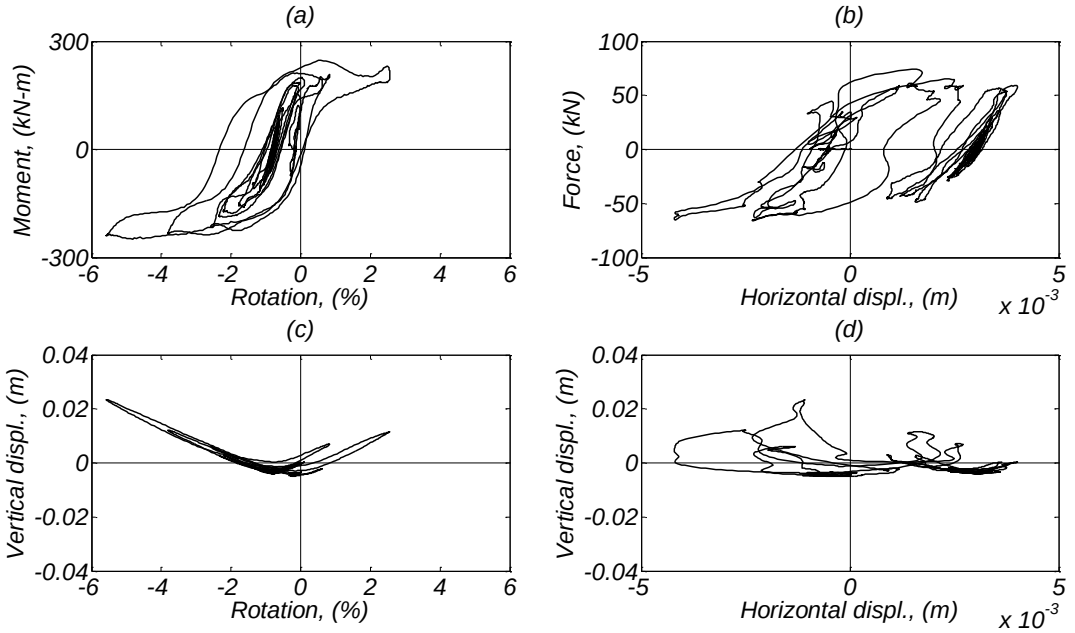

Figure C63. Aligned footing response; (a) moment vs rotation diagram (around NS direction), (b) base shear vs horizontal displacement (EW direction), (c) vertical displacement vs foundation rotation, and (d) vertical displacement vs horizontal displacement in the EW direction.

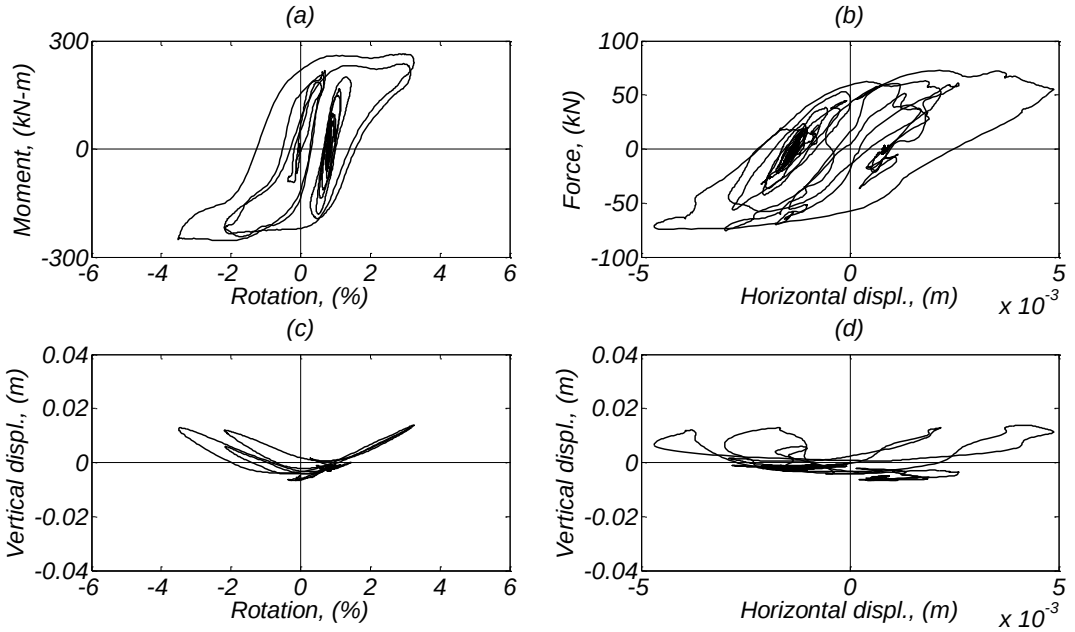

Figure C64. Skew footing response; (a) moment vs rotation diagram (around NS direction), (b) base shear vs horizontal displacement (EW direction), (c) vertical displacement vs foundation rotation, and (d) vertical displacement vs horizontal displacement in the EW direction.

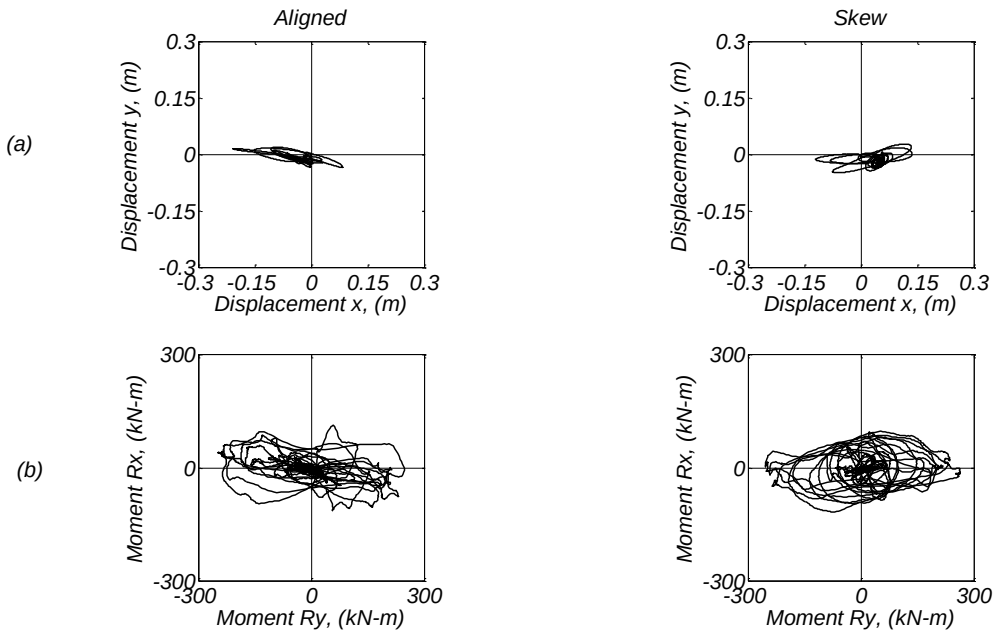

Figure C65. Bilateral response for the aligned and skew specimens; (a) mass displacement for the EW(x) and NS(y) direction, and (b) foundation moment for the corresponding directions.

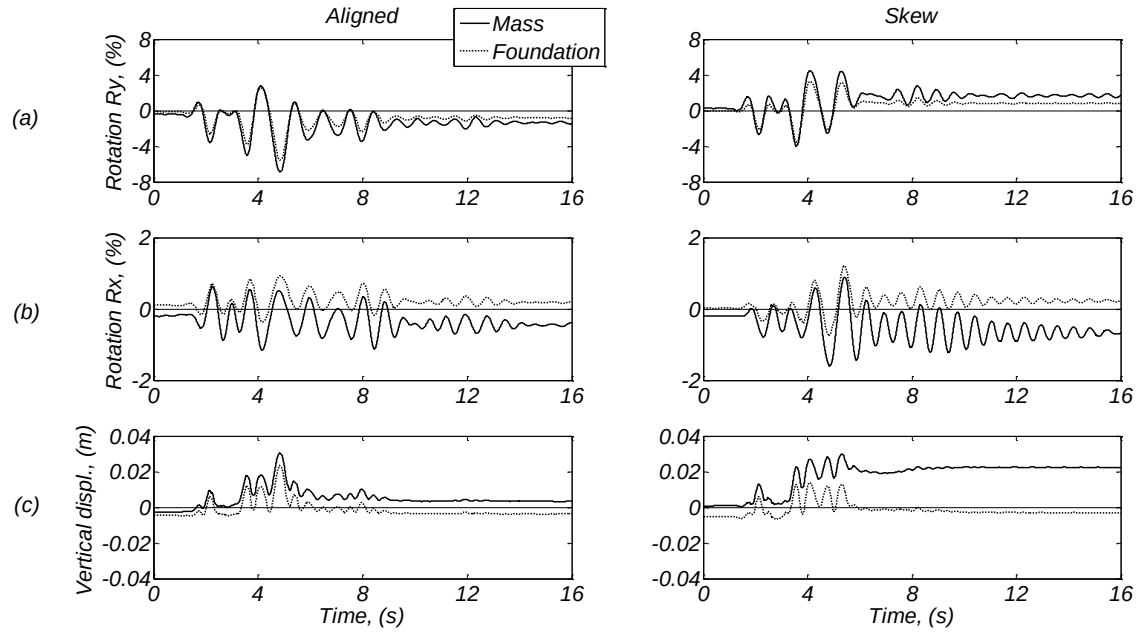

Figure C66. Time histories for the aligned and skew specimens; (a) mass drift ratio for the EW direction and equivalent foundation rotation, (b) mass drift ratio for the NS direction and equivalent foundation rotation, and (c) mass and footing vertical displacements.

Day 2, Takatori 1.0 Motion

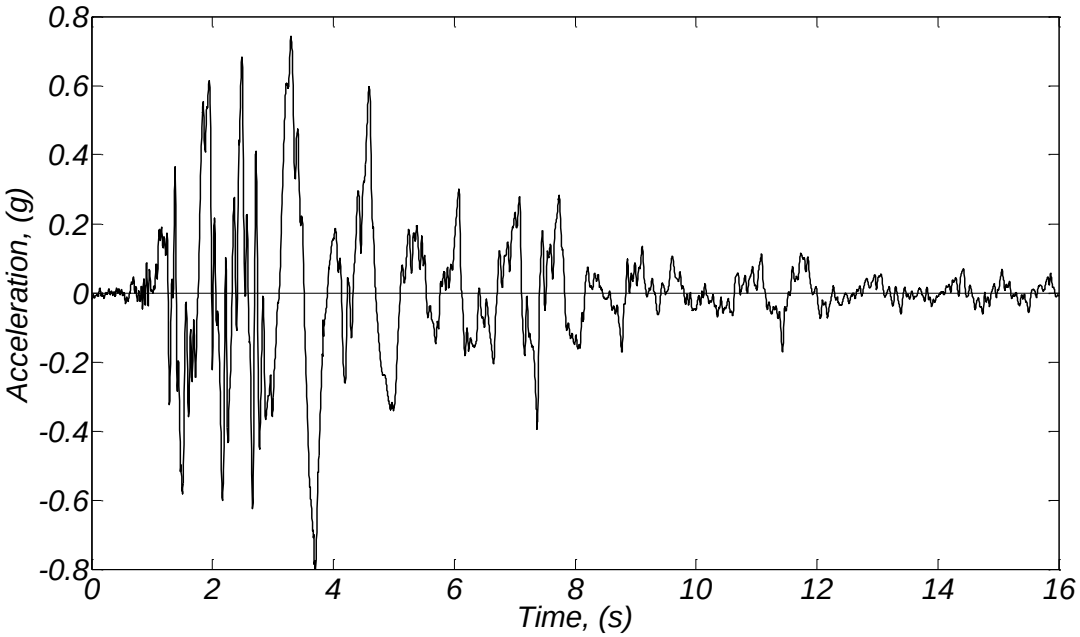

Figure C67. Soil free field acceleration time history (direction of shaking).

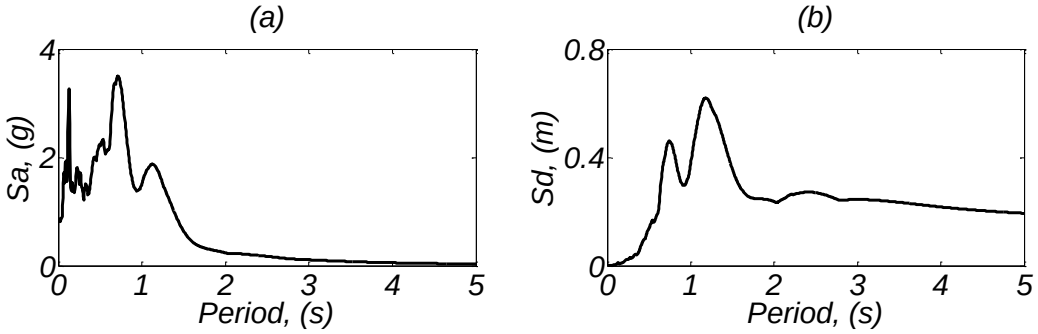

Figure C68. (a) Acceleration and (b) displacement response spectra for the recorded soil free field acceleration (direction of shaking) for damping ζ = 3%.

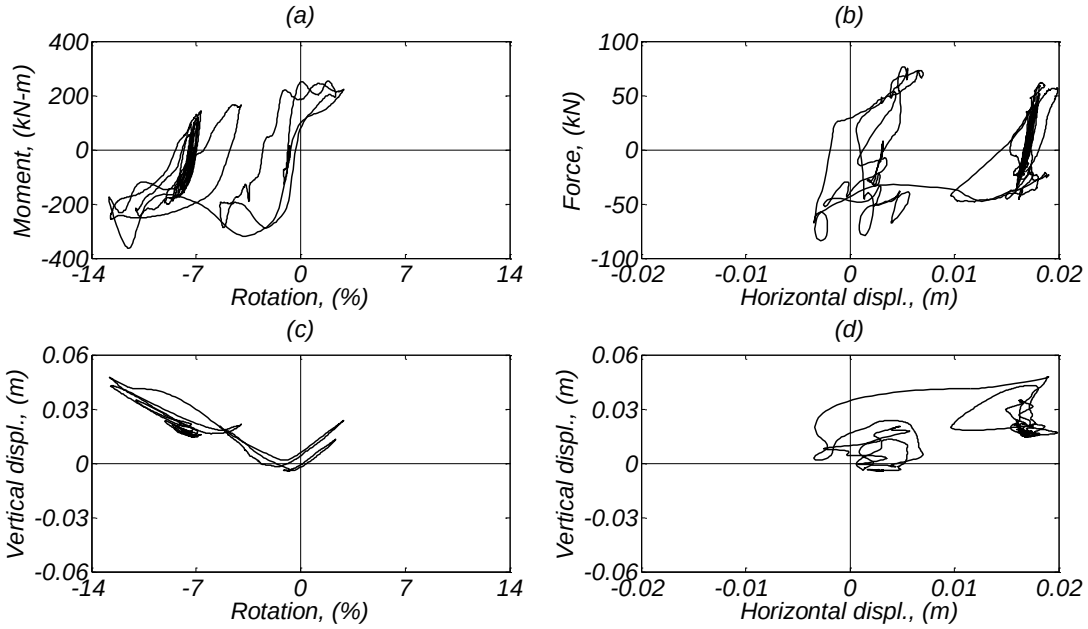

Figure C69. Aligned footing response; (a) moment vs rotation diagram (around NS direction), (b) base shear vs horizontal displacement (EW direction), (c) vertical displacement vs foundation rotation, and (d) vertical displacement vs horizontal displacement in the EW direction.

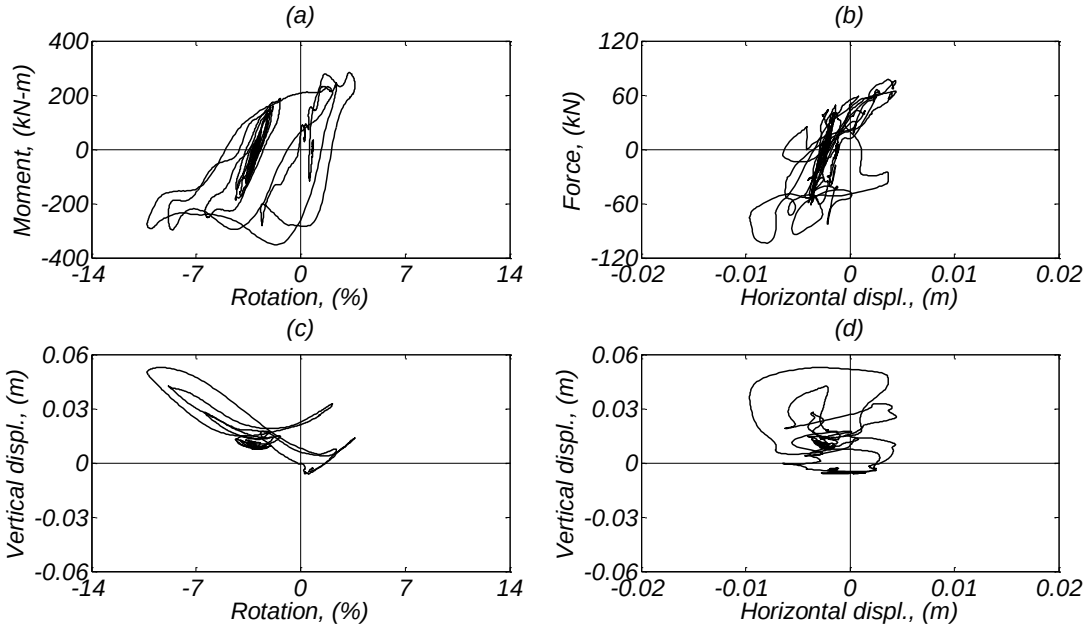

Figure C70. Skew footing response; (a) moment vs rotation diagram (around NS direction), (b) base shear vs horizontal displacement (EW direction), (c) vertical displacement vs foundation rotation, and (d) vertical displacement vs horizontal displacement in the EW direction.

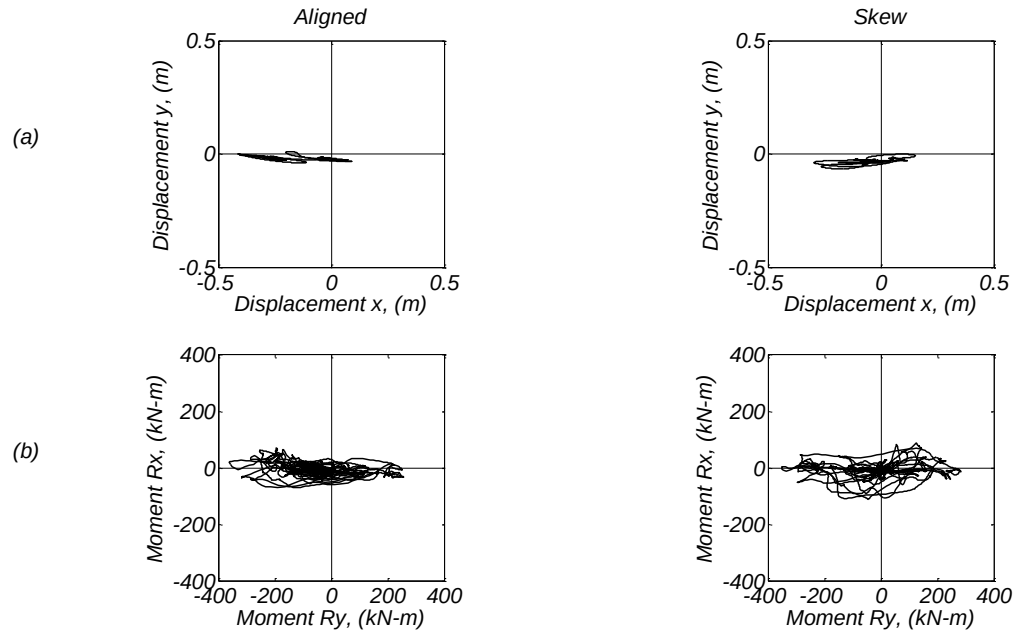

Figure C71. Bilateral response for the aligned and skew specimens; (a) mass displacement for the EW(x) and NS(y) direction, and (b) foundation moment for the corresponding directions.

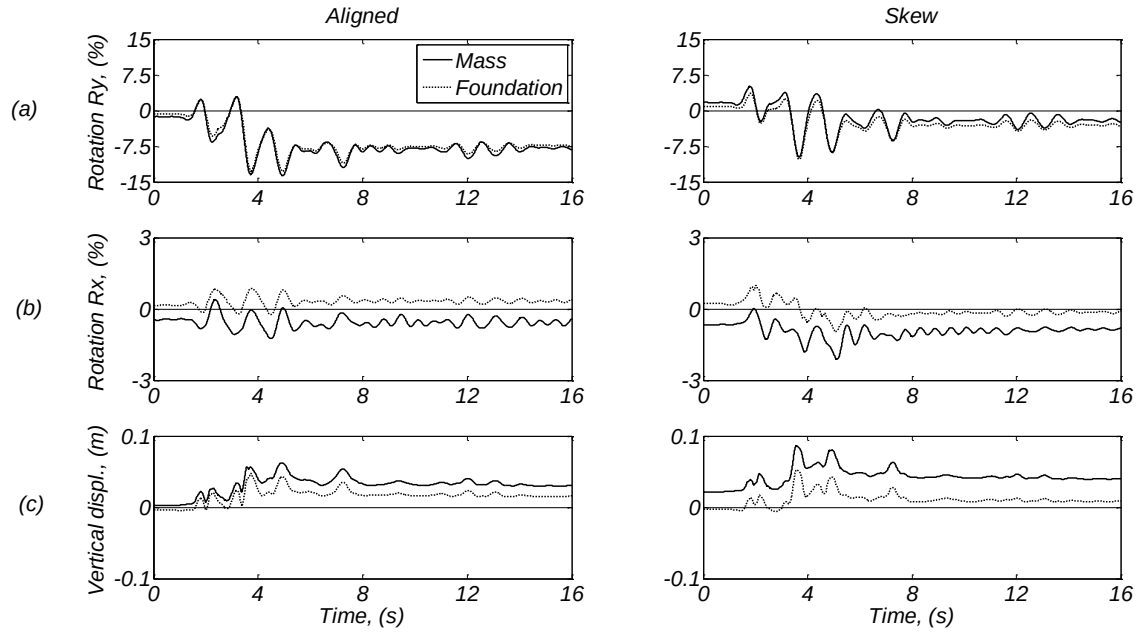

Figure C72. Time histories for the aligned and skew specimens; (a) mass drift ratio for the EW direction and equivalent foundation rotation, (b) mass drift ratio for the NS direction and equivalent foundation rotation, and (c) mass and footing vertical displacements.

Day 3, Gilroy #1 1.0 Motion

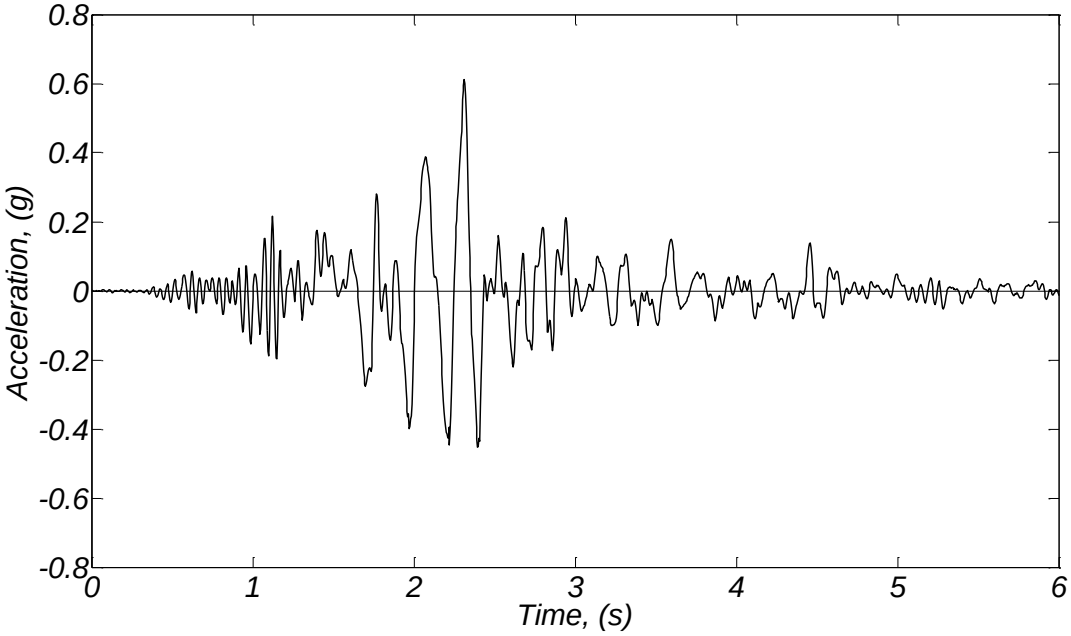

Figure C73. Soil free field acceleration time history (direction of shaking).

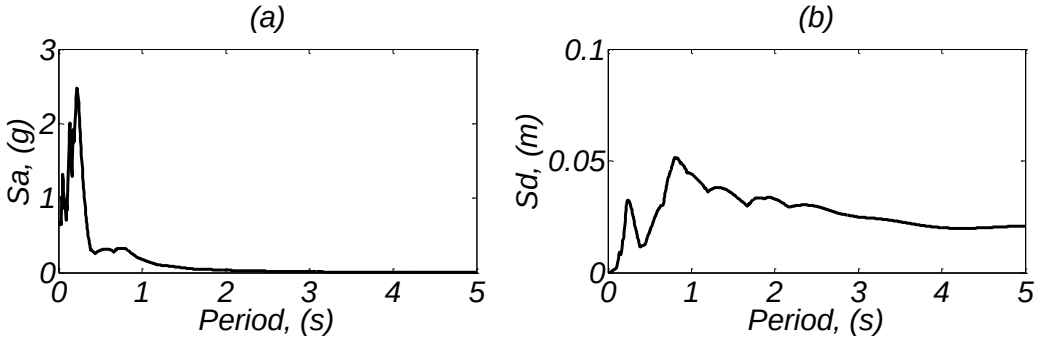

Figure C74. (a) Acceleration and (b) displacement response spectra for the recorded soil free field acceleration (direction of shaking) for damping $\zeta = 3\%$.

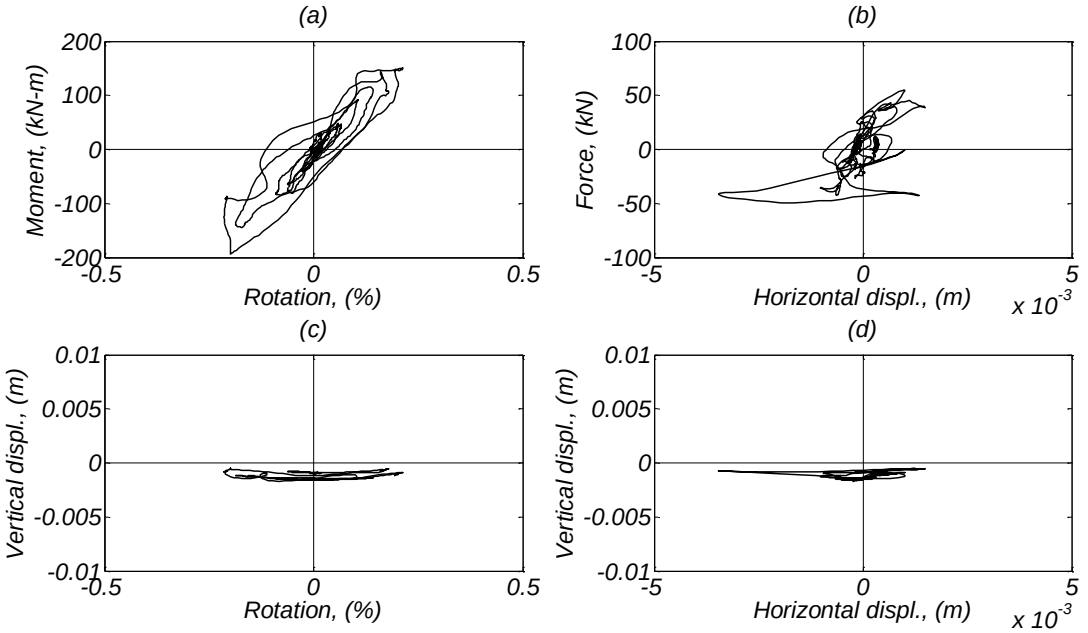

Figure C75. Aligned footing response; (a) moment vs rotation diagram (around NS direction), (b) base shear vs horizontal displacement (EW direction), (c) vertical displacement vs foundation rotation, and (d) vertical displacement vs horizontal displacement in the EW direction.

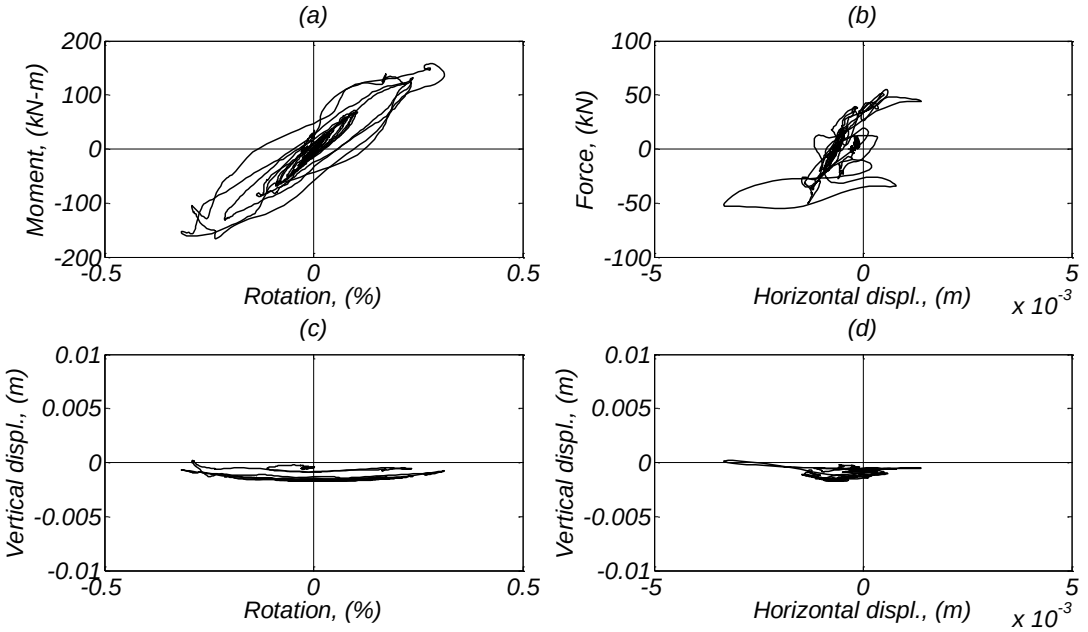

Figure C76. Skew footing response; (a) moment vs rotation diagram (around NS direction), (b) base shear vs horizontal displacement (EW direction), (c) vertical displacement vs foundation rotation, and (d) vertical displacement vs horizontal displacement in the EW direction.

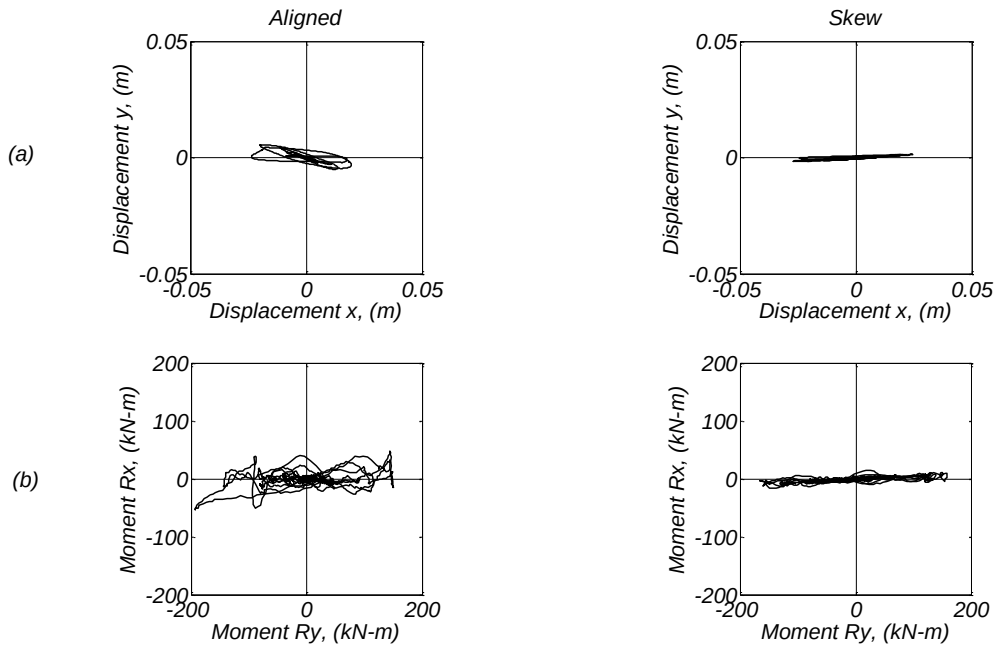

Figure C77. Bilateral response for the aligned and skew specimens; (a) mass displacement for the EW(x) and NS(y) direction, and (b) foundation moment for the corresponding directions.

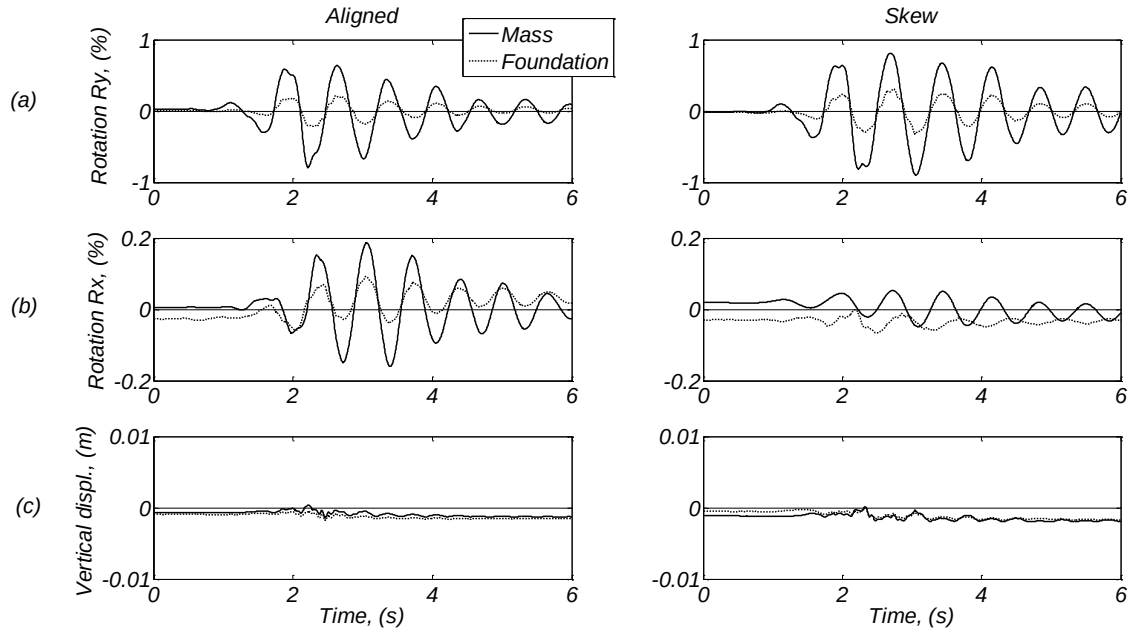

Figure C78. Time histories for the aligned and skew specimens; (a) mass drift ratio for the EW direction and equivalent foundation rotation, (b) mass drift ratio for the NS direction and equivalent foundation rotation, and (c) mass and footing vertical displacements.

Day 3, Corralitos 0.8 Motion

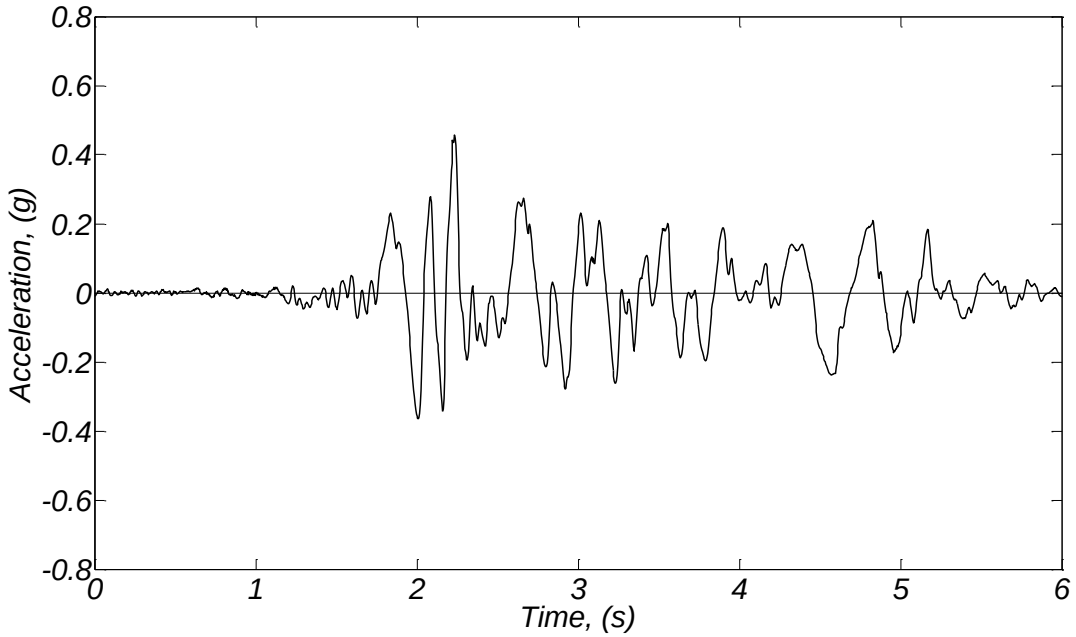

Figure C79. Soil free field acceleration time history (direction of shaking).

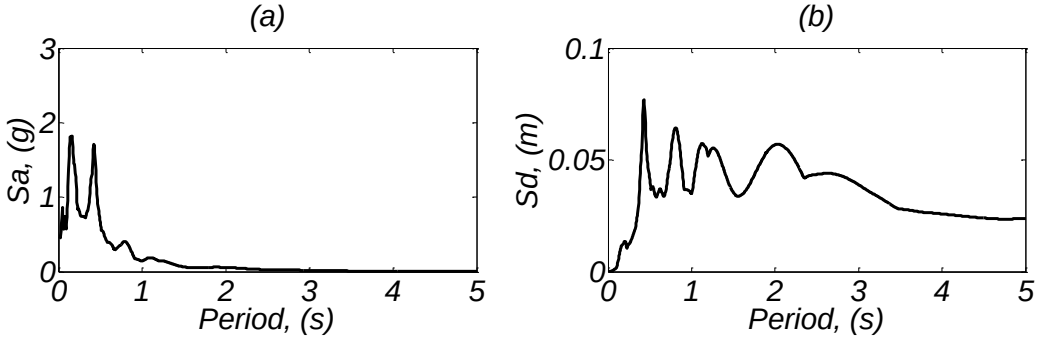

Figure C80. (a) Acceleration and (b) displacement response spectra for the recorded soil free field acceleration (direction of shaking) for damping $\zeta = 3\%$.

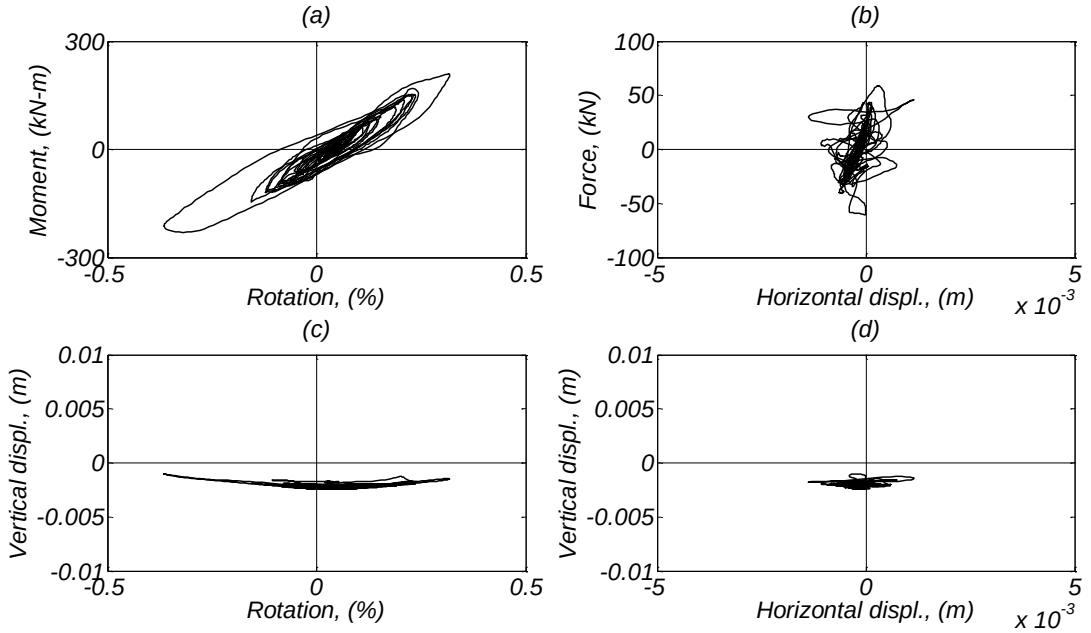

Figure C81. Aligned footing response; (a) moment vs rotation diagram (around NS direction), (b) base shear vs horizontal displacement (EW direction), (c) vertical displacement vs foundation rotation, and (d) vertical displacement vs horizontal displacement in the EW direction.

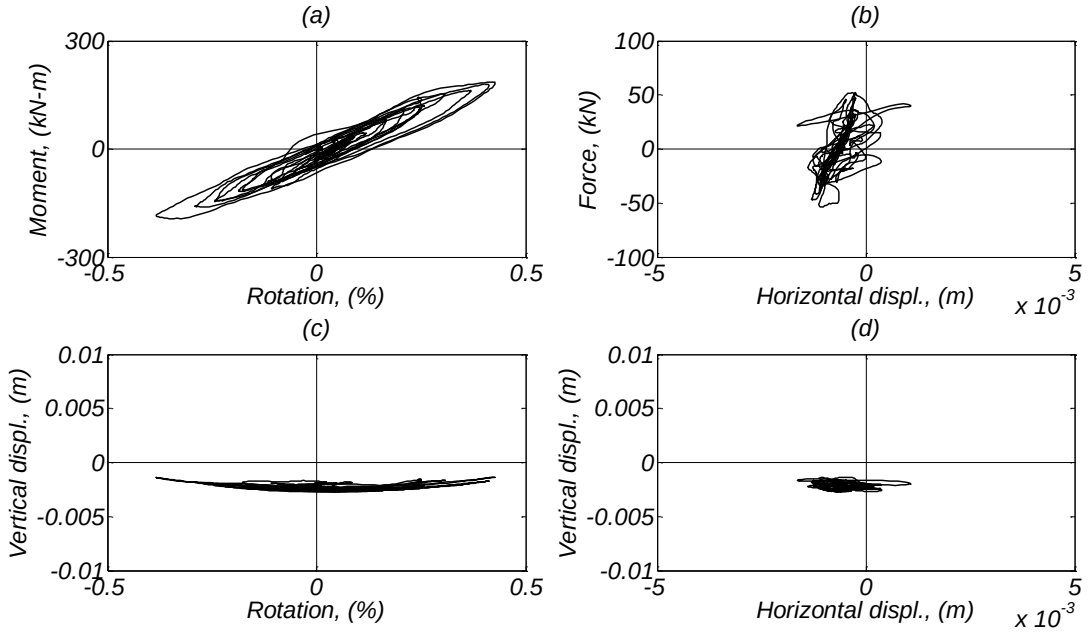

Figure C82. Skew footing response; (a) moment vs rotation diagram (around NS direction), (b) base shear vs horizontal displacement (EW direction), (c) vertical displacement vs foundation rotation, and (d) vertical displacement vs horizontal displacement in the EW direction.

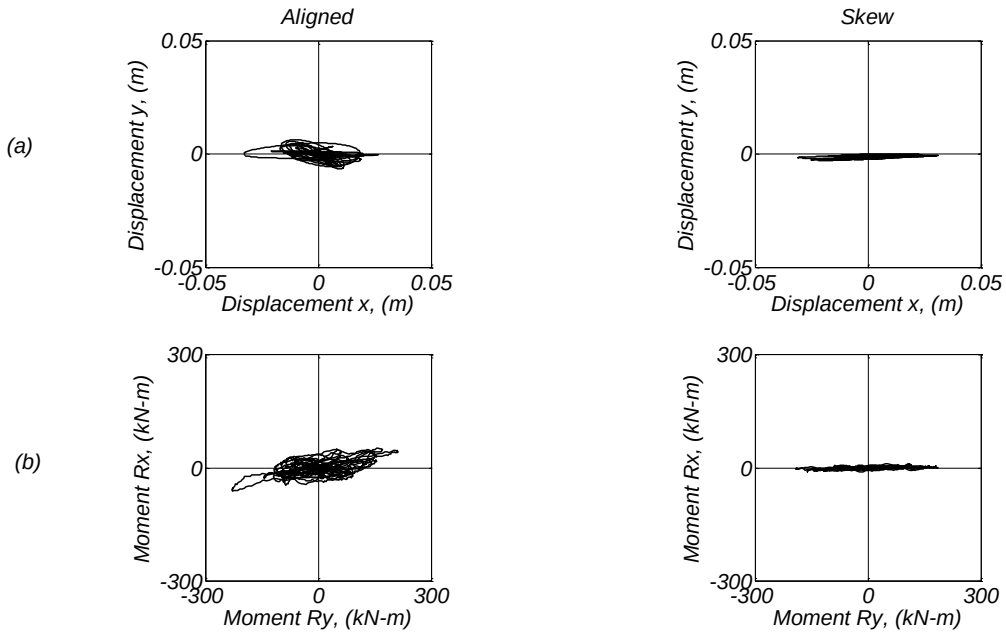

Figure C83. Bilateral response for the aligned and skew specimens; (a) mass displacement for the EW(x) and NS(y) direction, and (b) foundation moment for the corresponding directions.

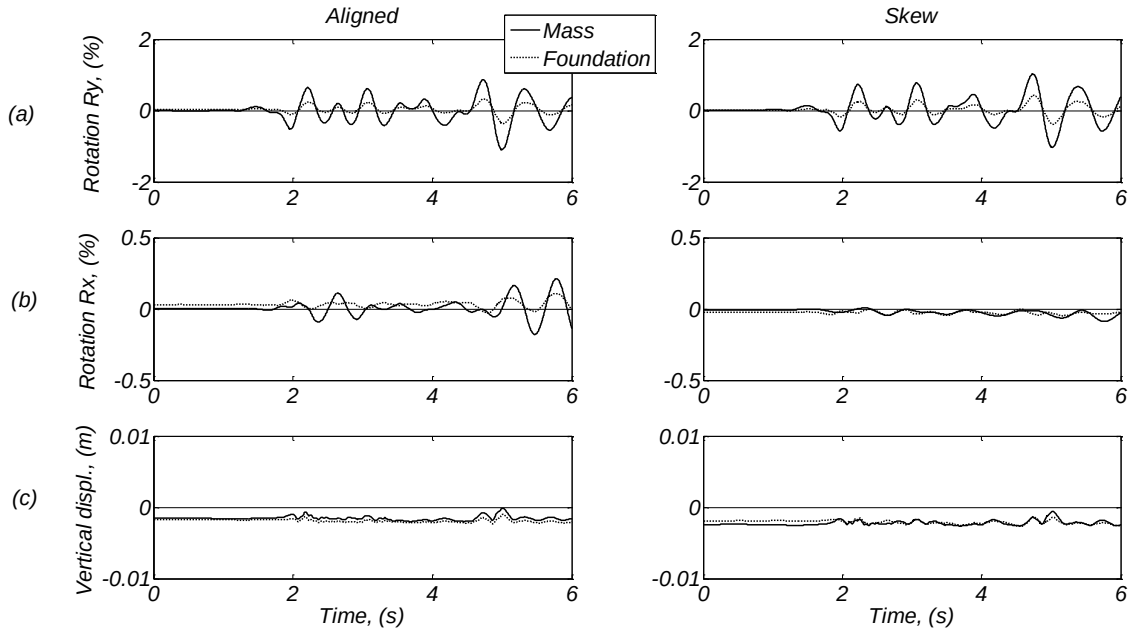

Figure C84. Time histories for the aligned and skew specimens; (a) mass drift ratio for the EW direction and equivalent foundation rotation, (b) mass drift ratio for the NS direction and equivalent foundation rotation, and (c) mass and footing vertical displacements.

Day 3, El Centro #6 1.1 Motion

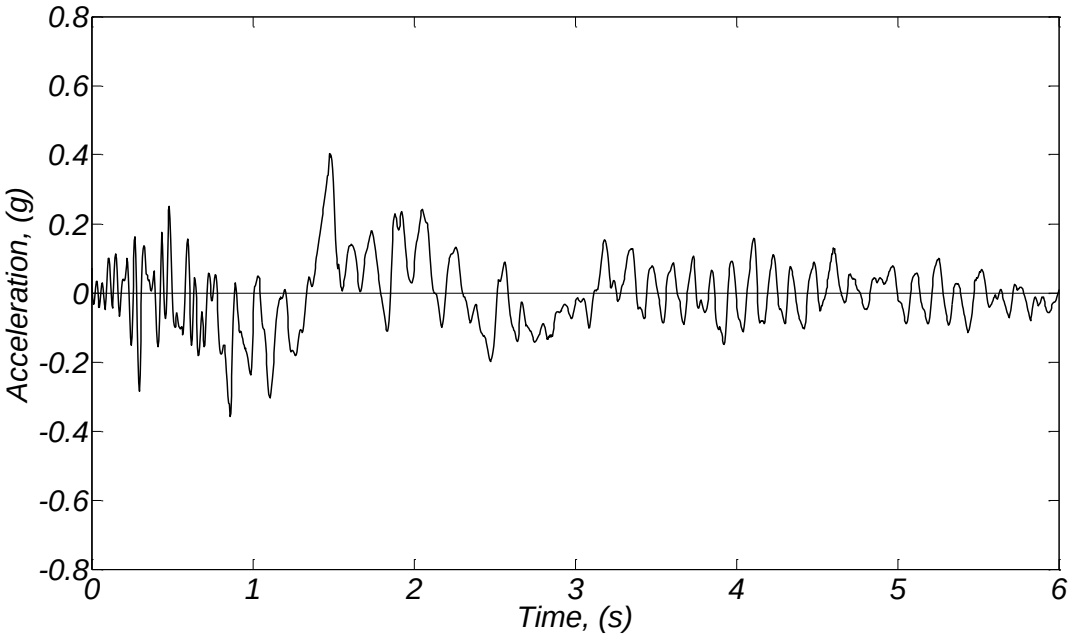

Figure C85. Soil free field acceleration time history (direction of shaking).

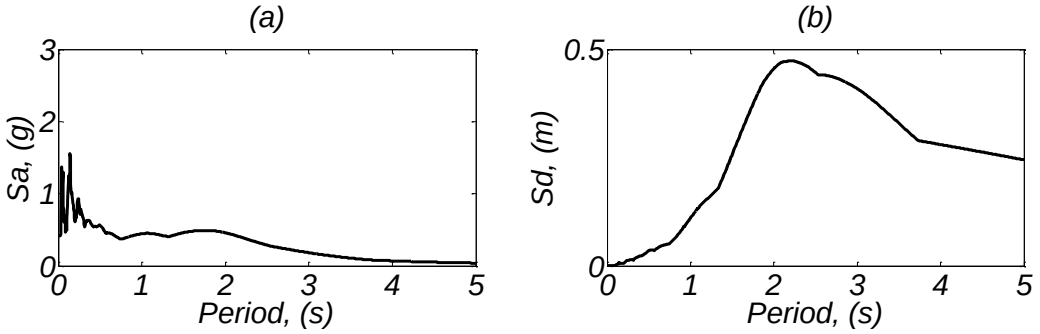

Figure C86. (a) Acceleration and (b) displacement response spectra for the recorded soil free field acceleration (direction of shaking) for damping ζ = 3%.

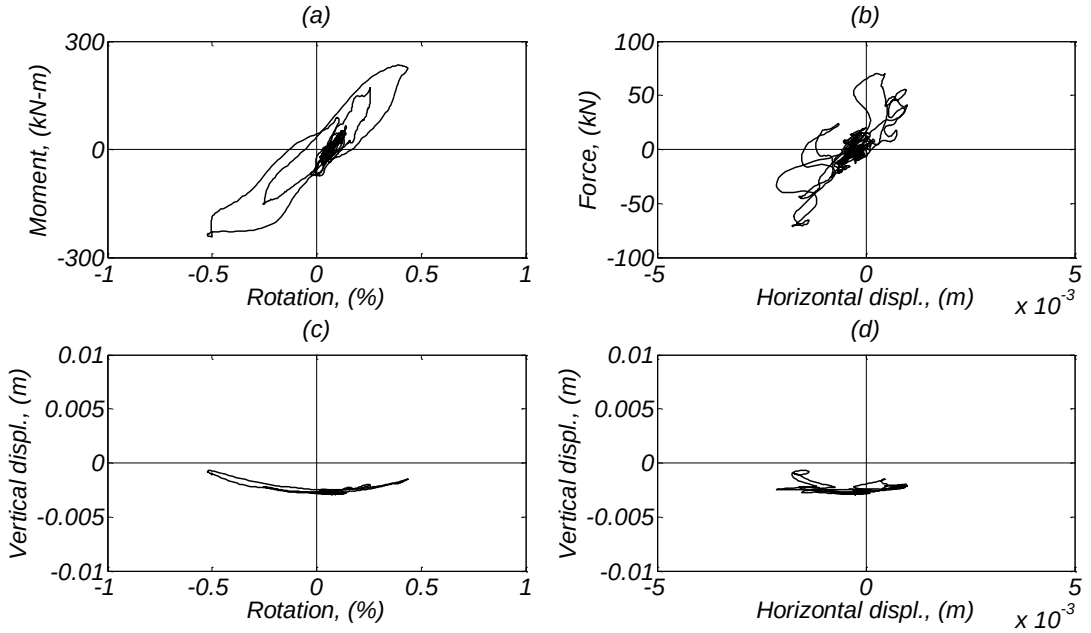

Figure C87. Aligned footing response; (a) moment vs rotation diagram (around NS direction), (b) base shear vs horizontal displacement (EW direction), (c) vertical displacement vs foundation rotation, and (d) vertical displacement vs horizontal displacement in the EW direction.

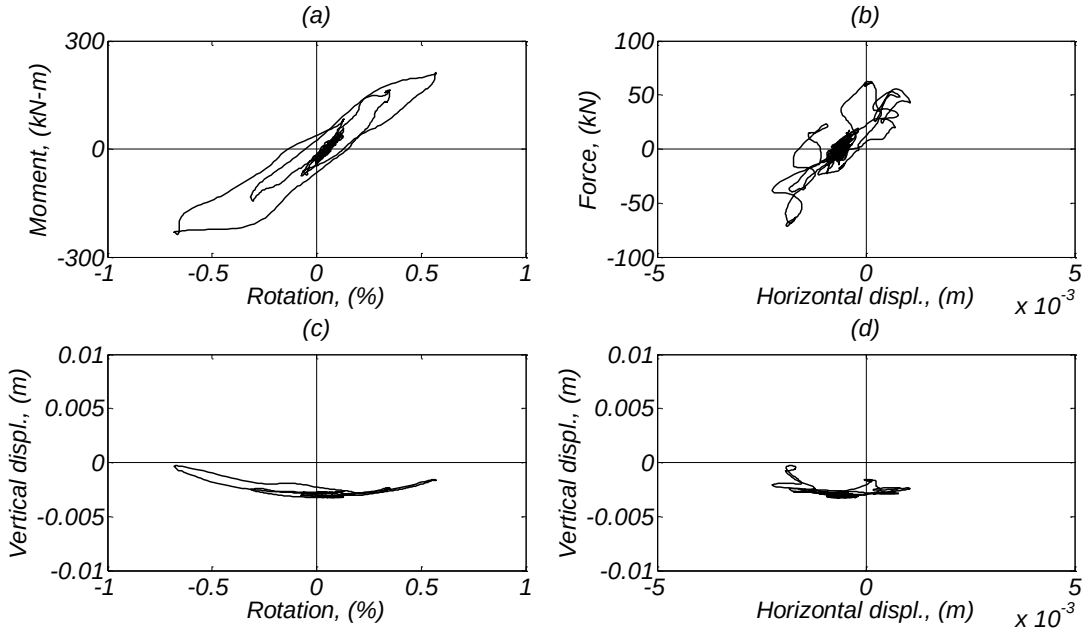

Figure C88. Skew footing response; (a) moment vs rotation diagram (around NS direction), (b) base shear vs horizontal displacement (EW direction), (c) vertical displacement vs foundation rotation, and (d) vertical displacement vs horizontal displacement in the EW direction.

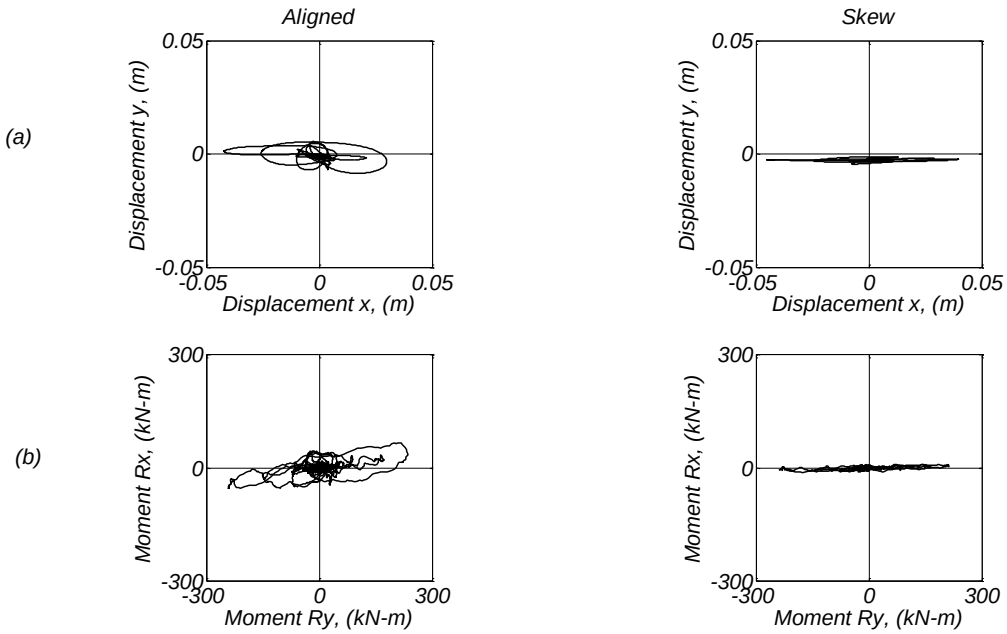

Figure C89. Bilateral response for the aligned and skew specimens; (a) mass displacement for the EW(x) and NS(y) direction, and (b) foundation moment for the corresponding directions.

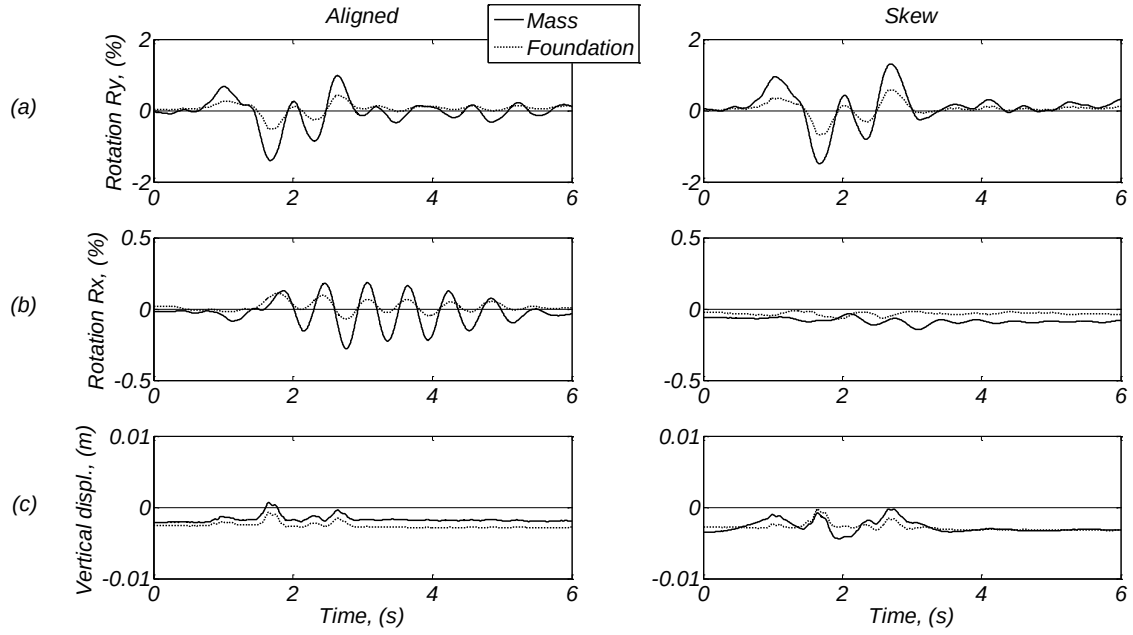

Figure C90. Time histories for the aligned and skew specimens; (a) mass drift ratio for the EW direction and equivalent foundation rotation, (b) mass drift ratio for the NS direction and equivalent foundation rotation, and (c) mass and footing vertical displacements.

Day 3, Pacoima dam 0.8 Motion

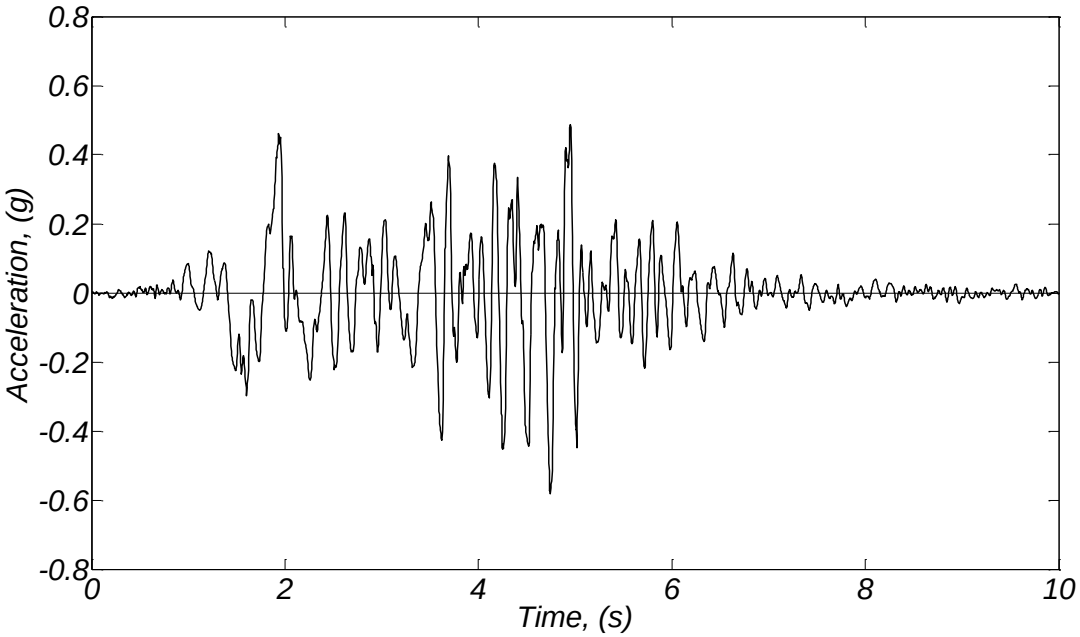

Figure C91. Soil free field acceleration time history (direction of shaking).

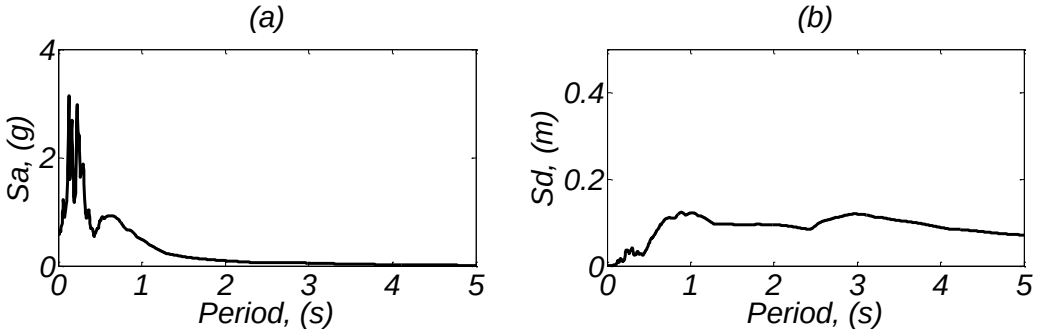

Figure C92. (a) Acceleration and (b) displacement response spectra for the recorded soil free field acceleration (direction of shaking) for damping ζ = 3%.

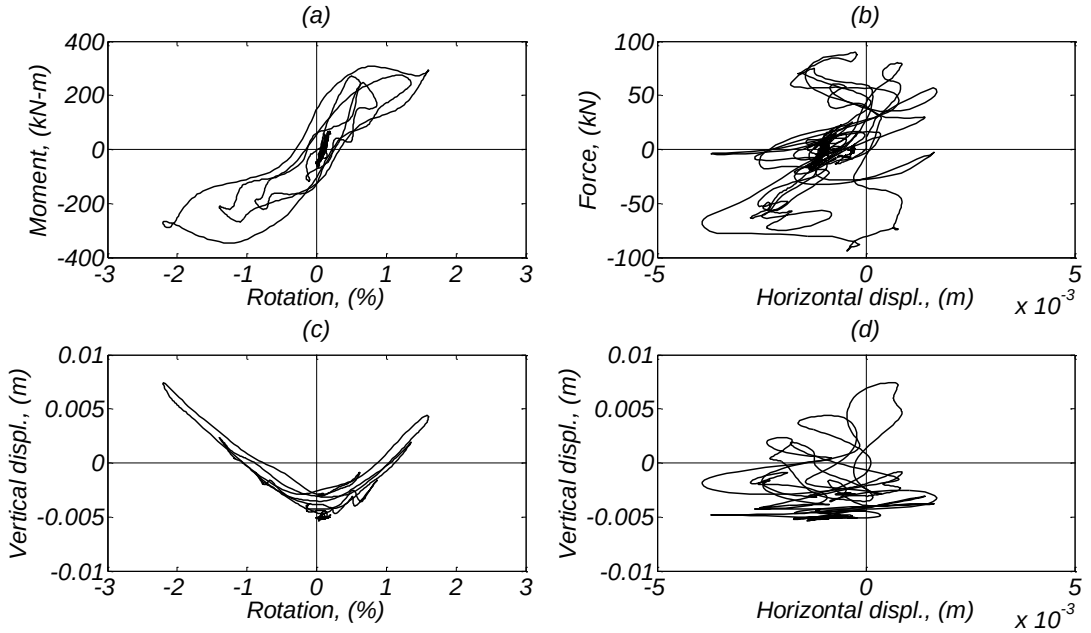

Figure C93. Aligned footing response; (a) moment vs rotation diagram (around NS direction), (b) base shear vs horizontal displacement (EW direction), (c) vertical displacement vs foundation rotation, and (d) vertical displacement vs horizontal displacement in the EW direction.

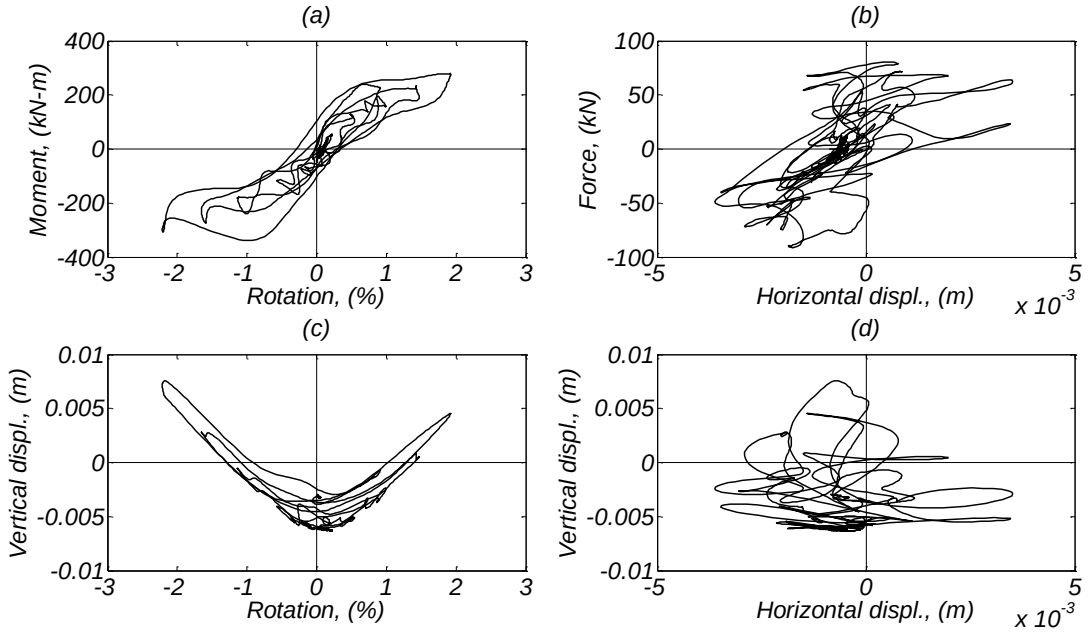

Figure C94. Skew footing response; (a) moment vs rotation diagram (around NS direction), (b) base shear vs horizontal displacement (EW direction), (c) vertical displacement vs foundation rotation, and (d) vertical displacement vs horizontal displacement in the EW direction.

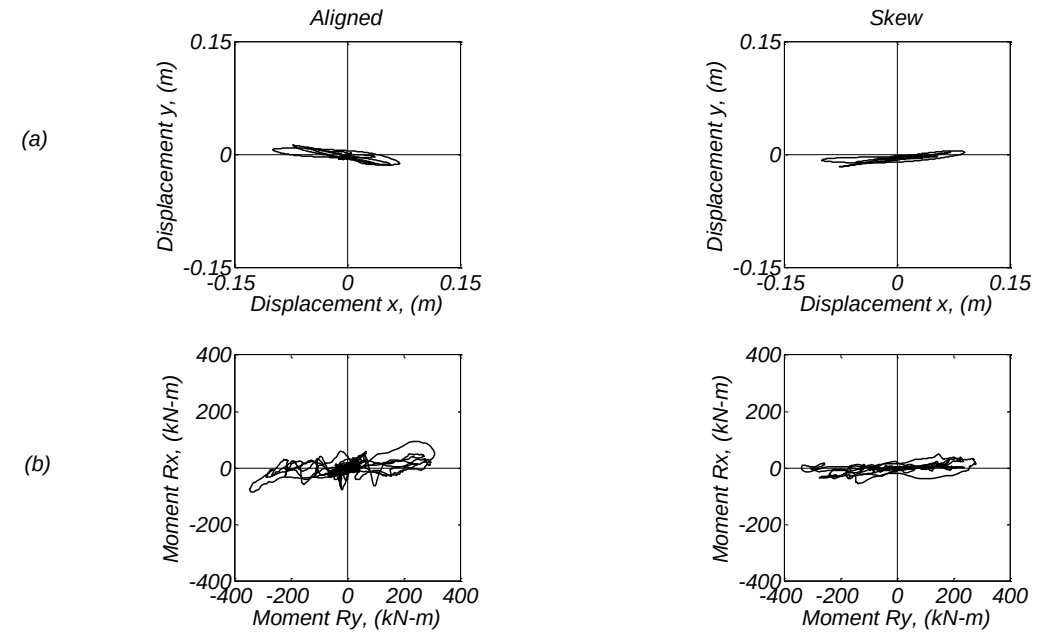

Figure C95. Bilateral response for the aligned and skew specimens; (a) mass displacement for the EW(x) and NS(y) direction, and (b) foundation moment for the corresponding directions.

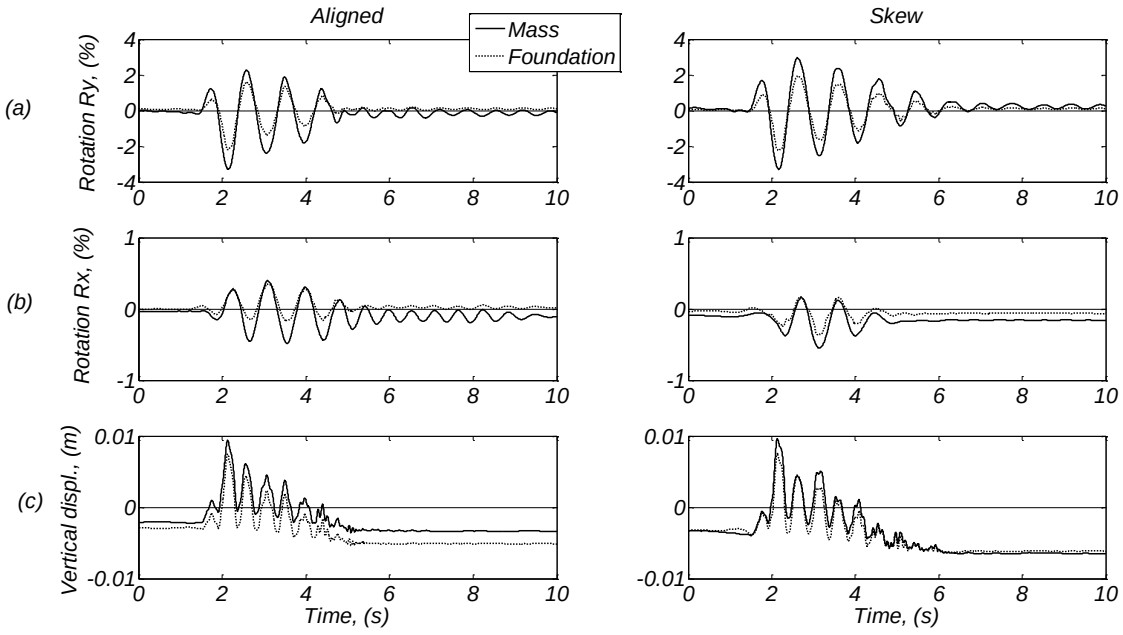

Figure C96. Time histories for the aligned and skew specimens; (a) mass drift ratio for the EW direction and equivalent foundation rotation, (b) mass drift ratio for the NS direction and equivalent foundation rotation, and (c) mass and footing vertical displacements.

Day 3, Takatori 0.5 Motion

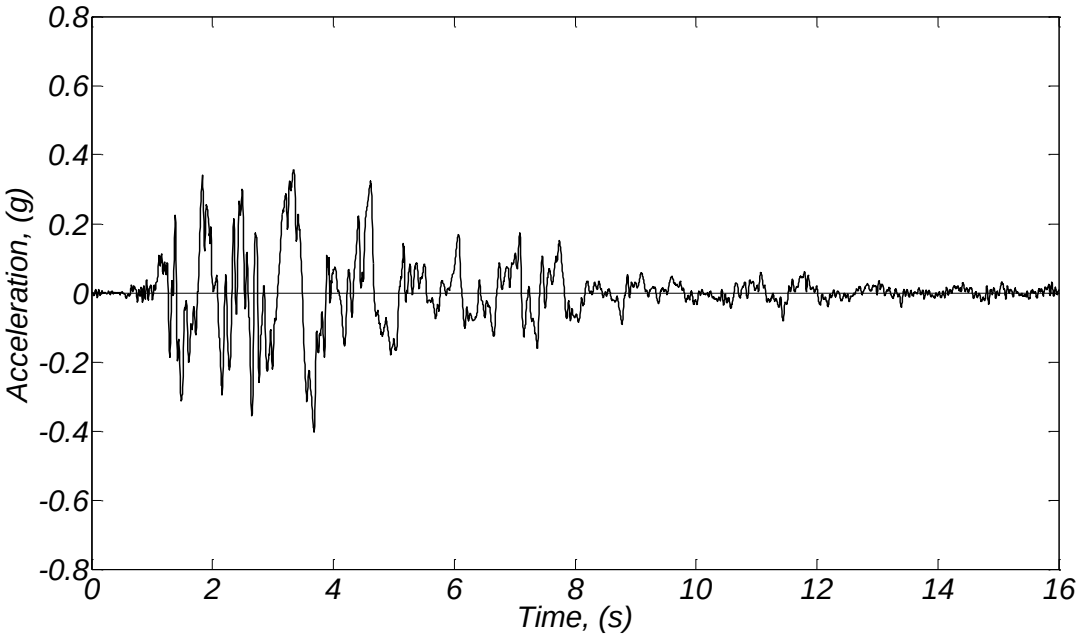

Figure C97. Soil free field acceleration time history (direction of shaking).

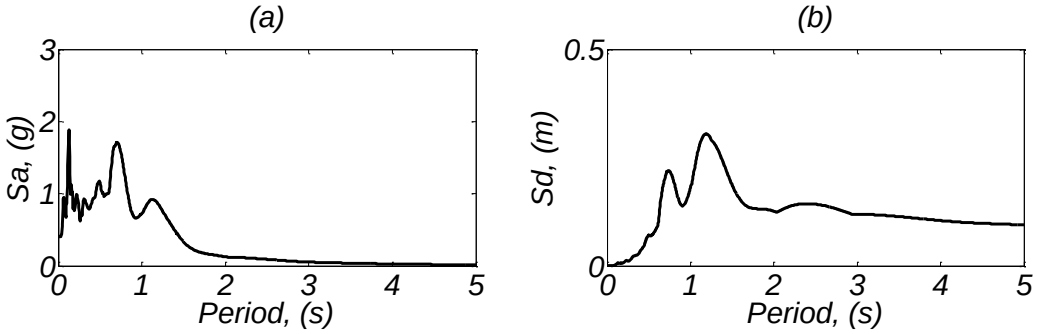

Figure C98. (a) Acceleration and (b) displacement response spectra for the recorded soil free field acceleration (direction of shaking) for damping ζ = 3%.

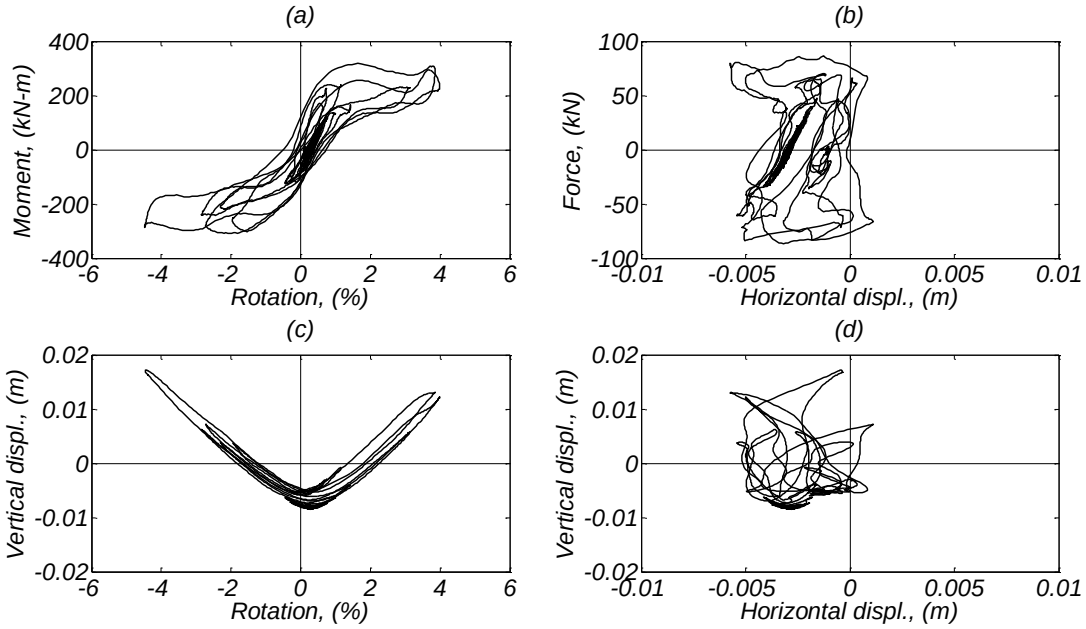

Figure C99. Aligned footing response; (a) moment vs rotation diagram (around NS direction), (b) base shear vs horizontal displacement (EW direction), (c) vertical displacement vs foundation rotation, and (d) vertical displacement vs horizontal displacement in the EW direction.

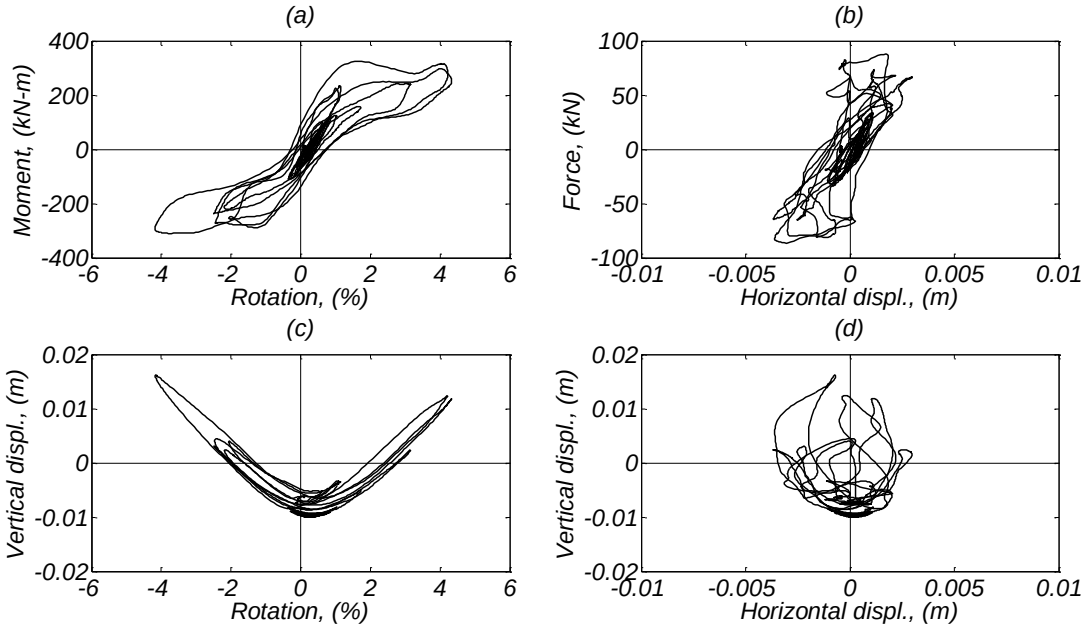

Figure C100. Skew footing response; (a) moment vs rotation diagram (around NS direction), (b) base shear vs horizontal displacement (EW direction), (c) vertical displacement vs foundation rotation, and (d) vertical displacement vs horizontal displacement in the EW direction.

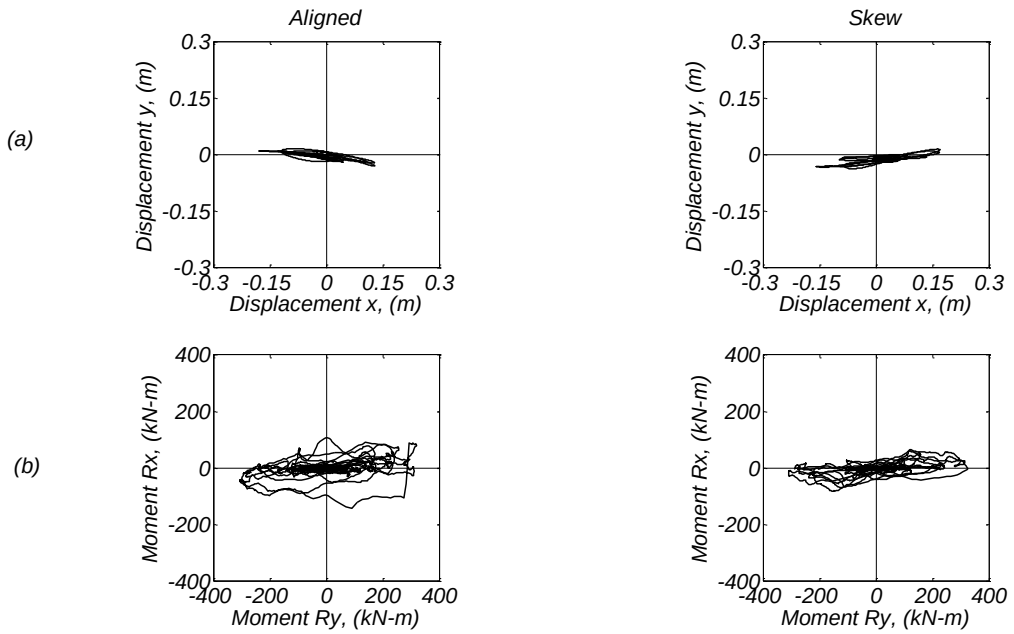

Figure C101. Bilateral response for the aligned and skew specimens; (a) mass displacement for the EW(x) and NS(y) direction, and (b) foundation moment for the corresponding directions.

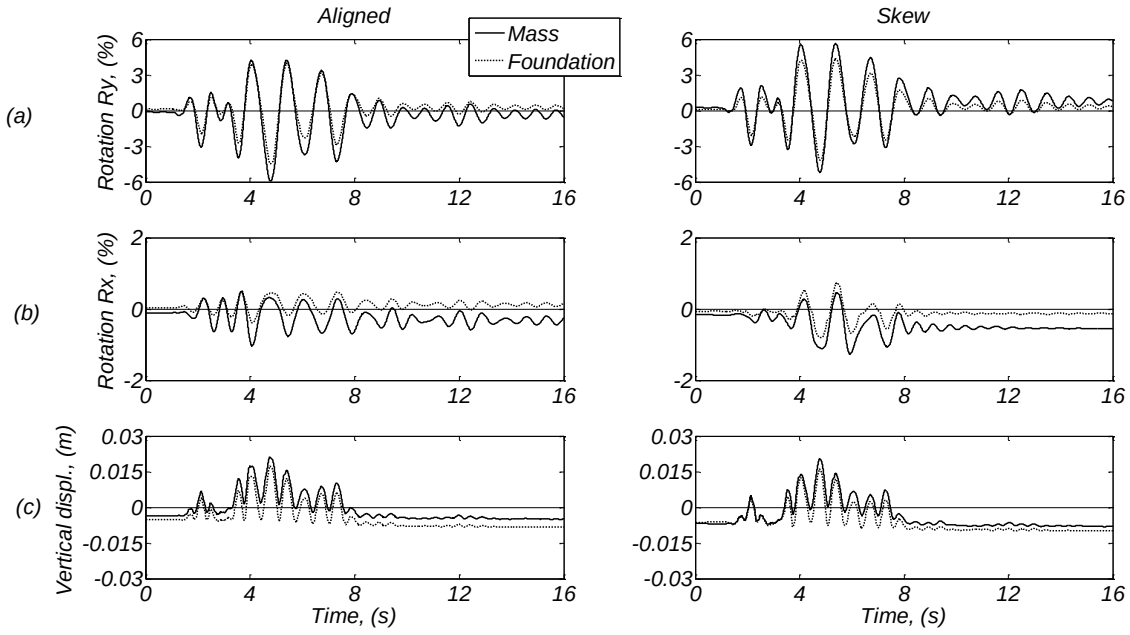

Figure C102. Time histories for the aligned and skew specimens; (a) mass drift ratio for the EW direction and equivalent foundation rotation, (b) mass drift ratio for the NS direction and equivalent foundation rotation, and (c) mass and footing vertical displacements.

Day 3, Takatori 1.0 Motion

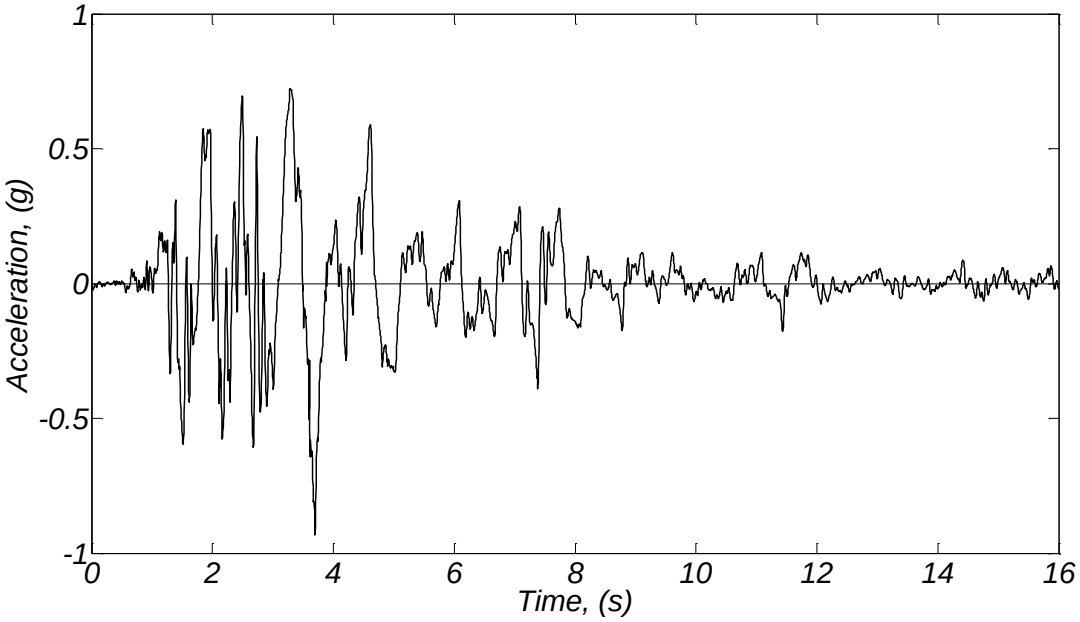

Figure C103. Soil free field acceleration time history (direction of shaking).

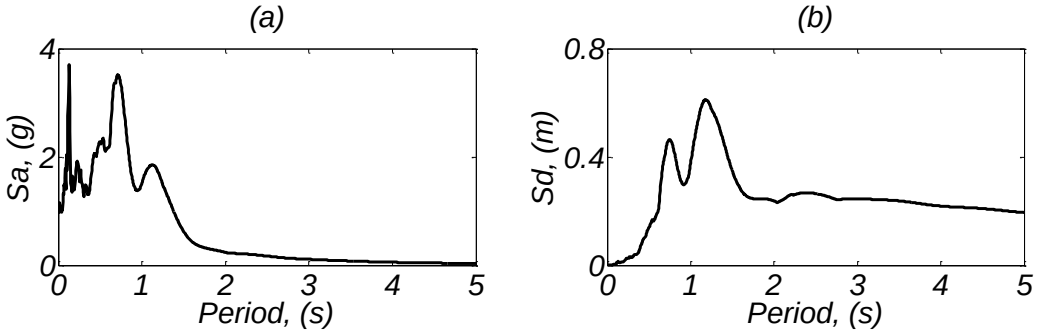

Figure C104. (a) Acceleration and (b) displacement response spectra for the recorded soil free field acceleration (direction of shaking) for damping $\zeta = 3\%$.

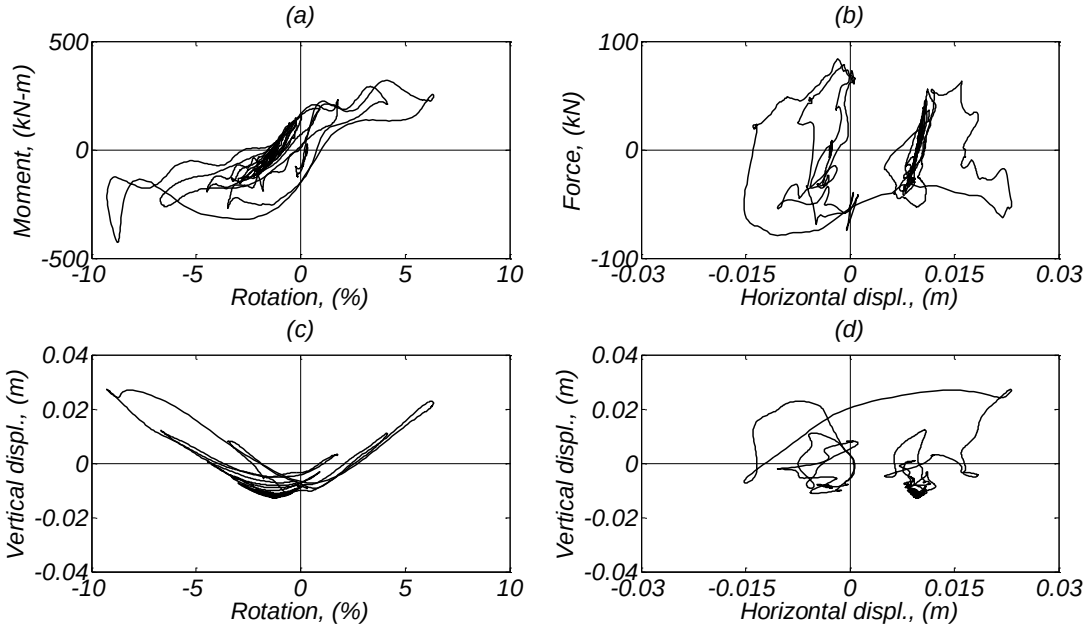

Figure C105. Aligned footing response; (a) moment vs rotation diagram (around NS direction), (b) base shear vs horizontal displacement (EW direction), (c) vertical displacement vs foundation rotation, and (d) vertical displacement vs horizontal displacement in the EW direction.

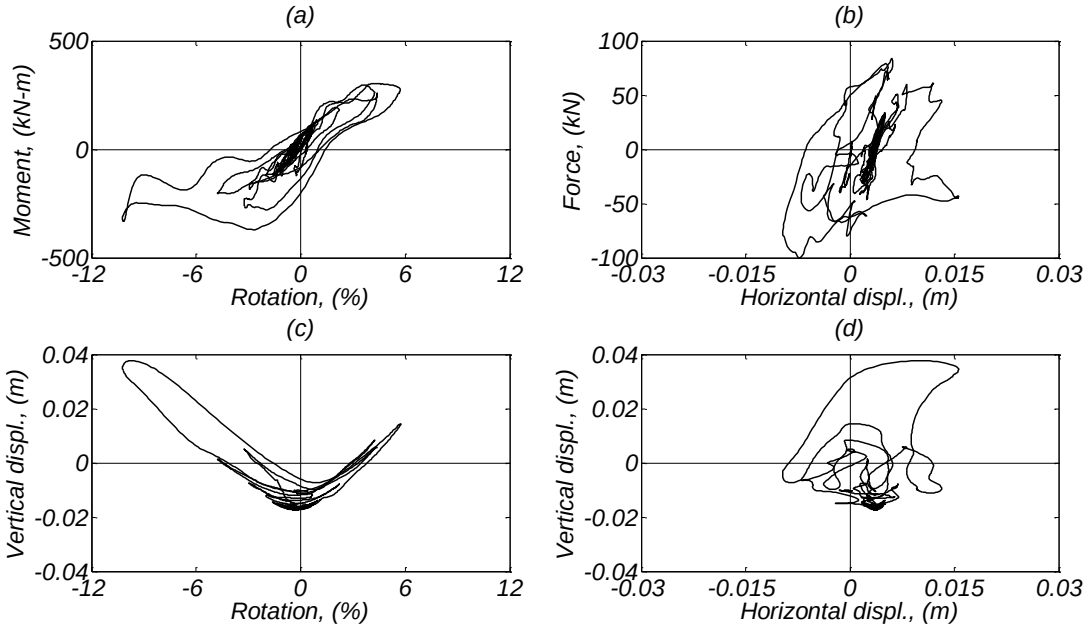

Figure C106. Skew footing response; (a) moment vs rotation diagram (around NS direction), (b) base shear vs horizontal displacement (EW direction), (c) vertical displacement vs foundation rotation, and (d) vertical displacement vs horizontal displacement in the EW direction.

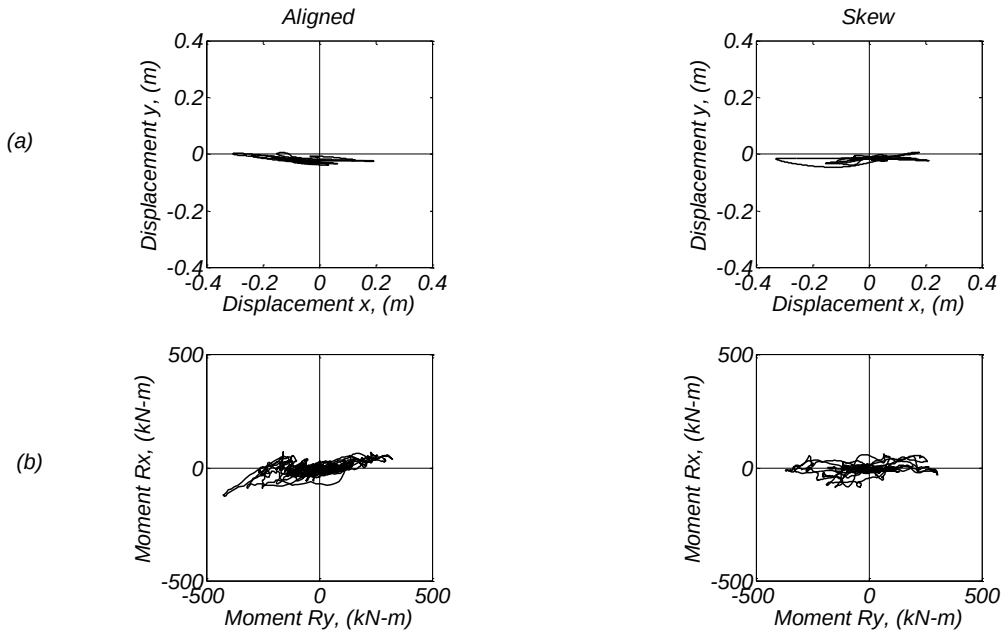

Figure C107. Bilateral response for the aligned and skew specimens; (a) mass displacement for the EW(x) and NS(y) direction, and (b) foundation moment for the corresponding directions.

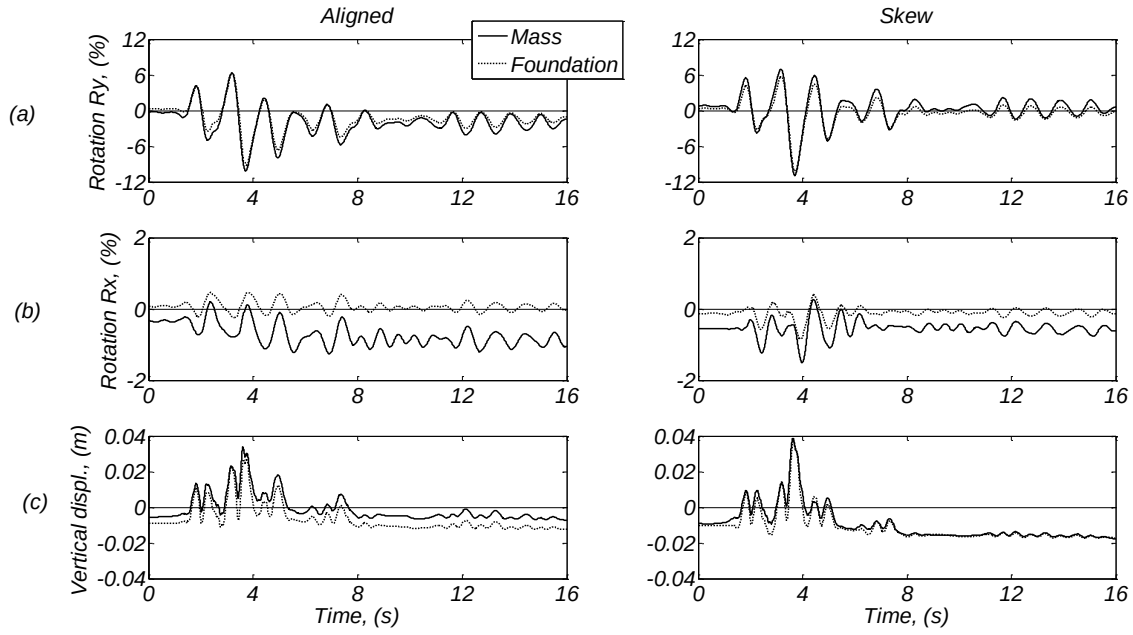

Figure C108. Time histories for the aligned and skew specimens; (a) mass drift ratio for the EW direction and equivalent foundation rotation, (b) mass drift ratio for the NS direction and equivalent foundation rotation, and (c) mass and footing vertical displacements.

Day 3, Parachute site 1.0 Motion

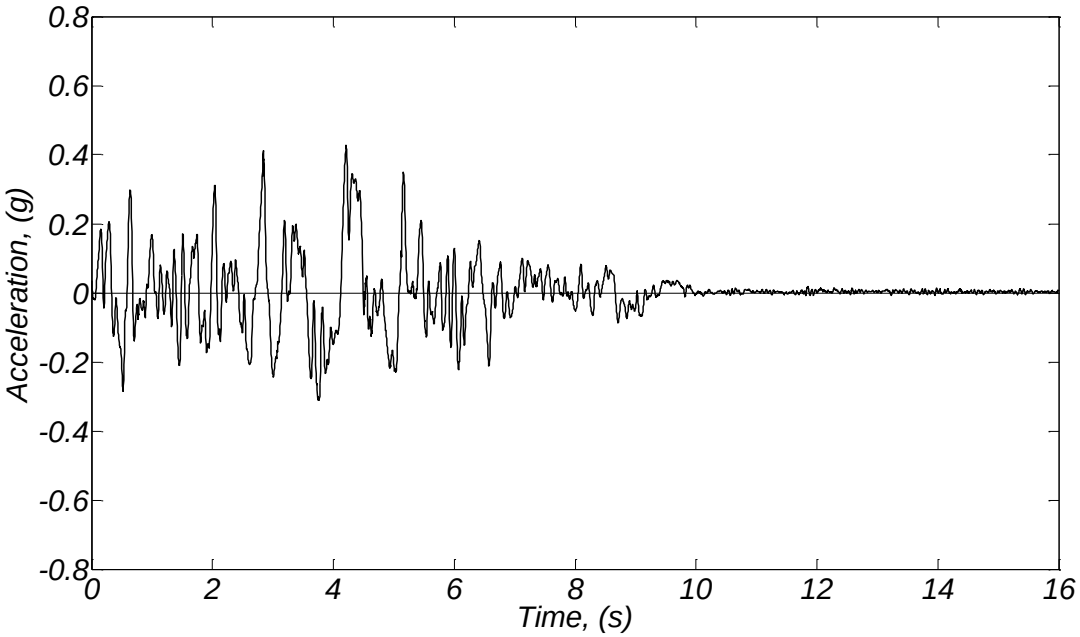

Figure C109. Soil free field acceleration time history (direction of shaking).

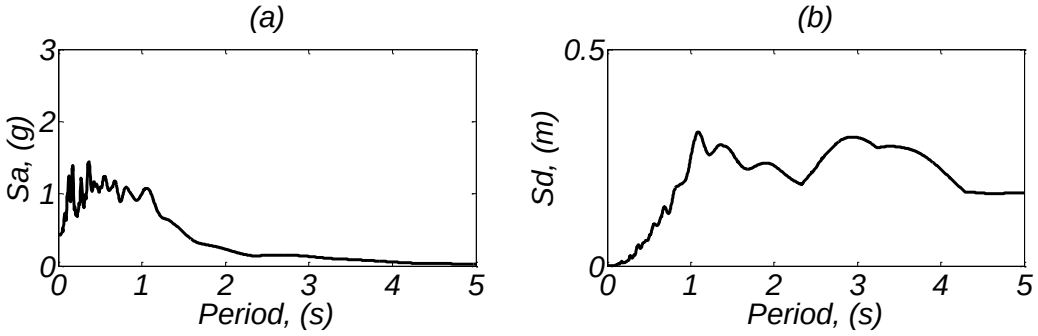

Figure C110. (a) Acceleration and (b) displacement response spectra for the recorded soil free field acceleration (direction of shaking) for damping $\zeta = 3\%$.

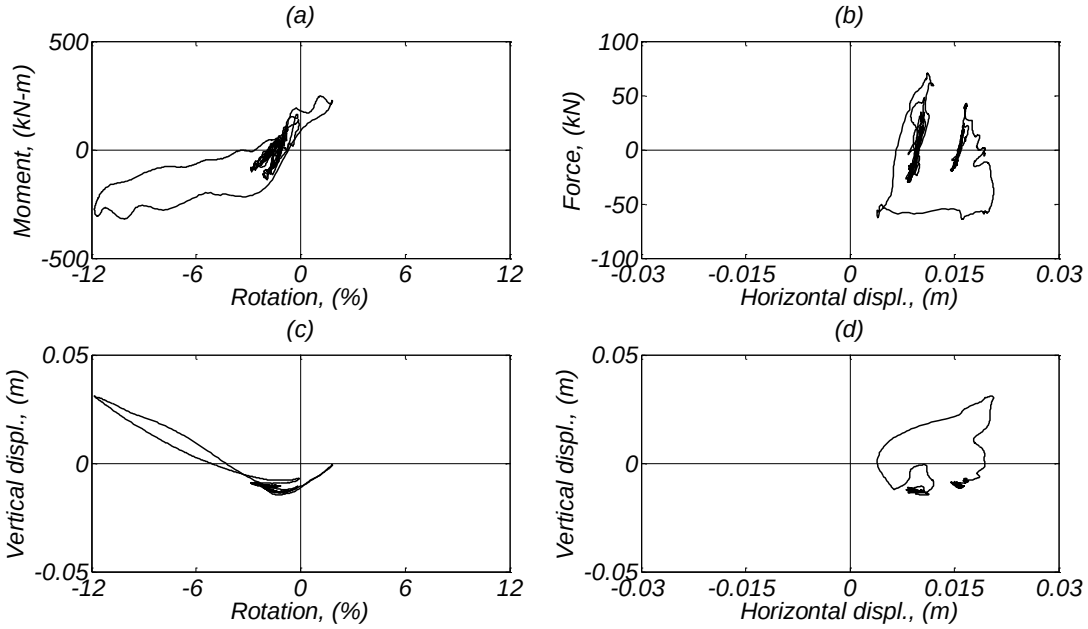

Figure C111. Aligned footing response; (a) moment vs rotation diagram (around NS direction), (b) base shear vs horizontal displacement (EW direction), (c) vertical displacement vs foundation rotation, and (d) vertical displacement vs horizontal displacement in the EW direction.

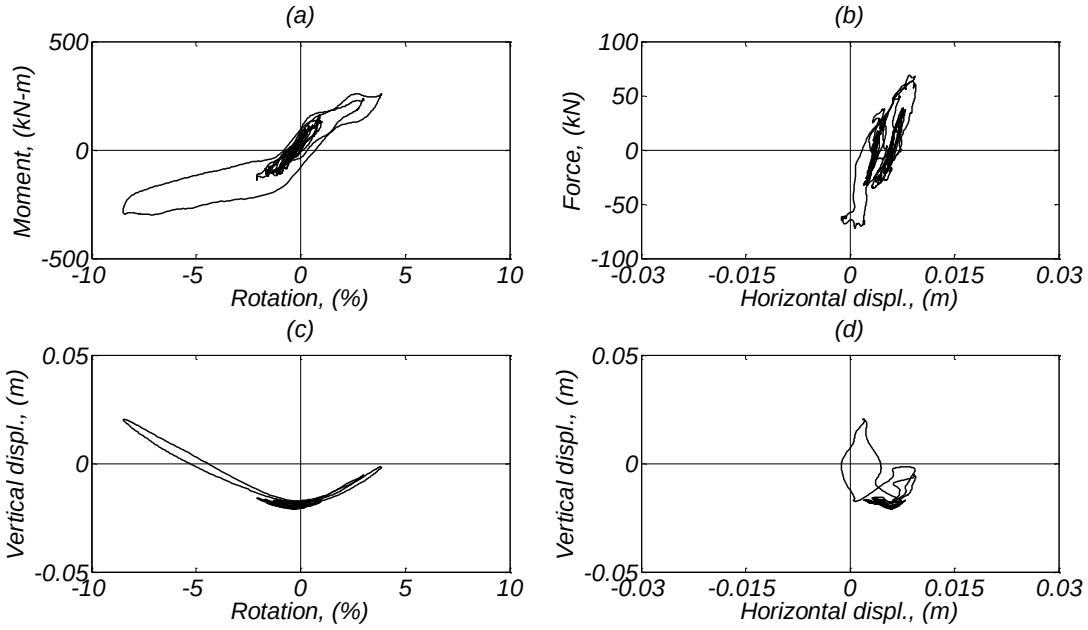

Figure C112. Skew footing response; (a) moment vs rotation diagram (around NS direction), (b) base shear vs horizontal displacement (EW direction), (c) vertical displacement vs foundation rotation, and (d) vertical displacement vs horizontal displacement in the EW direction.

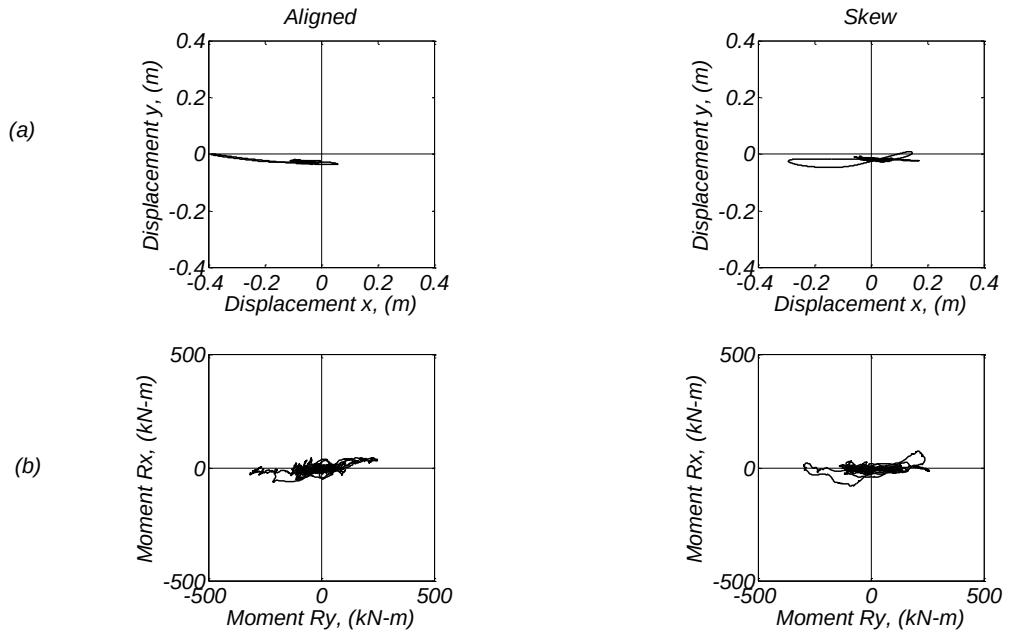

Figure C113. Bilateral response for the aligned and skew specimens; (a) mass displacement for the EW(x) and NS(y) direction, and (b) foundation moment for the corresponding directions.

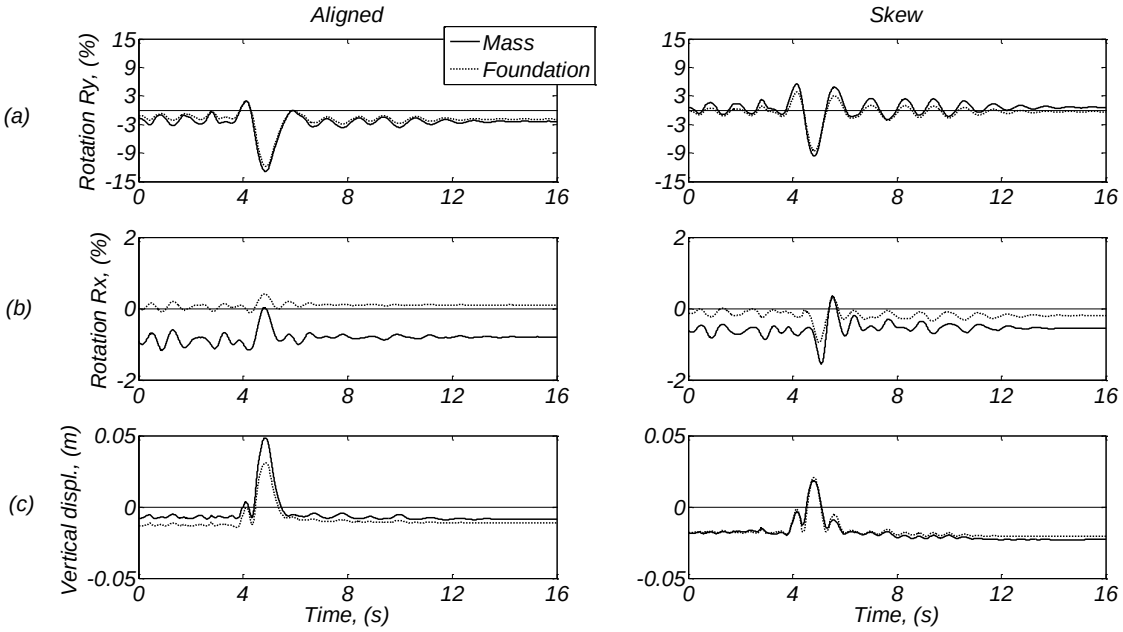

Figure C114. Time histories for the aligned and skew specimens; (a) mass drift ratio for the EW direction and equivalent foundation rotation, (b) mass drift ratio for the NS direction and equivalent foundation rotation, and (c) mass and footing vertical displacements.

Day 3, Parachute site -1.0 Motion

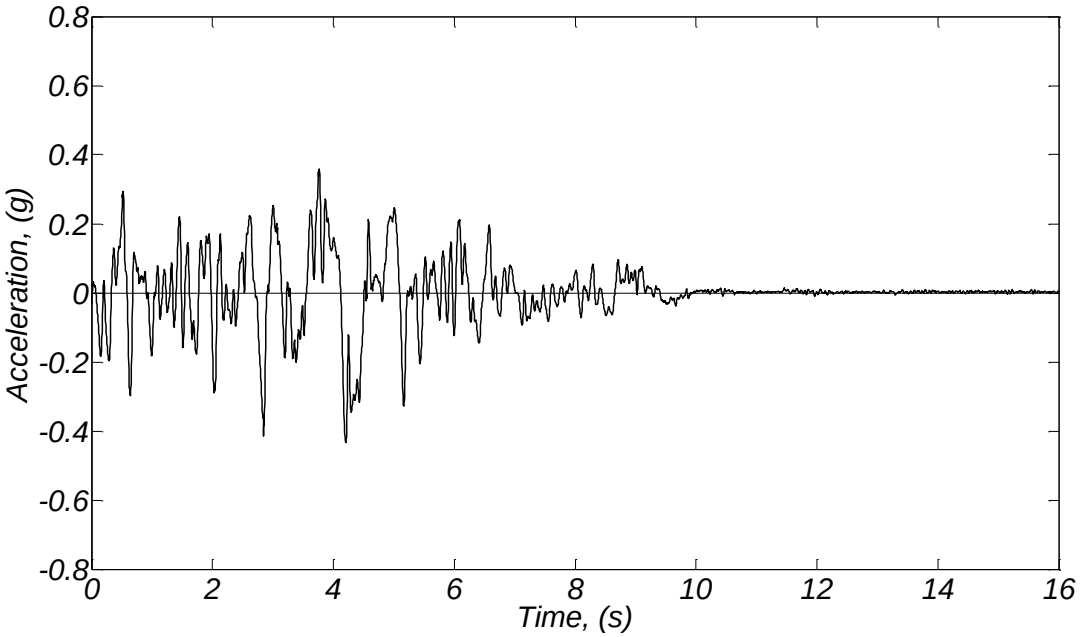

Figure C115. Soil free field acceleration time history (direction of shaking).

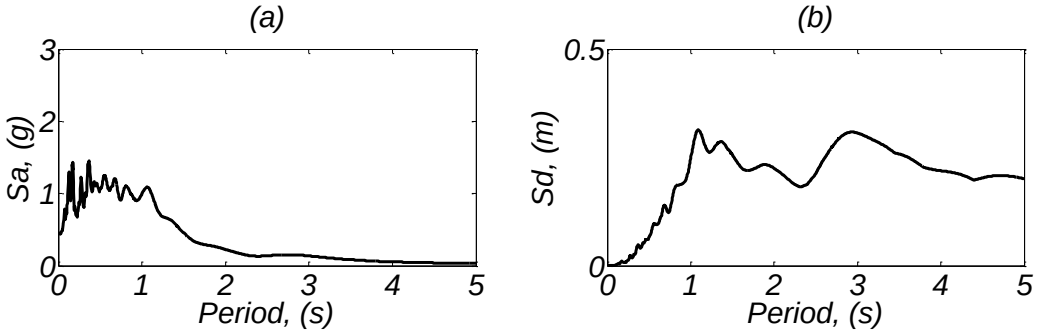

Figure C116. (a) Acceleration and (b) displacement response spectra for the recorded soil free field acceleration (direction of shaking) for damping ζ = 3%.

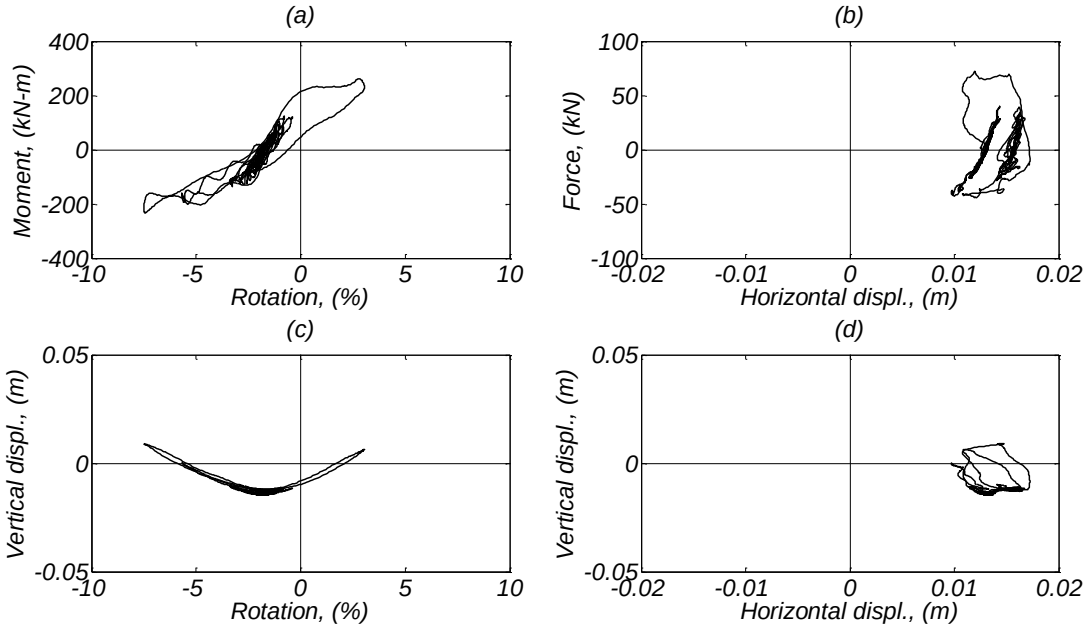

Figure C117. Aligned footing response; (a) moment vs rotation diagram (around NS direction), (b) base shear vs horizontal displacement (EW direction), (c) vertical displacement vs foundation rotation, and (d) vertical displacement vs horizontal displacement in the EW direction.

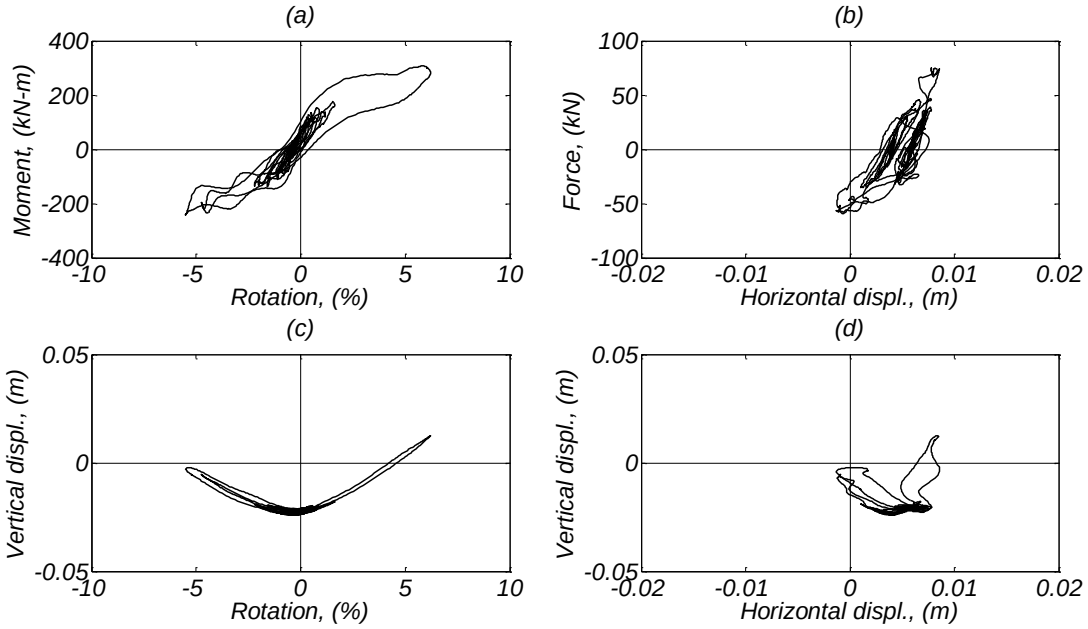

Figure C118. Skew footing response; (a) moment vs rotation diagram (around NS direction), (b) base shear vs horizontal displacement (EW direction), (c) vertical displacement vs foundation rotation, and (d) vertical displacement vs horizontal displacement in the EW direction.

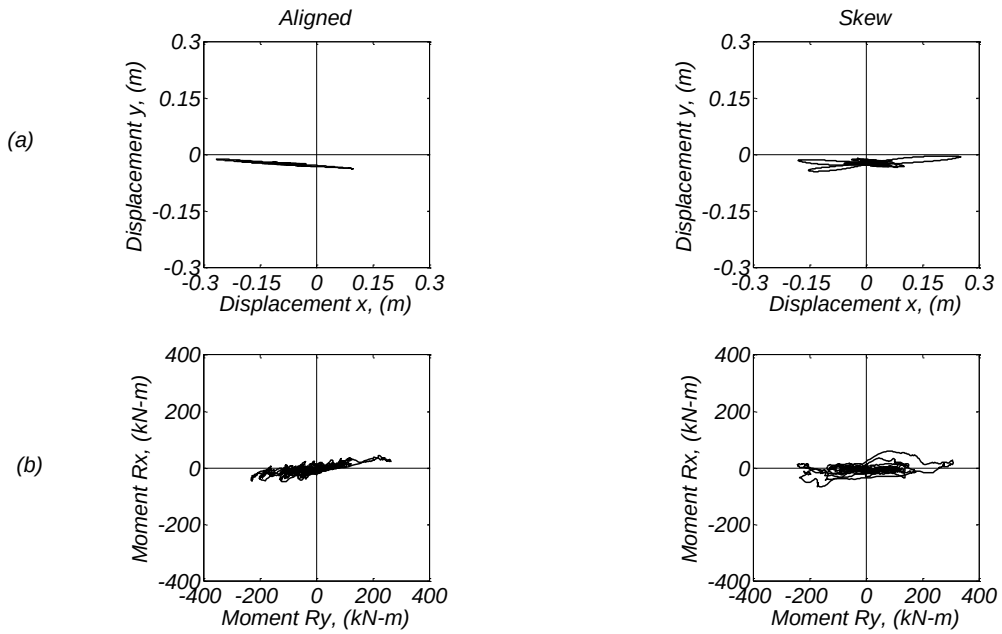

Figure C119. Bilateral response for the aligned and skew specimens; (a) mass displacement for the EW(x) and NS(y) direction, and (b) foundation moment for the corresponding directions.

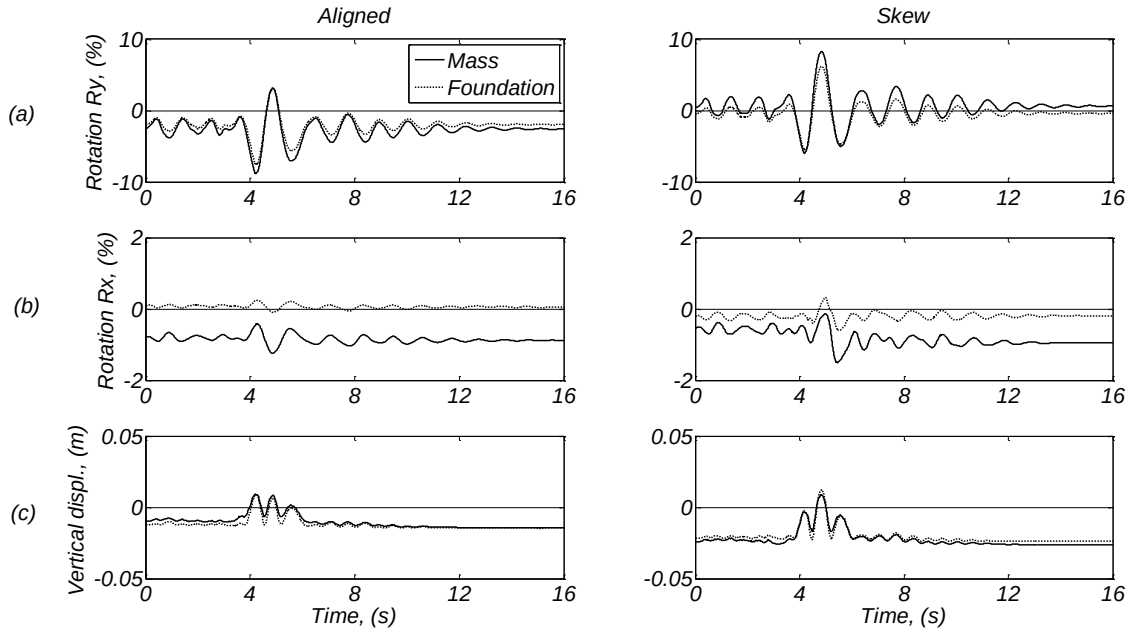

Figure C120. Time histories for the aligned and skew specimens; (a) mass drift ratio for the EW direction and equivalent foundation rotation, (b) mass drift ratio for the NS direction and equivalent foundation rotation, and (c) mass and footing vertical displacements.

Day 3, Parachute site 1.1 Motion

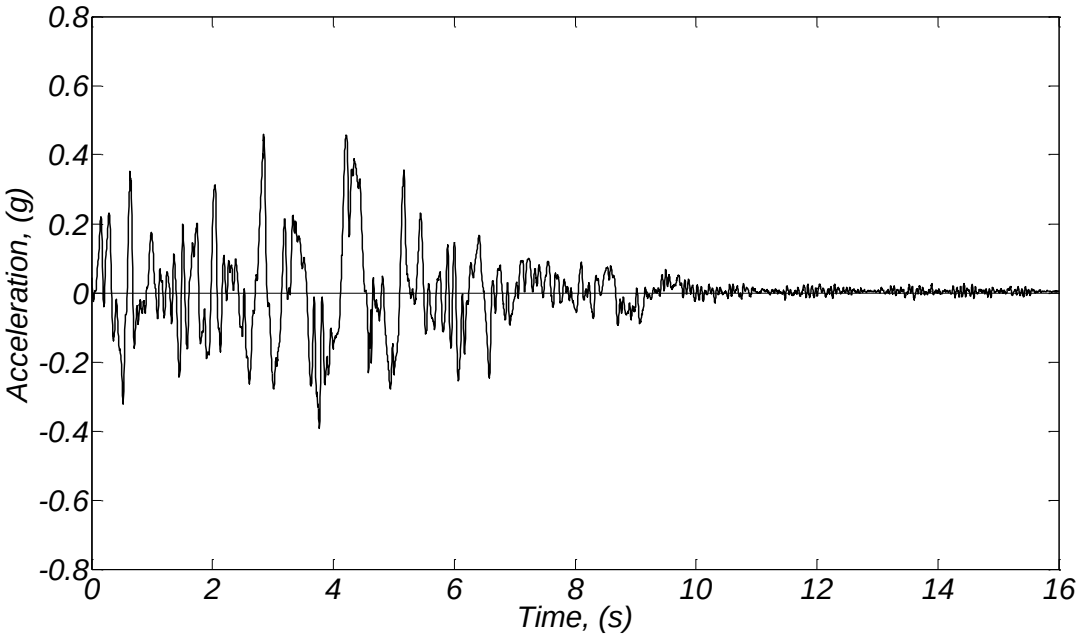

Figure C121. Soil free field acceleration time history (direction of shaking).

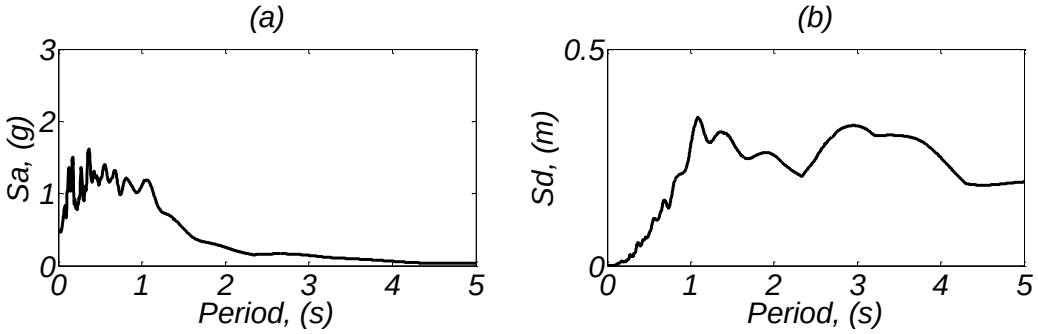

Figure C122. (a) Acceleration and (b) displacement response spectra for the recorded soil free field acceleration (direction of shaking) for damping $\zeta = 3\%$.

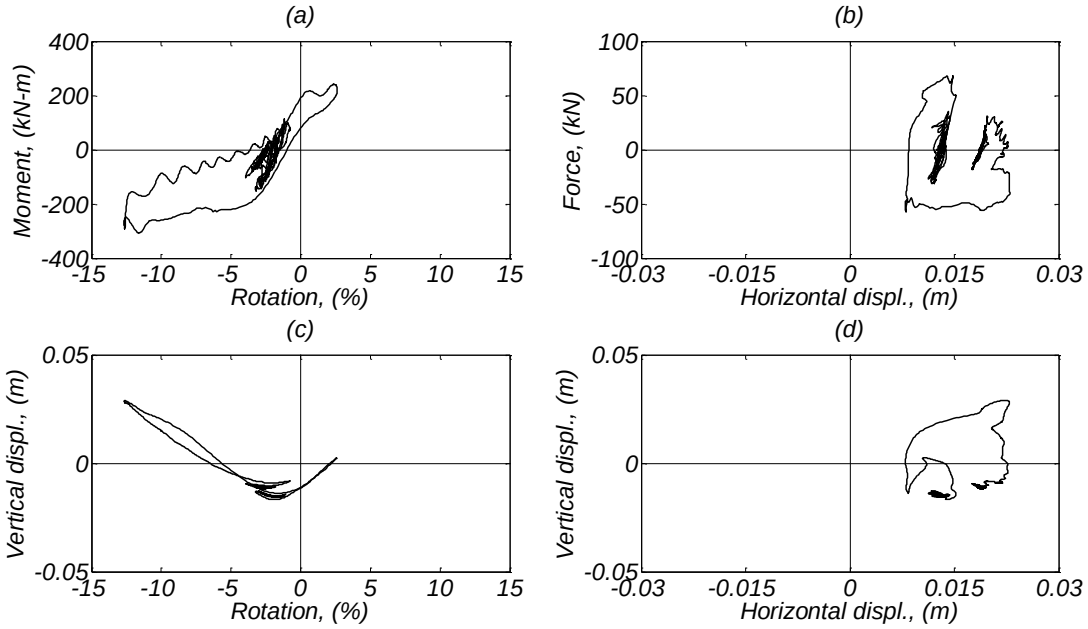

Figure C123. Aligned footing response; (a) moment vs rotation diagram (around NS direction), (b) base shear vs horizontal displacement (EW direction), (c) vertical displacement vs foundation rotation, and (d) vertical displacement vs horizontal displacement in the EW direction.

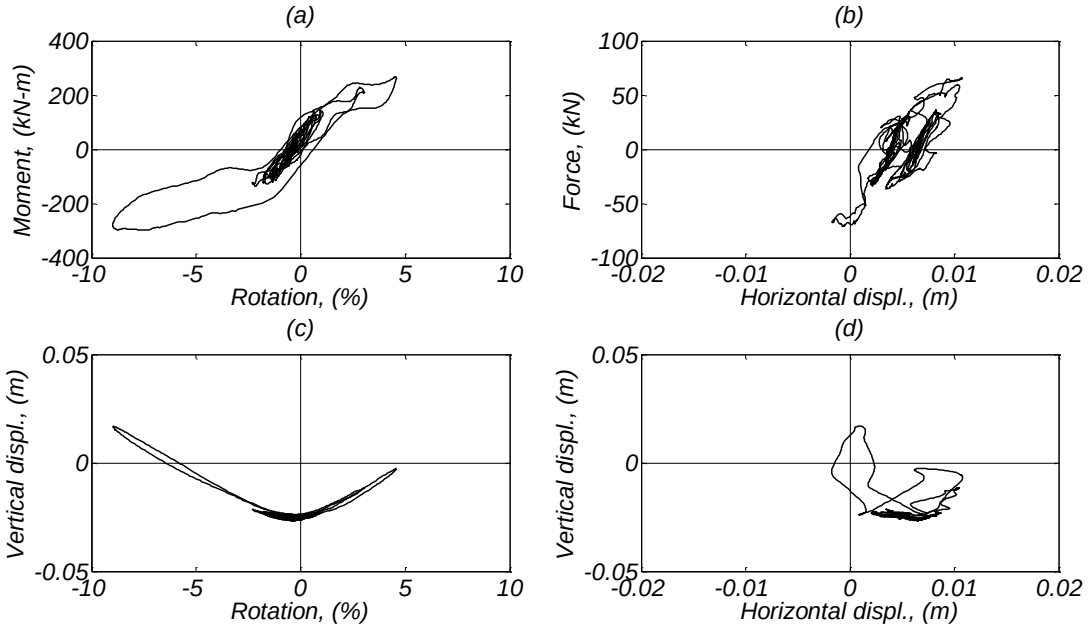

Figure C124. Skew footing response; (a) moment vs rotation diagram (around NS direction), (b) base shear vs horizontal displacement (EW direction), (c) vertical displacement vs foundation rotation, and (d) vertical displacement vs horizontal displacement in the EW direction.

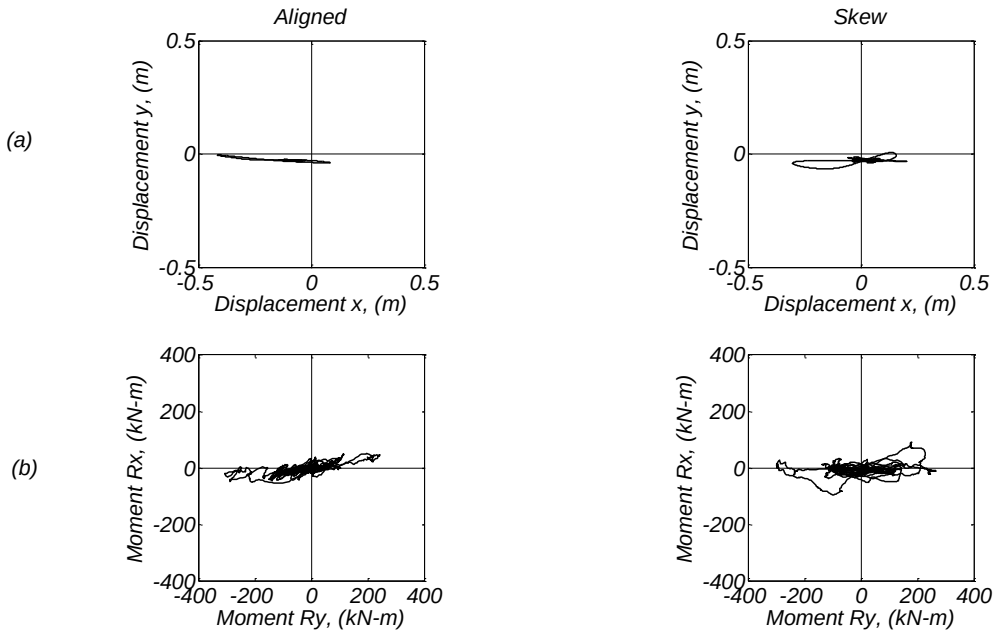

Figure C125. Bilateral response for the aligned and skew specimens; (a) mass displacement for the EW(x) and NS(y) direction, and (b) foundation moment for the corresponding directions.

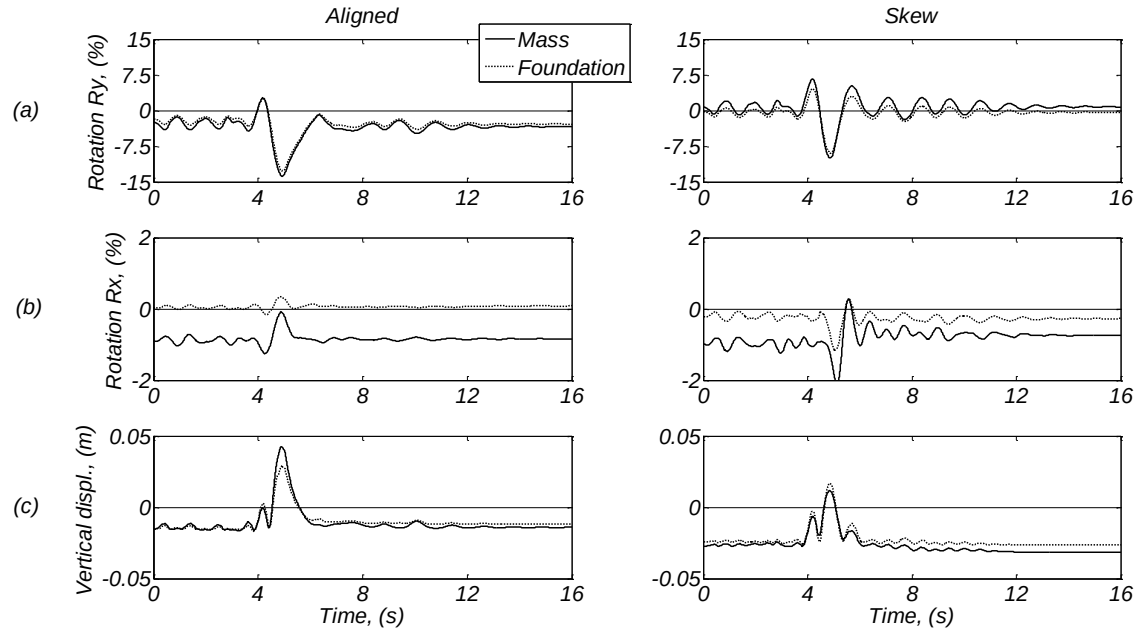

Figure C126. Time histories for the aligned and skew specimens; (a) mass drift ratio for the EW direction and equivalent foundation rotation, (b) mass drift ratio for the NS direction and equivalent foundation rotation, and (c) mass and footing vertical displacements.

Appendix D: Raw time history plots

Day 1, Takatori 0.5 Motion

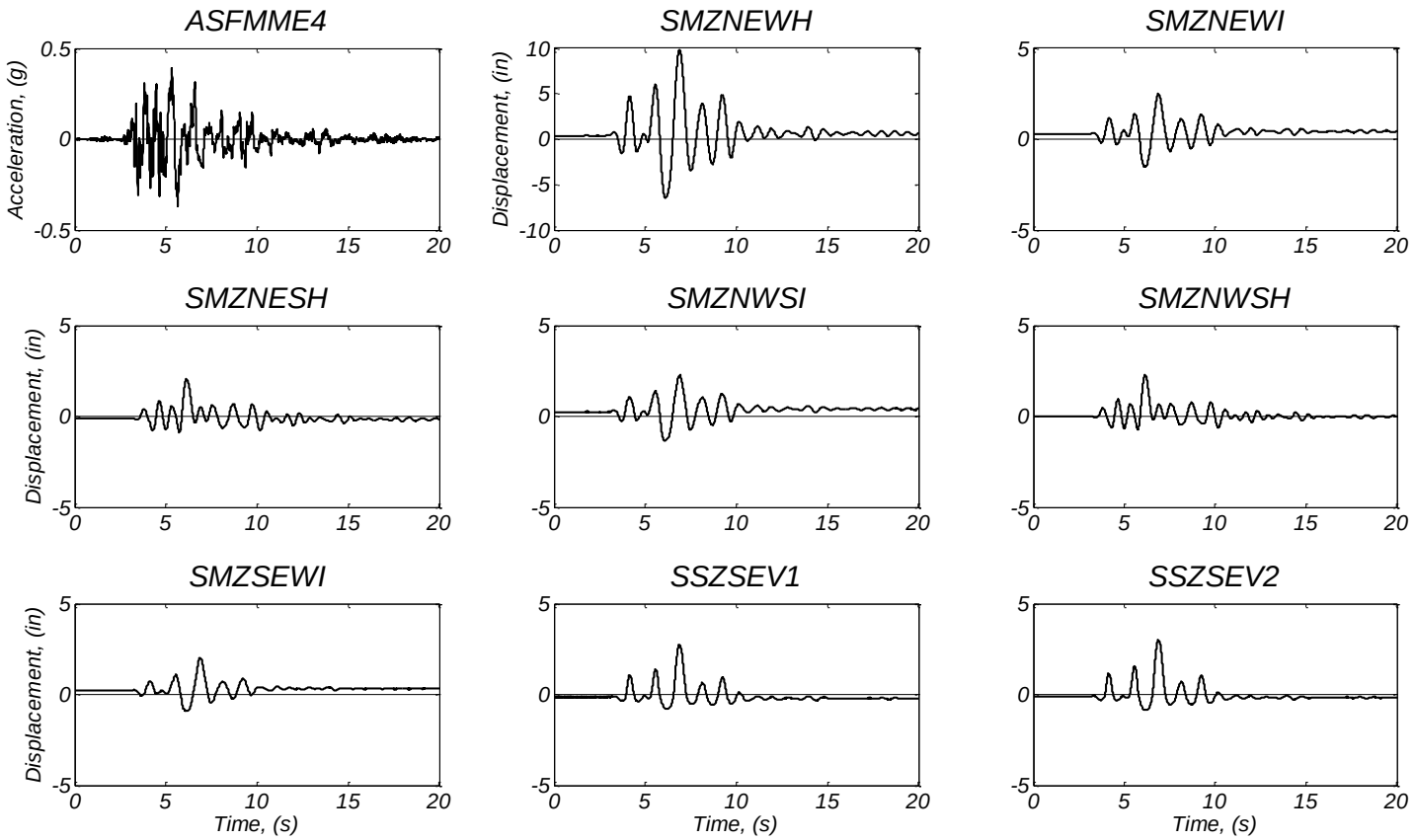

Figure D1. Raw data plots for string potentiometers.

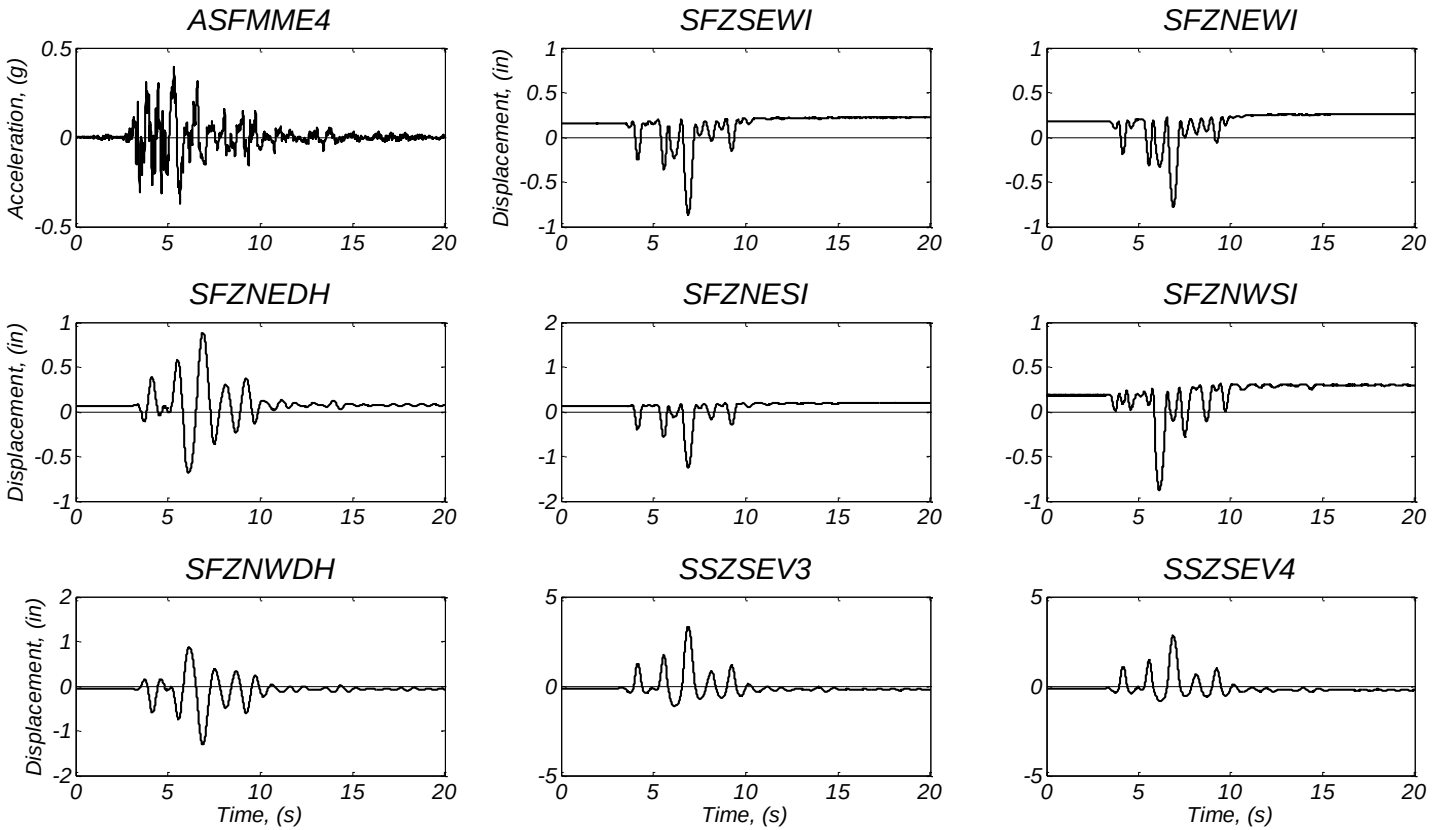

Figure D2. Raw data plots for string potentiometers.

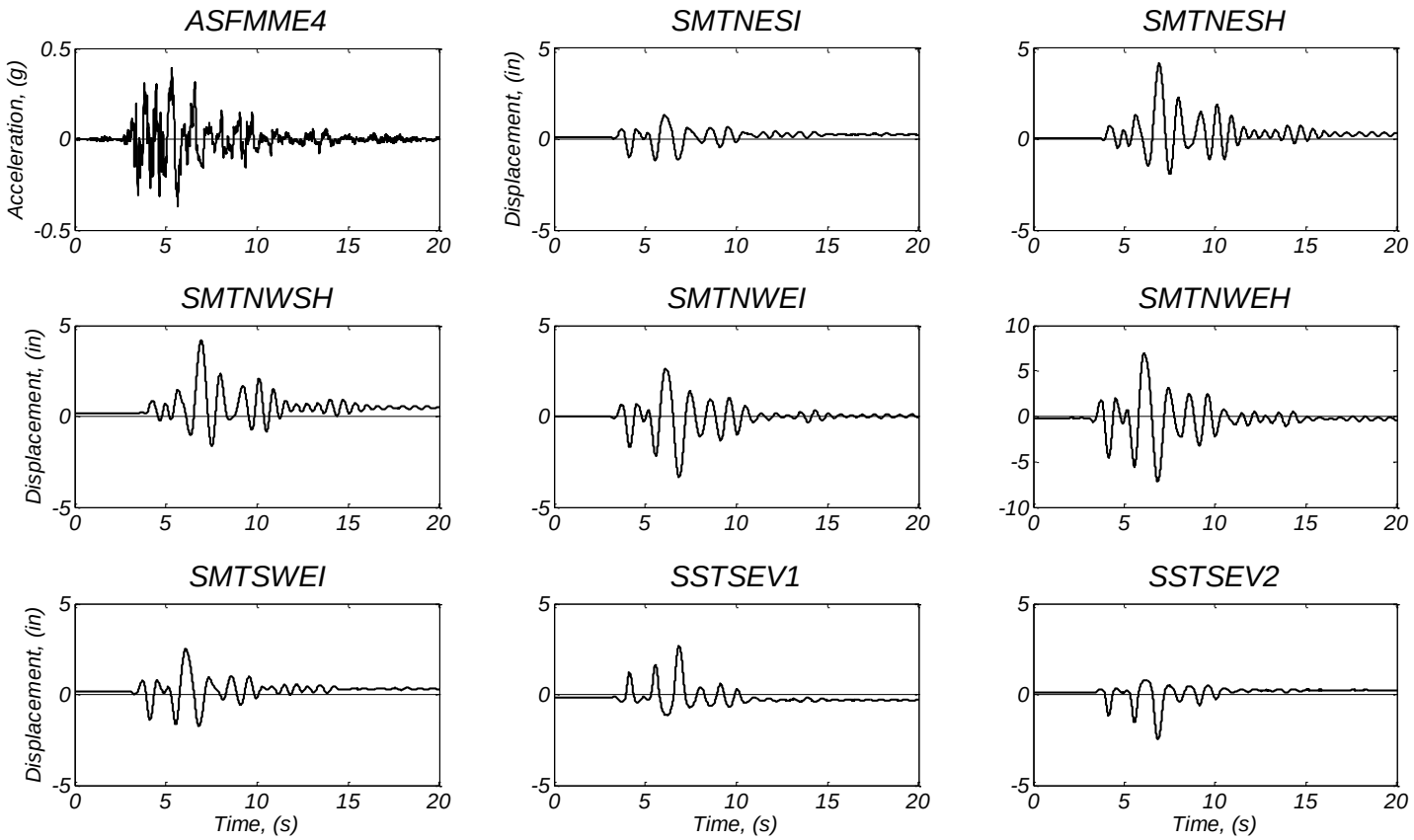

Figure D3. Raw data plots for string potentiometers.

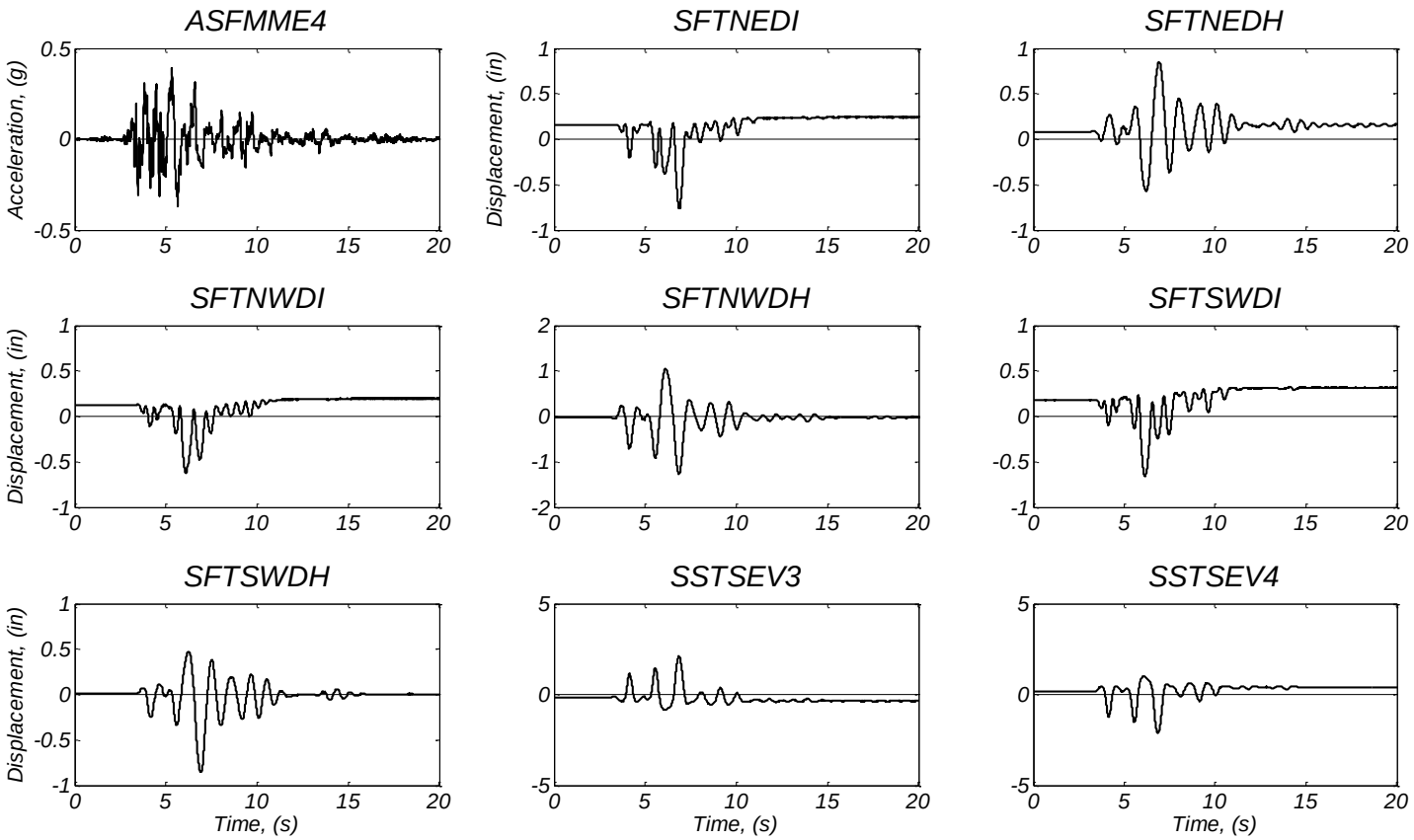

Figure D4. Raw data plots for string potentiometers.

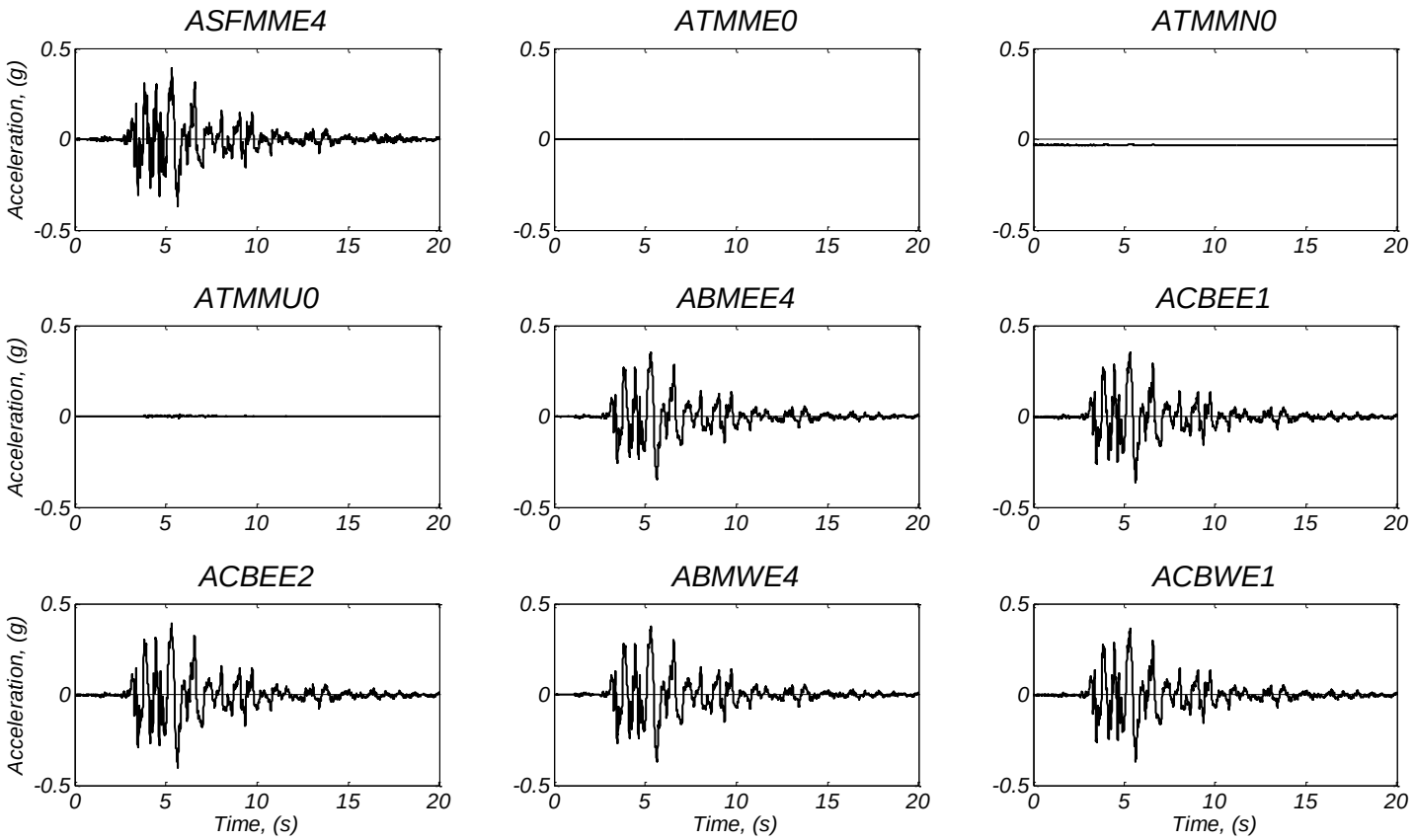

Figure D5. Raw data plots for accelerometers.

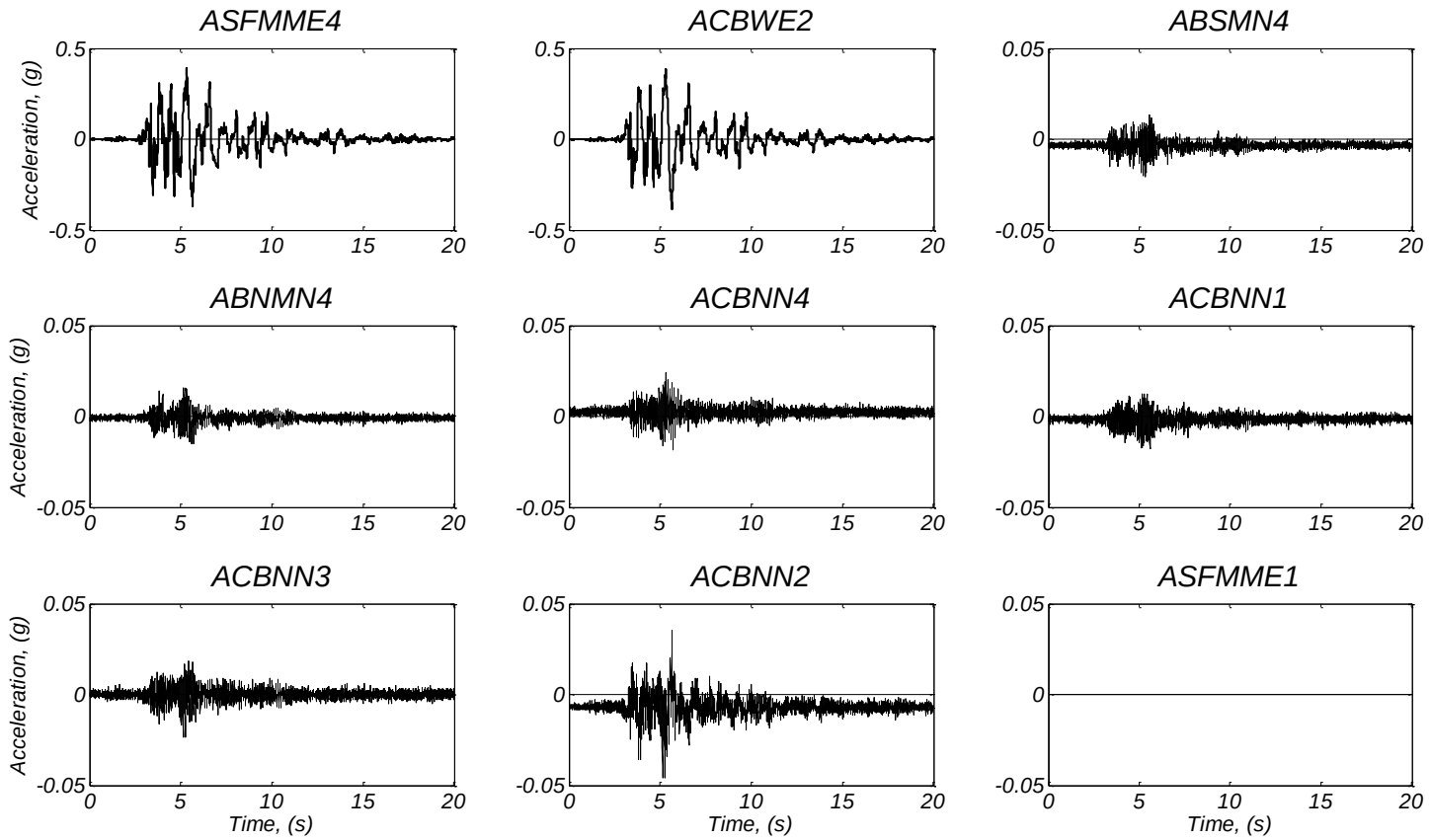

Figure D6. Raw data plots for accelerometers.

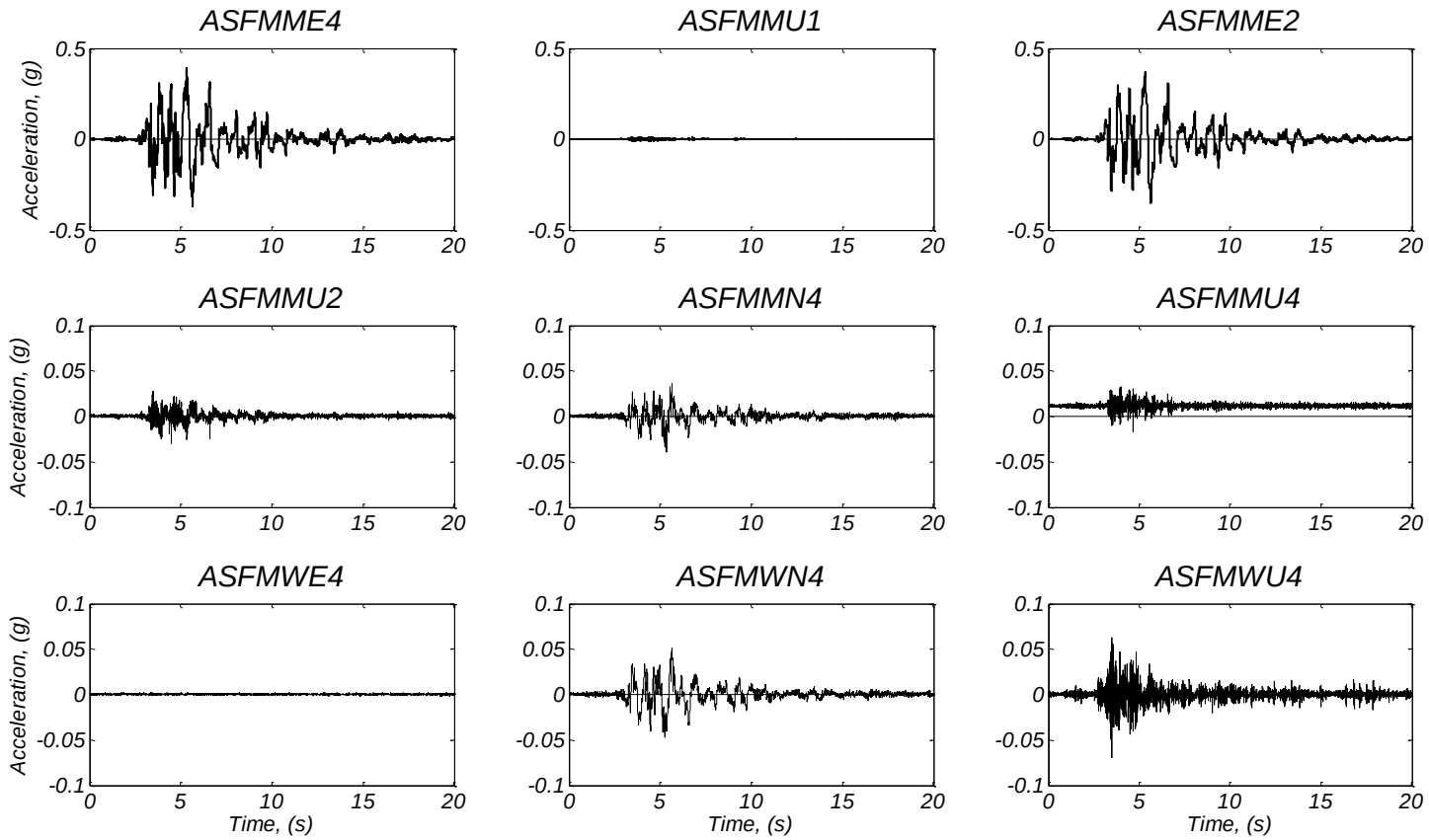

Figure D7. Raw data plots for accelerometers.

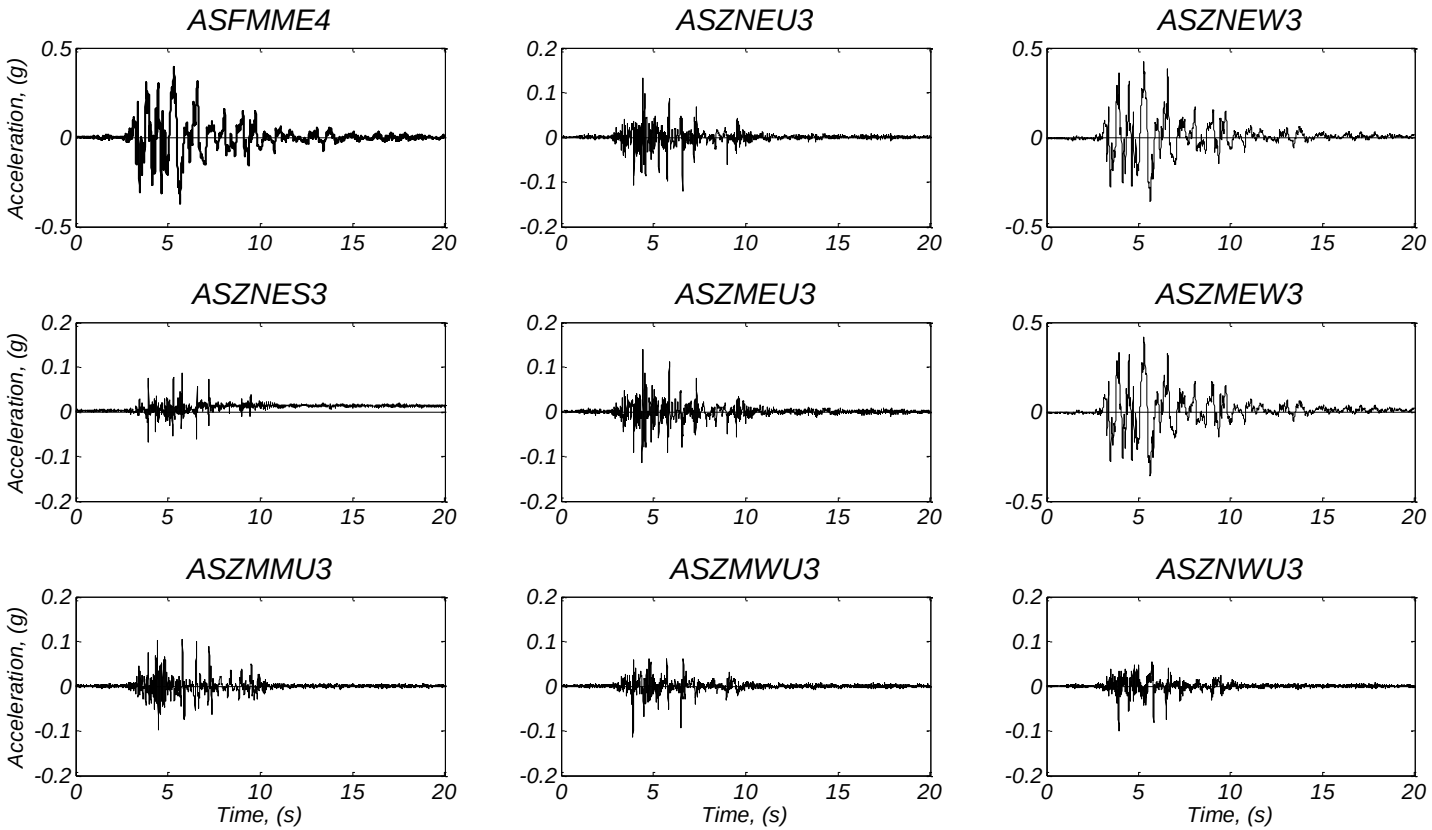

Figure D8. Raw data plots for accelerometers.

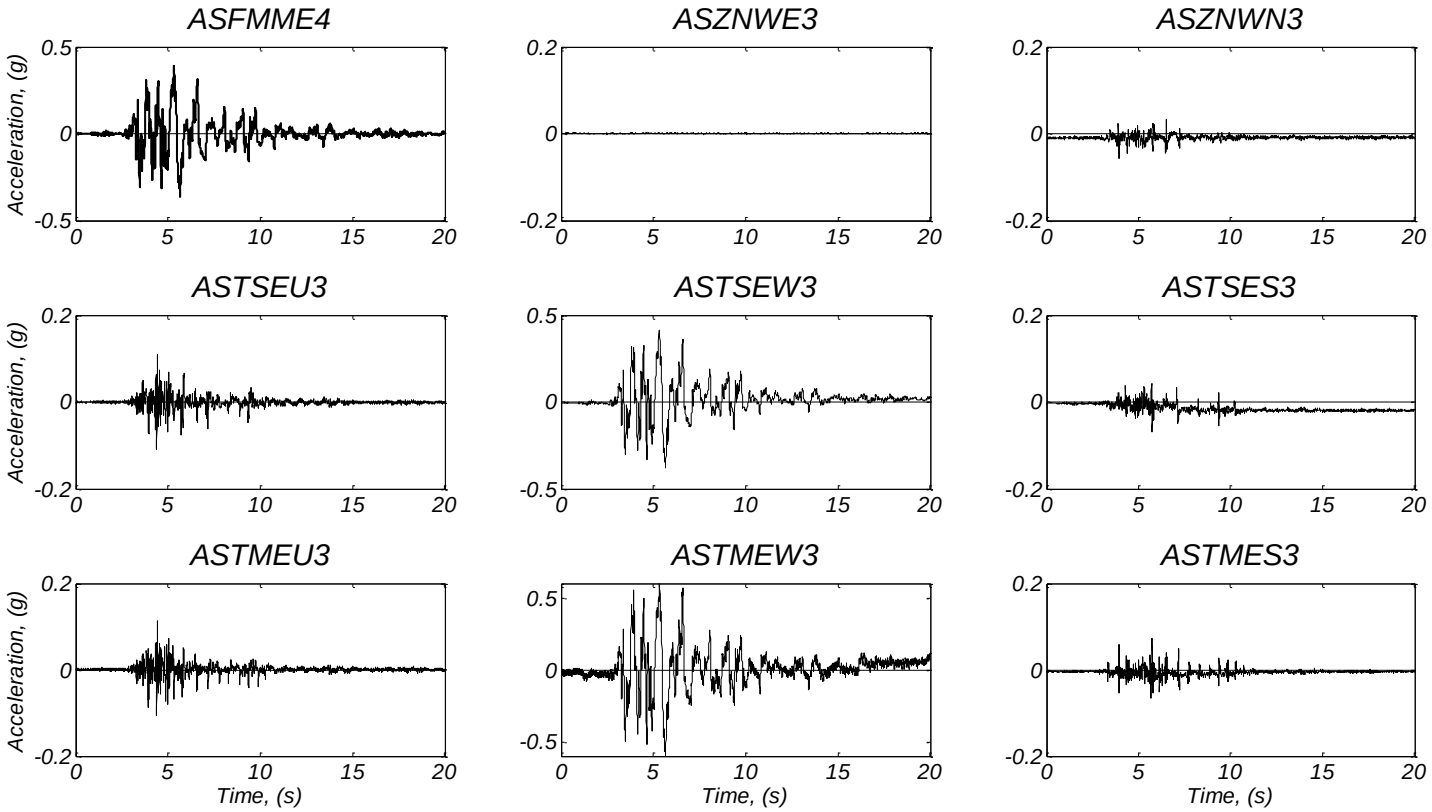

Figure D9. Raw data plots for accelerometers.

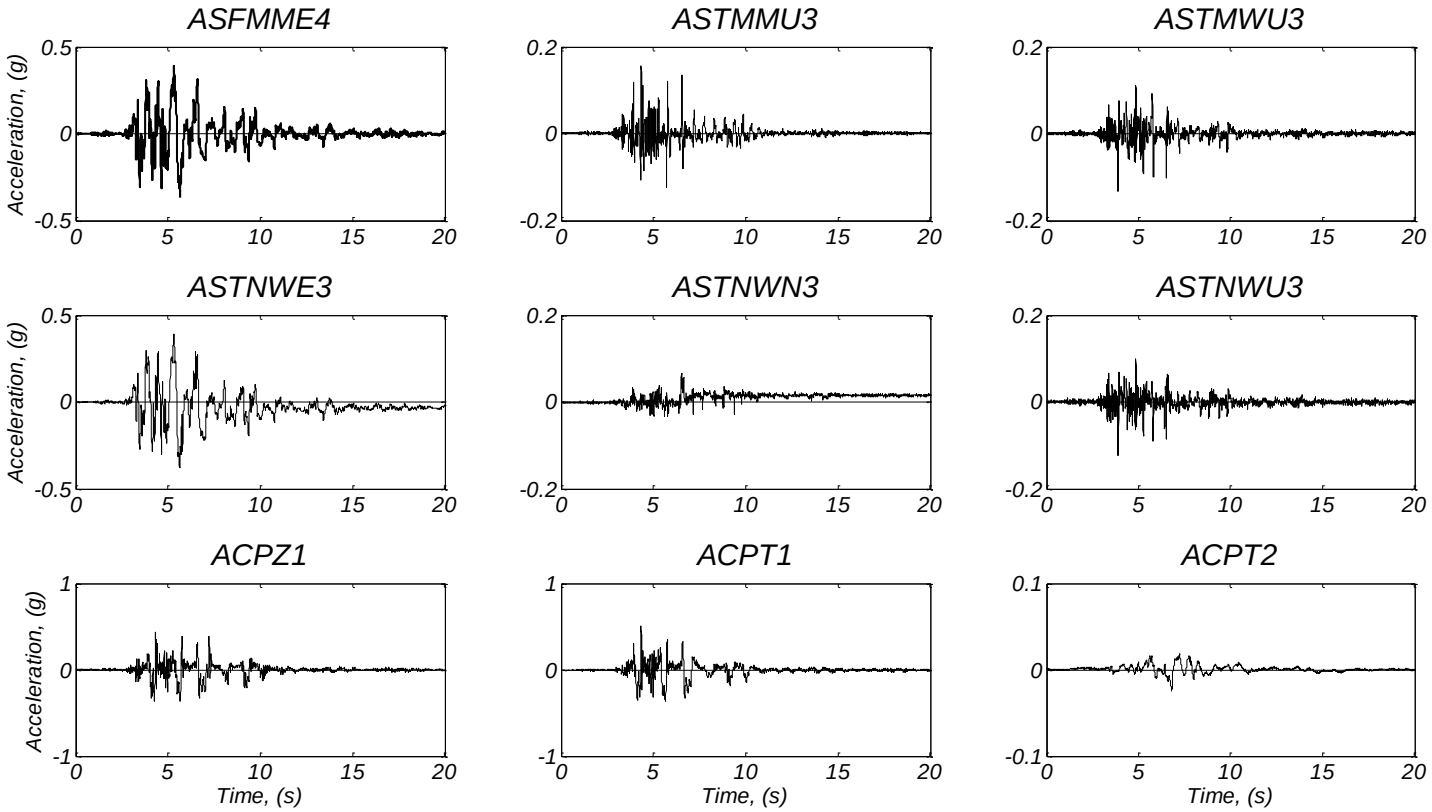

Figure D10. Raw data plots for accelerometers.

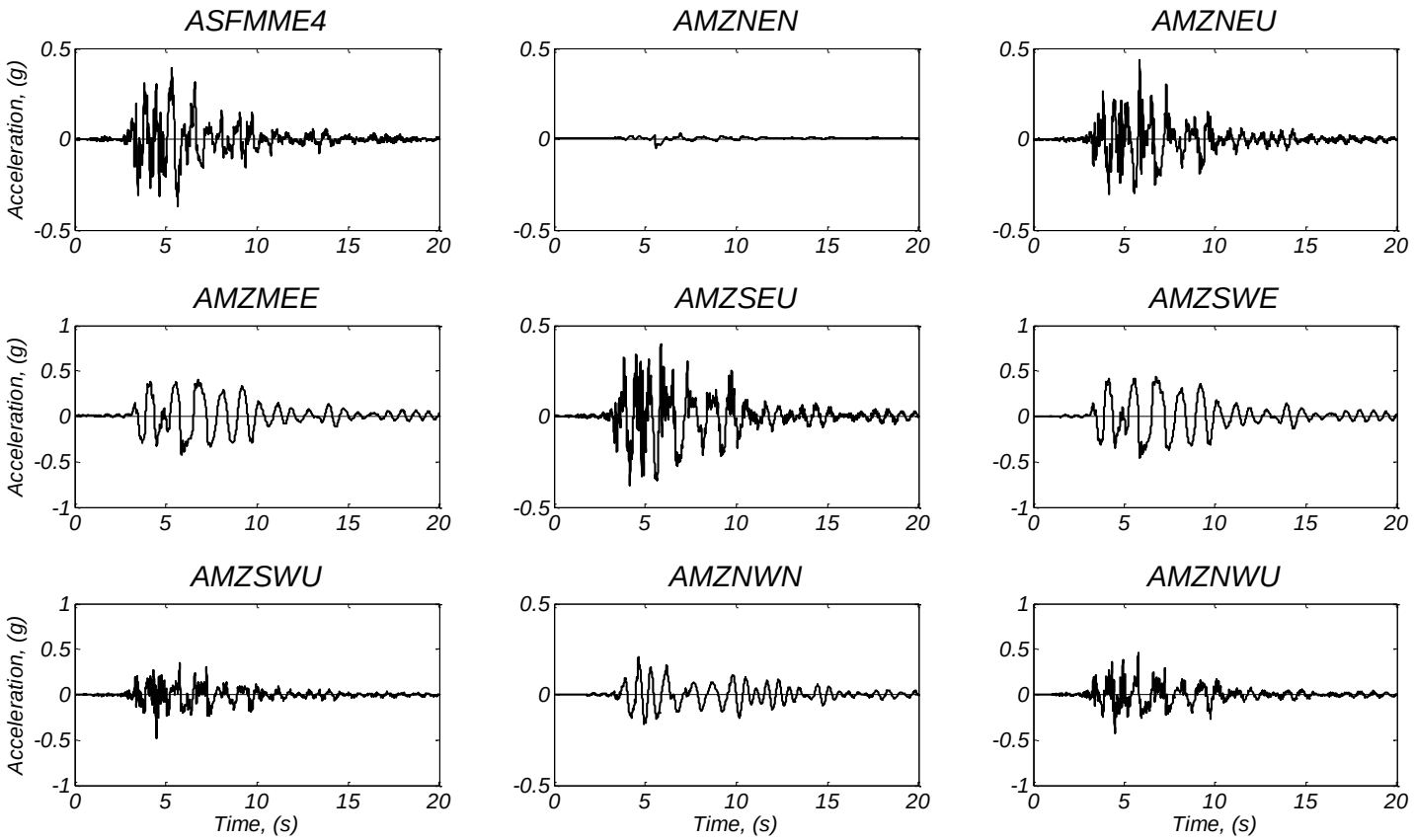

Figure D11. Raw data plots for accelerometers.

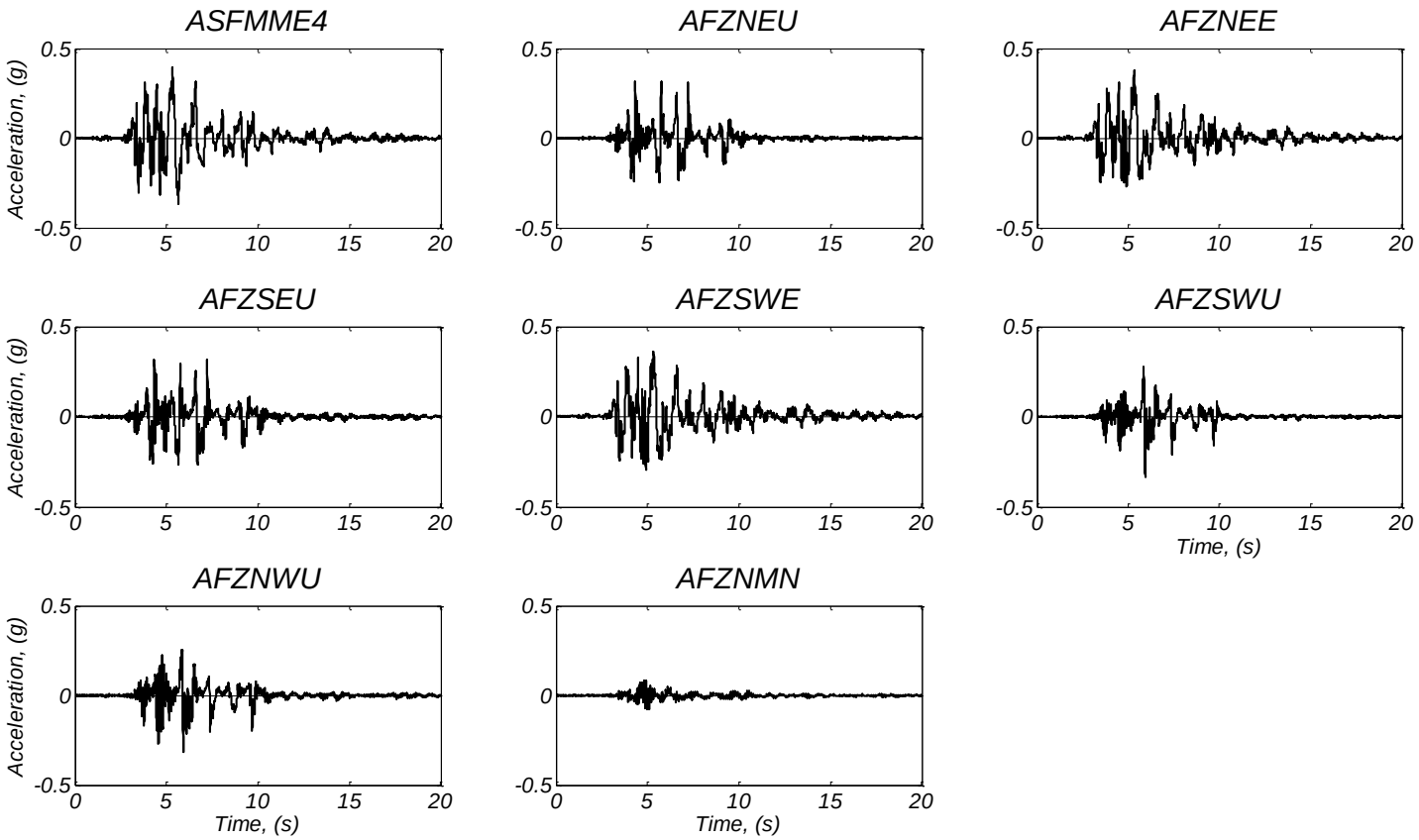

Figure D12. Raw data plots for accelerometers.

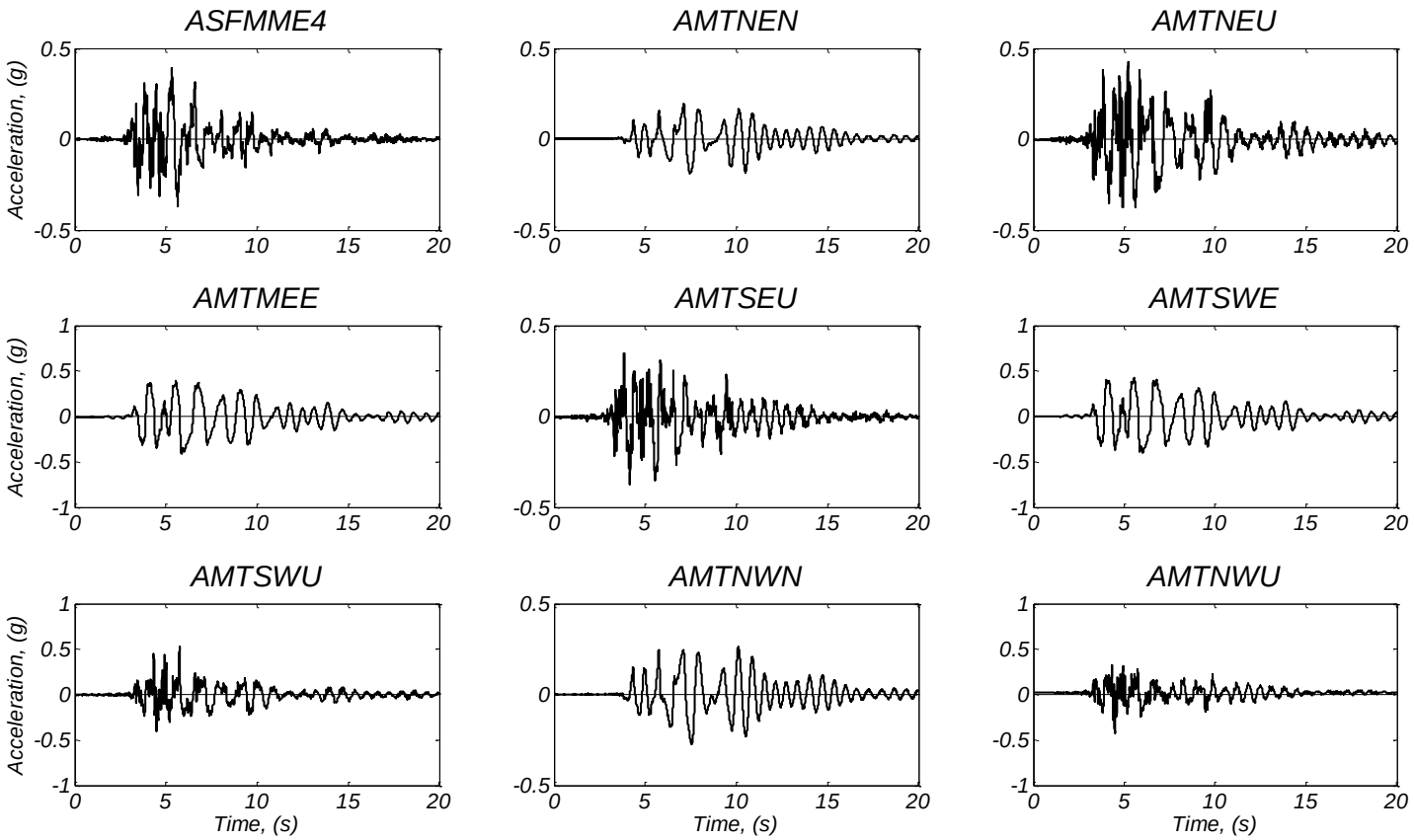

Figure D13. Raw data plots for accelerometers.

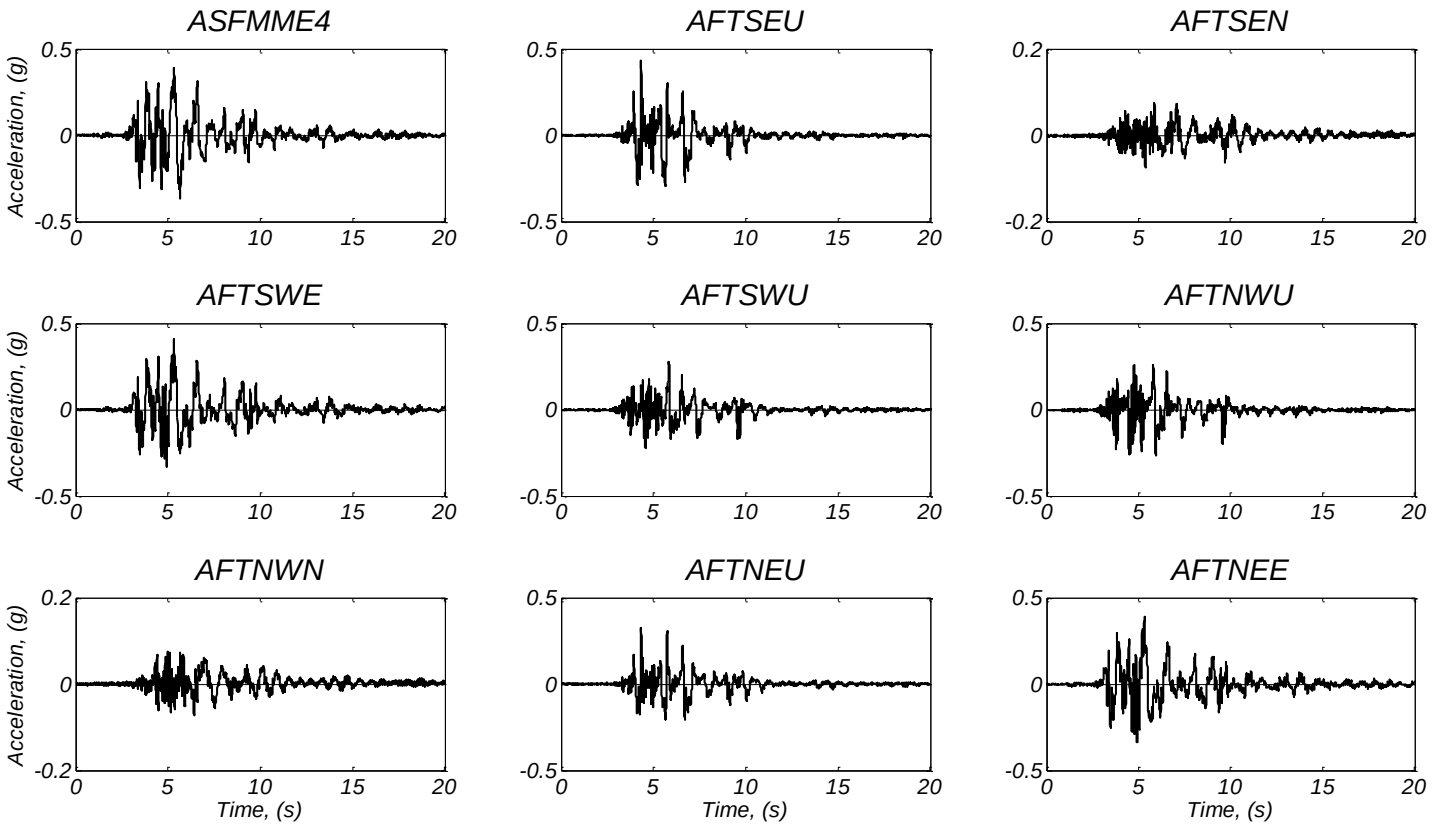

Figure D14. Raw data plots for accelerometers.

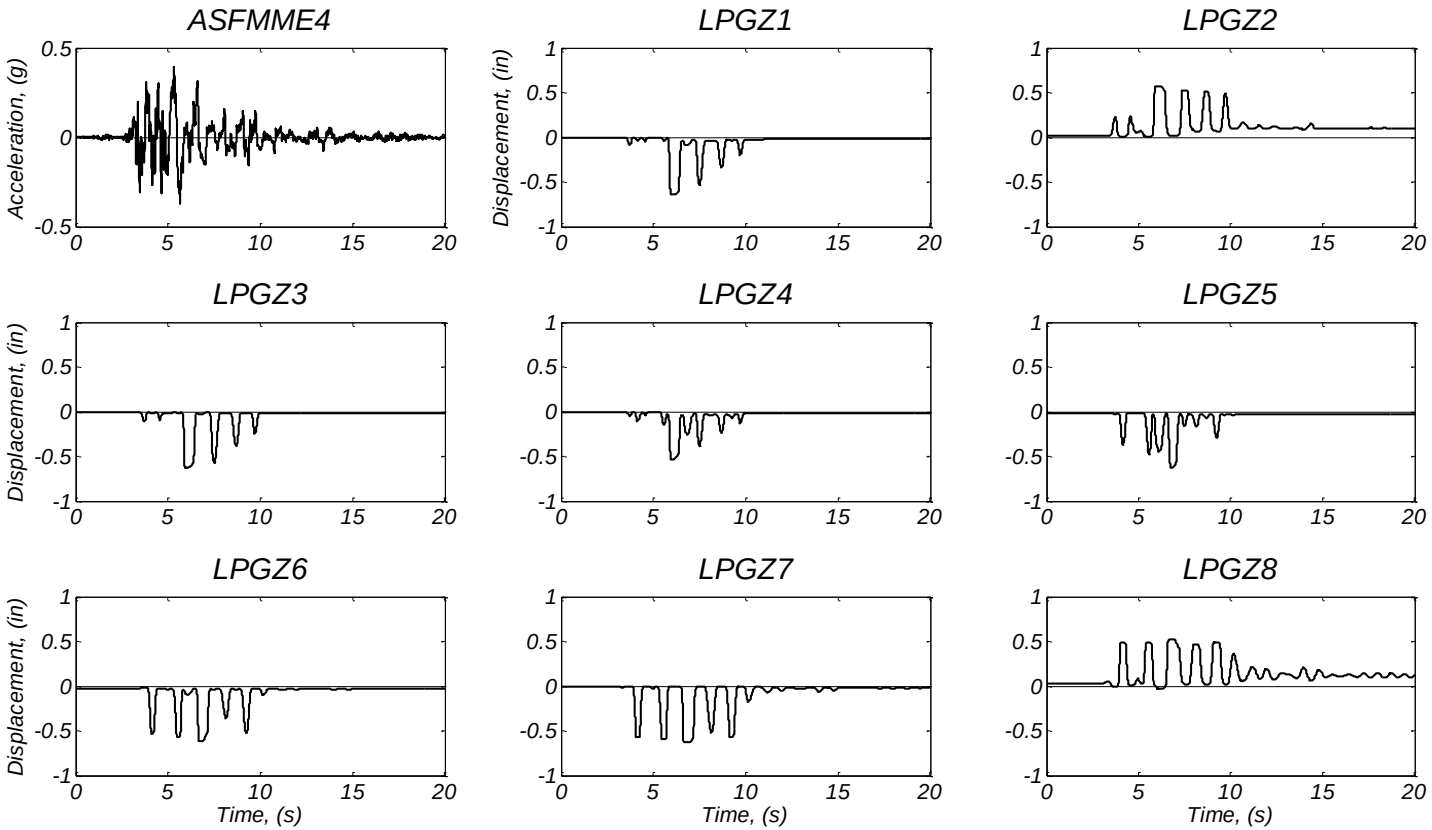

Figure D15. Raw data plots for linear potentiometers.

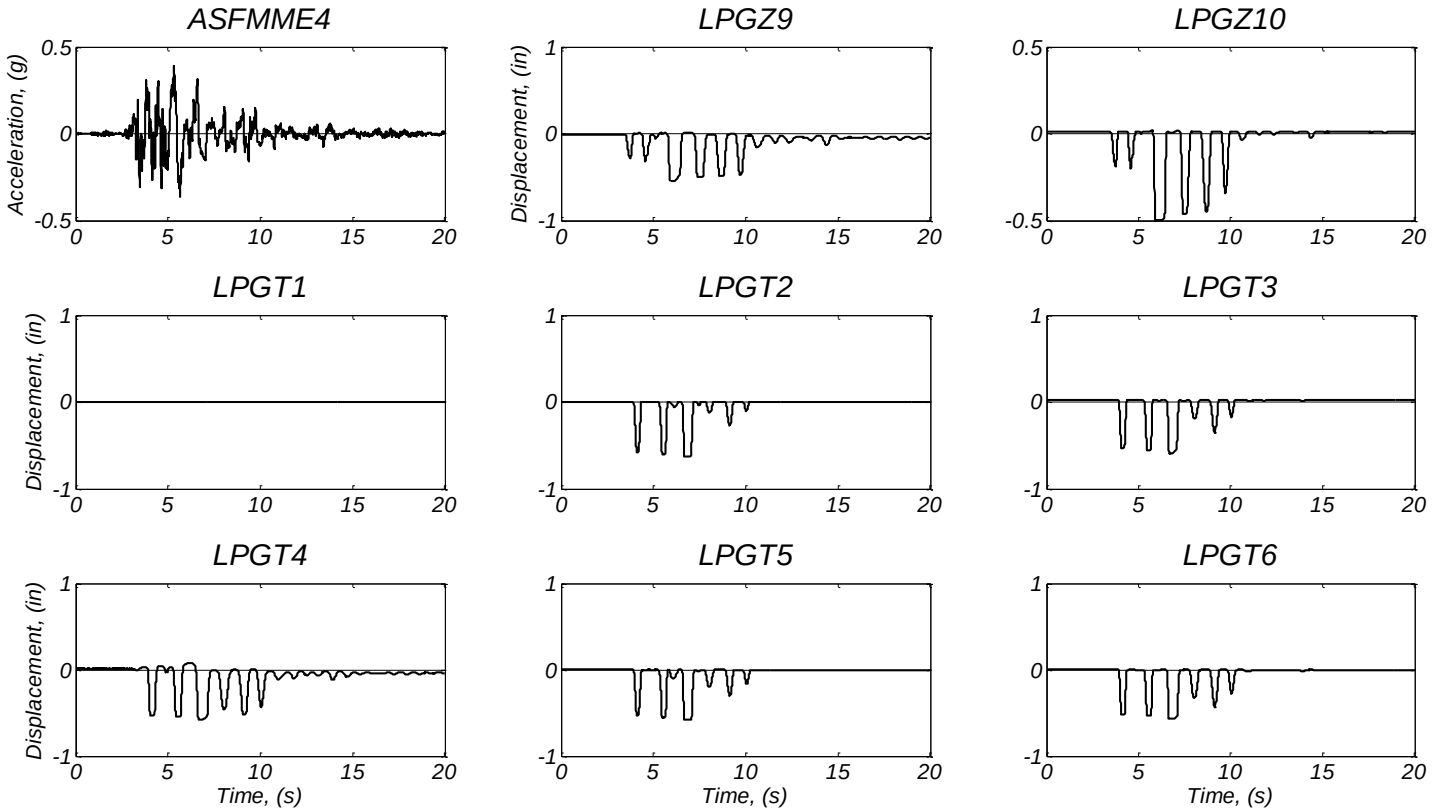

Figure D16. Raw data plots for linear potentiometers.

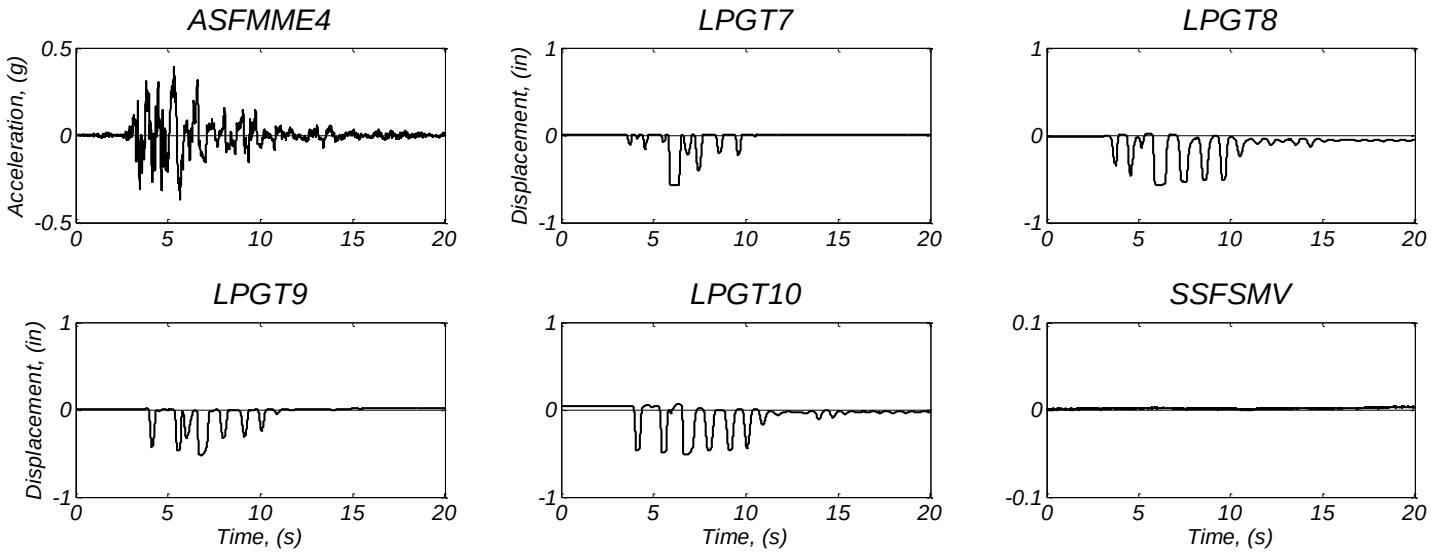

Figure D17. Raw data plots for linear and string potentiometers.

Day 3, Takatori 0.5 Motion

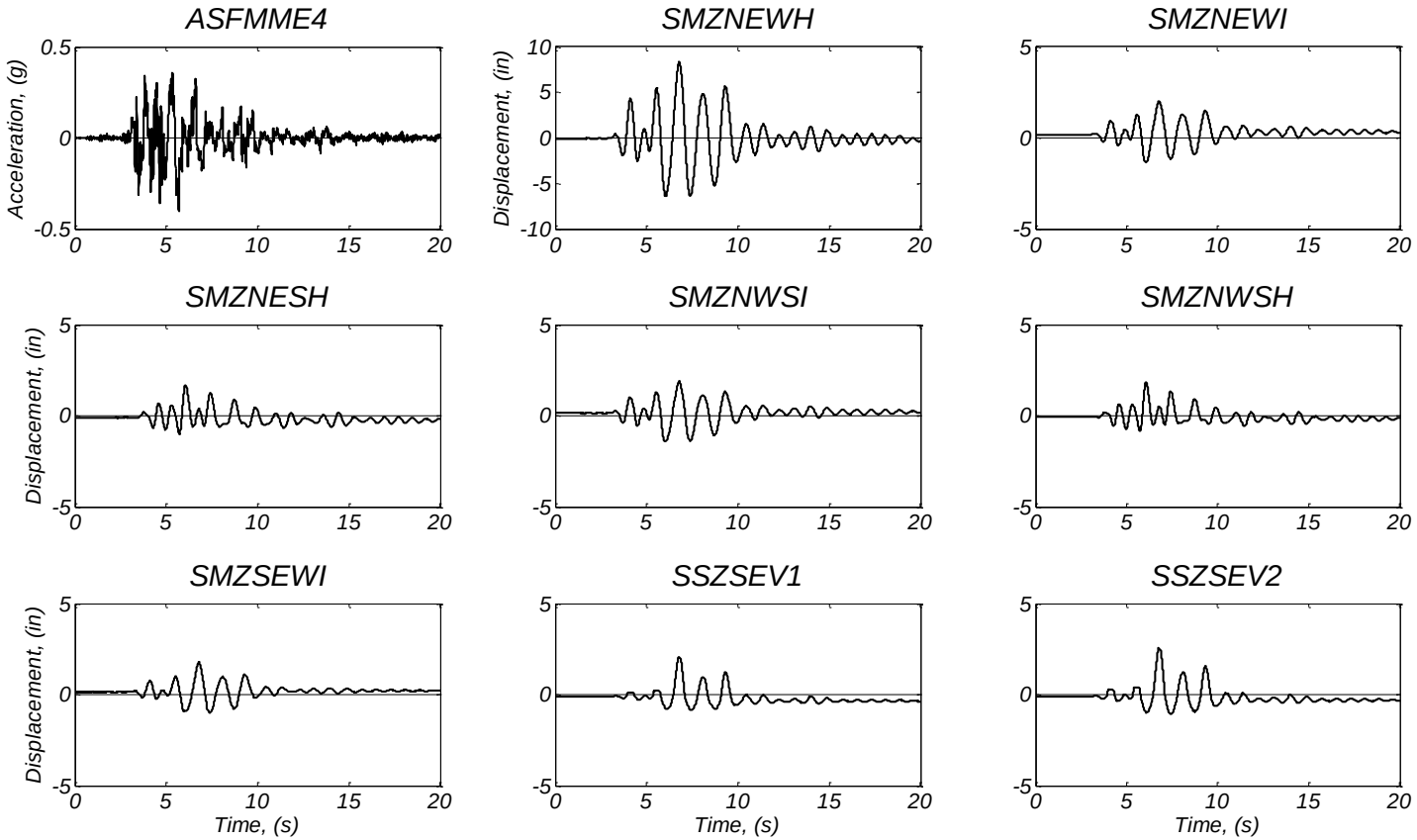

Figure D18. Raw data plots for string potentiometers.

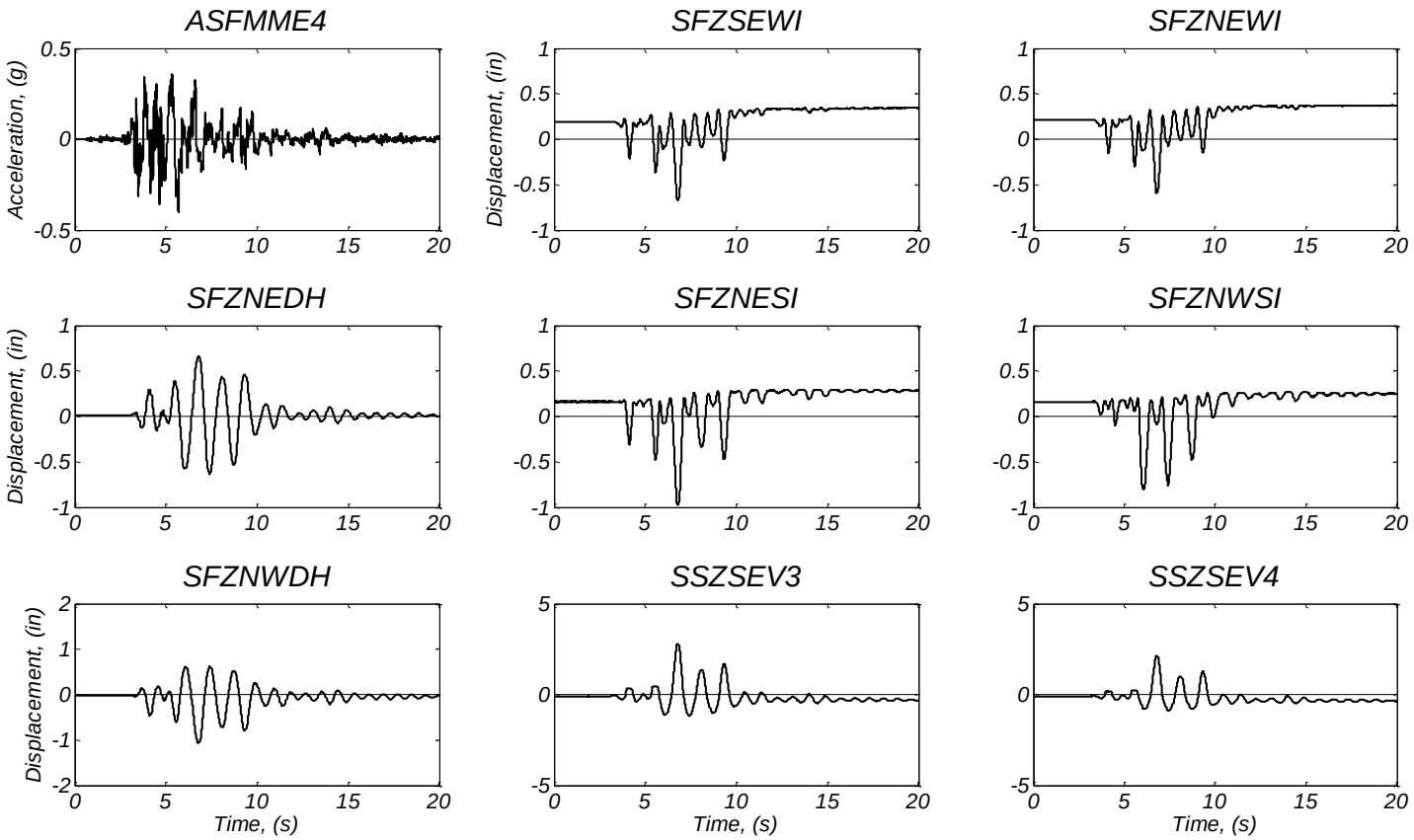

Figure D19. Raw data plots for string potentiometers.

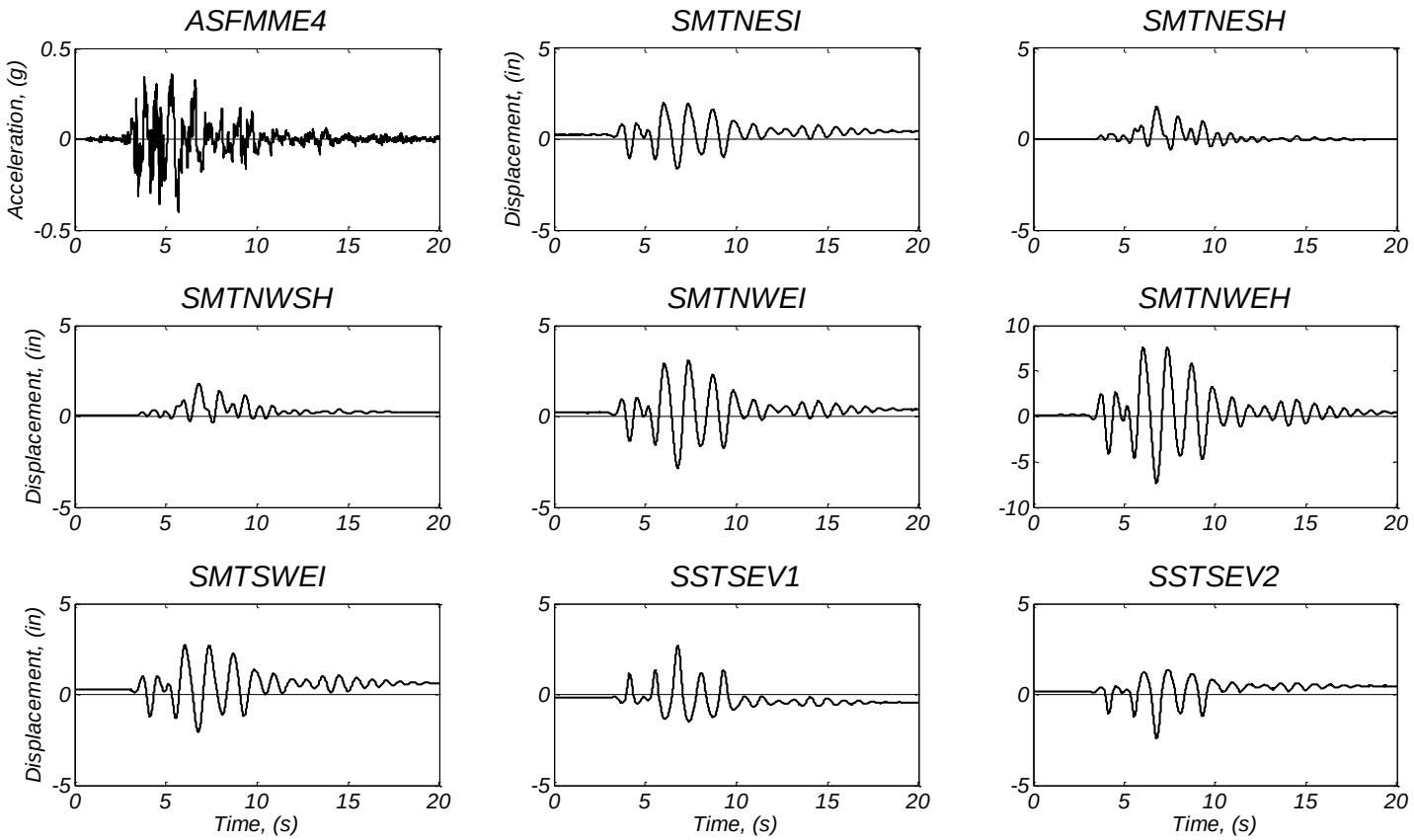

Figure D20. Raw data plots for string potentiometers.

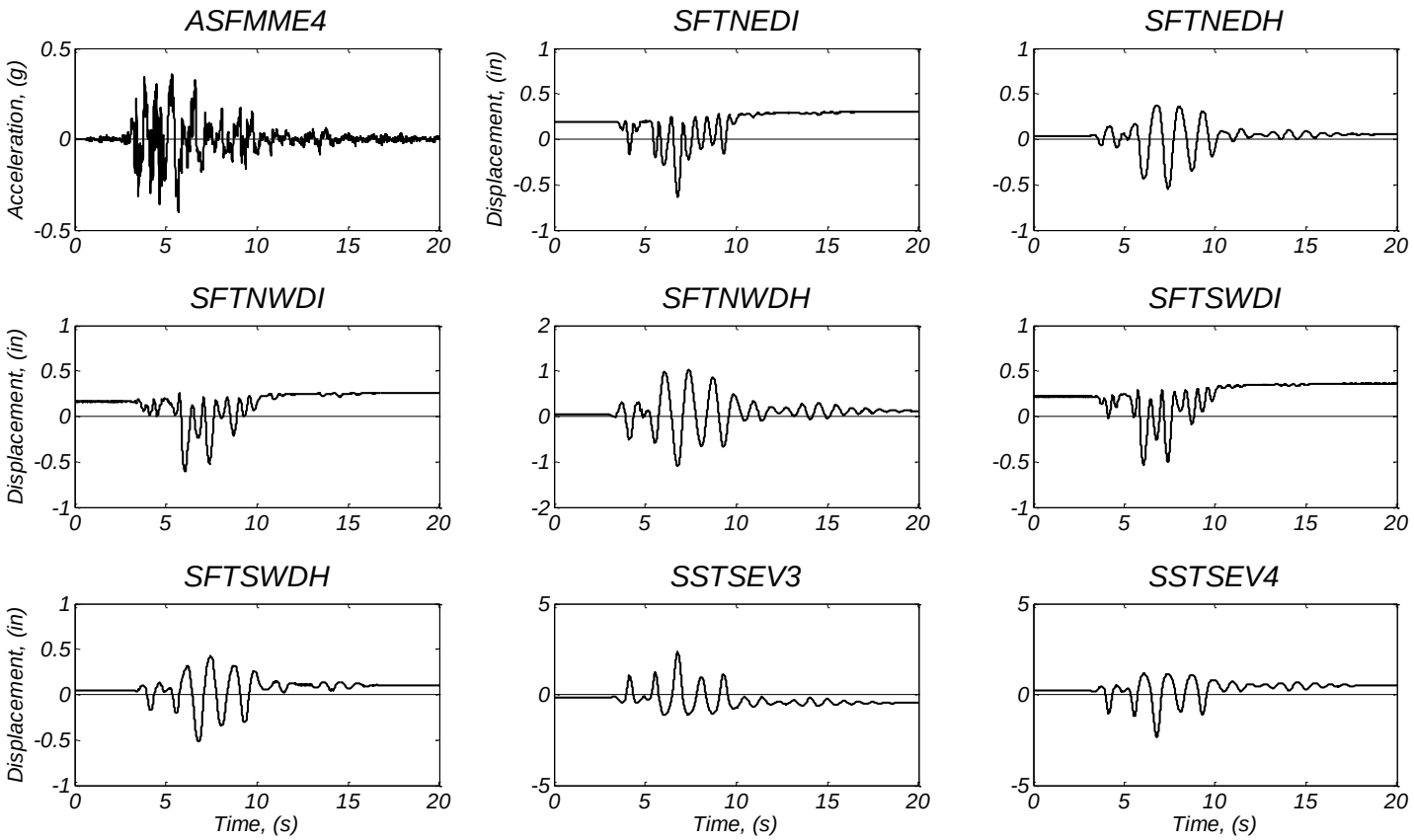

Figure D21. Raw data plots for string potentiometers.

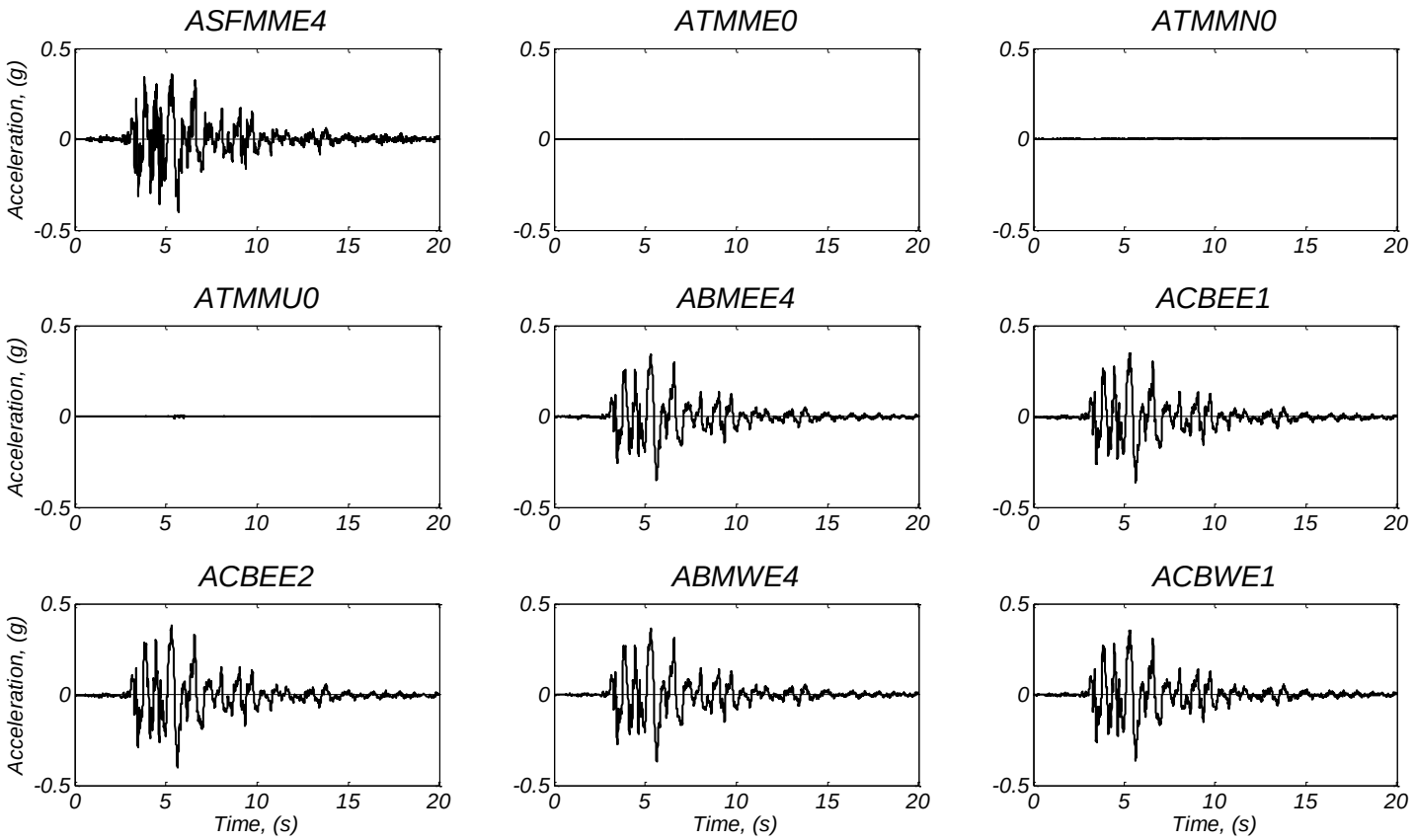

Figure D22. Raw data plots for accelerometers.

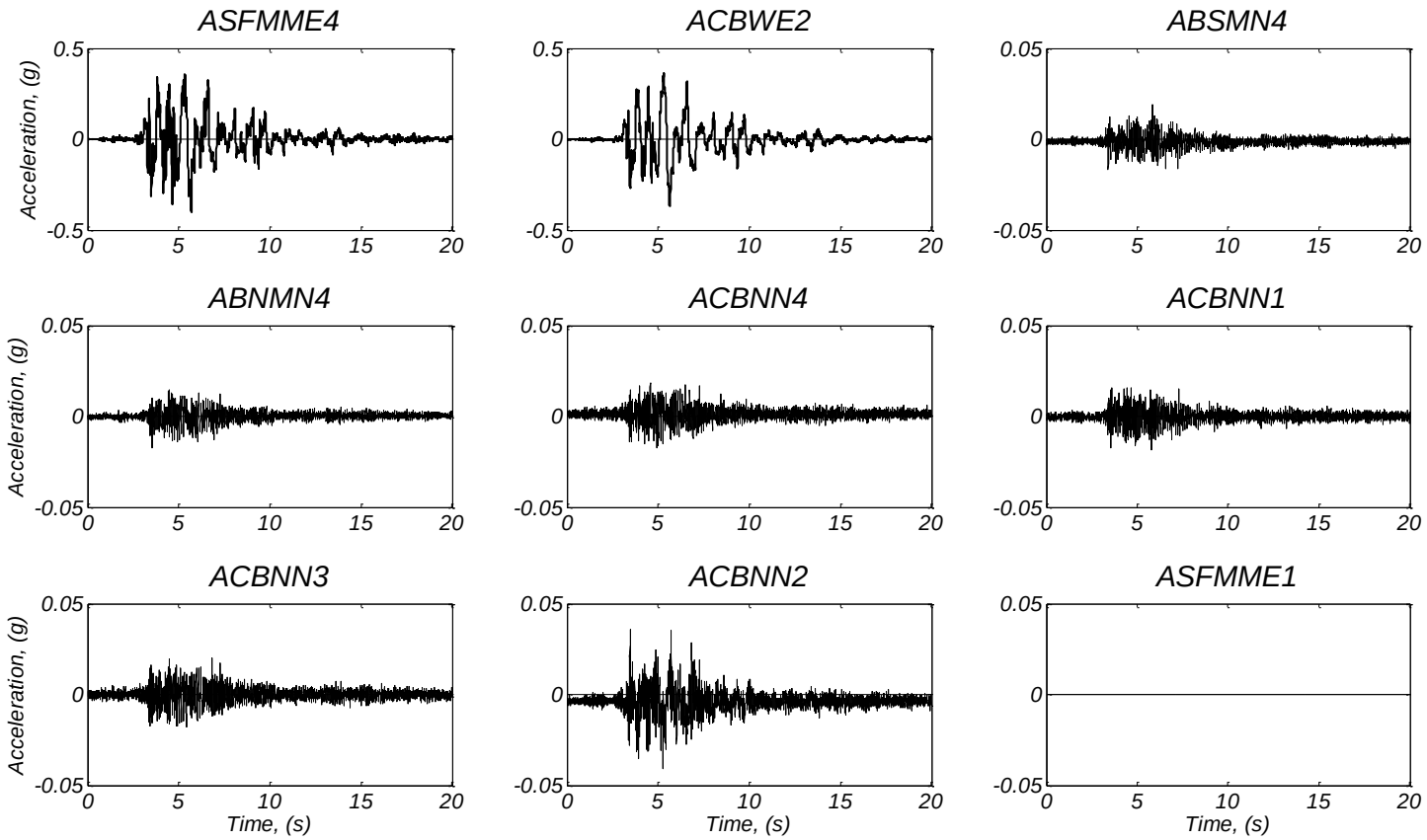

Figure D23. Raw data plots for accelerometers.

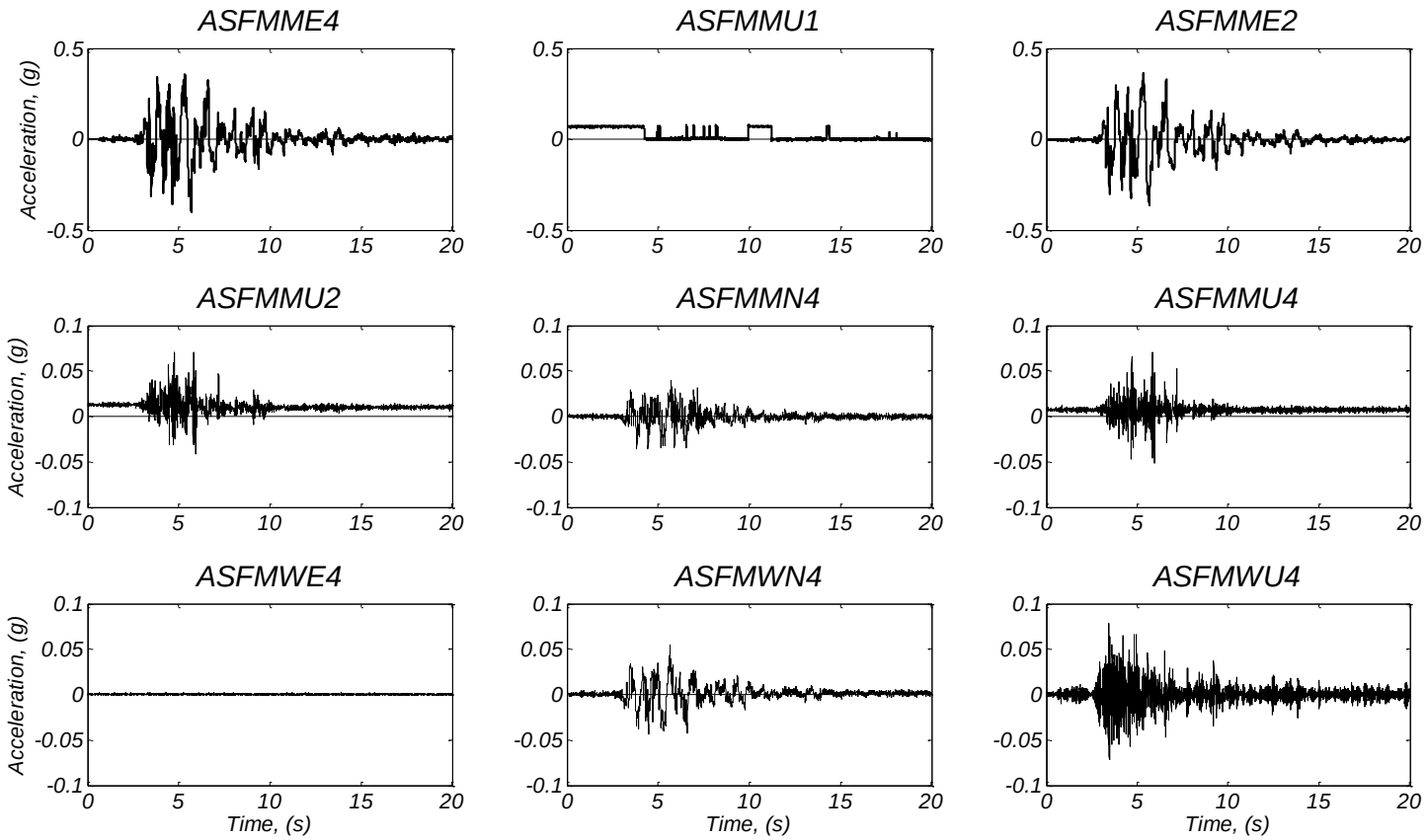

Figure D24. Raw data plots for accelerometers.

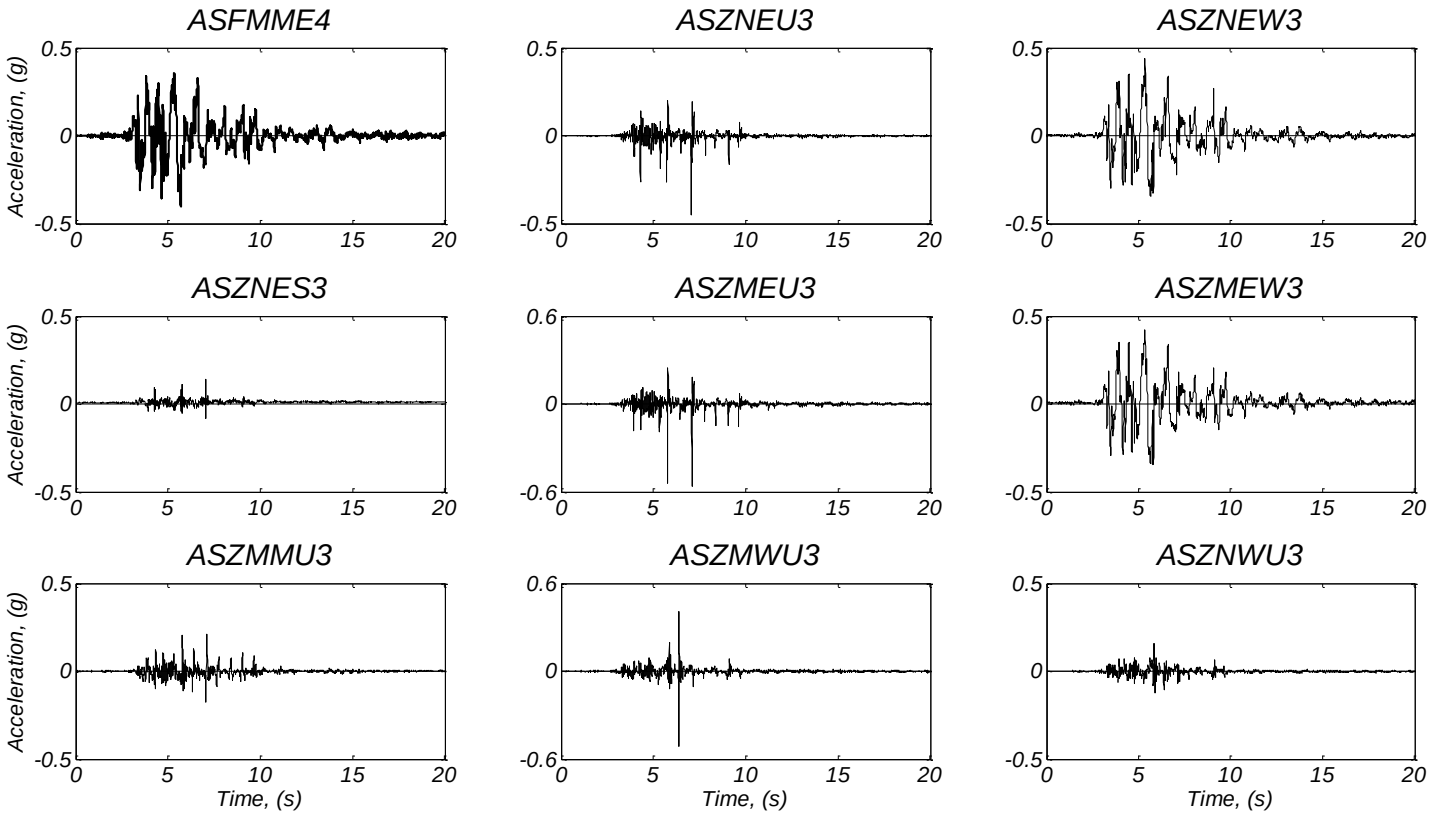

Figure D25. Raw data plots for accelerometers.

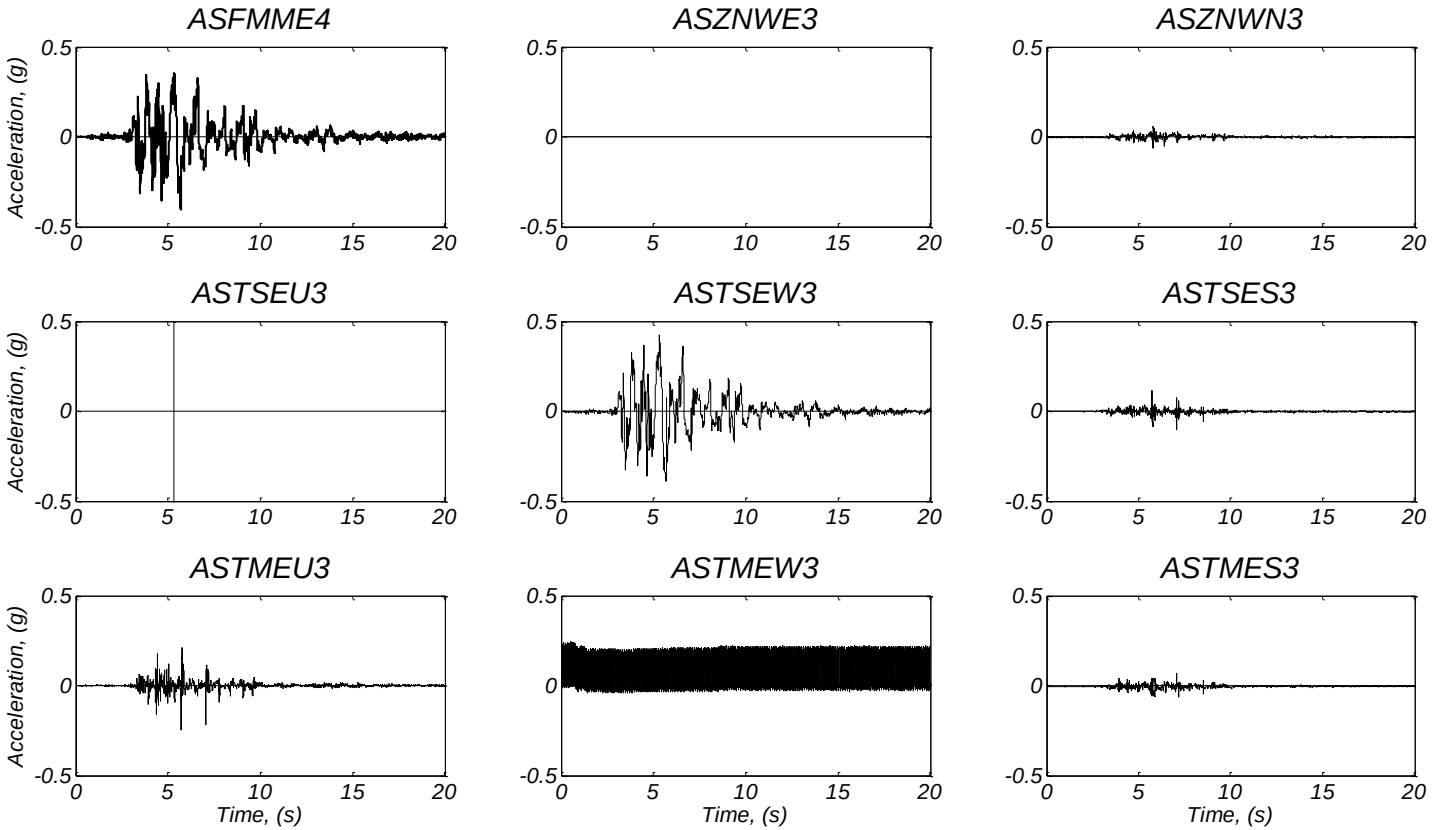

Figure D26. Raw data plots for accelerometers.

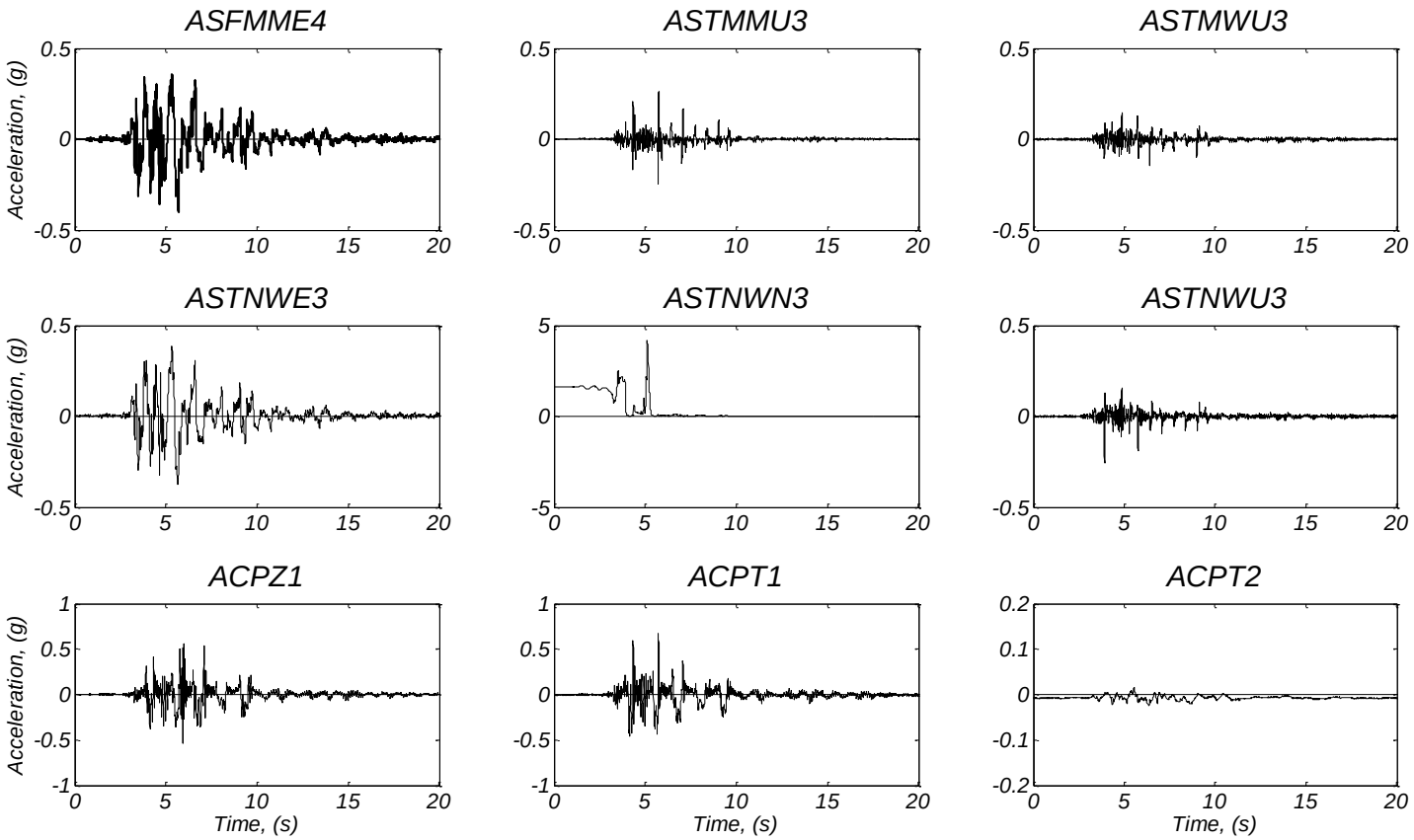

Figure D27. Raw data plots for accelerometers.

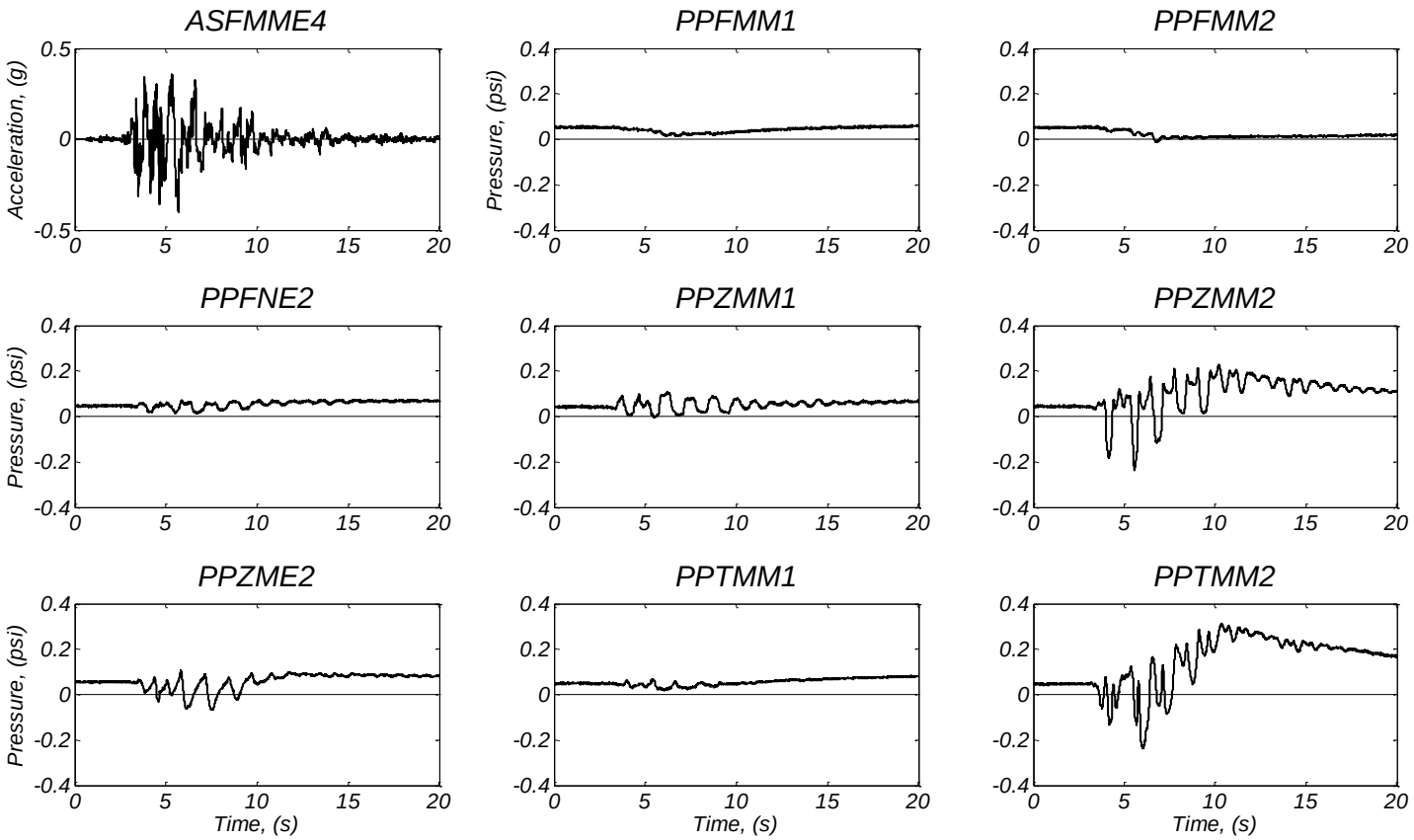

Figure D28. Raw data plots for pore pressure transducers.

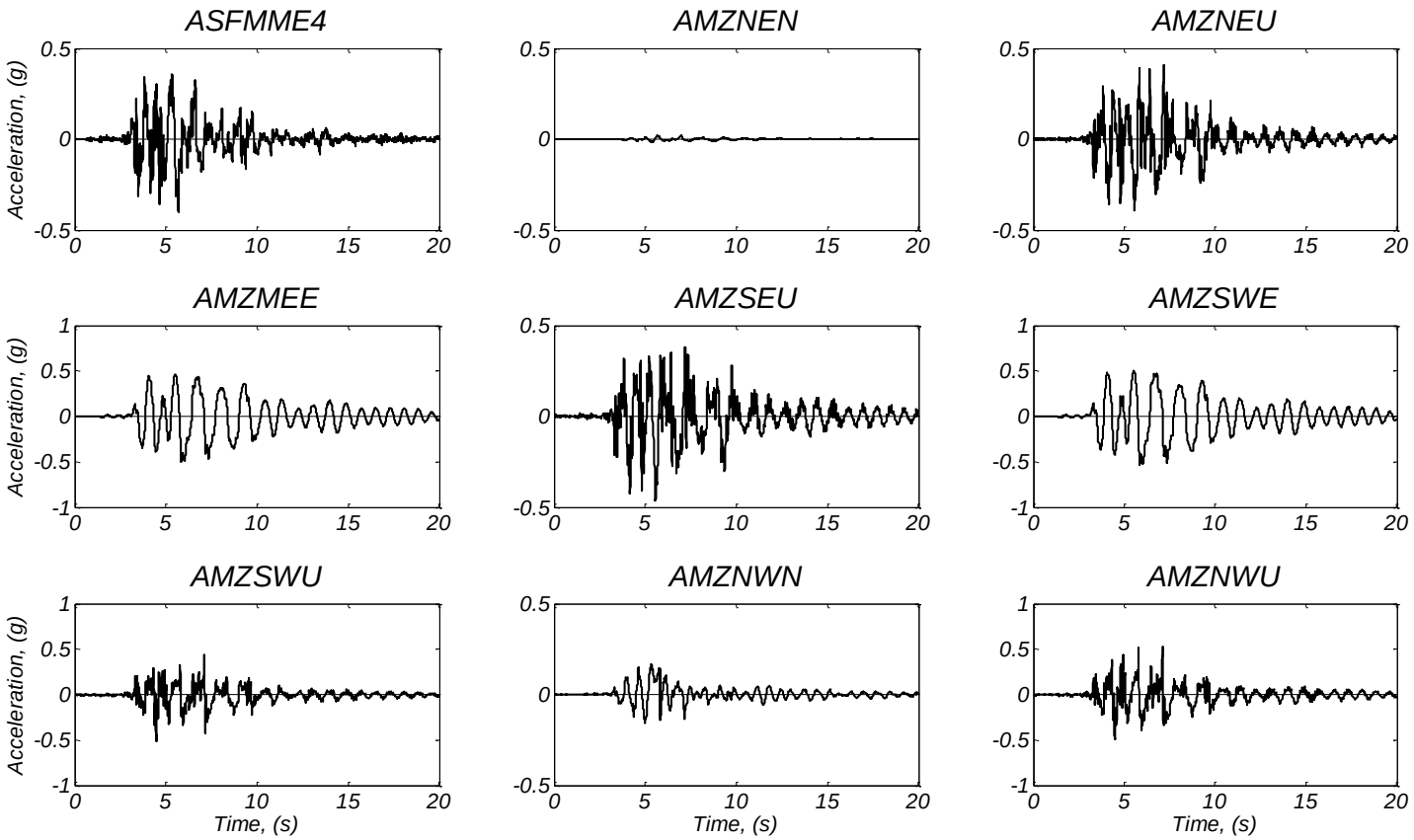

Figure D29. Raw data plots for accelerometers.

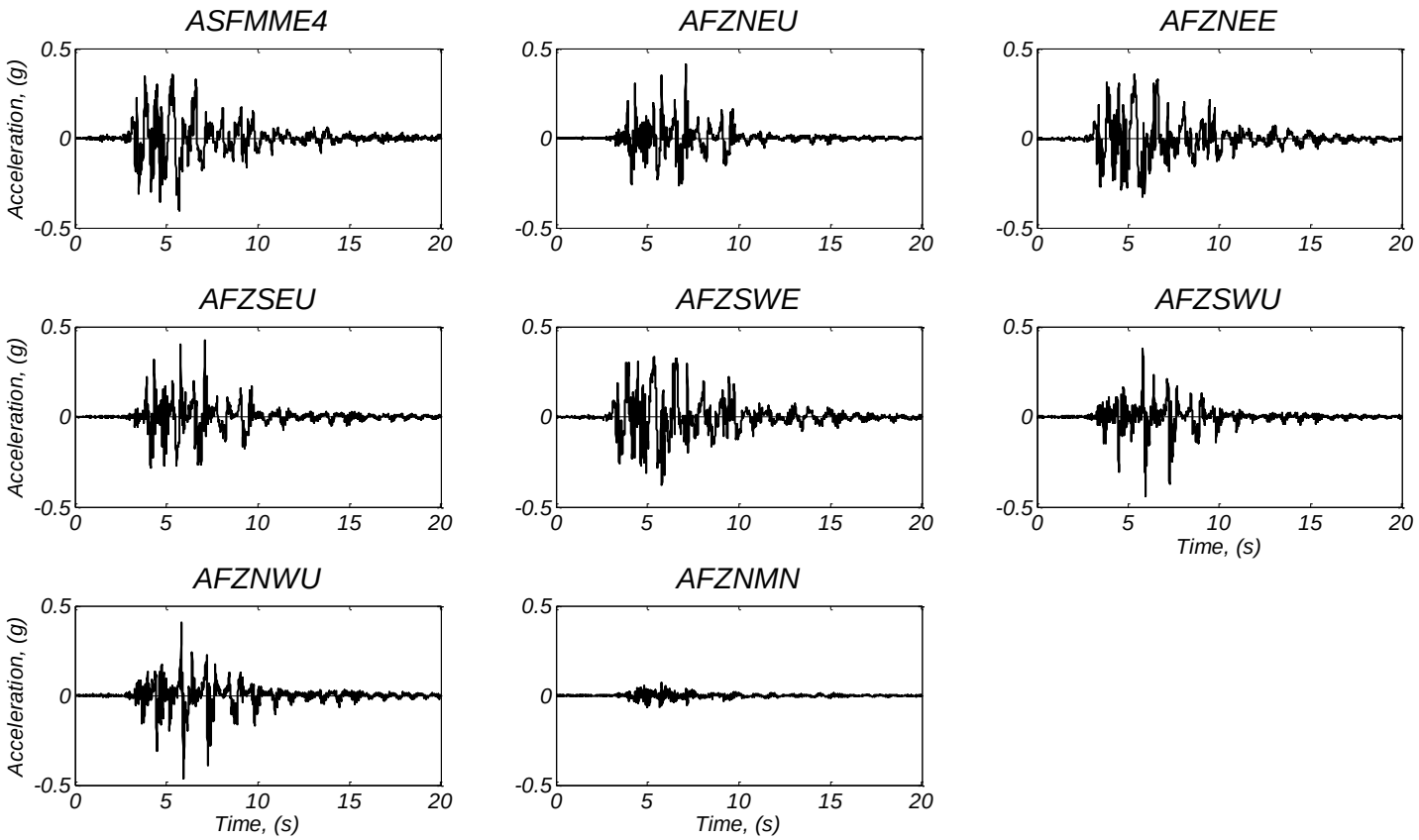

Figure D30. Raw data plots for accelerometers.

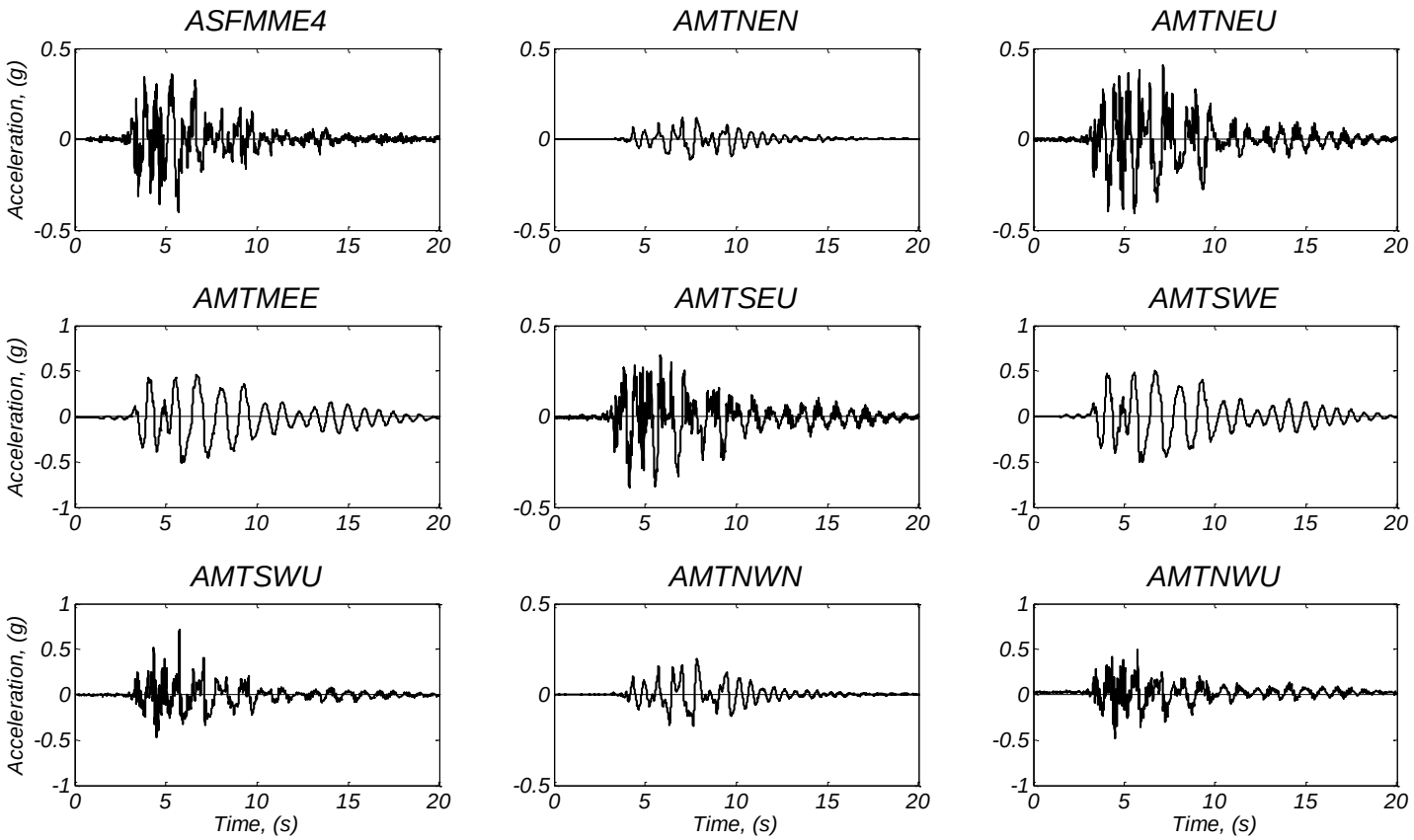

Figure D31. Raw data plots for accelerometers.

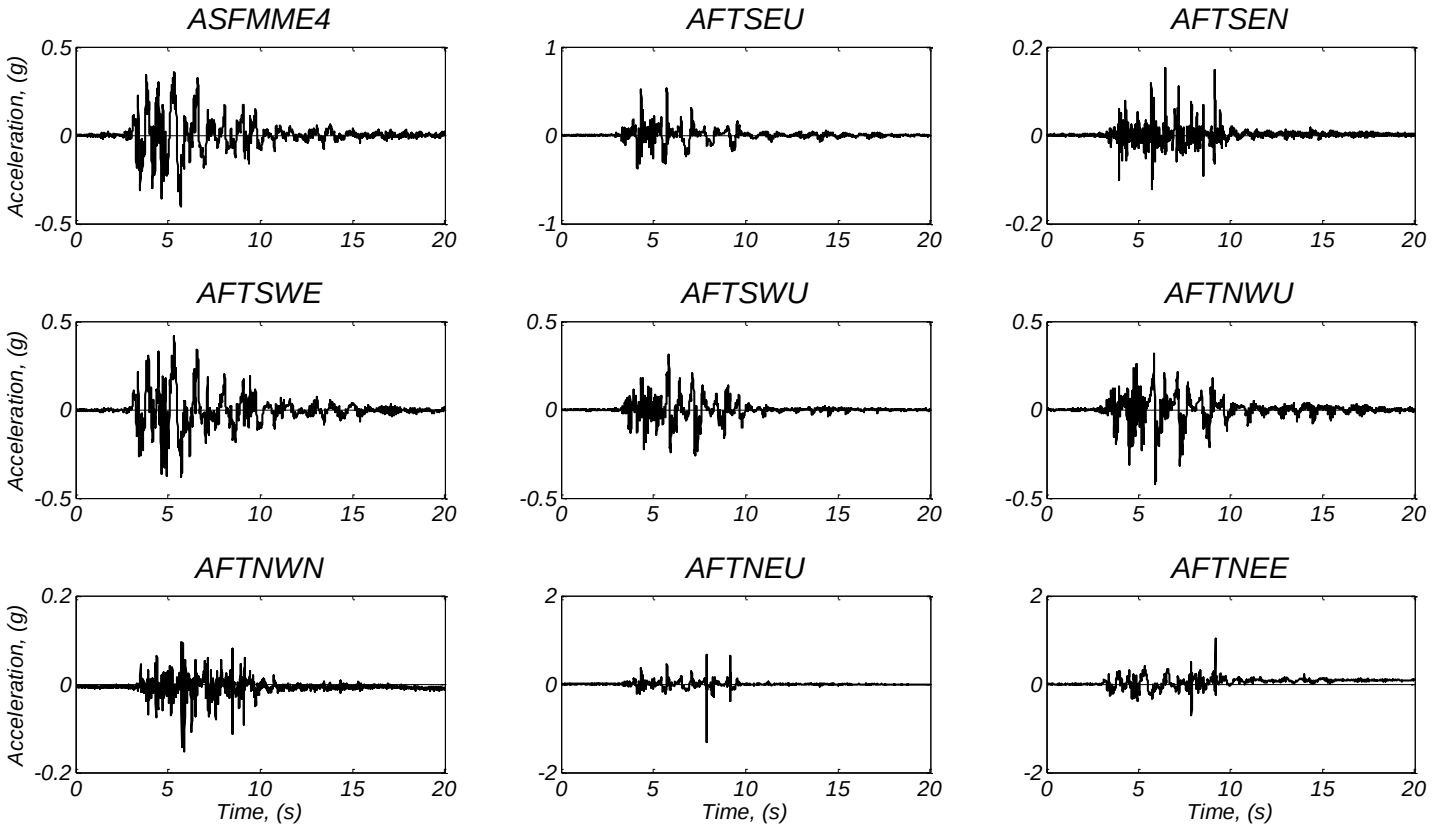

Figure D32. Raw data plots for accelerometers.

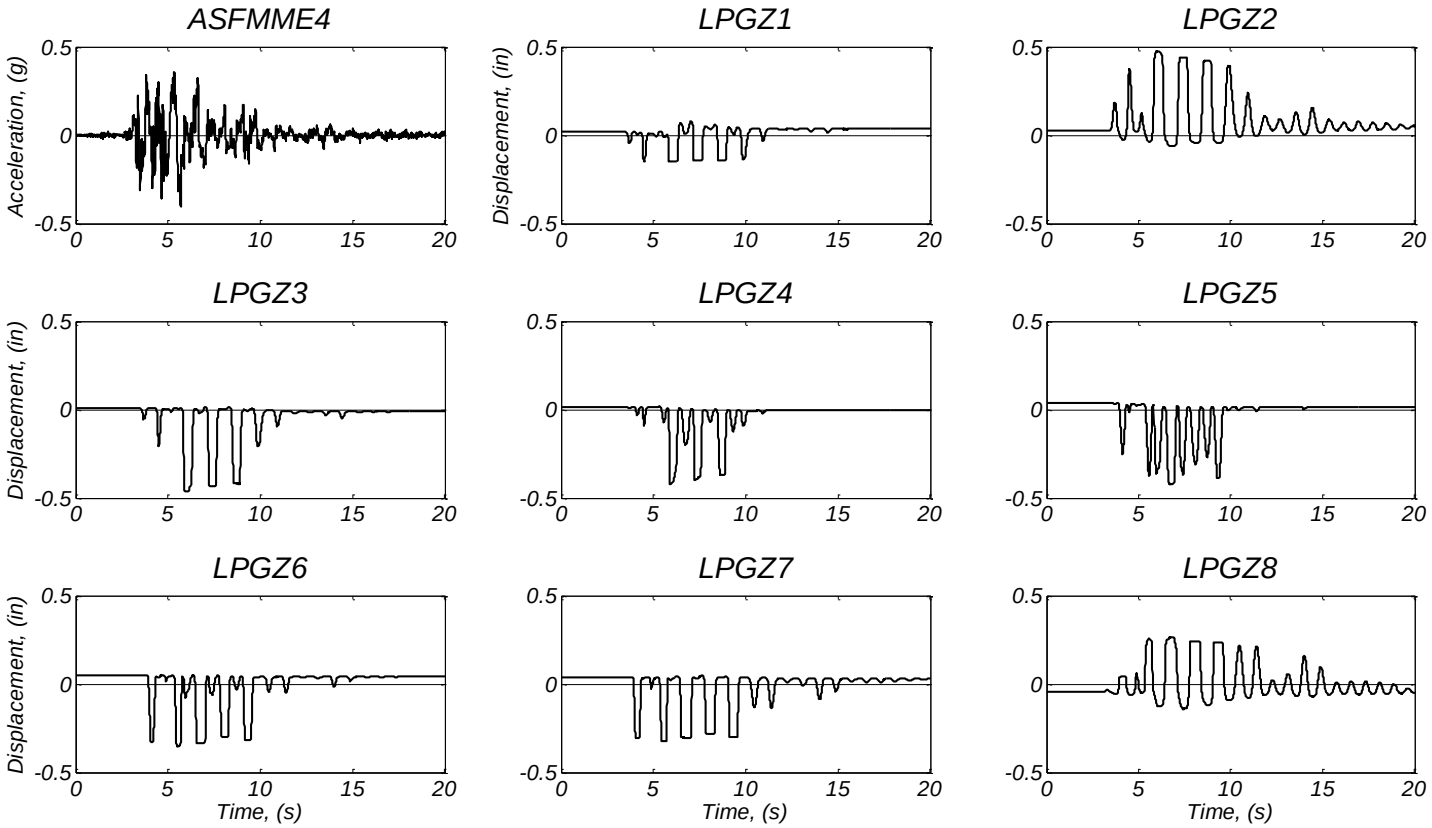

Figure D33. Raw data plots for linear potentiometers.

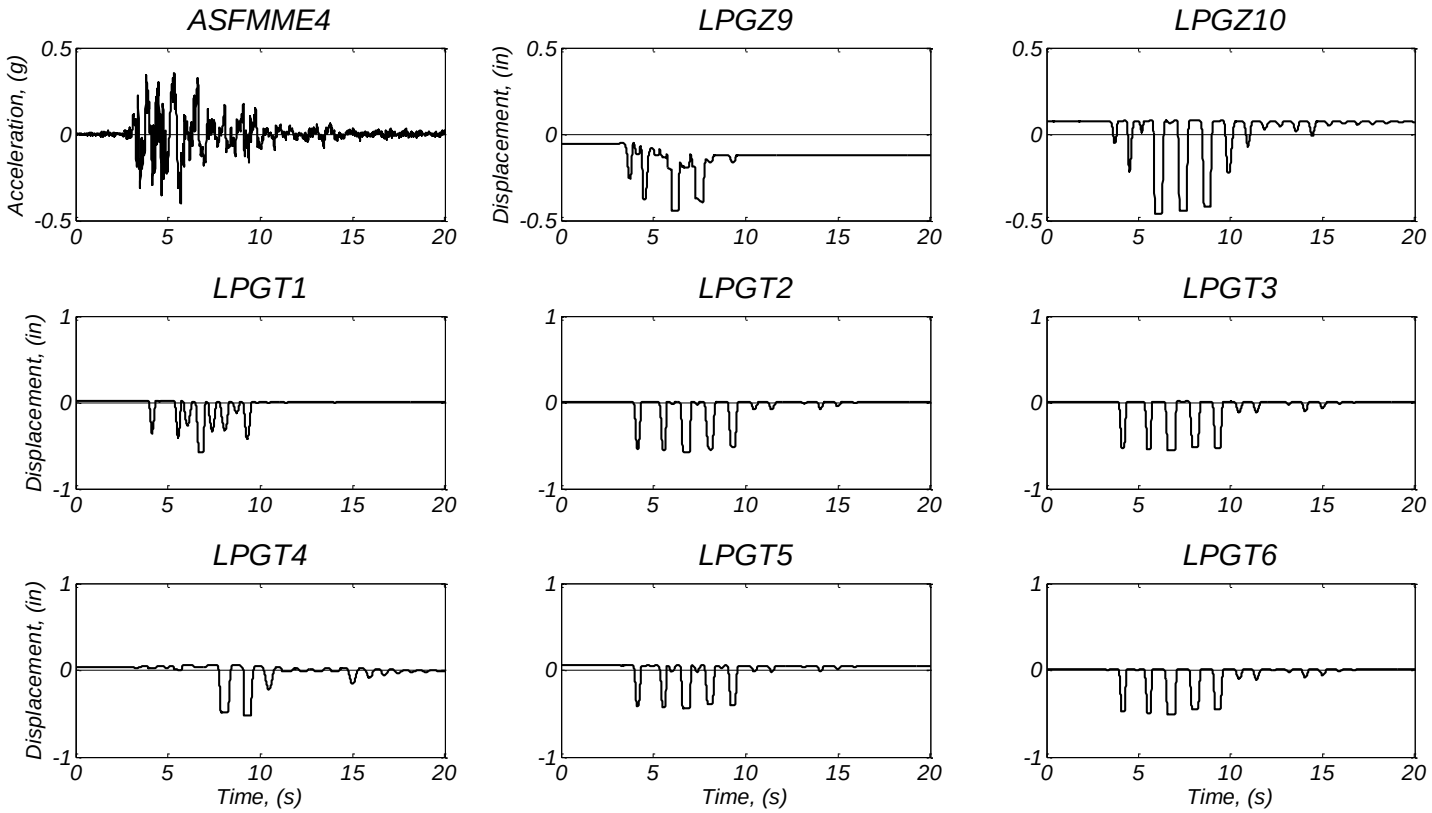

Figure D34. Raw data plots for linear potentiometers.

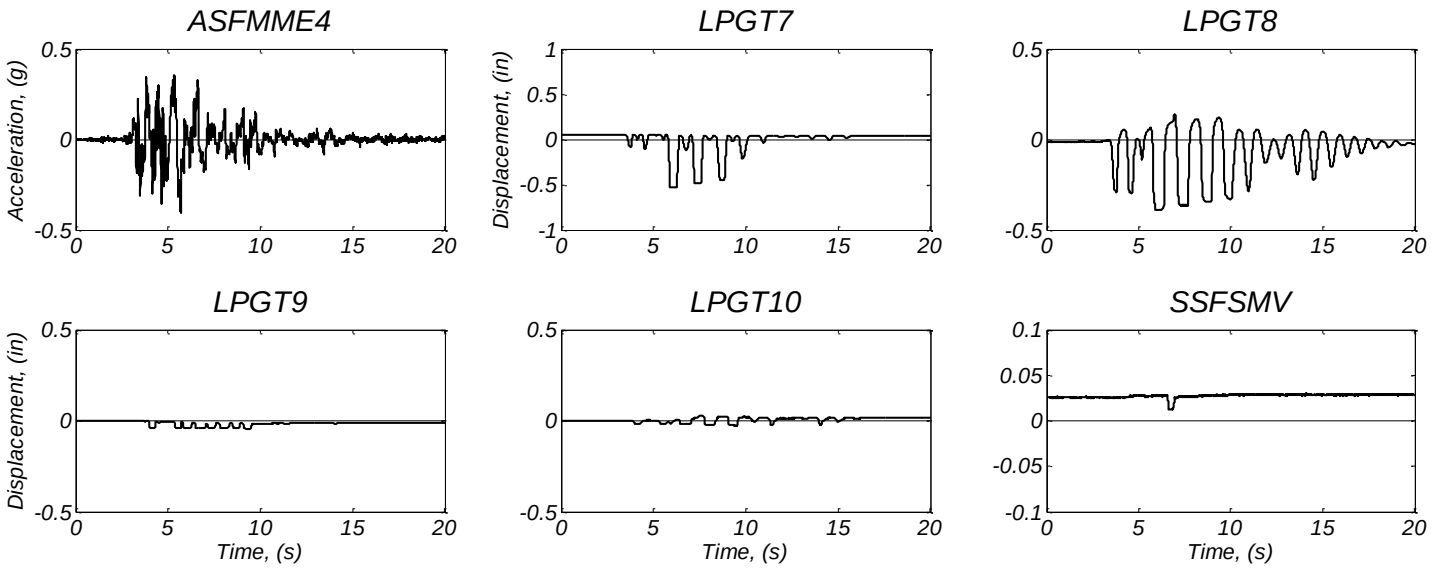

Figure D35. Raw data plots for linear and string potentiometers.